FLOW OF NON-NEWTONIAN FLUIDS IN OPEN CHANNELS

By

RAINER HALDENWANG

NH Dipl (Civ Eng), M Dip Tech (Civ Eng) (Cape Technikon)

Dissertation submitted in fulfilment of the degree
DOCTOR TECHNOLOGIAE
in the Department of Civil Engineering
Cape Technikon

August 2003

THE FLOW OF NON-NEWTONIAN FLUIDS IN OPEN CHANNELS

Rainer Haldenwang

Department of Civil Engineering, Cape Technikon,
PO Box 652, Cape Town, 8000, South Africa.
August, 2003.

ABSTRACT

Flume design for homogeneous non-Newtonian fluids is problematic and not much research has been conducted in this field. This application is industrially important in mining where slurries have to be transported to processing or disposal sites at higher concentrations because water is becoming a scarce and expensive commodity. This thesis addresses the problem of flume design and develops predictive models for the laminar, transitional and turbulent flow behaviour of non-Newtonian fluids in rectangular open channels.

The relevant literature pertaining to Newtonian and non-Newtonian pipe and open channel flow is reviewed and research aspects are identified.

A unique test facility was designed, constructed and commissioned for this project. The facility includes a 5 m-long by 75 mm-wide rectangular tilting flume, as well as a 10 m by 300 mm-wide rectangular tilting flume that can be partitioned to form a 150 mm wide flume. The flumes are in series with an in-line tube viscometer which has tubes of diameter 13, 28 and 80 mm. The experimental investigation covers a wide range of widths (75 mm-300 mm), slopes (1º-5º), flow rates (0.05 l/s-45 l/s), relative densities (1.0067-1.165), volumetric concentrations (0%-10%), and yield stresses (0-21.3 Pa). The fluids tested are kaolin and bentonite slurries and CMC and Carbopol polymer solutions. The resulting database of empirical flow behaviour enabled the identification of the important flow behaviour characteristics.

Existing models are compared and evaluated using the experimental database compiled for this thesis and it is concluded that no model exists to predict the database compiled for the various materials from laminar flow through the transition region into turbulence.

For the correlation of laminar flow data, a Reynolds number was developed from the Reynolds number proposed for pipe flow by Slatter (1994). Using this Reynolds number, all the laminar flow data available was collapsed onto the 16/Re line on a standard Moody diagram.

Criteria were developed to predict the onset of transition and the onset of ‘full turbulence’. These criteria are functions of the Froude and Reynolds number as well as the viscous characteristics of the fluids. These models performed better than the methods proposed by Naik (1983) and Coussot (1994), which were based on the Hanks criterion.

A turbulent flow model was developed based on the turbulent model presented by Slatter (1994) for pipe flow. Flow predictions using this model were more accurate than those presented by Torrance (1963), Naik (1983), Wilson and Thomas (1985), and Slatter (1994).

The new models were tested with the database compiled for this thesis as well as with two published data sets, one by Naik (1983) and the other by Coussot (1994). The new flow models predicted all the available data within acceptable limits, providing a basis for design.

A new and experimentally validated design protocol is presented for the design of rectangular non-Newtonian open channel flow in laminar, transitional and turbulent flow.

Declaration

I, Rainer Haldenwang, hereby declare that the contents of this dissertation/thesis represent my own unaided work, and that the dissertation/thesis has not previously been submitted for academic examination towards any qualification. Furthermore, it represents my own opinions and not necessarily those of the Cape Technikon.

Rainer Haldenwang

August 2003

DEDICATION

To Mariëtta,

Suzanne, Mario and Renate.

"Trust in the LORD with all your heart

and lean not on your own understanding;

in all your ways acknowledge him,

and he will make your paths straight."

Proverbs 3:5-6

Acknowledgements

I would like to thank the following persons and organisations:

Prof. Paul Slatter, my supervisor and friend, who guided me through the whole research process with much encouragement, wisdom and enthusiasm and helped to make the journey an exciting one.

The council of the Cape Technikon for study leave and financial support.

The financial assistance of the National Research Foundation towards this research is hereby acknowledged. Opinions expressed in this thesis and the conclusions arrived at, are those of the author and are not necessarily to be attributed to the National Research Foundation.

Rainer Haldenwang
August 2003

NOMENCLATURE

Symbol	Description	Unit
A	cross sectional area	m^2
A_r	Wilson and Thomas area ratio	
A_0	velocity function (Naik)	
a	geometric coefficient for channel shape	
B	breadth of channel	m
B	roughness function	
b	geometric coefficient for channel shape	
c_L	resistance coefficient for frontal correction in a cylinder measuring system	
C	concentration, constant	
C_{Chezy}	Chezy constant	$m^{0.5}s^{-1}$
C_v	solids volumetric concentration	percentage
C_w	solids concentration by weight	
d	particle diameter	µm
D	internal pipe diameter	m
D_{char}	characteristic geometric dimension	
D_e	equivalent diameter	m
D_v	diameter of vane	m
e	roughness	m
E	sum of mean error squared	
F	force	N
f	Fanning friction factor	
Fr	Froude number	
g	gravitational acceleration	m/s^2
G	pseudo shear rate	1/s
H	head	m
H_B	Herschel-Bulkley number	
He	Hedström number	
H_f	frictional head	m
h	flow depth in channel	m
h	gap in plate measuring system	m
i	hydraulic gradient m(water)/m(pipe)	
K	fluid consistency index	$Pa.s^n$
K	open channel shape constant	
K’	apparent fluid consistency index	$Pa.s^{n'}$
k	hydraulic roughness	m
L	pipe or channel length, characteristic length	m
L_v	length of vane	m
l	mixing length	µm
M	mass	kg
M_w	mass water	kg
m	slope	
m	1/n (inverse of the flow behaviour index)	

m_{Bazin}	Bazin constant	
N	number of data points	
n	flow behaviour index	
n’	apparent flow behaviour index	
n_{Cutter}	Cutter constant	
$n_{Manning}$	Manning constant	$m^{-0.3333}s$
P	wetted perimeter	m
P_m	average wetted perimeter over a section	m
p	pressure	Pa
Q	volumetric flow rate	m^3/s
R	radius	m
R_b	radius of rotary viscometer bob	m
R_c	radius of rotary viscometer cup	m
Re	Reynolds number	
Re_c	critical Reynolds number at onset of transition	
$Re_{c(turb)}$	critical Reynolds number at onset of ‘full turbulence’	
$Re_{K\&Tiu(BP)}$	Kozicki & Tiu Reynolds number (Bingham)	
$Re_{K\&Tiu(PP)}$	Kozicki & Tiu Reynolds number (Power law)	
Re_{Naik}	Naik Newtonian Reynolds number	
Re_{Zhang}	Zhang & Ren Reynolds number (Bingham)	
Re_2	general open channel flow Reynolds number	
$Re_{2(YPP)}$	open channel Reynolds number adapted for Hershel-Bulkley fluids	
$Re_{2(PP)}$	open channel Reynolds number adapted for power law fluids	
$Re_{2(BP)}$	open channel Reynolds number adapted for Bingham fluids	
Re_r	roughness Reynolds number	
R_h	hydraulic radius	m
r	correlation coefficient	
S	relative density	
T	torque	N.m
T_m	maximum torque measured	N.m
t	time	s
u	point velocity	m/s
u^+	dimensionless velocity	
V	average velocity	m/s
V_*	shear velocity	m/s
V_s	settling velocity	m/s
V_{turb}	new turbulent velocity	m/s
v	part of transition equation used by Coussot	
v	velocity	m/s
w	mass flow rate	kg/s
α	angle of inclination degrees	
β	cone angle degrees	
$\dot{\gamma}$	shear rate	s^{-1}
δ	viscous sub-layer thickness	μm
δ	ratio of cup : bob in rotary viscometer	
δ	ratio between cup and bob radius	

δ_N	Newtonian viscous sub-layer thickness	
δ_{NN}	non-Newtonian viscous sub-layer thickness	
Δ	increment	
ε	channel roughness factor	
λ	half width to depth ratio of channel	
μ	dynamic viscosity	Pa.s
μ_{app}	apparent dynamic or secant viscosity	Pa.s
μ_e	equivalent viscosity	Pa.s
μ_p	coefficient of mechanical sliding friction	
ν	kinematic viscosity	m^2s^{-1}
ρ	fluid or slurry density	$kg.m^{-3}$
ρ_w	density of water	$kg.m^{-3}$
τ	shear stress	Pa
τ_o	wall shear stress	Pa
τ_y	yield stress	Pa
ϕ	ratio of yield stress over wall shear stress	
ϕ	ratio of wall shear stress and yield stress	
Φ	part of shape factor equation	
φ	Kozicki and Tiu shape factor function	
χ	Von Karman constant	
ω	velocity function, angular velocity	$rad.s^{-1}$
Ω	velocity function	

Subscripts

85	85^{th} percentile of particles passing
0	at the wall of the pipe or flume
c	critical
calc	calculated
l	loss
m	mixture (slurry)
obs	observed (experimental)
r	roughness
s	solids
v	volumetric
w	water

TERMS AND CONCEPTS CITED

Open channel: Conduit for transporting liquids with a free surface open to atmosphere. A channel may be artificial or natural.

Flume: Artificial open channel carrying fluids, slurries or tailings. The word is used mainly in the mining and chemical industries.

Launders: In the mining industry short flumes with steeper slopes are often called launders.

Note: The above three terms are often used to describe the same object.

Rheology: The science of flow behaviour (from the Greek *rheos* - flow and *logos* - knowledge).

Newtonian fluid: Any fluid that has a directly proportional relationship between shear stress and shear rate.

Non-Newtonian fluid: Any fluid that does not have a simple proportional relationship between shear stress and shear rate.

Laminar flow: The effect of viscous forces dominates the flow behaviour and fluid particles appear to move in smooth paths, not crossing streamlines.

Turbulent flow: Here inertial forces dominate viscous forces so that the particles move in irregular paths which are not smooth or fixed and where streamlines are crossed.

Transition region: This is the region between the laminar and the turbulent region where the regimes are mixed.

Reynolds number: The ratio between viscous and inertial forces is proportional to

the Reynolds number. The number is expressed in terms of the density, velocity, characteristic length and the viscosity of the fluid.

Froude number: The ratio between gravity and inertial forces is proportional to the Froude number.

CONTENTS

LIST OF FIGURES

LIST OF TABLES

CHAPTER 1

INTRODUCTION

The flow of water in open channels has been well researched worldwide for a long time. As early as 1959, Chow wrote a textbook on open channel flow, and since then many more have been written. The same cannot be said of the flow of homogeneous non-Newtonian slurries in open channels. Only a few papers and chapters in books have been written by authors like Kozicki and Tiu (1967), Wilson (1991) and Coussot (1994 and 1997).

The flow of Non-Newtonian slurries in open channels has significant implications in the mining field where dense slurries have to be transported around plants and to tailings dams (Sanders, Schaan, Gillies, McKibben, Sun and Shook, 2002). As water becomes scarcer, limited by legislation and more expensive, higher concentrations need to be transported. Another application is the transport of sewage sludge. In the polymer processing and textile fiber industries, open channels are also used (Kozicki and Tiu, 1988). The fact that many of these open channels are designed without a properly researched and validated design procedure makes this a research topic that requires urgent attention.

Slurries flowing in open channels can be classified into three categories. In homogeneous slurries the particles are relatively small and are kept in suspension by the carrier fluid, which is generally water. If no flow occurs, these particles will eventually

settle at least partially. These slurries are classified as non-Newtonian and can be rheologically characterised.

Coarse particle mineral slurries in water are settling slurries. For these slurries, the velocity of the carrier fluid is critical, as the particles need to be in suspension to be transported. The third category is the mixed regime slurry that is a mixture of the slow settling and rapid settling slurries (Wilson, 1991).

This thesis deals with the flow of homogeneous non-Newtonian slurries in smooth rectangular open channels dealing specifically with:

- laminar flow
- the transition from laminar to turbulent flow
- turbulent flow.

1.1 STATEMENT OF THE PROBLEM

The fundamental problem is to predict the flow behaviour of non-Newtonian slurries in open channels. This problem can be divided into three flow regimes: laminar flow, turbulent flow and the transition zone in between the two regimes.

1.1.1 Laminar Flow

Laminar flow in open channels can be treated similarly to that of laminar flow in pipes. The difference is that there is a surface open to atmosphere that complicates the flow behaviour (Chow, 1959). There are some empirical models available in literature, that rely on various rheological models (Kozicki & Tiu, 1967; Zhang & Ren, 1982). The

rheological characterisation of the slurries is another important issue that has a direct effect on the effectiveness of the flow predictions. Although there are a few models available to predict laminar flow in open channels, some of them have not yet been experimentally tested (Kozicki & Tiu, 1967).

1.1.2 Laminar turbulent transition

For the laminar turbulent transition prediction of slurries in pipes, there are a number of methods described in literature (Slatter, 1994). The same cannot be said for open channel flow. What one finds, is that authors speculate that the methods used in pipelines should also work for open channel flow (Naik, 1983; Coussot, 1997; Wilson 1991). To be able to predict transition accurately is essential when open channels are designed, because the flow behaviour is very different for laminar and turbulent flow.

1.1.3 Turbulent flow

Turbulent flow in pipes and channels is still not well understood (McComb, 1994). Authors like Shook & Roco (1991) as well as Slatter (1994), have tested different models in pipelines and have found them to vary significantly. For open channel flow it is as difficult and again authors have speculated that models for pipeline turbulence can be used in open channels (Naik, 1983; Kozicki & Tiu, 1967; Wilson, 1991). Again, very little work has been done to verify this experimentally (Wilson, 1991).

1.2 OBJECTIVE

The objective of this thesis is to measure, analyse and describe the flow behaviour of different viscous fluids in three rectangular flumes of different size, with slopes varying

from one to five degrees, over a wide flow rate range and to establish design criteria for flow predictions of slurries in open channels specifically looking at the following:

- Laminar flow regime
- The transition between laminar and turbulent flow
- Turbulent flow in smooth wall channels.

1.3 METHODOLOGY

In order to reach the objectives, the following research methodology was followed.

Viscous fluids to be tested will cover a wide range of viscous characteristics and will include materials that can be characterised using the following rheological models, namely: Newtonian, Power law or Ostwald-de Waele, Bingham plastic and Hershel-Bulkley.

The overall approach is displayed in flow-chart format in Figure 1-1 below.

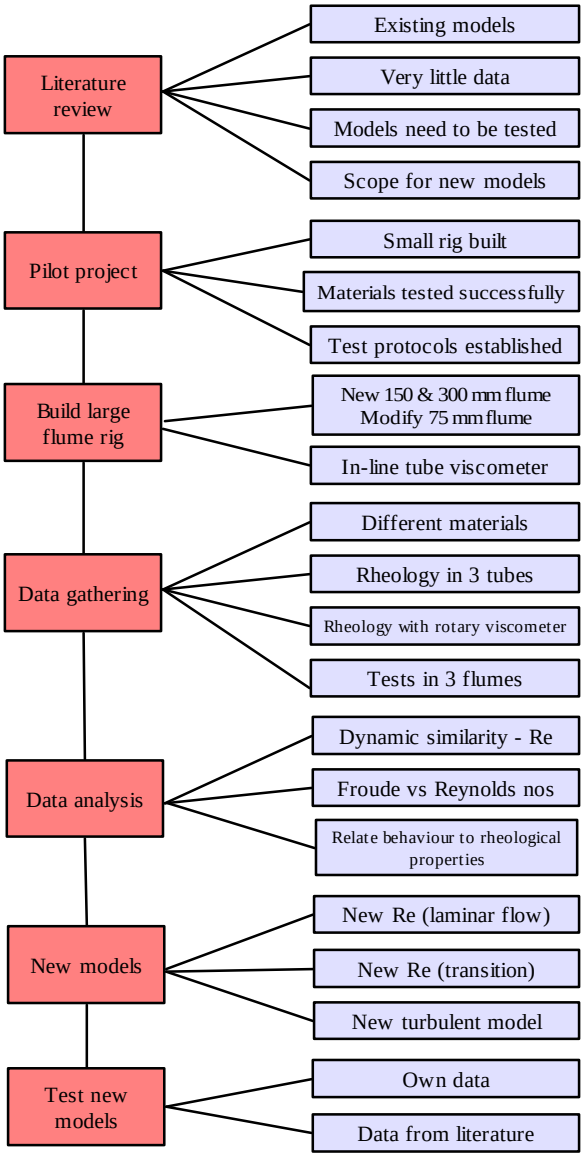

Figure 1-1 Flow chart of research approach

1.3.1 Literature review (Chapter 2)

Open channel flow fundamentals, as well as models suggested by Kozicki and Tiu (1967), Coussot (1994), and others are reviewed. The impact of rheology on the laminar flow models will also be discussed.

1.3.2 Experimental procedures (Chapter 3)

A special test rig was designed and constructed to conduct all the tests. It consists of three different size rectangular flumes linked to an in-line tube viscometer with three diameter tubes. This enabled us to rheologically characterise the materials tested in-line. Three rheologically different slurries were tested over a wide range of laminar and turbulent flow rates in three size flumes over a range of slopes varying from one to five degrees.

1.3.3 Analysis of data using models from the literature (Chapter 4)

The data obtained experimentally is used to test models presented in the literature. The results are then discussed.

1.3.4 New analysis (Chapter 5)

The data obtained experimentally will be used to develop and present new empirical models to predict non-Newtonian laminar flow, transition and turbulence in open channels.

1.3.5 Evaluation of new models (Chapter 6)

The new models will be evaluated and their limitations and accuracy described.

1.3.6 Summary, conclusions and recommendations (Chapter 7)

The significant contributions of this work will be presented, as well as the conclusions drawn and recommendations made for future work.

1.3.7 Open Channel Design Procedure (Appendix C)

The new design procedure will be described which will enable a design engineer to systematically go through the procedure of an open channel flow design for homogeneous slurries in rectangular flumes.

1.4 DELINEATION

The following topics will not be part of this dissertation but will be part of future research planned.

The effect of different shapes of open channels on the flow of non-Newtonian fluids in the different flow regimes.

The effect of roughness on open channel flow of non-Newtonian fluids.

Refining methods to measure velocity profiles in fluids that are not transparent.

Calibrating CFD (Computational Fluid Dynamics) models so that computer models can be used to examine open channel flow.

Time dependent fluids will not be tested.

1.5 SUMMARY

An introduction, the objectives, an overview and the layout of this thesis have been presented in this chapter. In Chapter 2, the theory and literature review will be presented.

CHAPTER 2

THEORY AND LITERATURE REVIEW

2.1 INTRODUCTION

The theory and literature of the flow of homogeneous, time independent, non-Newtonian slurries in open channels are presented. As the flow in pipes is closely linked to open channel flow and much theory for open channel flow is derived from pipe flow, there will be some reference to pipe flow and its relevance also (Chow, 1959).

The reason why pipe flow is discussed is that open channel flow models, both Newtonian and non-Newtonian, have to a large extent, been derived from pipe flow models. That there are similarities is not disputed, but that there is also a big difference should not be forgotten. The presence of a free surface adds an extra dimension to the complexity of open channel flow over that of full pipe flow (Chow, 1959).

A considerable amount of research has been conducted on the flow of Newtonian fluids in pipes and open channels, and therefore this type of flow will be presented first.

To classify the non-Newtonian slurries used in this thesis, the yield-pseudoplastic or Herschel-Bulkley rheological model will be reviewed. The strength of this model is that it can be easily simplified to satisfy Bingham and power-law fluids, and in its most basic form it reverts to the Newtonian model (Slatter, 1994).

Relevant non-Newtonian Reynolds numbers and criteria to predict transition will be discussed. Turbulence models will also be discussed.

2.2 FLOW REGIMES

Before dealing with pipe and open channel flow, it is necessary to define the different flow regimes that will be discussed at length in the following sections and chapters.

2.2.1 Newtonian laminar and turbulent flow

Fluid flow can be classified as either laminar or turbulent. If the flow is laminar, one fluid layer slides over the next in an ordered, streamlined fashion. In this region, the viscous forces dominate and obey Newton's law of viscosity where the shear stress is proportional to the velocity gradient and the coefficient of proportionality is the dynamic viscosity. The relationship is described as follows: (Chhabra & Richardson, 2000).

$$\tau = \mu\left(-\frac{du}{dy}\right). \qquad 2.1$$

In turbulent flow, which occurs most often when water is concerned, the fluid particles flow in erratic paths, which cause the velocity components to fluctuate. These fluctuations create momentum changes, which result in large increases in shear stresses (Featherstone & Nalluri, 1995).

Osborne Reynolds was the first to study these flow regions and developed the following relationship, which is now called the Reynolds number. The Reynolds number is proportional to the ratio between inertial and viscous forces and is defined as follows:

$$Re = \frac{\rho V L}{\mu}. \qquad 2.2$$

For pipe flow the characteristic length L becomes the diameter D (Streeter, 1971).

For open channel flow L becomes the hydraulic radius R_h, where the hydraulic radius is the ratio of area over the wetted perimeter of the flow cross-section (Chow, 1959).

By experiment Reynolds determined that laminar flow occurs when the Reynolds number was less than approximately 2 000, and that turbulent flow occurs with Reynolds numbers above 4 000. The region between laminar and turbulent flow is an unstable region called the transition zone.

2.2.2 Froude number

The Froude number is proportional to the ratio between inertial and gravity forces. If the Fr >1, it means that waves cannot propagate upstream (Chow, 1959).

The Froude number is defined by Chanson (1999) as a dimensionless number proportional to the square root of the ratio of the inertial force over the weight of the fluid:

$$Fr = \frac{V}{\sqrt{g D_{charac}}} = \frac{\rho V^2 A}{\rho g A L} \propto \sqrt{\frac{\text{inertial force}}{\text{weight}}}. \qquad 2.3$$

The D_{charac} is the characteristic geometric dimension. For a pipe it will be the diameter and for an open channel the flow depth.

For a rectangular open channel the Froude number is:

$$Fr = \frac{V}{\sqrt{gh}}. \qquad 2.4$$

If the Froude number is less than unity, the flow is called *sub-critical*. In this flow state

the gravity forces are more prominent.

If the Froude number is greater than unity, the flow is classified as *super-critical*. The inertial forces play a greater role in this flow state and the velocity is generally high.

When the Froude number is 1, the flow is critical and this is generally regarded as an unstable region.

Both the Reynolds and Froude numbers describe flow behaviour.

The possibility of propagating a gravity wave upstream can be used as a criterion to distinguish between sub- and super-critical flow (Chow, 1959).

2.2.3 Open channel flow types

Open channel flow can be categorised into several types. The two classifications that are relevant to this thesis are as follows:

- **Steady and unsteady flow**

  Open channel flow is *steady* when the flow depth h does not change with time over the time interval which is considered. Unsteady flow occurs when the flow depth changes with time.

- **Uniform and varied flow**

  The flow is *uniform* when the flow depth h is the same over a section of the channel. The flow is *varied* when the flow depth h varies over the length considered.

For open channel flow hydraulics, steady uniform flow is the flow that is treated (Chow, 1959). It is therefore important that this flow type occurs in the test section of a laboratory flume.

2.3 FLUID BEHAVIOUR

In this section, the fluid characteristics of single-phase liquids and pseudo-homogeneous mixtures such as slurries will be described. These liquids may be treated as a continuum if they are stable in the absence of turbulent eddies and vary according to their response to externally applied shear stresses (Chhabra & Richardson, 1999).

The term homogeneous also presents problems, because most slurries are not truly homogeneous as they contain two phases, namely the carrier fluid and the solid particles. Wilson, (1991) call slurries homogenous if there is a uniform spatial distribution and a uniform concentration of solids.

Most of these fine particle slurries are also not non-settling, but because they settle slowly they can be treated as homogenous non-settling slurries for the purpose of flow modelling (Shook & Roco, 1991).

2.3.1 Newtonian fluid behaviour

When a thin layer of fluid is contained between two parallel plates, a distance dy apart, as depicted in **Figure 2-1**, and a force, F, is applied to the plate; this force will be balanced by the opposite internal friction forces in the fluid. If the fluid is a Newtonian liquid and in laminar flow, the relationship between the total shear stress is equal to the product of the viscosity and the shear rate of the fluid.

The shear stress is equal to the force exerted on the fluid per unit area, and the shear rate is the change in velocity with respect to y, which is measured normal to the plane.

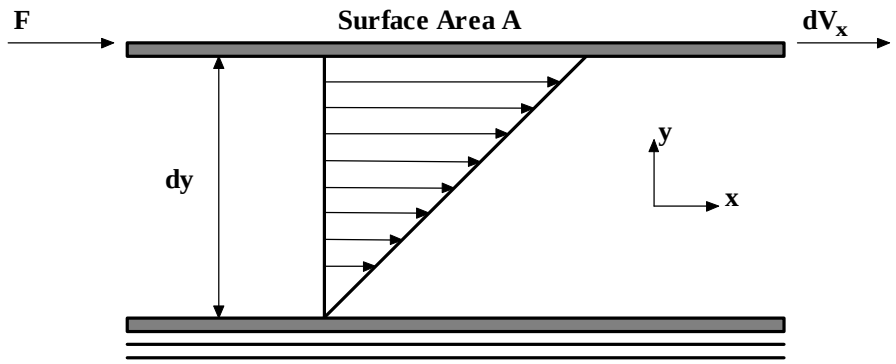

Figure 2-1 Schematic representation of one directional shearing flow

The relationship is mathematically formulated as follows: (Chhabra & Richardson, 1999).

$$\frac{F}{A} = \tau_{yx} = \mu\left(-\frac{dV_x}{dy}\right) = \mu\dot{\gamma}_{yx} \quad . \qquad 2.5$$

The first subscript in τ and $\dot{\gamma}$ indicate that the direction is normal to the shear force, and the second subscript refers to the direction of the fluid flow (Chhabra & Richardson, 2000).

Sir Isaac Newton was the first person to describe this relationship in 1687 (Barr, 1931). The constant of proportionality μ is called the coefficient of dynamic viscosity. A fluid is called a Newtonian fluid if it obeys the relationship between shear stress and shear rate as described in Equation 2.1. This relationship is linear and is only applicable to the laminar flow region.

The coefficient of dynamic viscosity is also called the Newtonian viscosity and is dependent on the material, temperature and pressure.

A plot of shear stress τ versus shear rate $\dot{\gamma}$ at constant temperature will be a straight line

and will pass through the origin. This graph is called a flow curve or a rheogram. The slope of this graph will be μ and this one term (the Newtonian viscosity) will describe the fluid flow behaviour fully.

The Newtonian relationship is depicted Figure 2-2.

2.3.2 Non-Newtonian fluid behaviour

If the relationship between shear stress τ, and shear rate $\dot{\gamma}$, at constant temperature, is not linear, then the material is called a non-Newtonian fluid. This refers also to relationships where the line does not go through the origin. As one can imagine, there are an infinite number of such relationships that make the rheological classification of fluids and slurries very difficult.

Some of these relationships are depicted in **Figure 2-2** (Chhabra & Richardson, 1999). It must be noted that the flow behaviour depicted is only for time-independent fluids; that means that the fluid behaviour does not change with time.

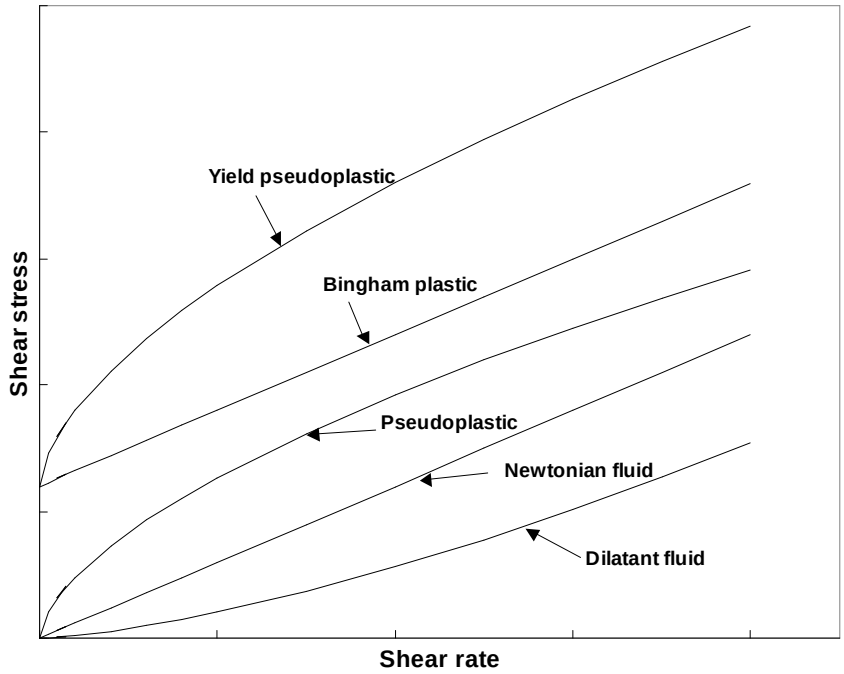

Figure 2-2 Rheological models

2.3.3 Non-Newtonian models

The models used to rheologically classify the slurries used in this thesis are the pseudoplastic, Bingham and yield-pseudoplastic models.

2.3.3.1 Pseudoplastic or shear-thinning model

These fluids are characterised by an apparent viscosity which decreases with an increase of shear rate. This means that the gradient of the graph becomes smaller as the shear rate increases. The equation for this behaviour is as follows:

$$\tau_0 = K\dot{\gamma}^n . \qquad 2.6$$

The two parameters K and n are empirical curve fitting parameters where n is the fluid consistency index and K the flow behaviour index.

If n < 1, the fluid exhibits shear-thinning behaviour.

If n > 1, the fluid exhibits shear-thickening or dilatant behaviour.

If n = 1, the equation reverts back to the Newtonian equation with K= μ

(Chhabra & Richardson, 1999).

The CMC tested in the open channels behaved like a pseudoplastic shear-thinning fluid.

2.3.3.2 Viscoplastic flow behaviour

The following two models describe fluids with a yield stress τ_y. This means that the fluid will not flow before the internal yield stress has been overcome by the externally applied stresses. Hyper-concentrated mud and kaolin suspensions exhibit such behaviour. The Yellow River in China is a classical example of a fluid with such behaviour. When the hyper-concentrated mud concentration is high, due to severe siltation and erosion, and the discharge decreases, the yield stress increases and the whole river stops flowing for short periods (Wan & Wang, 1994).

There is an on-going debate about whether a yield stress is real or not (Barnes & Walters, 1985). The hypothesis is that if the shear rate measured is low enough, there will be no yield stress. For engineering design, the yield stress is a reality for certain fluids and has to be dealt with.

2.3.3.3 Bingham plastic model

The simplest way to describe a fluid with a yield stress is with the Bingham model.

The equation is as follows:

$$\tau_0 = \tau_y + K\dot{\gamma} \quad . \qquad 2.7$$

The equation is linear and the shear stress intercept is the yield stress (Chhabra & Richardson, 1999). This is a simple two-parameter equation and has been used extensively to characterise hyper-concentrated mud (Wan & Wang, 1994).

The bentonite used in the flume tests was characterised as a Bingham fluid.

2.3.3.4 Herschel-Bulkley or yield-pseudoplastic model

If a Bingham fluid exhibits a non-linear relationship, then the yield pseudoplastic three constant model can be used. The flow curve can be described as follows:

$$\tau_0 = \tau_y + K\dot{\gamma}^n . \qquad 2.8$$

This equation is mathematically more complex than the others but it adequately describes kaolin suspensions (Slatter, 1986; Slatter, 1994). This model was also used to characterise the kaolin suspensions used in the flume tests conducted in this thesis.

It will be noted that the yield pseudoplastic model can be easily modified to describe the previously mentioned models.

If $\tau_y = 0$, the equation reverts to the pseudoplastic equation.

If $n = 1$, the equation becomes the Bingham equation.

If $n = 1$, and $\tau_y = 0$, the equation describes the Newtonian flow equation.

2.3.3.5 The yield stress debate

Barnes (1999) has presented an excellent synopsis of the so-called yield stress debate which has been going on for a long time. This is a follow-up of another paper which resulted in an extended debate (Barnes and Walters 1985).

The advent of low shear rate rotary viscometers has clearly shown that at very low shear rates, less than 10^{-4} s^{-1}, non-Newtonian fluids display a Newtonian viscosity, discounting the validity of a true yield stress. Barnes (1999) proceeds to show that in no fewer than seventeen highly diverse cases, the Cross model provides adequate prediction over a very large shear rate range. One of these cases is a bentonite slurry.

Malkin, Masalova, Pavlovski and Slatter (2003) show that the Cross model can also adequately fit an 8% kaolin slurry.

Both bentonite and kaolin slurries are used for testing purposes in this thesis.

For pipe and open channel flow we are more interested in the intermediate shear rate range between 1-1000 s^{-1}, where models such as the Herschel-Bulkley, Bingham and power law are just as competent as the Cross model (Chhabra & Richardson, 1999).

While on the one hand there is clearly great practical benefit to using simpler 2 and 3 parameter models for engineering purposes, it is also prudent to bear in mind the bigger picture, and not attach too much significance to the 'rheological parameters' τ_y, K and n, which are in the extreme argument simply curve fitting constants.

2.3.4 Rheometry for non-Newtonian models

From what has been described in the previous section, it can be concluded that it is not easy to characterise non-Newtonian fluids rheologically. One problem is that when one tries to measure the shear rate, it should be constant throughout the measuring system

employed. When using a rotary viscometer, the shearing gap of the cone and plate and cup and bob systems are generally small to try to overcome this problem, but when dealing with suspensions, the size of the particles often prohibits the use of narrow gaps (Chhabra & Richardson, 1999).

Rheometry or viscometry deals with the establishment of a relationship between shear stress and shear rate to establish the rheological parameters used in the relevant rheological model for the specific fluid or suspension. The rheological parameters are τ_y, K and n. To establish these parameters, tube, capillary or rotational viscometers are used.

2.3.4.1 Rotary viscometry

Rotational viscometers of various configurations are used to rheologically characterise the flow behaviour of non-Newtonian fluids.

The main types are controlled shear rate and controlled shear stress instruments. Both these types can be fitted with various types of measuring geometries such as parallel plate, cone and plate, and concentric cylinder systems (Chhabra & Richardson, 1999). In all these systems the torque applied to the rotation is related to the shear stress and the speed of rotation is related to the shear rate. Some of the measuring systems are depicted in **Figure 2-3** below.

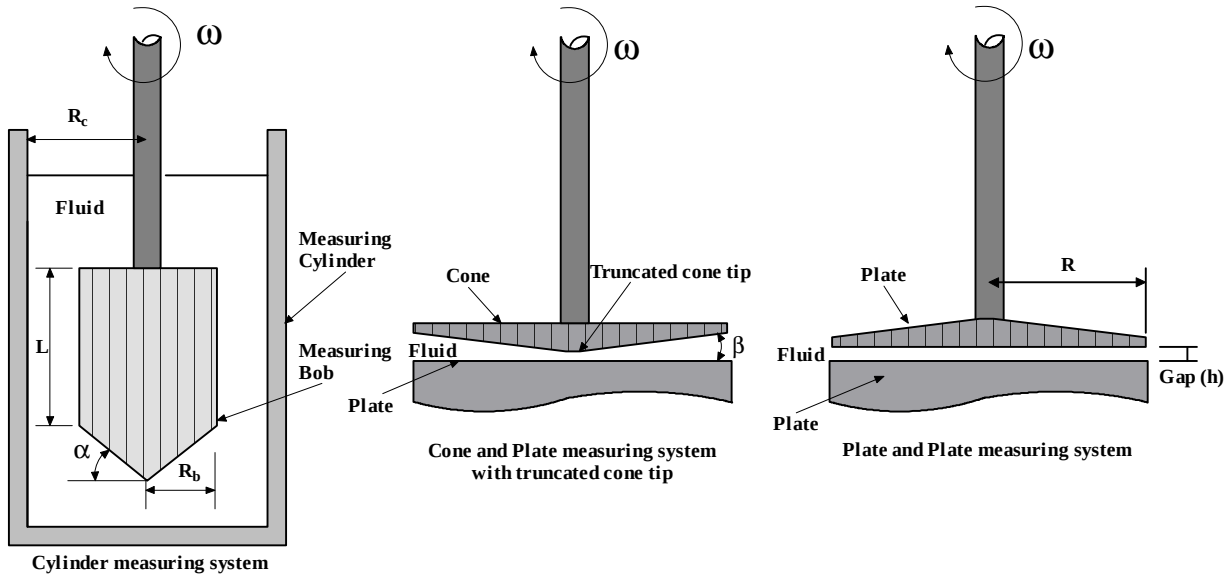

Figure 2-3 Rotational viscometer measuring systems

- Concentric Cylinder measuring system

There are a variety of concentric cylinder measuring systems of which the one depicted above in **Figure 2-3** is only one type. This system has a truncated cone at the lower end to minimise end effects (Metzger, 1998).

The shear stress and shear rate in the shearing gap are only valid for very thin gaps. Most suppliers of systems make assumptions when calculating the shear stress and shear rates.

For the Cylinder measuring system, the representative shear stress (τ) and the shear rate ($\dot{\gamma}$) is as follows according to Metzger (1998):

$$\tau = \frac{\delta^2}{2\delta^2} \frac{T}{2\pi L \left(R_b\right)^2 c_L} \quad \text{and} \quad \dot{\gamma} = \omega \frac{\left(\delta^2\right)}{\left(\delta^2 - 1\right)} \qquad 2.9$$

where $\delta = \frac{R_c}{R_b}$, and c_L = the resistance coefficient for the frontal area correction. This is found empirically.

Some of the errors arrive from end effects, wall slip, secondary flows, viscous heating and misalignment of the geometry (Macosko, 1994).

- Cone and Plate configuration

The main advantage of this configuration, where the cone angle is small and generally less than four degrees, is that the shear rate is constant across the shearing gap. A disadvantage is that this small angle can also produce large errors because of misalignment and eccentricities (Chhabra and Richardson, 1999).

The truncation is generally very small, therefore this configuration is not suitable for fluids with particles, as they will be trapped in the gap and cause errors (Metzger, 1998).

For the cone and plate configuration, the shear stress (τ) in the gap of the cone and the shear rate ($\dot{\gamma}$) is as follows according to Metzger (1998):

$$\tau = \frac{3T}{2\pi R^3} \quad \text{and} \quad \dot{\gamma} = \frac{\omega}{\beta}. \qquad 2.10$$

- Parallel plate measuring system

The upper plate in this configuration rotates while the lower plate is fixed. The shear rate is not constant but varies from the centre to the edge of the plate.

This configuration is more suitable for measuring fluids with particles as the gap can be adjusted and should be at least five times the diameter of the largest particles according to Metzger, (1998).

For the plate and plate measuring system, the shear stress stress (τ) in the gap between the plates and the shear rate ($\dot{\gamma}$) can be calculated as follows according to Metzger (1998):

$$\tau = \frac{2T}{\pi R^3} \quad \text{and} \quad \dot{\gamma} = \frac{\omega R}{h}. \qquad 2.11$$

The equations that are presented above are used by manufacturers of rheometers in their software, together with compensation for some of the errors listed above.

2.3.4.2 Tube viscometry

Although there are advantages in using rotational viscometers, certain authors prefer tube viscometers for non-Newtonian slurries (Wilson *et al.*, 1996; Slatter, 1994). In the rotary viscometer, lower shear rates can be obtained, but the tube viscometer, on the other hand, is a miniature pipeline and therefore has the advantage of being geometrically similar.

The ideal tube viscometer consists of a fluid flowing in steady laminar flow at constant temperature and with a pressure drop Δp due to laminar friction between its ends.

The relationship between the wall shear stress τ_0 and the volumetric flow rate Q and the shear stress τ is as follows:

$$\frac{Q}{\pi R^3} = \frac{1}{\tau_0^3}\int_0^{\tau_0} \tau^2 f(\tau) d\tau \qquad 2.12$$

$\tau_0 = \frac{R}{2}\left(-\frac{\Delta p}{L}\right)$ and $\left(-\frac{\Delta p}{L}\right)$ is equal to the pressure drop per unit length of tube.

The shear stress at any radius r is:

$$\tau = \frac{r}{2}\left(-\frac{\Delta p}{L}\right). \qquad 2.13$$

A plot of $\frac{Q}{\pi R^3}$ vs τ_0 will give a unique line for a given material for all values of R and $\left(-\frac{\Delta p}{L}\right)$ (Chhabra & Richardson, 1999).

The problem with tube viscometry is that 8V/D is not true shear rate but the wall shear rate for a Newtonian fluid, therefore the pseudo shear rate has to be transformed to the true shear rate, ($\dot{\gamma}$).

For a flow curve where the form is unknown Equation 2.12, after some manipulation, will yield the following according to Chhabra & Richardson, (1999):

$$\left(-\frac{du}{dr}\right)_0 = \frac{8V}{D}\left(\frac{3}{4} + \frac{1}{4}\frac{d\log(8V/D)}{d\log\tau_0}\right). \qquad 2.14$$

Various forms of this equation exist, one being the Rabinowitsch-Mooney Equation:

$$\dot{\gamma}_0 = \left(-\frac{du}{dr}\right)_0 = \frac{8V}{D}\left(\frac{3n'+1}{4n'}\right) \qquad 2.15$$

where

$$n' = \frac{d(\log\tau_0)}{d\left(\log\left(8V/D\right)\right)}. \qquad 2.16$$

If one plots a log-log pseudo shear diagram with τ_o versus 8V/D for the laminar flow region, then n′ is the slope of the tangent of the graph. The slope will only be approximately constant if the fluid is a power-law fluid (Chhabra & Richardson, 1999).

The Rabinowitsch-Mooney transformation procedure for pipe data can be summarised as follows:

- Plot the laminar flow data $\log\frac{D\Delta P}{4L}$ vs $\log\frac{8V}{D}$ obtained from a tube viscometer. Different diameter tubes will coincide in the laminar region, whereas the turbulent data will not.
- Fit a mathematical function to the laminar flow data and obtain the first derivative of the equation. This will be the equation for n′.
- Calculate $\dot{\gamma}_0$ using Equation 2.14.
- Plot τ_o versus $\dot{\gamma}_0$ on arithmetic or logarithmic co-ordinates.
- Fit the appropriate equation to suit the data (for example, the yield-pseudoplastic, power-law or Bingham plastic model).
- From these equations the rheological parameters τ_y, K and n can be obtained.

2.3.4.3 The Lazarus and Slatter approach to rheological classification of tube viscometer data

The following approach was developed by Lazarus and Slatter (1988).

Later in this chapter it will be shown how Equation 2.17 was developed (see Section 2.6.1).

$$\frac{32Q}{\pi D^3}=\frac{8V}{D}=\frac{4n}{K^{\frac{1}{n}}\tau_0}\left(\tau_0-\tau_y\right)^{\frac{1+n}{n}}\left(\frac{\left(\tau_0-\tau_y\right)^2}{1+3n}+\frac{2\tau_y\left(\tau_0-\tau_y\right)}{1+2n}+\frac{\tau_y{}^2}{1+n}\right). \qquad 2.17$$

Equation 2.16 can be used to rheologically classify a fluid. The process is as follows:

- Plot the laminar flow data $\frac{D\Delta P}{4L}$ vs $\frac{8V}{D}$ of N data points obtained from a tube viscometer. Different diameter tubes will coincide in the laminar region, whereas the turbulent data will not.
- Calculate the values $\frac{8V}{D}_{calc}$ of the N data points using Equation 2.18 and assuming values for τ_y, K and n.
- These values for τ_y,K and n must now be optimised by minimising the sum of the mean error square of the N data points.

$$E = \sum_{i=1}^{N} \left(\frac{\frac{8V}{D_{i\ obs}} - \frac{8V}{D_{i\ calc.}}}{\frac{8V}{D_{i\ obs}}} \right)^2 . \qquad 2.18$$

For a yield-pseudoplastic fluid, τ_y, K and n will be optimised, for a Bingham fluid, n will become 1, and for a pseudoplastic fluid, τ_y will become 0.

2.3.4.4 The Tikhonov regularisation method to transform tube viscometer data

Nguyen, Vu, Wong, and Yeow (1999) describe how Tikhonov regularisation can be applied to solve the inverse problem of capillary viscometry.

The problem with tube or capillary viscometers is that the flow data is presented on a pseudo shear diagram and the pseudo shear rate needs then to be transformed to true shear rate. This can be done by using the Rabinowitsch-Mooney transformation method. The problem is that the method depends on the accuracy of the differentiation of the log-log plot of τ_y against 8V/D. It is unavoidable that there will be experimental noise in

the data. The numerical value of the derivative can therefore be very sensitive to the way the differentiation is performed.

The Tikhonov regularisation, used by Nguyen *et al.* (1999) does not use direct differentiation of experimental data. They show that this method can accurately process tube data and is accurate even at low shear rates where the experimental noise is normally the most problematic.

2.3.4.5 Errors in tube viscometry

- **Wall slip**

Chhabra and Richardson (1999) warn that serious errors can occur when wall slip is not accounted for. Wall slip occurs when the layer of particles near the wall are more dilute than the bulk flow. As a result the viscosity near the wall will be reduced and apparent slip will occur.

It is important that more than one diameter tube is used. If three diameter tubes are used, the laminar flow regions of the three data sets will coincide if there is no wall slip. If they do not coincide, then the slip velocity must be calculated for each tube and deducted from the measured mean velocity.

- **Entrance and exit losses**

It is important that the entrance and exit losses in the tubes that are used be minimised. To do this one needs to make sure that the flow is developed fully before differential pressure readings are taken. Slatter (1994), uses 50 pipe diameters unobstructed flow

before and after the test sections. He relates this to previous studies by Govier and Aziz (1972) and Hanks (1981).

2.4 NEWTONIAN PIPE FLOW

2.4.1 Laminar flow of Newtonian fluids in circular tubes

Consider steady laminar flow of a Newtonian liquid in a circular tube of radius R as depicted in Figure 2-4 below. The force balance on the fluid element, which is at a distance r from the centre line, can be written as:

$$p\left(\pi r^2\right) - \left(p + \Delta p\right)\pi r^2 = \tau_{rz}\, 2\pi r L \qquad 2.19$$

$$\tau_{rz} = \left(\frac{\Delta p}{L}\right)\frac{r}{2}. \qquad 2.20$$

Figure 2-4 is applicable both in laminar and turbulent flow (Chhabra & Richardson, 1999).

The shear stress at the wall at radius R is:

$$\tau_0 = \frac{D\Delta p}{4L}. \qquad 2.21$$

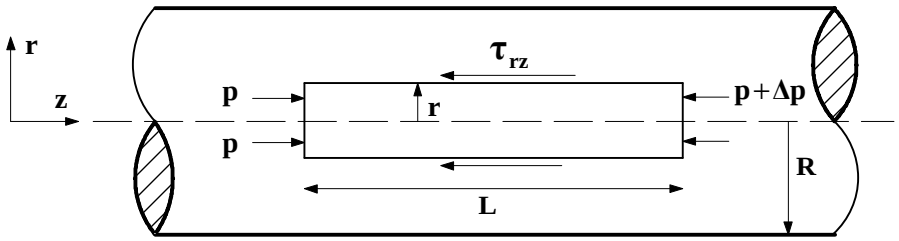

Figure 2-4. Force balance in pipe

Figure 2-5 depicts a representation of the shear stress and velocity distribution in laminar flow in a pipe.

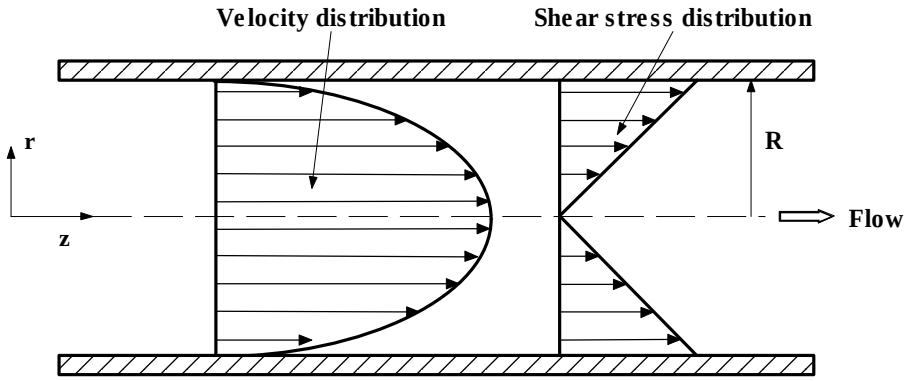

Figure 2-5. Pipe section showing velocity and shear stress distribution. (Chhabra & Richardson, 1999)

It can be seen that the shear stress is a maximum at the wall and zero in the middle of the pipe. The velocity distribution is parabolic and therefore a maximum in the middle of the pipe and zero at the wall.

2.4.1.1 Relationship between shear stress, shear rate and viscosity.

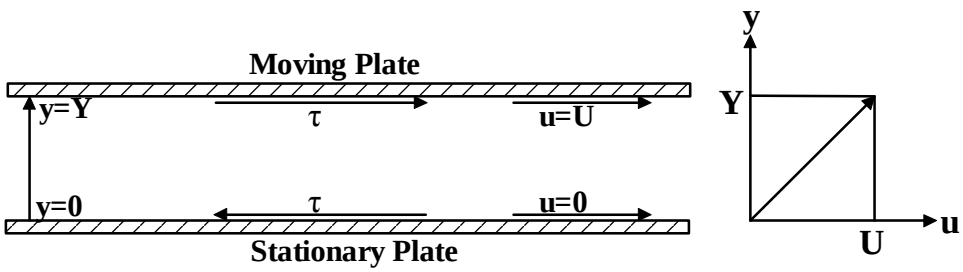

Figure 2-6. Relationship between shear stress and shear rate between two plates

Viscosity is the measure of the resistance of the fluid to deformation by shearing.

In **Figure 2-6** above two plates are parallel with fluid in between. The bottom plate is stationary and the top plate is moved to right with a steady velocity U. No-slip occurs at the plate faces. At y=0, u=0 and at y=Y, the velocity is U. At any intermediate position u=U/Y. The velocity gradient is du/dy. This represents the rate of shear deformation of the fluid, or shear rate.

To keep the plate moving at a steady rate, a force has to be applied to the plate. The force per unit area is the shear stress τ. The shear stress in the fluid at any plane parallel to the plate is also τ.

For a simple fluid like water, the relationship between shear stress and shear rate is linear and the slope is μ (viscosity).

Sir Isaac Newton was the first to describe the relationship as shown below:

$$\tau = \mu\left(-\frac{du}{dy}\right). \qquad 2.1$$

(The negative sign indicates that τ is a measure of the resistance to motion.) (Chhabra & Richardson, 1999).

2.4.1.2 Relationship between pipe flow, shear stress, viscosity and pipe diameter.

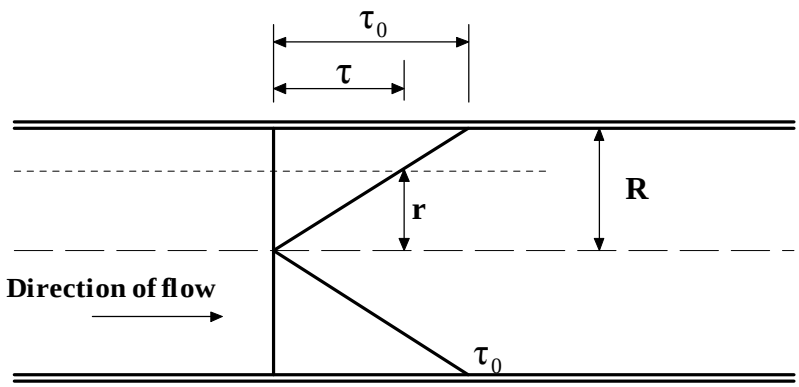

Figure 2-7 Shear stress in a pipe

The flow in the pipe is a function of the wall shear stress, viscosity and diameter

$Q = \text{function of } (\tau_0, \mu, D)$.

The shear stress at a distance r from the centreline of the pipe is:

$$\tau_r = r\frac{\tau_0}{R}. \qquad 2.22$$

Integrating over the pipe radius

$$V = \frac{\tau_0 D}{8\mu}. \qquad 2.23$$

From this the relationship between the wall shear stress and 8V/D is derived:

$$\tau_0 = \mu \frac{8V}{D}. \qquad 2.24$$

The Reynolds number for pipe-flow is defined as follows:

$$Re = \frac{\rho V D}{\mu}. \qquad 2.25$$

The Fanning friction factor is defined as follows:

$$f = \frac{\tau_0}{0.5\rho V^2}. \qquad 2.26$$

Substituting Equation 2.26 in Equation 2.24 is as follows:

$$\frac{2}{\rho V^2}\tau_0 = \mu \frac{8V}{D}\frac{2}{\rho V^2}. \qquad 2.27$$

The relationship between friction factor and Reynolds number in laminar flow for a Newtonian fluid is therefore:

$$f = \frac{16}{Re}. \qquad 2.28$$

This relationship, if plotted on the Moody diagram where the Fanning friction factor is plotted against the Reynolds number on a log-log plot is a straight line of slope –1. It will be convenient to define the open channel friction factor the same way so that the friction factor:Reynolds number relationship will be presented the same way on the Moody diagram (Douglas, Gasiorek & Swaffield, 1985).

2.4.2 Turbulent flow of Newtonian fluids in circular tubes.

There are a number of turbulence models for pipe flow available. The most well known are the following:

2.4.2.1 The Blasius equation

Blasius proposed this empirical relationship between friction factor and Reynolds number for smooth pipes in 1913, and defined it as follows: (Douglas *et al*, 1985):

$$f = \frac{0.079}{\mathrm{Re}^{0.25}}. \qquad 2.29$$

This relationship is works well up to a Reynolds number of 100 000 (Streeter, 1971).

2.4.2.2 Colebrook-White

Prandtl and Nikuradze tested artificially roughened pipes and established a relationship between the friction factor and a roughness ratio, which they defined as k/D. They subdivided turbulent flow into three regions and formulated each region separately (Featherstone & Nalluri, 1995).

In 1939, Colebrook and White combined the equations in the following form: (Featherstone & Nalluri, 1995).

$$\frac{1}{\sqrt{4f}} = -2\log\left(\frac{\mathrm{k}}{3.7\mathrm{D}} + \frac{2.51}{\mathrm{Re}\sqrt{4f}}\right). \qquad 2.30$$

This equation can be transposed to yield a pipe flow equation in terms of the velocity (Featherstone & Nalluri, 1995):

$$V = -2\sqrt{2g\,D\sin\alpha}\,\log\left(\frac{k}{3{,}7D} + \frac{2{,}51\mu}{D\sqrt{2g\,D\sin\alpha}}\right). \qquad 2.31$$

2.4.3 Laminar turbulent transition of Newtonian fluids in circular tubes

The end of the laminar flow regime in pipes is shown to be at a Reynolds number of approximately 2 100 on the Moody chart (Douglas *et al.*, 1985). The transition region, however, occurs over a region of Reynolds numbers varying from 2 000 to several thousand (Featherstone & Nalluri, 1995).

2.5 NEWTONIAN OPEN CHANNEL FLOW

2.5.1 Newtonian laminar flow in open channels

Laminar flow of Newtonian liquids in open channels has been well recorded in many textbooks and none is more famous than that of Chow (1959).

2.5.1.1 Relationship between friction factor and Reynolds number (wide channel)

The following derivation is for smooth open channel flow for a wide channel.

By writing the momentum equation over a small control volume,

$$\tau_{yx} = \rho g(h - y)\sin\alpha\,. \qquad 2.32$$

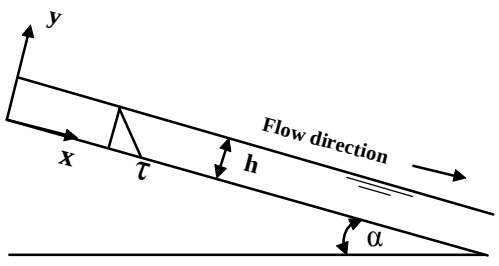

Figure 2-8 Flow down an inclined slope

Since du_x/dy is positive here, one can write:

$$\tau_{yx} = \mu \frac{du_x}{dy} \therefore \frac{du_x}{dy} = \left(\frac{\rho g \sin\alpha}{\mu} \right)(h - y) \qquad 2.33$$

Integration w.r.t y yields:

$$u_x = \frac{\rho g \sin\alpha}{\mu}\left(hy - \frac{y^2}{2} \right) + C \qquad 2.34$$

where C is evaluated by applying the boundary condition at y = 0, $u_x = 0$ C = 0

$$\therefore u_x = \frac{\rho g \sin\alpha}{\mu}\left(hy - \frac{y^2}{2} \right). \qquad 2.35$$

The volumetric flow rate per unit width is:

$$\frac{Q}{B} = \int_0^h u_x dy = \frac{\rho g \sin\alpha}{\mu} \int_0^h \left(hy - \frac{y^2}{2} \right) dy \qquad 2.36$$

$$= \frac{\rho g \sin\alpha}{\mu}\left(\frac{hy^2}{2} - \frac{y^3}{6} \right)_0^h = \frac{\rho g \sin\alpha}{\mu}\left(\frac{h^3}{2} - \frac{h^3}{6} \right) = \frac{\rho g \sin\alpha}{3\mu} h^3 \qquad 2.37$$

The average velocity is:

$$V = \frac{Q}{Bh} = \frac{\rho g \sin\alpha}{3\mu} h^2 . \qquad 2.38$$

For this geometry,

$$R_h = \frac{A}{P} = \frac{Bh}{B} = h \qquad 2.39$$

$$\therefore V = \frac{\rho g \sin\alpha R_h^2}{3\mu} \Rightarrow R_h g \sin\alpha = \frac{3V\mu}{\rho R_h} . \qquad 2.40$$

By definition,

$$f = \frac{8 R_h g h_f}{L V^2} \text{ , but } \frac{h_f}{L} = \sin\alpha \qquad 2.41$$

$$\therefore f = \frac{8 R_h g \sin\theta}{V^2} = \frac{3V\mu}{\rho R_h}\frac{8}{V^2} = \frac{24}{Re} \text{ (wide channels)} \qquad 2.42$$

and setting

$$\mathrm{Re} = \frac{\rho V R_h}{\mu} \therefore f = \frac{K}{\mathrm{Re}} \ , \qquad 2.43$$

where K depends on the shape of the open channel. For a rectangular channel K is 16 (Kozicki & Tiu, 1967).

The Reynolds number and friction factor in laminar flow for a Newtonian fluid is similar to pipe flow and can be similarly plotted on the standard Moody diagram. This is done by substituting D_e with $D_e = 4R_h$.

For a rectangular channel the fanning friction factor is as follows:

$$f = \frac{gD_e \sin\theta}{2V^2} \text{ (for pipe flow)} \qquad 2.44$$

$$f = \frac{g4R_h \sin\theta}{2V^2} = \frac{g2R_h \sin\theta}{V^2} \qquad 2.45$$

The Reynolds number is as follows:

$$\mathrm{Re} = \frac{\rho V D_e}{\mu} = \frac{\rho V 4R_h}{\mu} \qquad 2.46$$

2.5.1.2 The effect of shape

The oldest reference to the effect of shape that could be found was by Straub, Silberman and Nelson (1956). They studied Newtonian open channel flow at low Reynolds numbers and derived values for K for several open channel shapes. The values they produced for rectangular flumes ranged between 15/Re and 20/Re. They show that the value of K varies with the change of the ratio of width over breadth of the flume.

The relationship they developed for K is as follows:

$$K = \frac{24}{\left(1+\frac{h}{0.5B}\right)^2}\frac{1}{\left(1-\frac{192}{\pi^5}\frac{h}{0.5B}\sum_{n=0}^{\infty}\left(\frac{1}{(2n+1)^5}\tanh\left(\left(\frac{2n+1}{2}\right)\left(\frac{\pi\,0{,}5B}{h}\right)\right)\right)\right)} \quad 2.47$$

Kozicki and Tiu (1967) used this relationship to develop geometric coefficients a and b which are characteristic for a particular cross-section. The Reynolds numbers that they propose for non-Newtonian flume flow incorporate these coefficients. This will be discussed later in this chapter.

2.5.1.3 Wall shear stress for rectangular channels

Sanders, Schaan, Gillies, McKibben, Sun & Shook (2002) did work on solids transport in laminar flow of non-Newtonian slurries in a half-round flume. They calculated the average wall shear stress from the momentum equation if the flow is not uniform as follows:

The rectangular flume shown in **Figure 2-9** below is tilted at α degrees to the horizontal. The mass flow rate is w kg/s, the average wetted perimeter is $P_{m.}$ It can be seen from **Figure 2-9** that the conditions at 1 and 2 may not necessarily be the same.

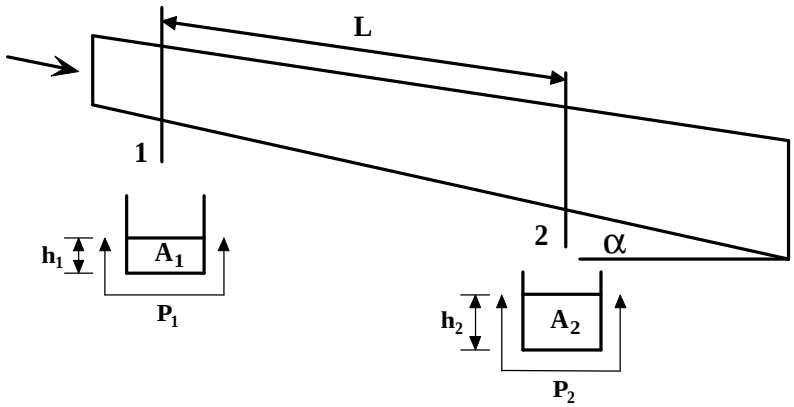

Figure 2-9 Rectangular flume depicting non-uniform flow

A momentum balance for the element bounded by planes 1 and 2 in **Figure 2-9** is written as:

$$\tau_0 L P_m = A_m \rho g L \sin\alpha + p_1 A_1 - p_2 A_2 + w(V_1 - V_2) \qquad 2.48$$

where $w = \rho A_1 V_1 = \rho A_2 V_2$.

Equation 2.48 can be re-arranged to yield:

$$\tau_0 = \left(\frac{A}{P}\right)_m \rho g L \sin\alpha + \frac{p_1 A_1 - p_2 A_2}{P_m L} + \rho \frac{A_1 V_1^{\,2} - A_2 V_2^{\,2}}{P_m L} \qquad 2.49$$

Equation 2.49 describes the mean wall shear stress that occurs between planes 1 and 2. If, however, the conditions at 1 and 2 are the same, the wall shear stress reduces to:

$$\tau_0 = \rho g R_h \sin\alpha . \qquad 2.50$$

This shear stress formula is intended to take into account the shear stress distribution around the boundary of the rectangular flume. For the wide channel, the hydraulic radius R_h is replaced by the flow depth h.

2.5.2 Turbulent flow of Newtonian fluids in open channels

There are a number of Newtonian open channel models, some of which have been adapted from pipe flow by substituting the diameter with hydraulic radius.

2.5.2.1 The Blasius Equation for flume flow

Blasius formulated the relationship between friction factor and Reynolds number for smooth pipes. When the diameter is substituted by the hydraulic radius in the definition of the Reynolds number, the pipe flow formula can be used for open channel flow (Chow, 1959):

$$f = \frac{0.079}{\mathrm{Re}^{0.25}}. \qquad 2.51$$

The Blasius formula is applicable for Reynolds numbers from transition to 10^6.

2.5.2.2 Chezy Equation for flume flow

The Chezy equation was introduced in 1768 by Chezy, who designed a water supply for Paris. The formula applies to turbulent flow.

The Chezy equation is defined as follows by (Chanson, 1999):

$$V = C_{Chezy}\sqrt{R_h \sin\alpha}. \qquad 2.52$$

The Chezy constant C was originally thought to be a constant, but research has shown that it is not, and there are a number of formulae available to calculate the value of C_{Chezy}. One of them is the Bazin formula that is defined as follows (Chow, 1959):

$$C_{Chezy} = \frac{157.6}{1 + \frac{m_{Bazin}}{\sqrt{R_h}}}. \qquad 2.53$$

The values of the Bazin constant vary from 0.11 for smooth cement to 3.17 for a rough earth channel.

2.5.2.3 Manning Equation for flume flow

The Manning equation was derived from the Chezy equation and is defined as follows by Chanson (1999):

$$V = \frac{1}{n_{Manning}}\left(R_h\right)^{\frac{2}{3}}\sqrt{\sin\alpha}. \qquad 2.54$$

The Manning n value ranges typically from 0.01 for glass to 0.030 for gravel (Chanson, 1999).

This formula applies to fully turbulent flow and has most probably been the most widely used open channel formula.

2.5.2.4 Colebrook-White equation for flume flow

The Colebrook-White equation for pipe flow as described in paragraph 2.4.2.2 can be transposed to open channel flow by substituting the diameter with the hydraulic diameter which is four times the hydraulic radius. The formula is then as follows (Chanson, 1999):

$$\frac{1}{\sqrt{4f}} = -2\log\left(\frac{k}{14{,}84R_h} + \frac{2.51}{Re\sqrt{4f}}\right). \qquad 2.55$$

The k-value is the equivalent roughness height.

The formula is valid for turbulent flow in rough and smooth channels.

The Colebrook-White equation can also be expressed in terms of viscosity and velocity as follows (Featherstone & Nalluri, 1995):

$$\frac{1}{\sqrt{4f}} = -2\log\left(\frac{k}{14{,}84R_h} + \frac{2.51\mu}{4R_h\rho V\sqrt{4f}}\right). \qquad 2.56$$

This can be transformed to an explicit equation in terms of the velocity to be:

$$V = \sqrt{32R_h \sin\alpha}\,\log\left(\frac{k}{14{,}84R_h} + \frac{1.255\mu}{R_h\rho\sqrt{32gR_h \sin\alpha}}\right). \qquad 2.57$$

The Colebrook-White equation is cited as it was used to calculate the flume roughness, and is regarded as one of the more sophisticated approaches to open channel design (Wallingford & Barr, 1994).

2.5.3 Laminar-turbulent transition of Newtonian fluids in open channels

As for pipe flow, the laminar turbulent transition does not occur at one point but over a range of Reynolds numbers. Straub *et al.* (1958), concluded that the transition Reynolds number depended somewhat on the shape of the flume and ranged from 2 000 to 3 000. They also suggested that this is slightly higher than for closed conduit flow.

On the Moody diagram published by Chanson (1999), the transition range is shown between a Reynolds number 2 000 and 4 000.

2.6 NON-NEWTONIAN PIPE FLOW

2.6.1 Non-Newtonian laminar pipe flow

Govier & Aziz (1972) developed the following laminar pipe flow equation for Herschel-Bulkley fluids.

The velocity gradient across the pipe is presented as follows:

$$-\frac{du}{dr}=\left(\frac{1}{K}\right)^{\frac{1}{n}}\left(\frac{r}{2}\frac{\Delta p}{L}-\tau_y\right)^{\frac{1}{n}}. \qquad 2.58$$

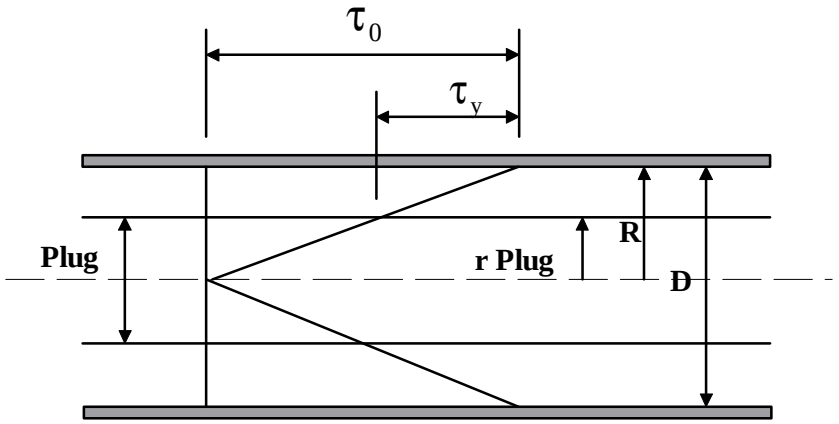

Figure 2-10 Shear stress distribution in a pipe

For the case when the shear stress is less than the yield stress, $\tau = r\Delta p/2L \le \tau_y$ and when

$r \le r_{plug}$, the fluid does not shear and $r_{plug} = \frac{R\tau_y}{\tau_0}$. 2.59

This is depicted in **Figure 2-10**.

For a yield stress fluid:

$$u = \frac{\left(\frac{1}{K}\right)^{\frac{1}{n}}}{\left(\frac{\Delta p}{2L}\right)} \frac{n}{n+1}\left(\left(\tau_0 - \tau_y\right)^{\frac{n+1}{n}} - \left(\tau - \tau_y\right)^{\frac{n}{n+1}} \right) \qquad 2.60$$

$$Q = \left(2\pi \int_{r_{plug}}^{R} u\, r\, dr \right) + \left(\pi r_{plug}^2\, u_{plug} \right). \qquad 2.61$$

This can be integrated to obtain the flow and the average velocity.

$$\frac{32Q}{\pi D^3} = \frac{8V}{D} = \frac{4n}{K^{\frac{1}{n}}\left(\tau_0\right)^3} \left(\tau_0 - \tau_y\right)^{\frac{1+n}{n}} \left(\frac{\left(\tau_0 - \tau_y\right)^2}{1+3n} + \frac{2\tau_y\left(\tau_0 - \tau_y\right)}{1+2n} + \frac{\tau_y{}^2}{1+n} \right). \qquad 2.16$$

This formula can be used to obtain the flow rate and velocity for a specific wall shear stress if the rheological parameters τ_y, K and n are known.

2.6.2 Non-Newtonian turbulent pipe flow

In turbulent flow there are several models available that have been developed over many years. As this is such a difficult flow regime to predict and as most of these models are empirical, they may vary considerably depending on what fluid and concentration is used. Only a few well known models will be described.

2.6.2.1 The Torrance turbulence model

Torrance (1963) developed a turbulent flow model for non-Newtonian slurries in pipes. His model uses the Herschel-Bulkley or yield-pseudoplastic rheological model and is derived from the Newtonian turbulent model.

The Von Karman constant used in the formula is 0.36 n, which means it depends on the viscous characteristics of the fluid.

For smooth pipe flow the average turbulent velocity is derived as follows:

$$\frac{V}{V_*} = \frac{3.8}{n} + \frac{2.78}{n}\ln\left(1 - \frac{\tau_y}{\tau_0}\right) + \frac{2.78}{n}\ln\left(\frac{V_*^{2-n}\rho(R)^n}{K}\right) - 4.17\,. \qquad 2.62$$

This model does take the rheological parameters of the fluid into consideration.

2.6.2.2 The Slatter model

Slatter (1994) developed a new turbulence model that can be interpreted in terms of a particle roughness effect. The roughness Reynolds number formulated takes the complete rheology and the representative particle size of the solids into account. The representative particle size that he found to be the most representative was the d_{85}. This worked well for the slurries tested in his work.

The roughness Reynolds number is presented as follows:

$$Re_r = \frac{8\rho(V_*)^2}{\tau_y + K - \left(\frac{8V_*}{d_x}\right)^n}\,. \qquad 2.63$$

For smooth wall turbulent flow when $Re_r \leq 3.32$ the average velocity is:

$$V = V_* \left(2.5 \ln \left(\frac{R}{d_{85}} \right) + 2.5 \ln Re_r + 1.75 \right). \quad 2.64$$

For fully developed rough wall turbulent flow when $Re_r > 3.32$ the flow velocity is:

$$V = V_* \left(2.5 \ln \left(\frac{R}{d_{85}} \right) + 4.75 \right). \quad 2.65$$

The assumption made is that the transition from smooth wall to rough wall turbulent flow is abrupt. The model takes the rheological parameters into consideration in turbulence.

2.6.2.3 Wilson and Thomas model

Wilson and Thomas (1985), developed a model for turbulent pipe flow that predicts the thickening of the laminar sub-layer by an area ratio factor A_r. For a yield- pseudoplastic fluid the area ratio is as follows:

$$A_r = 2 \left(\frac{1 + \frac{\tau_y}{\tau_0} n}{1 + n} \right). \quad 2.66$$

The area ratio is graphically illustrated in **Figure 2-11**.

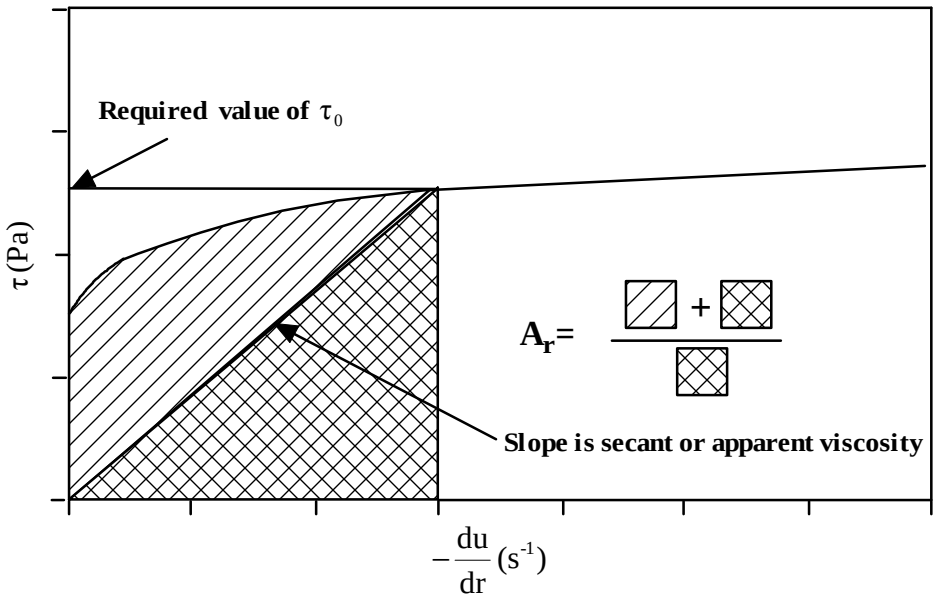

Figure 2-11 Area ratio and apparent viscosity – Wilson and Thomas model

The non- Newtonian sub-layer thickness is described as follows:

$$\delta_{NN} = A_r \delta_N \qquad 2.67$$

and the Newtonian sub-layer is:

$$\delta_N = \frac{11.6\mu}{\sqrt{\rho\tau_0}}. \qquad 2.68$$

For a specific wall shear stress the shear rate is:

$$\dot{\gamma}_0 = \left(\frac{\tau_0 - \tau_y}{K} \right)^{\frac{1}{n}}. \qquad 2.69$$

From this the Newtonian or secant viscosity can be calculated:

$$\mu_N = \frac{\tau_0}{\dot{\gamma}_0}. \qquad 2.70$$

The secant viscosity μ' is obtained from the yield-pseudoplastic rheogram.

The mean velocity according to Wilson and Thomas is then:

$$V = V_*\left(\frac{V_N}{V_*} + 11.6(A_r - 1) - 2.5\ln A_r - \Omega\right). \qquad 2.71$$

The Newtonian mean velocity V_N for pipe flow, derived from the logarithmic velocity distribution was derived by Schlichting (1960), and yields a mean velocity as shown below:

$$V_N = V_*\left(2.5\ln\left(\frac{\rho V_* R}{\mu}\right) + 1.75\right). \qquad 2.72$$

The value Ω is a term which takes into account the blunting of the velocity profile caused by the yield stress.

$$\Omega = -2.5\ln\left(1 - \frac{\tau_y}{\tau_0}\right) - 2.5\frac{\tau_y}{\tau_0}\left(1 + 0.5\frac{\tau_y}{\tau_0}\right) \qquad 2.73$$

This model can accommodate partially rough and rough wall turbulent flow to some extent if the appropriate roughness is used when calculating V_N (Slatter, 1994).

2.6.3 Non-Newtonian Transitional Pipe Flow

As for Newtonian pipe flow, the Reynolds number is used to predict the onset of transition. Because the non-Newtonian characteristics are complicated, various Reynolds numbers have been developed to account for these.

2.6.3.1 Newtonian Approximation

One approach is to use the apparent viscosity as suggested by Wilson (1986), and which is shown graphically in **Figure 2-11** and is defined as:

7 $$\mu_{app} = \frac{\tau_0}{\left(-\frac{du}{dr}\right)_0}\ . \qquad 2.74$$

The viscosity μ in the standard Reynolds number equation is just replaced by μ_{app}.

This is not so straightforward, as the value of μ_{app} has to be calculated for every value of τ_o.

Transition is then estimated to occur at Reynolds number 2 100.

2.6.3.2 The Hanks criteria

Chhabra and Richardson (1999) describe the Hanks criterion to predict transition pipe flow of Bingham fluids.

The critical Reynolds number is expressed in terms of the Hedström number.

$$Re_c = \frac{\rho VD}{K} = \frac{1 - \frac{4}{3}\phi + \frac{\phi^4}{3}}{8\phi} He \qquad 2.75$$

Where $\phi = \frac{\tau_y}{\tau_0}$ is defined as follows:

$$\frac{\phi}{(1-\phi)^3} = \frac{He}{16800}. \qquad 2.76$$

The Hedström number is defined as follows:

$$He = \frac{\rho D^2 \tau_y}{K^2}. \qquad 2.77$$

2.6.3.3 The Slatter and Lazarus Reynolds Number

Slatter and Lazarus (1993) show that the representative viscous stress across a pipe if the representative shear rate is 8V/D can be expressed for a yield-pseudoplastic fluid as:

$$\tau_{visc} = \tau_y + K\left(\frac{8V}{D}\right)^n, \qquad 2.78$$

which results in the viscous force being:

$$\text{Viscous force} \propto D^2\left(\tau_y + K\left(\frac{8V}{D}\right)^n\right). \quad 2.79$$

The pipe Reynolds number is:

$$Re_2 \propto \frac{\rho V^2}{\tau_y + K\left(\frac{8V}{D}\right)^n}. \quad 2.80$$

When the proportionality constant is taken as 8, the Reynolds number in Equation 2.80 reduces to the Newtonian Reynolds number under Newtonian conditions, which results in the final form of Re_2 in Equation 2.81.

$$Re_2 = \frac{8\rho V^2}{\tau_y + K\left(\frac{8V}{D}\right)^n}, \quad 2.81$$

2.6.3.4 Slatter and Wasp Approach

Slatter and Wasp (2000) present three correlations between Re_c and He for Bingham plastic pipe flow data.

The low He range Re_c=2 100 for He < 1.7 x 10^3.

For the intermediate He range $Re_c=155He^{0.35}$ for $1.7x10^3$ <He < 1.5 x 10^5.

For the high He range $Re_c=26He^{0.5}$ for He > 1.5 x 10^5.

This correlation was obtained by analysing a large pipe flow database, and it predicts the onset of transition reasonably well.

It is necessary to characterise the fluid as a Bingham plastic.

2.7 NON-NEWTONIAN OPEN CHANNEL FLOW

Some work has been done on laminar flow of non-Newtonian fluids in open channels. A few of the models will be discussed.

2.7.1 Work done by Kozicki and Tiu

Kozicki and Tiu (1967), published analytical work on the effect of shape in laminar flow on open channels. The study of the effect of shape is not part of this thesis but the relevance of their shape factor for rectangular shaped flumes is.

2.7.1.1 Shape Factors

Shape factors were defined by Straub *et al.* (1958) in their open channel investigation. Kozicki and Tiu (1967) built on this work and the shape factors a and b they propose are defined as follows:

$$a = 0.5\left(\frac{\lambda}{1+\lambda}\right)^2\left(1-\frac{32}{\pi^3}\sum_0^\infty\left(\frac{(-1)^n}{(2n+1)^3}\left(\frac{1}{\cosh\frac{(2n+1)}{2}\pi\lambda}\right)\right)\right)^{-1}, \qquad 2.82$$

with

$$\lambda = {}^{B}\!/_{h} \qquad 2.83$$

$$b = a(3\varphi - 1) \qquad 2.84$$

with

$$\varphi = \frac{\left(1 - \frac{32}{\pi^3}\sum_0^{\infty}\left(\frac{(-1)^n}{(2n+1)^3}\right)\left(\frac{1}{\cosh\left(\frac{(2n+1)}{2}\pi\lambda\right)}\right)\right)}{\left(1 - \frac{192}{\pi^5}\frac{1}{\lambda}\sum_0^{\infty}\left(\frac{1}{(2n+1)^5}\right)\tanh\left(\frac{(2n+1)}{2}\pi\lambda\right)\right)}. \qquad 2.85$$

It can be seen that the shape factors a and b are mathematically rather complex. As far as can be ascertained these formulae have not been tested against experimental data.

2.7.1.2 Kozicki and Tiu Reynolds number for pseudoplastic or power-law fluids

The Reynolds number that they propose for a power-law fluid in a rectangular flume is as follows:

$$Re = \frac{\rho V^{(2-n)} R_h^n}{2^{n-3} K\left(\frac{a+bn}{n}\right)^n}. \qquad 2.86$$

This Reynolds number includes the shape factors a and b which are to account for the variation in aspect ratio as the depth increases.

2.7.1.3 Kozicki and Tiu Reynolds number for Bingham fluids

For Bingham fluids, Kozicki and Tiu propose a different Reynolds number, which is as follows:

$$Re = \frac{4VR_h\rho}{K}\left[\frac{1}{a+b} - \frac{1}{b}\left(\frac{\tau_y}{\tau_{ave}}\right) + \frac{a}{b(a+b)}\left(\frac{\tau_y}{\tau_{ave}}\right)^{\left(1+\frac{b}{a}\right)}\right] \qquad 2.87$$

with

$$\tau_{ave} = \rho g R_h \sin\alpha . \qquad 2.50$$

In Chapter 4 these models will be tested with data compiled for this thesis.

2.7.2 Hyperconcentration Flow Research By Zhang & Ren

Zhang & Ren (1982) studied the flow of mud. They simulated Yellow river mud by adding to water particles with d_{90} = 0.063 mm, d50 = 0.042 mm and d_{10} = 0.010 mm. This together with some sediment formed a slurry which they tested with a capillary viscometer and classified as a Bingham fluid.

The laminar flow equation developed by Zhang and Ren is the same as Re_2 (Bingham Plastic) used in this thesis. It is only written in a slightly different form. The Reynolds number is valid for Bingham fluids only and is given as:

$$Re_{Zhang} = \frac{4R_h V}{K + \frac{\tau_y R_h}{2V}} . \qquad 2.88$$

The friction factor was defined as:

$$f = \frac{2gR_h \sin\alpha}{V^2} . \qquad 2.89$$

All their tests were conducted in a concrete flume at one flume slope, as the flume was 43 m long.

2.7.3 Concentrated mud suspension flow research by Coussot

Coussot (1994) did work on kaolin suspensions, which he characterises as a Herschel-Bulkley fluid; for the concentrations used he fitted all his data by fixing the value of n to 0.333. From this he derived a value for average wall shear stress in a rectangular flume:

$$\tau_0 = \tau_y\left(1 + a\left(H_B\right)^{-0.9}\right). \qquad 2.90$$

Coussot also introduces a shape factor, which he defines as follows:

$$a = 1.93 - 0.43\left(\arctan\left(\left(\frac{10h}{B}\right)^{20}\right)\right). \qquad 2.91$$

Coussot claims that this is relevant for h/B<1, which means that for a 300 mm wide channel the shape factor should work for h up to 300 mm deep. The value of 'a' reaches a minimum value at a depth of approximately 60 mm, which means an h/B ratio of about 0.2. This contradicts the initial assumption of 'a' being correct for an h/B ratio of up to 1.

The Herschel-Bulkley number is defined by Coussot as follows:

$$H_B = \frac{\tau_y}{K}\left(\frac{h}{V}\right)^n. \qquad 2.92$$

Re-writing Equation 2.89 in terms of H_B

$$H_B = \left(\frac{\frac{\rho g R_h \sin\alpha}{\tau_y} - 1}{a}\right)^{1/-0.9}. \qquad 2.93$$

By using Equation 2.90 to determine the shape factor and equating 2.92 and 2.93 to each other, one can, for a given value of h determine a flow velocity.

This will be tested in Chapter 4.

2.7.4 Non-Newtonian turbulent open channel flow

Few turbulent flow models are available for non-Newtonian open channel flow. The data presented by Coussot (1994), does not reach turbulence because the slurries that he tested were very viscous. (See Section 4.1.3).

2.7.4.1 The Naik Turbulence Model

Naik (1983) presents the formula published by Chow (1959) for rough wall turbulent Newtonian open channel flow and derives from it a formula for the mean velocity of a Bingham fluid

$$V = 2.5V_*\left(1-\frac{\tau_y}{\tau_0}\right)^{0.5}\left(A_0+\ln\left(\frac{R_h}{k}\right)\right), \qquad 2.94$$

where:

$$A_0 = \ln\left(\left(\frac{30h}{R_h}\right)^{\left(-1-\left(\frac{\left(\frac{B}{h}+2\right)h^2}{4A}\right)\right)}\right). \qquad 2.95$$

This model was developed from a half-round open channel section and modified for the rectangular channel. The fluid, kaolin, was characterised as a Bingham fluid.

The Bingham parameters that are used are derived from the particle size distribution and reduced volume fraction of the solids, and not from pipe or rotary viscometer tests. This is the only reference that was found where the rheological parameters were established in such a way. As the method is not mentioned or discussed anywhere else, it is difficult to discuss or comment on.

Our experience indicates that rheology is a complex function of many other variables such as pH, zeta potential, surface chemistry effects etc, and should be measured for meaningful flow behaviour investigations.

Although Equation 2.94 is for rough wall turbulent flow it will be tested with the data compiled for this thesis and will presented in Chapter 4.

2.7.4.2 Wilson (1991) design protocol

Wilson (1991) does not present a specific turbulence model but describes a method for homogeneous slurries which he reasons should flow at a Froude number higher than 1.2, which Faddick (1986) proposes for settling slurries.

Wilson reasons that the shear velocity, which is a measure of the vertical velocity in turbulence, must be taken into account and minimum values are specified.

The minimum value of the velocity must then be set in terms of the minimum Froude number value of 1.2.

Pipes used for testing are smooth and therefore more complicated friction formulations may be necessary, e.g., the adapted Colebrook-White equation which can be written as

$$\frac{V}{V_*} = -2.43 \ln\left(\frac{k}{3.7 D_e} + \frac{0.89 \mu_e}{\rho V_* D_e} \right). \qquad 2.96$$

The equivalent viscosity μ_e replaces the fluid viscosity in the equation for non-Newtonian liquids and k is the roughness size.

μ_e is a variable and depends on the shear velocity. Because the values vary for different slurries, the values for μ_e and V_* must be obtained empirically from pipe loop tests and

plotted on graphs.

For any value of shear velocity V_* the value of μ_e can be found from the graph and can be substituted in Equation 2.96 together with the known or assumed values of k and D_e.

The values for equivalent diameter and slope calculated previously by the Manning formula will produce a certain shear velocity.

From the graph the μ_e will be read off. This will be entered in Equation 2.96 and produce a velocity that can be checked against the velocity obtained earlier. The slope may have to be adjusted to obtain that velocity.

Finally it must be established whether V_* will be enough to prevent the settling of particles. The minimum value of V_* can be read off the same graph. At this point deposition has already taken place and therefore the value must be increased by a factor of approximately 1.2.

The method suggested by Wilson should work well if the viscous forces are not very high. For high concentration, high yield stress fluids, it is debatable whether the flow rates will reach turbulence. Whether the Froude number of 1 has the same implications for highly viscous non-Newtonian open channel flow is also not certain.

The Manning formula is for Newtonian flow and again it is debatable whether it will work for highly viscous fluids.

2.7.5 Non-Newtonian laminar turbulent transition in open channel flow

Only a few references exist which describe the laminar turbulent transition for non-Newtonian fluids in open channels.

2.7.5.1 Transition By Zhang & Ren

Zhang & Ren (1982) discovered by measuring flow pulsations with a pressure micro-transducer that the pulsations in the transitional regions start in the lower regions of the flume and weaken towards the surface. In full turbulence the pulsations reach a maximum over the full depth of the flume.

The transition range occurs between Reynolds number 3 000 and 5 000 for different channel roughnesses and the friction factor ranges from 0.005 to 0.01.

It is also interesting to note that the laminar-turbulent transition published in their paper occurs at a specific point for a certain flume roughness and that the transition is typically as for a Newtonian fluid where a sudden jump or increase in friction factor occurs.

2.7.5.2 Hedström number approach

Naik (1983) derives a method to predict the onset of transition using the Hedström number that is defined by Hedström (1952) for Bingham plastic pipe flow as:

$$He = \frac{D^2 \rho \tau_y}{K^2}. \qquad 2.97$$

For open channel flow the number becomes:

$$He = \frac{16\left(R_h\right)^2 \rho \tau_y}{K^2}. \qquad 2.98$$

For a Bingham fluid, Naik derives a condition to predict the laminar turbulent transition by the following equation:

$$\frac{\phi_c}{\left(1-\phi_c\right)^3} = \frac{He}{48000}. \qquad 2.99$$

The value of the constant may vary according to Naik between 24 000 and 96 000. This in turn depends on the Newtonian Reynolds number being between 2 000 and 8 000.

The relationship between the Hedström number and the Reynolds number for a Bingham fluid, Naik presents as follows:

$$Re = \left(\frac{He}{12\phi}\right)\left(1-1.5\phi+0.5\phi^3\right). \qquad 2.100$$

Chhabra & Richardson (1999), present the formula for the Bingham Reynolds number for pipes in a slightly different form

$$Re_c = \frac{1-\frac{4}{3}\phi_c+\frac{\phi_c^4}{3}}{8\phi_c} He, \qquad 2.101$$

with:

$$\frac{\phi_c}{\left(1-\phi_c\right)^3} = \frac{He}{16800}. \qquad 2.102$$

Coussot (1997) uses the Hanks criteria to derive a formula to predict the onset of turbulence for mudflow which he rheologically characterises as a yield-pseudoplastic suspension.

He suggests that the flow becomes turbulent when the depth of flow is larger than:

$$h = \frac{1}{\rho g \sin\alpha}\left[\tau_y + K\left(\frac{404(m+1)\rho(g\sin\alpha)^2}{Kv}\right)^{\left(\frac{1}{2m+1}\right)}\right] \qquad 2.103$$

with: m=1/n

and

$$V = \left[\left(\frac{m}{2m+1}\right)^{\left(\frac{m}{m+1}\right)} - \left(\frac{m}{2m+1}\right)^{\left(\frac{2m+1}{m+1}\right)}\right]. \qquad 2.104$$

2.7.5.3 The laminar/turbulent transition according to Wilson

Wilson (1991), suggests the following method to predict transition. He strongly recommends that pipe viscometer data be used to plot a pseudo shear diagram with τ_o against 8V/D. All the pipe diameters in laminar flow should collapse on one line if there is no wall-slip. On a log-log plot in turbulence the data for different diameters are parallel with a slope of approximately 2.

For each value of τ_w for a diameter of the tested diameter D_1, the value of V can be scaled up or down for any pipe diameter D_2.

$$V_2 = V_1 + 2.5V_* \ln\left(D_2 / D_1\right) \qquad 2.105$$

where the shear velocity is:

$$V_* = \sqrt{gR_h \sin\alpha}\,. \qquad 2.106$$

By substituting D_e for D, the turbulent data can be scaled down and the velocity at the laminar turbulent intersection can be read off the graph.

Wilson's method pre-supposes that the pipe flow behaviour in the transition region is exactly the same as for open channel flow and that the transition will occur at a Reynolds number of certain value. This has not been experimentally verified as far as can be ascertained.

2.8 RESEARCH ISSUES IDENTIFIED

The main objective of this thesis is to develop an experimentally validated design protocol to predict non-Newtonian open channel flow in a rectangular flume in laminar and turbulent flow and be able to predict the onset of transition. This review has shown that very few studies have been conducted, and even though some open channel flow models have been presented, most of them like that of Kozicki and Tiu (1967) have not been experimentally validated.

Researchers have generally restricted their research to one fluid, or one slope, or one channel width. If only one material was used, that means that usually only one rheological model was used to characterise the fluid.

- Rheological characterisation in the light of the yield stress debate

While it is pragmatic to continue to use the yield pseudoplastic, pseudoplastic and Bingham models for engineering purposes, it is clear that the apparent viscosity over the relevant shear rate range of application is the more important fundamental issue (Malkin *et al*., 2003).

- Laminar flow

Some work has been done but no one has looked at different materials to see if one Reynolds number can be used for materials with different rheological parameters. The same Reynolds numbers presented are only for Bingham fluids.

Most of the researchers also used rotary or capillary viscometers. Small samples used and rotary viscometers used for suspensions can be problematic to test as segregation can occur.

- Turbulent flow

A few models have been described mainly for Bingham fluids. Some authors suggest that pipe flow models can be transformed to open channel flow (Wilson, 1991). This needs to be validated experimentally.

- Transition

Transition has only been addressed by a few researchers and here again the only model has been the Hanks criteria, developed for pipe flow, which has been modified for open channel flow.

- Wall shear stress

Wall shear stress presents a big problem in open channel flow. For pipe flow it is not complicated as the cross-section of the pipe is symmetrical. This enables one to develop flow equations from the shear stress distribution. For open channel flow, the shear stress distribution is not known, and many assumptions are made, one of them being the infinite width model, which then ignores the sidewall effects.

From the above it can be concluded that some form of empirical approach will have to be used to solve the problems of open channel flow, especially if the transition

behaviour is to be somehow predicted. The complexity of using different rheologically classified fluids further complicates the issue.

2.9 CONCLUSION

In conclusion it can be said that there is sufficient evidence to prove that the field of non-Newtonian open channel flow has not been adequately studied. The application of this knowledge to the mining industry, where higher concentration slurries need to be transported, could be significant.

CHAPTER 3

EXPERIMENTAL WORK

3.1 INTRODUCTION

In this chapter, the apparatus used to gather all the data used in the evaluation of models used in literature, as well as the new models, are described.

All of the apparatus was built specifically for this project to establish the following:

- Accurate in-line rheological characterisation of all the slurries used.
- Testing of various slurries in three different sized flumes with various slopes, aspect ratios and over a wide range of flow rates to include laminar, transition and turbulent flow.

The design of the test rig was such that the same slurry could be tested in three pipe diameters to establish the in-line rheology as well as the flow in three different size flumes.

Materials tested were water and a sucrose solution for calibration purposes, kaolin clay slurries, bentonite slurries, aqueous Carbopol solutions and Carboxymethyl cellulose solutions or CMC, all of various concentrations.

The rheology measurements were carried out in the flume pipe rig with pipe sizes 13 mm, 28 mm and 80 mm, and the rheometer with a cone and plate and cup and bob configuration.

3.2 APPARATUS

The different apparatus used for gathering the experimental data for the work presented in this thesis were the rheometer, the flume pipe rig and three size flumes.

3.2.1 Rheometer

The rheometer used was a Paar Physica instrument that is equipped with an air bearing. The configurations that were used to test the slurries were a cone and plate and cup and bob. The cup and bob and cone and plate measuring systems are depicted in **Figure 3-1**below.

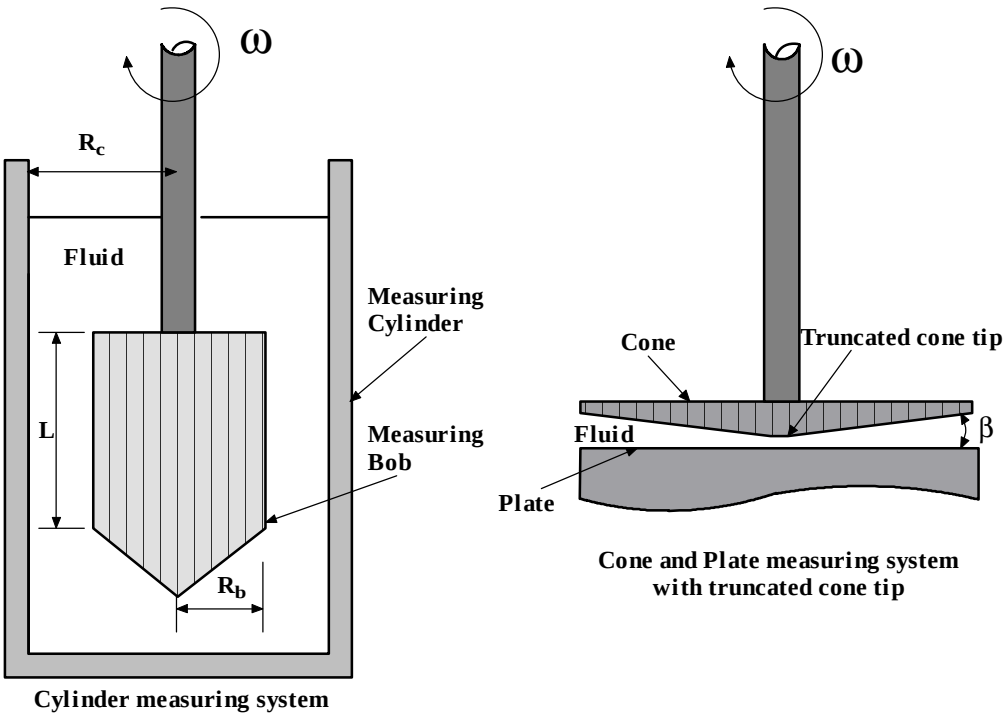

Figure 3-1 Rheometer: Cylinder and cone and plate measuring systems.

Flow curves were created for all the slurries tested and the rheological parameters obtained were compared with those obtained from the pipe viscometer.

3.2.2 The flume pipe rig

The flume pipe rig and the two flumes were all linked with a network of pipes. The design was such that the pump, mixing tank, weigh tank, flow meters, differential pressure transducers (DPTs) and heat exchanger could be shared between the flumes. The flume pipe rig is basically an in-line pipe viscometer.

The flume pipe rig consists of a 100 mm, 30 bar, progressive cavity positive displacement pump with variable speed drive which feeds through a heat exchanger to three PVC tubes. The tubes are in parallel and have 13 mm, 28 mm and 80 mm diameters respectively. The rest of the pipe work is mostly steel. Each pipe has an in-line magnetic flow meter. The 13 mm line also has an in-line mass-flow meter, which can also measure temperature and density. The flow meters are calibrated with a 500 litre weigh tank suspended over the mixing tank. The one end of the tank swivels and the other side is connected to the roof with a load cell. A temperature probe is fitted at the end of the heat exchanger.

All the outputs of the flow meters, DPTs, temperature probes and load cell of the weigh tank are connected to a data acquisition unit linked to a personal computer (PC).
The schematic layout is depicted in
Figure **3-2**.

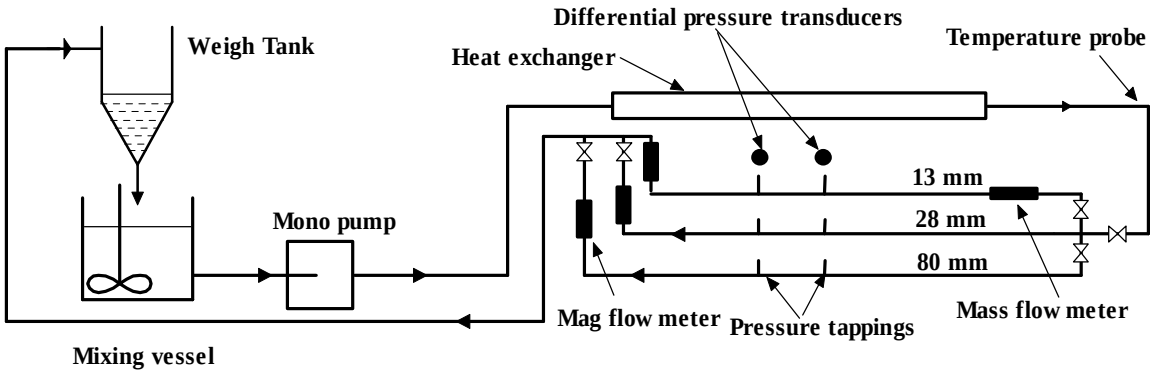

Figure 3-2 Flume pipe rig layout

3.2.3 Pressure tappings

On all three lines there are pressure tappings 1 m apart that provide two static pressure points so that differential pressure can be measured. The holes drilled into the pipe walls are 3 mm in diameter and the inside of the pipe is carefully cleaned so that no roughness is left at the tapping entry.

From the tapping the fluid is fed to the isolation pod that ensures that no solids can reach the manometer or differential pressure transducer (DPT). A water line is fed into the pod to flush the system. This is done regularly during testing. The same water line is also used to flush the DPTs. The layout of a flushing pod is depicted in **Figure 3-3**.

Before the pressure tappings a straight unobstructed pipe section of at least 50 pipe diameters was observed (Govier & Aziz, 1972; Hanks, 1981). This is to ensure that flow is fully developed and does not influence the pressure readings.

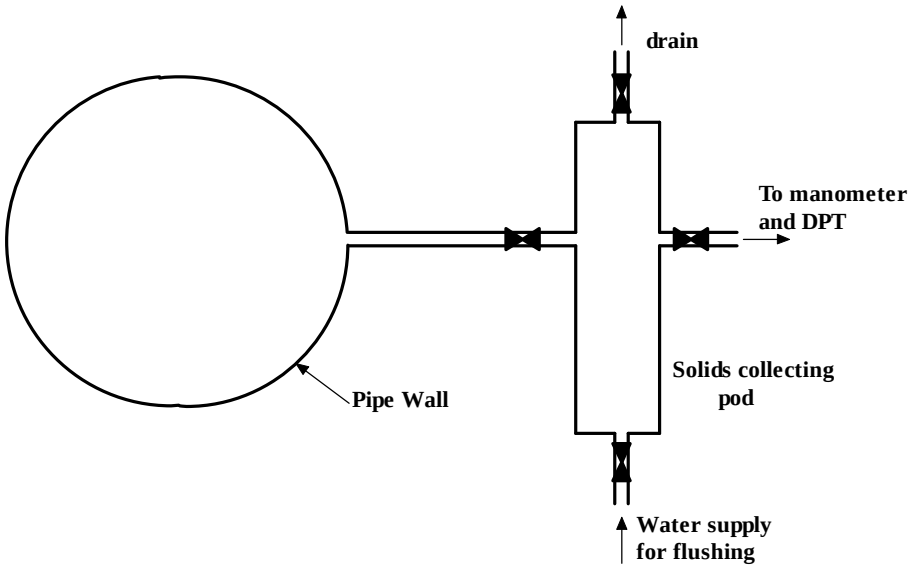

Figure 3-3 Detail of pressure tapping and pod

3.2.4 Weigh tank

The weigh tank is a 500 litre plastic tank mounted over the mixing tank. The platform on which the tank rests, swivels on bearings on one side and is supported from a roof beam on the other side. In this support there is a 500 kg load cell. The load cell is connected to the data logger. At the bottom of the tank is a valve that can let the fluid out into the main mixing tank. The tank is fed on a bypass from the flume pipe rig to calibrate the magnetic flow meters. Flow rates can then be checked with time by measuring the change in mass measured by the load cell. The weigh tank configuration is schematically depicted in **Figure 3-4**.

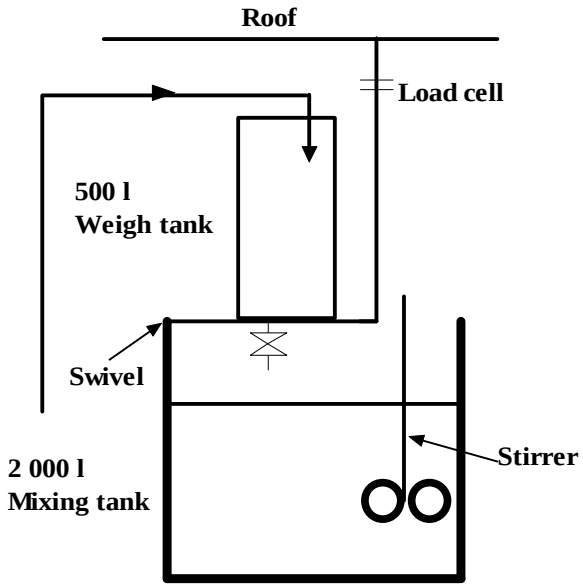

Figure 3-4 Layout of weigh tank

3.2.5 Manometer and pressure tapping layout

The layout of the manometer board and the connections to the pressure tappings on the lines is depicted on **Figure 3-5**. The manometer is used to calibrate the two differential pressure transducers (DPTs). This is done by setting up a range of air over water differential heads and comparing them with the DPT outputs.

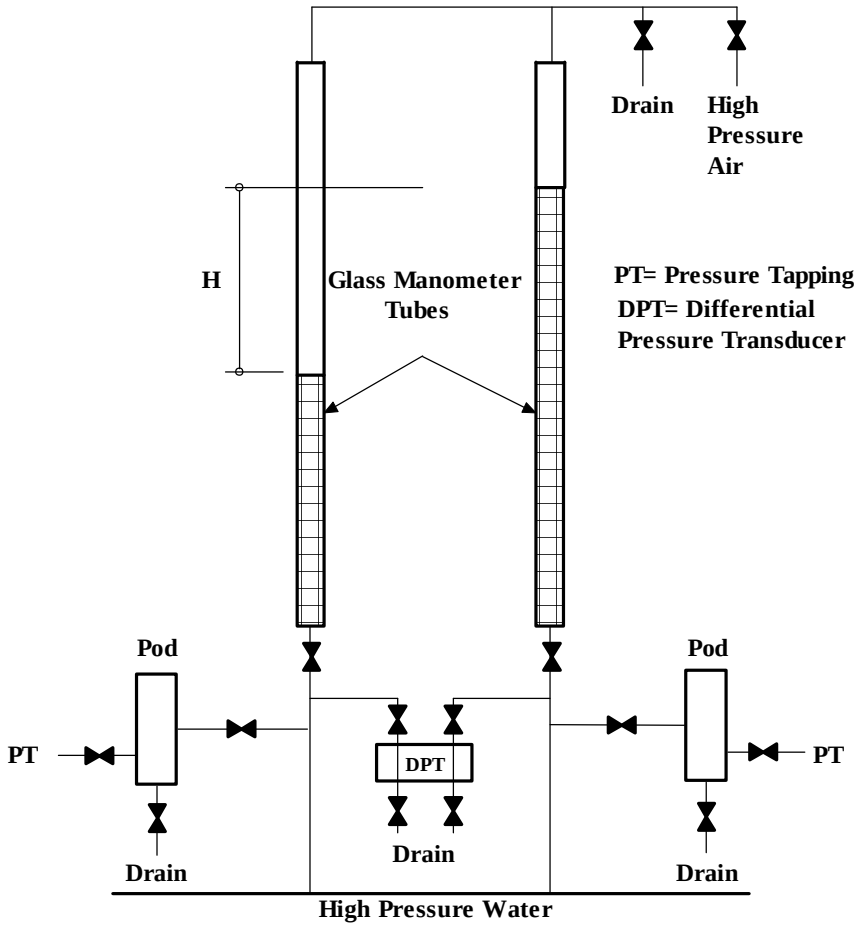

Figure 3-5 Layout of the manometer board and pressure tappings

3.2.6 Small flume

The small flume is a standard hydraulics laboratory flume, manufactured by a commercial company. The flume is 5 m long with a rectangular cross-section of 75 mm wide and 150 mm high. The bottom and sides are constructed of clear Perspex. The flume was modified to tilt from the initial 0.5 degrees to 5 degrees by fitting a screw type device. The supply tank was also modified to enable larger flow rates to be pumped through the system. The small flume is linked to the in-line pipe viscometer and the main supply tank and progressive cavity pump by a system of pipes.

To measure the flow depth, two electronic vernier-type depth gauges are fitted to the flume.

These depth gauges are electronically linked to the data acquisition unit via RS232 interfaces.

3.2.7 Large Flume

The large flume is 10 m long with a width of 300 mm and a depth of 300 mm with a partitioning section that can be fitted to the centre of the flume to form a 150 mm wide flume. These panels can be taken out to change the flume width. To change the slope of the flume an electrically powered hydraulic ram was fitted which can tilt the flume from 0 to 5 degrees.

The inlet tank has a capacity of 600 l and is fitted with baffles to streamline the flow.

The mixing tank has a capacity of 2000 l and is fitted with an electrically driven mixer that runs continuously during the tests.

The layout of the large flume is schematically depicted in **Figure 3-6**.

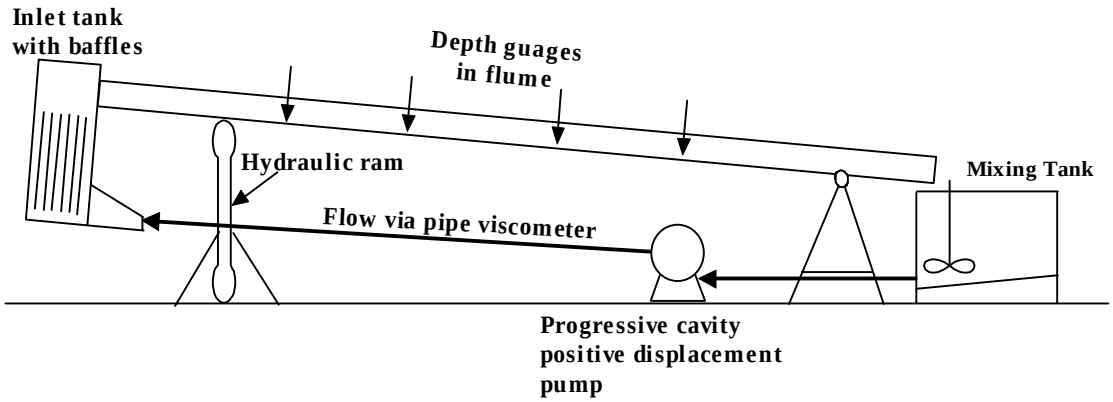

Figure 3-6 Layout of the 10 m tilting flume

3.2.8 Pumps

A 100 mm, 30 Bar progressive cavity positive displacement pump, driven by a 17 kW motor which is regulated by a variable speed drive, feeds the closed system linking the flumes and the pipe viscometer. This pump is able to deliver approximately 25 l/s of water through the pipe rig.

To minimise pump pulsations, a damper was fitted at the supply end of the pump. This is depicted in **Figure 3-7**. The effectiveness of the damper unit could be observed by observing the pulsations of the fluids in the clear section of the unit. The vertical pipes are 100 mm clear pipes with steel end caps on and steel nipples to let air into the system when required. The clear section is protected by stainless steel wire mesh. The flow in the flumes was more regular after fitting the damping unit.

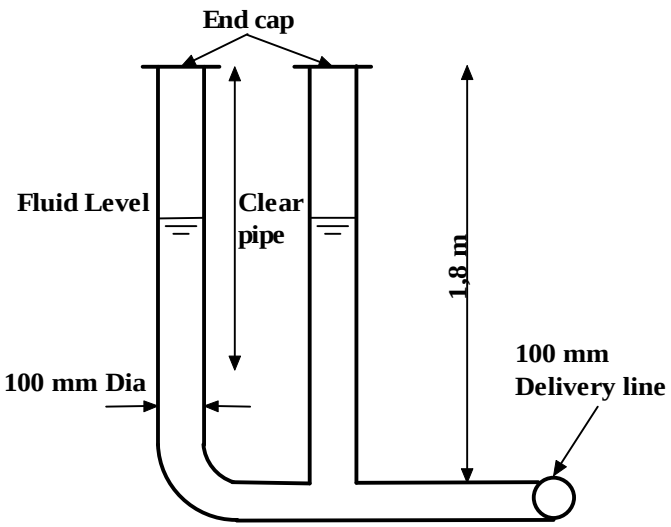

Figure 3-7 Pulsation damping unit

As the progressive cavity pump could not supply sufficient flow to obtain turbulence with the denser slurries, a centrifugal pump was added to the rig.

The Warman 4x3 centrifugal pump was installed and is driven by a 37 kW motor and regulated by a variable speed drive. To minimise losses, the pump was not linked to the in-line pipe viscometer, but linked via a heat exchanger and 100 mm electromagnetic flow meter directly to the inlet of the large flume. The layout is depicted in **Figure 3-8**.

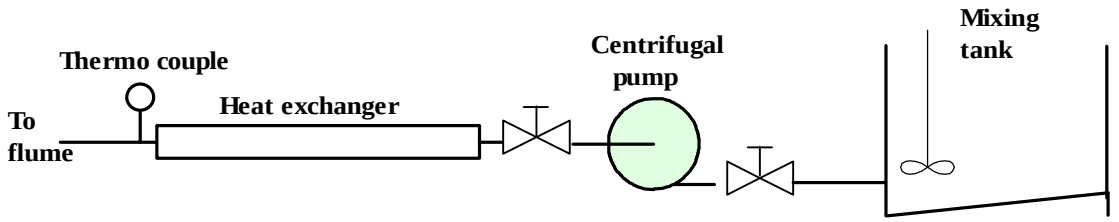

Figure 3-8 Layout of the centrifugal pump linked to large flume

3.3 CALIBRATION PROCEDURES

As most of the measuring instruments are electronic, they require calibration, and the calibration procedure is explained in the following section. Most signal outputs from the instruments are standard 4-20 mA current source. By fitting a 100 ohm resistor to the circuitry this is converted to 1-5 V. This voltage can then be read by the HP-data-logger.

3.3.1 Weigh tank

The weigh tank used for the flow meter calibration and depicted in **Figure 3-4** is swivelled on one side and suspended from the roof by means of a load cell. The load cell is used to weigh the fluid collected from the flow meters. To calibrate the load cell, water is weighed in a container on a scale. The water is then poured into the weigh tank and the voltage output recorded. For every increase of load, the increase in voltage is recorded.

The plot of load against voltage is depicted on the graph in **Figure 3-9**. A linear regression of the points will give the relationship between the loads and the equivalent voltages. This is then entered in the program to be used to calculate the flow rate.

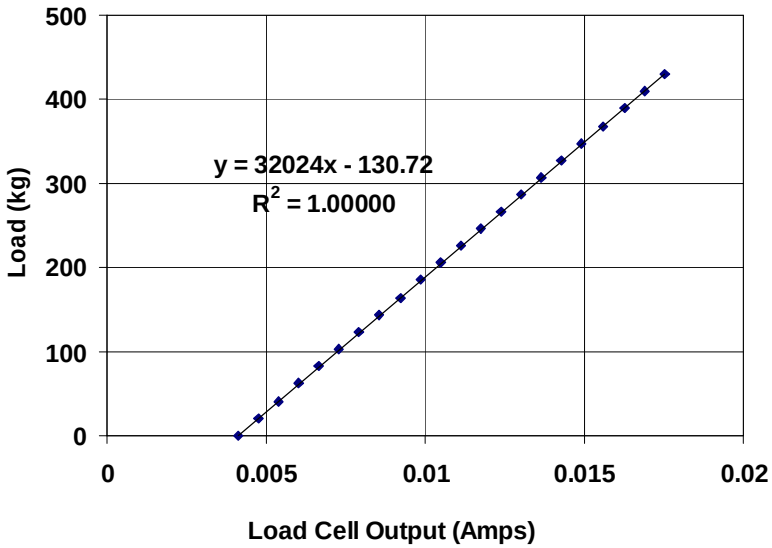

Figure 3-9 Load cell calibration (linear regression)

The linear regression over the range tested gives an R^2 value of 0.99999. To analyse the data further, the residual values are calculated and plotted. The relationship between the linear regression residual values against the loads is plotted on **Figure 3-10**.

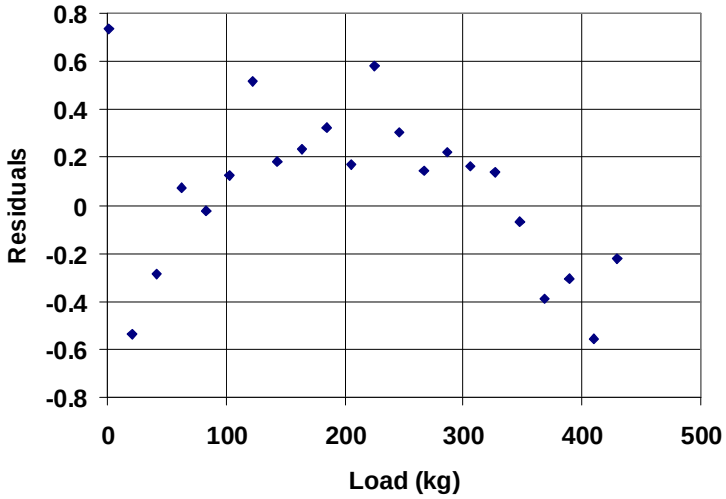

Figure 3-10 Graphical plot of linear regression residual values for the load cell calibration

Over the range tested, the residuals show some structure. It was then decided to fit a second order polynomial to the data, which is depicted in **Figure 3-11**.

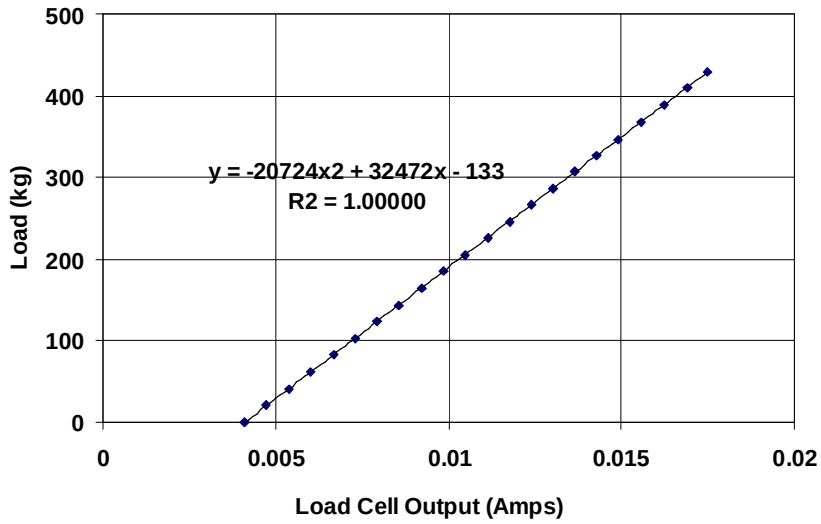

Figure 3-11 Load cell calibration (first order polynomial regression)

The R^2 value for this was 0.999999. The residual values are again calculated and plotted. The relationship between the linear regression residual values against the loads is plotted on **Figure 3-12**.

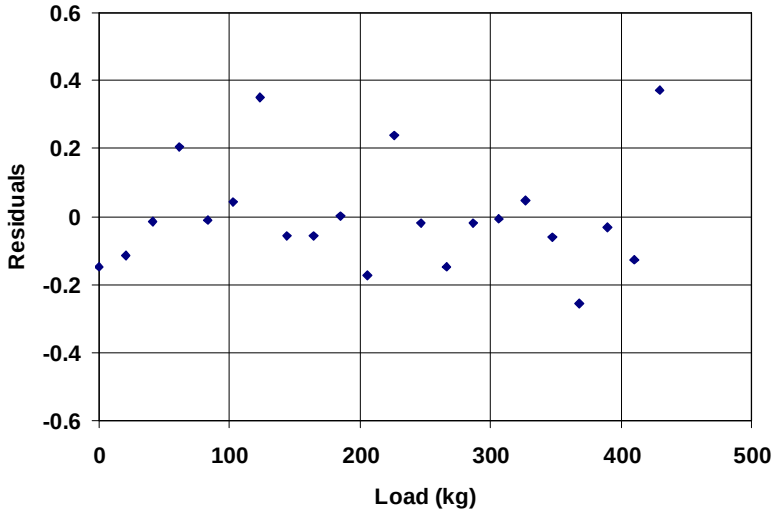

Figure 3-12 Graphical plot of second order regression residual values for the load cell calibration

Over the range tested, this shows a random distribution of the residuals. This indicates that the second order fit is better. However, the difference in error between the first and second order fit is very small. The R^2 value only differs with the 6th decimal place. It was decided that this does not really warrant the use of the more complex equation. The first order relationship is therefore used to obtain the calibration constants.

3.3.2 Flow meters

As the materials tested varied in chemical composition and concentration, each material and concentration is tested over the flow rates used by diverting the flow into the weigh tank. Several magnetic flow meters have been evaluated by Heywood, Mehta and Popler (1993), and they suggest that because the magnetic flux lines can never be exactly parallel, the velocity profile must influence the output. According to the

manufacturers the flow meters are accurate for slurries. The only way to make sure that this is true is to calibrate each slurry and concentration and, if necessary, introduce new calibration factors for each fluid and concentration.

The procedure is as follows:
For a flow meter the flow rate range is divided into about 12 different flow rates over the whole range.

Each flow rate is then weighed with time in the weigh tank. The data logger continuously samples the change in weight with time, and from these readings the average flow rate is calculated. The sampling period varies from 120 s for low flow rates to 12 s for the high flow rates. This is repeated for all the flow rates.

The flow rates versus voltages are then plotted and the straight-line regression gives the relationship between flow rate and volts as well as the error fit.

A typical test result for the 28 mm magnetic flow meter calibration is shown in **Figure 3-13** below.

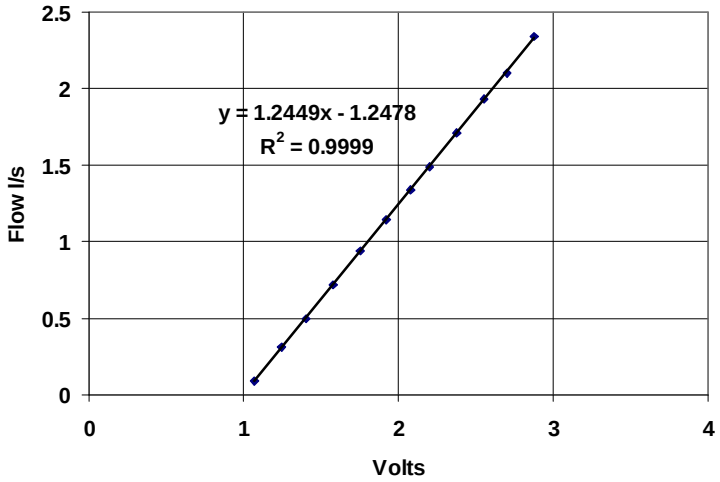

Figure 3-13 28 mm magnetic flow meter calibration for 6% kaolin

The calibration of the 80 mm magnetic flow meter was difficult as the higher flow rates filled the tank in a short time. The impact of the inflow on the tank and frame also caused vibrations. This resulted in inaccurate results. This was not the case with the 13mm and 28 mm calibrations.

The calibration values for the different concentrations kaolin for the 80 mm flow meter were then compared to the water calibration values and the deviations calculated. This is depicted in **Table 3-1**.

From the results it can be seen that only in the very low flow rates that result in low voltages are the deviations significant. Over the remainder of the range the deviation is less than 2%, except for the 8% concentration. From the results it can also be concluded that there is no increase in deviation with increase in concentration, as the 10% concentration shows less deviation than the 8% concentration.

Table 3-1 80 mm flow meter calibration constants deviation comparison for kaolin

Slurry	Water	Kaolin 3%		Kaolin 4.50%		Kaolin 6%		Kaolin 8%		Kaolin 10%	
m	7.5573	7.57		7.6792		7.6529		7.7757		7.5076	
c	-7.55975	-7.5815		-7.7553		-7.732		-8.0737		-7.5053	
volts	l/s	l/s	%dev from water	l/s	%dev from water	l/s	%dev from water	l/s	%dev from water	l/s	%dev from water
1.05											
1.15	1.13	1.12	0.63%	1.08	4.89%	1.07	5.51%	0.87	23.23%	1.13	0.24%
1.25	1.89	1.88	0.31%	1.84	2.29%	1.83	2.80%	1.65	12.77%	1.88	0.41%
1.35	2.64	2.64	0.17%	2.61	1.17%	2.60	1.63%	2.42	8.29%	2.63	0.48%
1.45	3.40	3.40	0.10%	3.38	0.55%	3.36	0.99%	3.20	5.80%	3.38	0.52%
1.55	4.15	4.15	0.05%	4.15	0.16%	4.13	0.58%	3.98	4.22%	4.13	0.54%
1.65	4.91	4.91	0.02%	4.92	-0.11%	4.90	0.30%	4.76	3.13%	4.88	0.56%
1.75	5.67	5.67	-0.01%	5.68	-0.31%	5.66	0.09%	5.53	2.33%	5.63	0.57%
1.85	6.42	6.42	-0.03%	6.45	-0.47%	6.43	-0.07%	6.31	1.71%	6.38	0.58%
1.95	7.18	7.18	-0.04%	7.22	-0.59%	7.19	-0.20%	7.09	1.23%	7.13	0.59%
2.05	7.93	7.94	-0.05%	7.99	-0.69%	7.96	-0.30%	7.87	0.83%	7.89	0.60%
2.15	8.69	8.69	-0.06%	8.75	-0.77%	8.72	-0.38%	8.64	0.51%	8.64	0.60%
2.25	9.44	9.45	-0.07%	9.52	-0.83%	9.49	-0.45%	9.42	0.24%	9.39	0.61%
2.35	10.20	10.21	-0.08%	10.29	-0.89%	10.25	-0.51%	10.20	0.01%	10.14	0.61%
2.45	10.96	10.97	-0.09%	11.06	-0.94%	11.02	-0.57%	10.98	-0.19%	10.89	0.61%
2.55	11.71	11.72	-0.09%	11.83	-0.98%	11.78	-0.61%	11.75	-0.37%	11.64	0.62%
2.65	12.47	12.48	-0.10%	12.59	-1.02%	12.55	-0.65%	12.53	-0.52%	12.39	0.62%
2.75	13.22	13.24	-0.10%	13.36	-1.06%	13.31	-0.69%	13.31	-0.66%	13.14	0.62%
2.85	13.98	13.99	-0.10%	14.13	-1.09%	14.08	-0.72%	14.09	-0.78%	13.89	0.62%
2.95	14.73	14.75	-0.11%	14.90	-1.11%	14.84	-0.74%	14.86	-0.88%	14.64	0.63%
3.05	15.49	15.51	-0.11%	15.67	-1.14%	15.61	-0.77%	15.64	-0.98%	15.39	0.63%
3.15	16.25	16.26	-0.11%	16.43	-1.16%	16.37	-0.79%	16.42	-1.07%	16.14	0.63%
3.25	17.00	17.02	-0.11%	17.20	-1.18%	17.14	-0.81%	17.20	-1.15%	16.89	0.63%
3.35	17.76	17.78	-0.12%	17.97	-1.20%	17.91	-0.83%	17.97	-1.23%	17.65	0.63%
3.45	18.51	18.54	-0.12%	18.74	-1.22%	18.67	-0.85%	18.75	-1.29%	18.40	0.63%
3.55	19.27	19.29	-0.12%	19.51	-1.23%	19.44	-0.87%	19.53	-1.36%	19.15	0.63%
3.65	20.02	20.05	-0.12%	20.27	-1.25%	20.20	-0.88%	20.31	-1.41%	19.90	0.63%
3.75	20.78	20.81	-0.12%	21.04	-1.26%	20.97	-0.90%	21.09	-1.47%	20.65	0.63%
3.85	21.54	21.56	-0.13%	21.81	-1.27%	21.73	-0.91%	21.86	-1.52%	21.40	0.64%
3.95	22.29	22.32	-0.13%	22.58	-1.28%	22.50	-0.92%	22.64	-1.56%	22.15	0.64%
4.05	23.05	23.08	-0.13%	23.35	-1.29%	23.26	-0.93%	23.42	-1.61%	22.90	0.64%
4.15	23.80	23.83	-0.13%	24.11	-1.30%	24.03	-0.94%	24.20	-1.65%	23.65	0.64%
4.25	24.56	24.59	-0.13%	24.88	-1.31%	24.79	-0.95%	24.97	-1.69%	24.40	0.64%
4.35	25.31	25.35	-0.13%	25.65	-1.32%	25.56	-0.96%	25.75	-1.72%	25.15	0.64%
4.45	26.07	26.11	-0.13%	26.42	-1.33%	26.32	-0.97%	26.53	-1.76%	25.90	0.64%
4.55	26.83	26.86	-0.13%	27.19	-1.34%	27.09	-0.98%	27.31	-1.79%	26.65	0.64%
4.65	27.58	27.62	-0.14%	27.95	-1.35%	27.85	-0.99%	28.08	-1.82%	27.41	0.64%
4.75	28.34	28.38	-0.14%	28.72	-1.35%	28.62	-0.99%	28.86	-1.85%	28.16	0.64%
4.85	29.09	29.13	-0.14%	29.49	-1.36%	29.38	-1.00%	29.64	-1.87%	28.91	0.64%

From the test results it could also be concluded that for the concentrations used, the effect of the density and higher viscosity of the slurries did not significantly influence the accuracy of the magnetic flow meters. This convinced us that the water calibration constants could be used over the range of concentrations used in this thesis.

The 80 mm flow meter, which was calibrated at a flow rate of 8.33 l/s, has a calibration accuracy according to the manufacturers which is as follows:

At 98% of the range	-0.08% deviation	0.0065 l/s
At 45% of the range	-0.06% deviation	0.0022 l/s
At 21% of the range	+0.32% deviation	0.0056 l/s

These tests were for water and the deviations are very small.

From all of the above we consider that the maximum error of the flow meters in the range measured to be of the order of 4%: provided that the 80 mm was not used below 2 l/s and the 28 mm flow meter not less than 0.4 l/s.

3.3.3 Differential pressure transducers

The two differential pressure transducers (DPTs), one with a range of 0-4 kPa and the other 0-30 kPa, were calibrated with a water-over-air glass U-tube manometer. The procedure was as follows:

- The two ends of the DP cell are connected to the two legs of the manometer.
- The whole system is flushed to make sure that all the air and solids are out of the system.
- The U-tube manometer is then zeroed and a differential pressure is set up. The difference between the two legs is then measured and the pressure head calculated.

$$\Delta p = \rho_{water}\, g\, H \quad (m). \tag{3.1}$$

- The voltage recorded by the DP cell is also recorded with the data-logger.
- The differential pressure is then increased and the same procedure is followed. Several points over the range of the DP cell are recorded.

- The differential pressures versus voltages are then plotted and the least square linear regression gives the relationship between differential pressure and volts as well as the error of fit.

A typical test result for the high DP cell is shown in **Figure 3-14** below.

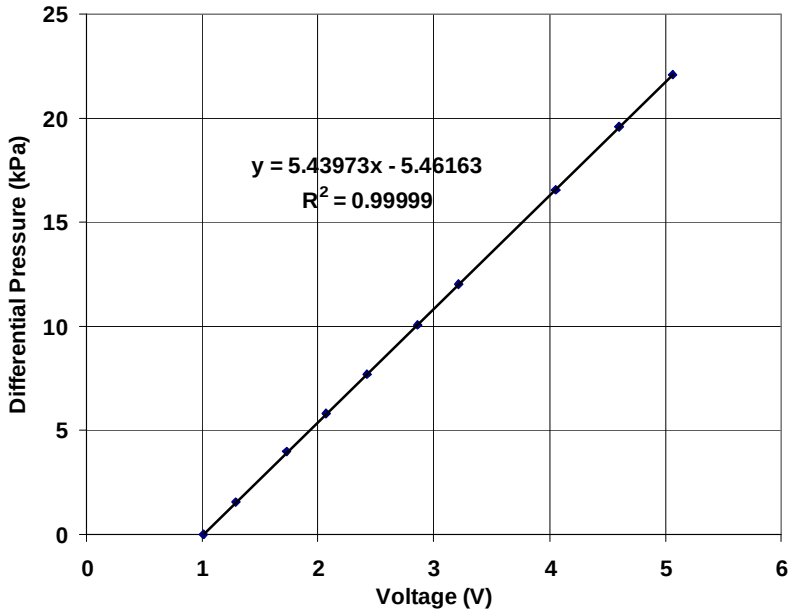

Figure 3-14 High differential pressure transducer calibration constants

According to the manufacturers, the accuracy of the DPTs are within 0.1% of full scale. This means that for the high range DPT the differential pressure error is +/- 25 Pa and for the low range DPT the differential pressure error is +/-4 Pa.

3.3.4 Clear water test in pipe viscometer

Once the flow meters and the DPTs have been calibrated, water tests are conducted in all the three pipes of the tube viscometer, namely the 13 mm, 28 mm and 80 mm.

The Colebrook-White equation 2.30 for turbulent flow in pipes is used to calculate the friction factor (f).

$$\frac{1}{\sqrt{4f}} = -2\log\left(\frac{k}{3.7D} + \frac{2.51}{Re\sqrt{4f}}\right). \qquad 2.30$$

By using the Darcy expression for friction head:

$$h_f = \frac{4fLV^2}{2gD} \qquad 3.2$$

and

$$\tau_0 = \frac{D\Delta p}{4L} = \frac{D\rho g h_f}{4L} \qquad 3.3$$

and combining equations 3.2 and 3.3 one can deduce that :

$$\tau_0 = \frac{f\rho V^2}{2}. \qquad 3.4$$

The procedure is as follows:

- The flow in each tube is measured and the average velocity is calculated.
- The differential pressure is measured over a distance L that is 1 m for all three pipes.
- The average wall shear stress is calculated by $\tau_0 = \frac{D\Delta p}{4L}$ (Equation 3.3).
- The wall shear stress in then plotted versus the average velocity V.
- The Colebrook-White equation is then used to calculate the theoretical value of τ_o for a range of wall shear stresses. The range is the same as that covered in the pipe test.
- This is done by assuming a value for pipe roughness (k), calculating the Reynolds number and optimising the Colebrook-White equation to obtain the friction factor (f).

- The friction factor is then used to calculate the theoretical value for wall shear stress using Equation 3.4.

The theoretical and actual data is then plotted on linear axes as shown for the three pipes in **Figure 3-15**, **Figure 3-16** and **Figure 3-17** below.

If the pipe is not smooth, the values for k can be optimised to find the actual pipe roughness (Slatter, 1994).

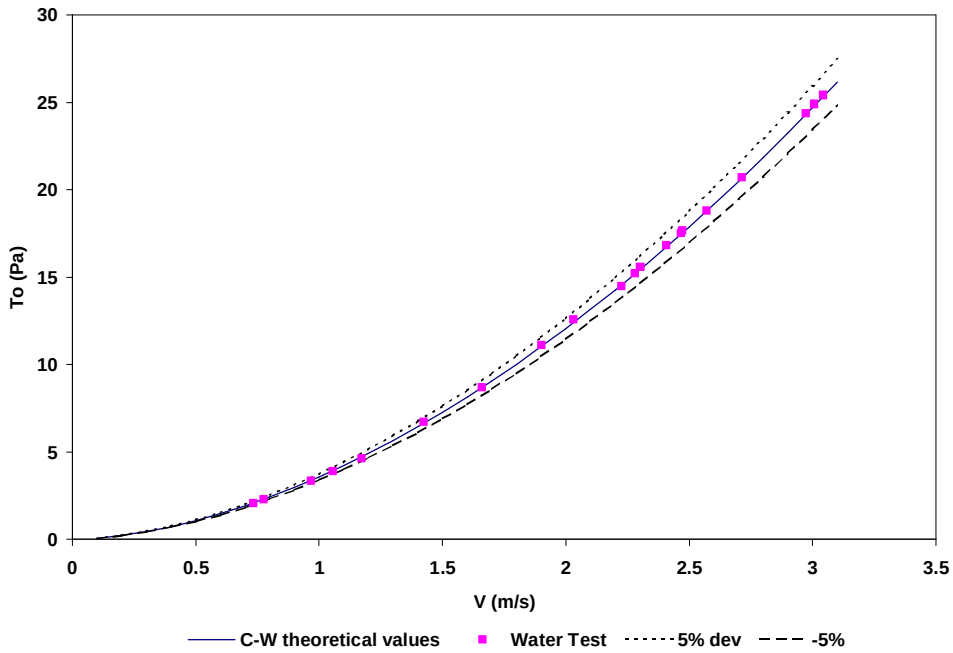

Figure 3-15 Clear water data against Colebrook-White test in 13 mm pipe

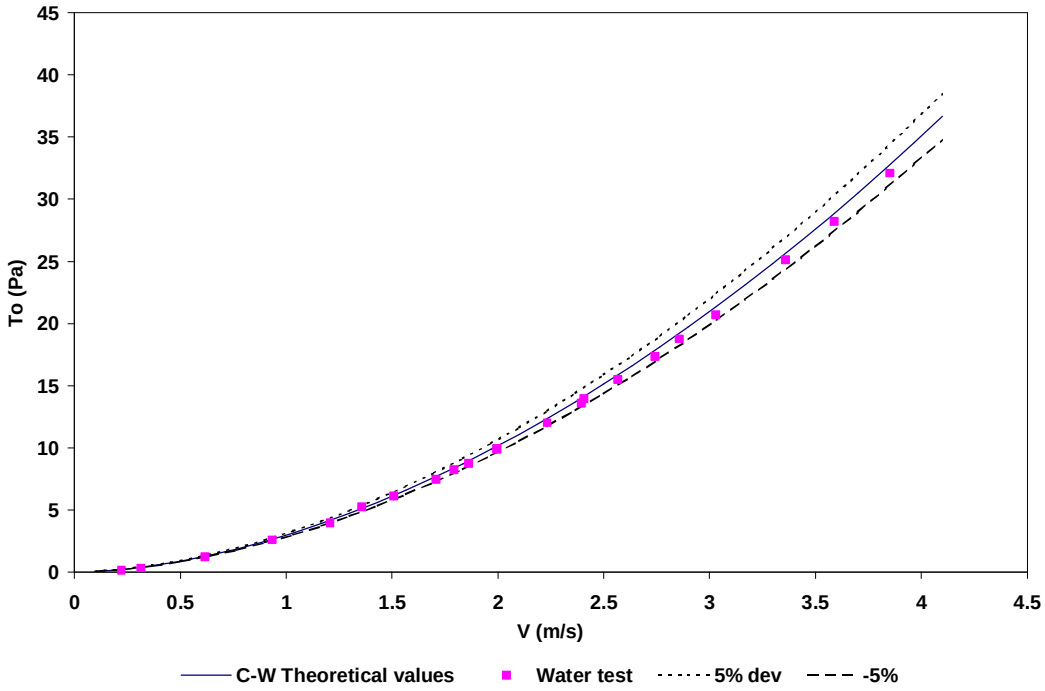

Figure 3-16 Clear water data against Colebrook-White test in 28 mm pipe

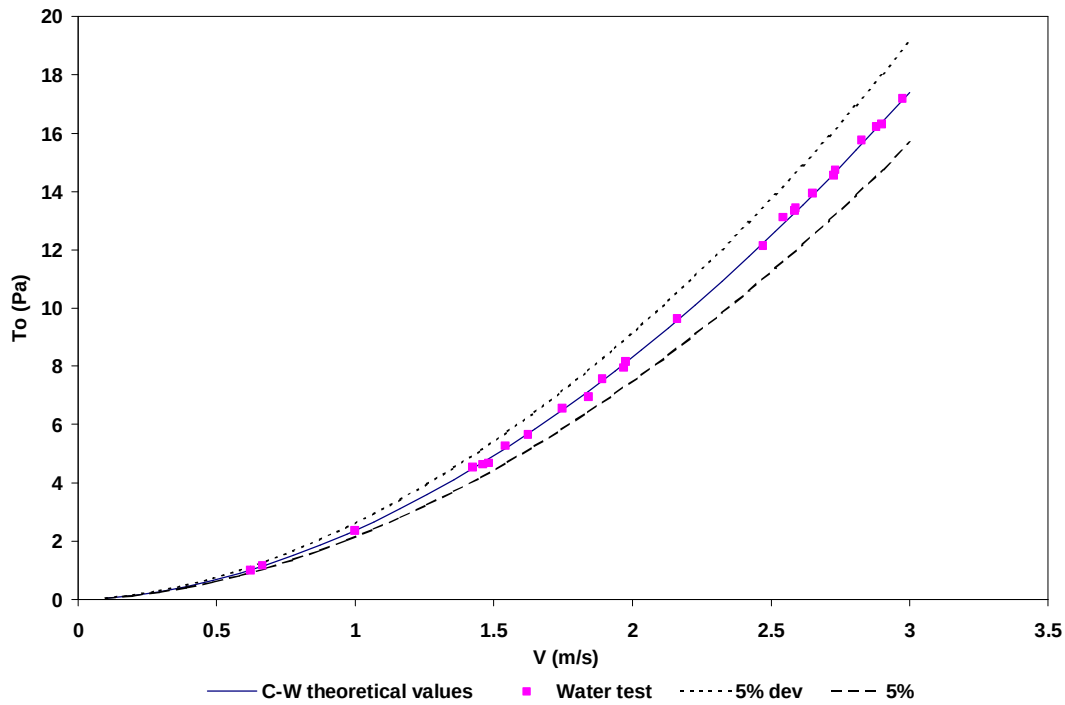

Figure 3-17 Clear water data against Colebrook-White test in 80 mm pipe

The k-values of the different diameter tubes were as follows:

13 mm tube k=1 μm

28 mm tube k=1 μm

80 mm tube k=3 μm.

From the Colebrook-White water tests the flow meter and differential pressure transducers can be tested together. If that is correct, then one can commence with the other tests. The results also indicate that the combined error from the flow meters and differential pressure transducers is less than 5% over the range tested.

3.3.5 Digital depth gauges

To measure the flow depth, each flume is fitted with two digital vernier type depth gauges. They are mounted perpendicular onto the flow surface. The depth gauges are linked electronically to the PC with an RS232 interface. The gauges are calibrated with a standard depth vernier. The electronic vernier is held against the standard vernier and various depths over the range of measurements are checked. The interface of the depth gauges transmits the depth signal directly to the PC as mm, and no calibration has to be performed.

3.3.6 Slope measurement of flumes

The flumes were levelled using a contractors' automatic dumpy level. By setting up in the middle of the flume, the level can be checked to within 1 mm over 10 m (0.01%).

The vertical displacement distances for the slopes of 1 2 3 4 and 5 degrees were then calculated and used to set the slopes required. A ruler was placed vertically on the frame next to the flume and a marker was connected to the flume. This was done at the position where the hydraulic ram is positioned. The various slopes can then easily be set to within 1 mm.

3.4 MEASURED VARIABLES

3.4.1 Measurement of pipe diameters

To check the internal diameter of the PVC pipes used in the test section of the pipe viscometer, the test sections are unscrewed at the unions linking them to the rig. The pipes with the pressure tappings are plugged at one end and placed in the vertical position on a scale. The pipe is filled with water until the water just flows out at the first tapping. The valve at the tapping is then closed.

The pipe is then weighed and more water added until water just flows out at the second tapping. The valve at the second tapping is then closed. The pipe is then weighed again.

The difference in mass of water (M_w) and the distance between tapping distances (L) is then used to calculate the internal pipe diameter (D) (Slatter, 1994).

$$D = \sqrt{\frac{4M_w}{\pi \rho_w L}} \,. \tag{3.5}$$

This process was repeated and the average of the three calculations was used.

The actual diameters of the three pipes used in the pipe viscometer rig are depicted in

Table 3-2:

Table 3-2 Actual pipe diameters of tube viscometer rig

Pipe diameter	Actual pipe diameter
13 mm	13.3 mm
28 mm	28.2 mm
80 mm	80.9 mm

The deviation may not look significant, but if the worst case, the 13 mm diameter is considered, the error introduced when using the pipe diameter given by the manufacturers, calculating the resulting cross-sectional area, is 5%. For the 80 mm pipe the error is 2% and for the 28 mm pipe, 0.75%.

3.4.2 Slurry density

The process to obtain the slurry density (ρ) and relative density (S_m) are calculated according to standard procedures as follows.

- The equipment required is a one litre volumetric flask and a scale that can measure to a milligram.
- Dry the flask thoroughly and weigh (M_1).
- Take a well-mixed slurry sample from the mixing tank. This can be done by taking a few samples from different places in the tank and mixing them.
- Fill the flask partially with slurry and weigh (M_2).
- Fill up the remainder of the flask to the graduated mark with water and weigh (M_3).

- Empty the flask, clean and fill with water to the same graduated mark, and weigh (M_4).
- The procedure is repeated at least three times to check the accuracy of testing.
- The relative density (S_m) is defined as:

$$S_m = \frac{\rho}{\rho_w} \qquad 3.6$$

and can also be written as:

$$S_m = \frac{\text{Mass of slurry sample}}{\text{Mass of equal volume of water}}$$

$$\therefore S_m = \frac{M_2 - M_1}{(M_3 - M_2) - (M_4 - M_1)} \qquad 3.7$$

From Equation 3.6:

$$\rho_m = S_m \rho_w \qquad 3.8$$

3.4.3 Slurry temperature

The temperature of the slurry is measured at two positions in the pipe loop with thermocouples. The two positions are at the end of the first heat exchanger, that is, just before the pipe viscometer, and the second is at the inlet to the large fume. Both thermocouples are directly linked to the data acquisition unit that reads the temperature in degrees Celsius. As the data acquisition unit reads the thermocouple directly, no signal calibration is required. The heat exchangers are linked to a central water-cooling system. The accuracy of the thermocouples, according to the manufacturer's specification, is in the order of 1 degree Celsius. The temperature was only monitored to try to stay within a range during tests. Most of the tests were done during the winter

months. The slurry temperature during the tests varied from 19-25 degrees Celsius. The pumps did heat up the slurries that were tested but the cooling system kept them from rising above 25 degrees. During any test the temperature did not vary more than 2 degrees. The effect of temperature on the tests was therefore deemed negligible.

3.4.4 Particle size distribution

No particle size distribution could be done at the Flow Process Research Centre. The particle size distribution test data for the kaolin was obtained from the suppliers. The test was done in a Microtek Sedigraph 5100 X-ray particle sizer. The particle size distribution of the bentonite was done by a local soils laboratory using the ASTM D41/85 for particle size analysis of soils.

The particle size distribution for kaolin and bentonite are depicted in **Figure 3-18** and **Figure 3-19**.

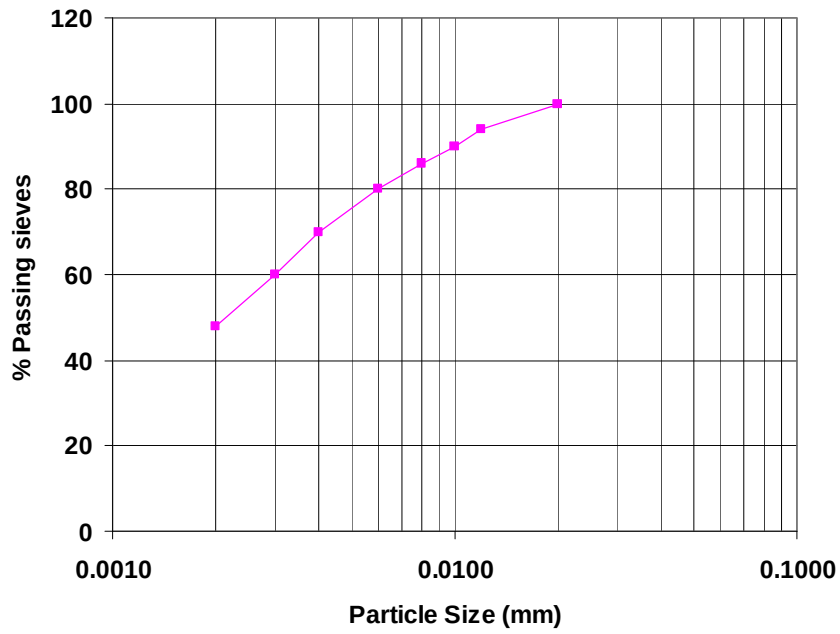

Figure 3-18 Particle size distribution of kaolin

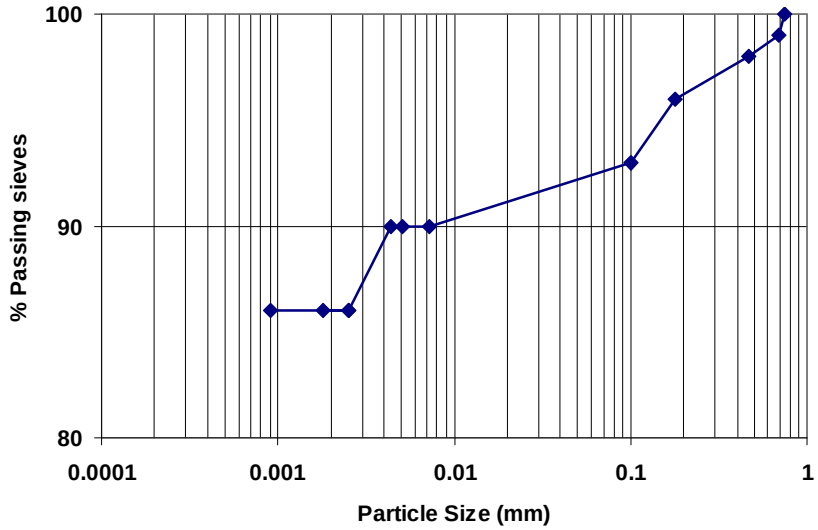

Figure 3-19 Particle size distribution of bentonite

3.4.5 Flume flow depth

A big problem when designing a test flume is the length. To simulate open channel flow in an experimental flume the flow in the test region needs to be fully developed, which means that the flow conditions in that region need to be constant. This is not so easy to obtain when space is restricted. The length of 10 m for the large flume was deemed to be sufficient at design stage from the literature available (Coussot, 1994; De Sutter, Huygens & Verhoeven, 1997). This was also the maximum length that could be fitted in the laboratory.

To investigate the flow development in the flume and also to ascertain in which flume region the flow was the closest to steady uniform flow so that the depth gauges could be fitted in that region, the following tests were conducted.

The flow depth of the 10 m flume was measured at a position 5 m and 6 m from the entrance. A long-section of the free surface was plotted from levels taken at 1 m intervals for various slopes and between 5 m and 6 m the flow was found to be closest to uniform. For a typical set of data see **Figure 3-20**, **Figure 3-21**, **Figure 3-22** and **Figure 3-23** below. The accuracy of the flow depth was estimated to be within 5%. The accuracy depends on the surface of the fluid. In laminar flow for a viscous fluid the accuracy is better than 5%, but in turbulence the fluid level is very difficult to establish as the surface, especially with the less viscous fluids, is very rough owing to turbulence.

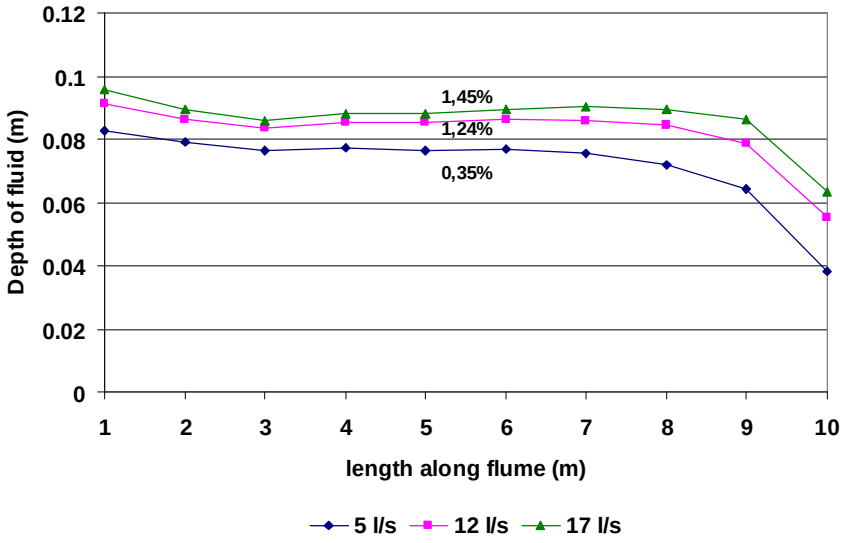

Figure 3-20 Fluid long-section in 300 mm flume for 10% kaolin at a 2 degree slope

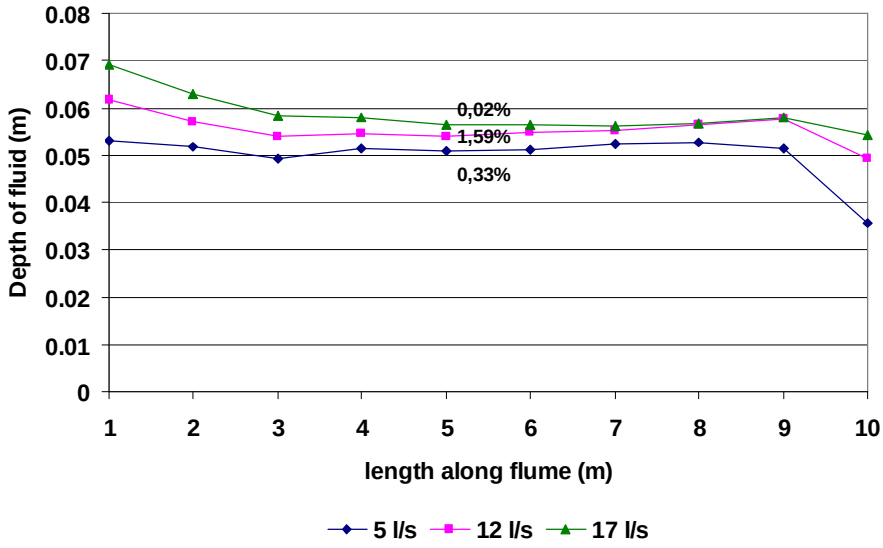

Figure 3-21 Fluid long-section in 300 mm flume for 10% kaolin at a 3 degree slope

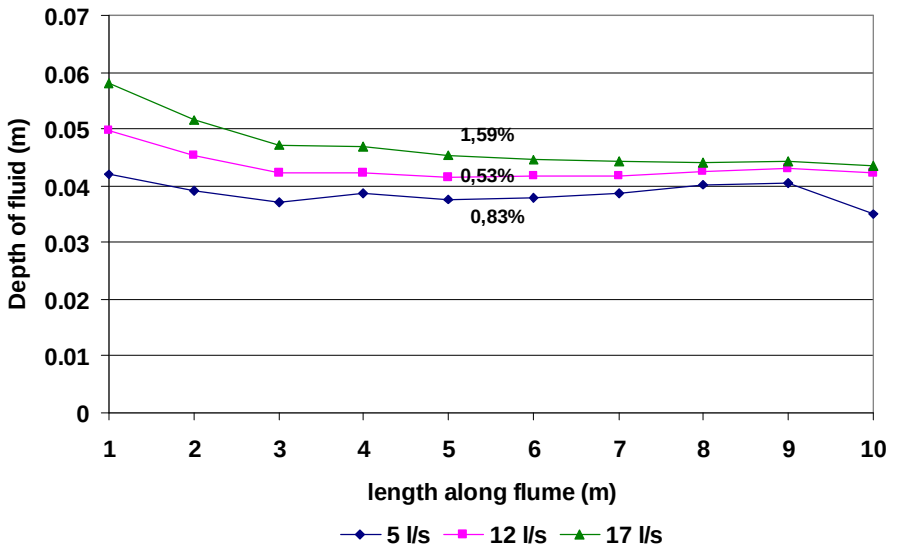

Figure 3-22 Fluid long-section in 300 mm flume for 10% kaolin at a 4 degree slope

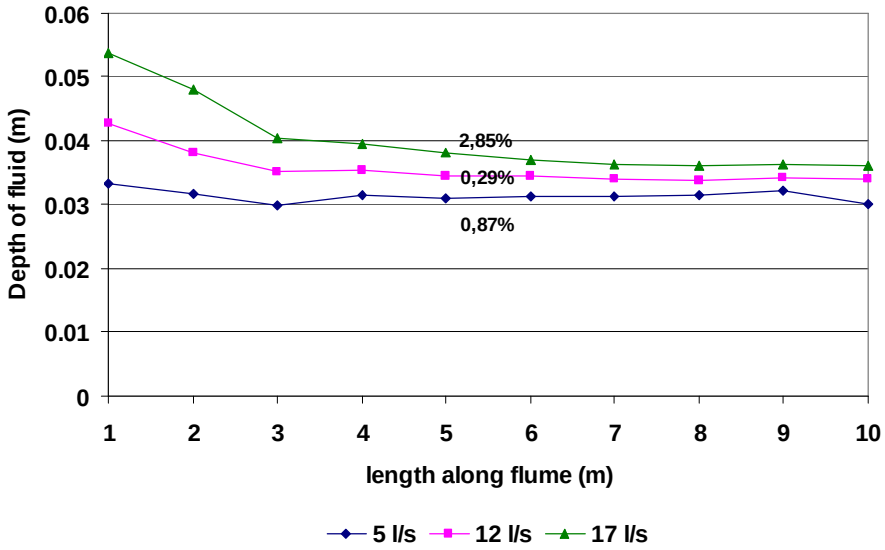

Figure 3-23 Fluid long-section in 300 mm flume for 10% kaolin at a 5 degree slope

On each of the graphs the difference in fluid height between 5 and 6 m along the length of the flume expressed as a percentage is indicated. For the 10% kaolin which was very viscous, the maximum difference was only 2.9%.

From the long-sections above it can be seen that for all the slopes there is an entrance and exit effect, which is very noticeable. The largest entrance effect occurred at 5 degrees' slope and the largest exit effect at 2 degrees' slope. The entrance effect also increased with flow rate whereas the exit effect increased with a decrease of flow rate.

For calculation purposes, the average of the fluid depths at 5 m and 6 m was used in calculations as for that range, over the range of slopes and flow rates used, the difference in surface heights was the least. The 10 m length of the flume is not totally adequate as there is a small difference in flume level between 5 m and 6 m. Taking the

slope of the surface into account is not part of the scope of this research. The length of the flume could not be increased, as the laboratory could not facilitate a longer flume.

3.5 COMBINED ERRORS

Certain derived quantities like pipe diameter, shear stress, shear rate and flow velocity in the flume are dependent on more than one measurement. These measurements all randomly influence the value of the quantity. Slatter (1994) refers to Brinkworth (1968), and Naik (1983) refers to Kline and McClintock (1953), for the same procedure that quantifies this error using a root mean square approach.

The highest expected error ΔX, if X is a function of N quantities is:

$$\left(\frac{\Delta X}{X}\right)=\sum\left(\frac{\partial X}{\partial N}\right)^2\left(\frac{N}{X}\right)^2\left(\frac{\Delta N}{N}\right)^2. \qquad 3.9$$

This is used to calculate the following errors.

3.5.1 Pipe diameter

The internal pipe diameter (D) was accurately calculated using Equation 3.5. By using equation 3.10, the errors calculated for pipe diameter are as follows:

$$\left(\frac{\Delta D}{D}\right)^2=\left(\frac{1}{2}\sqrt{\frac{4}{\pi\rho_w M_w L}}\,\frac{M_w \Delta M_w}{D M_w}\right)^2+\left(-\frac{1}{2}\sqrt{\frac{4M_w}{\pi\rho_w L^3}}\,\frac{L}{D}\,\frac{\Delta L}{L}\right)^2. \qquad 3.10$$

Pipe diameter (mm)	Measurement error $\frac{\Delta D}{D}$ %
13.318	0.106%
28.105	0.050%
80.879	0.017%

3.5.2 Wall Shear Stress

The highest expected error calculating the wall shear stress using Equation 3.11

$$\left(\frac{\Delta\tau_0}{\tau_0}\right)^2=\left(\frac{DP}{4L}\frac{D}{\tau_0}\frac{\Delta D}{D}\right)^2+\left(\frac{D}{4L}\frac{DP}{\tau_0}\frac{\Delta DP}{DP}\right)^2+\left(-\frac{D\,DP}{4L^2}\frac{L}{\tau_0}\frac{\Delta L}{L}\right)^2, \qquad 3.11$$

is graphically displayed in **Figure 3-24**.

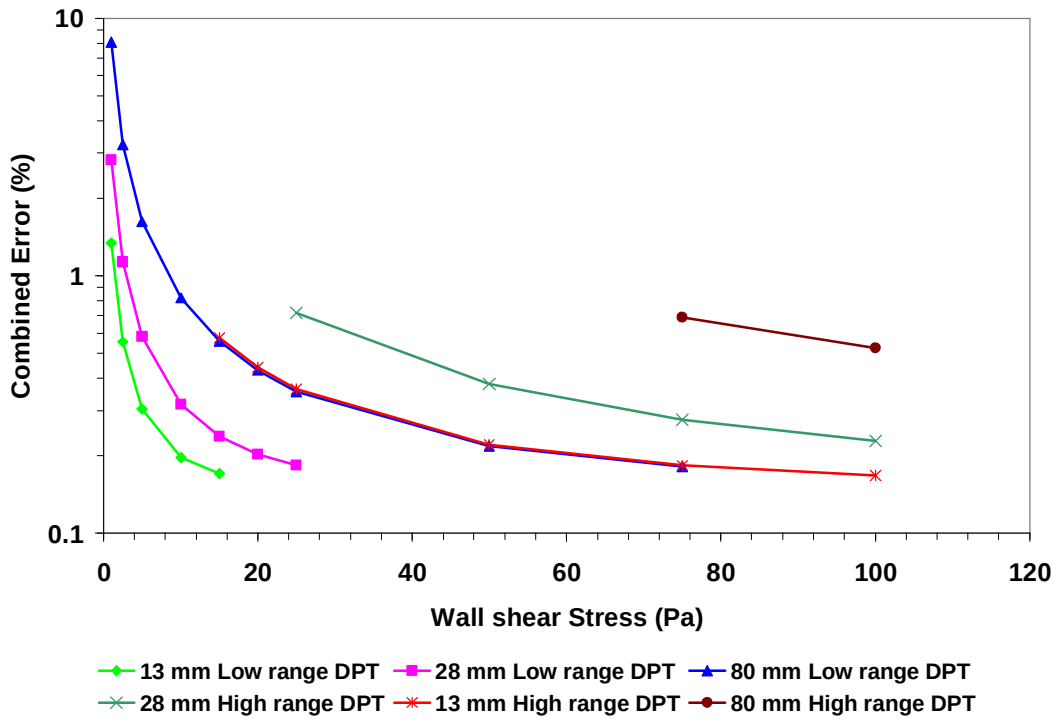

Figure 3-24 Pipe wall shear stress combined error.

The sudden jump in the percentage error occurs when one has to switch from the low range differential pressure transducer (DPT) to the high range DPT. There is a steep increase in error at the very low range, which is expected.

3.5.3 Pseudo Shear Rate

The highest expected error calculating the pseudo shear rate using Equation 3.12

$$\left(\frac{\Delta 8V/D}{8V/D}\right)^2 = \left(\frac{\Delta G}{G}\right)^2 = +\left(-\frac{32Q}{\pi D^3}\frac{Q}{G}\frac{\Delta Q}{Q}\right)^2 + \left(-\frac{96Q}{\pi D^4}\frac{D}{G}\frac{\Delta D}{D}\right)^2 \qquad 3.12$$

is graphically displayed in **Figure 3-25**.

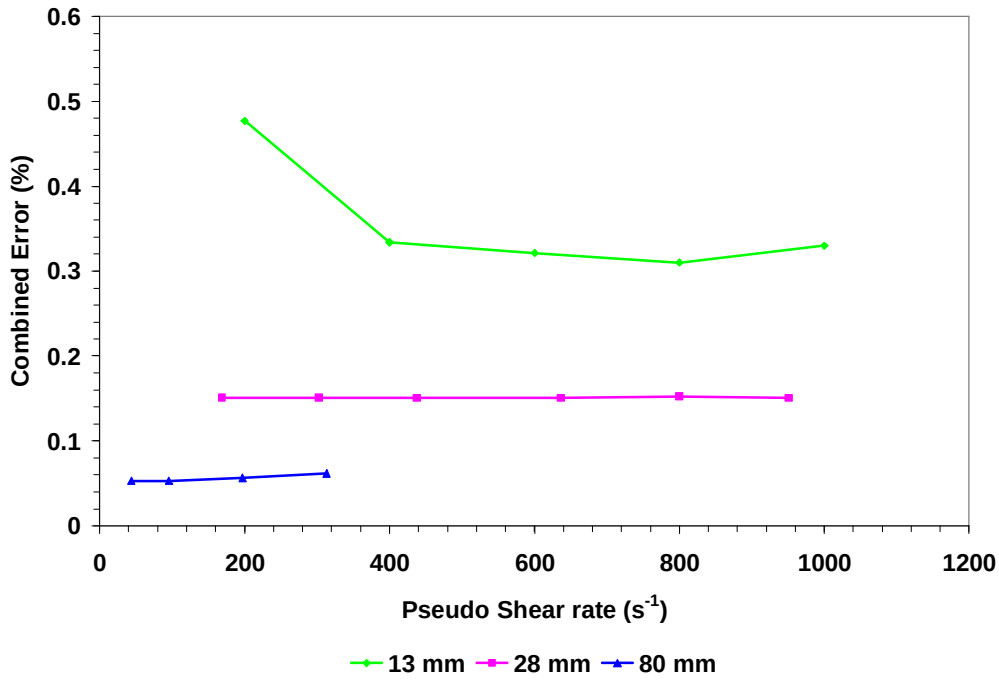

Figure 3-25 Highest combined errors for calculating pseudo shear rate

The combined errors for pseudo shear rate are low because shear rate is only related to the flow measured by the meter output and the diameter of the tube.

3.5.4 Flume Flow Velocity

The flume flow velocity is calculated from the flow rate measured by the magnetic flow meters and the cross-sectional area of the flume.

$$V = \frac{Q}{Bh} \tag{3.13}$$

The highest expected error is calculated from 3.14

$$\left(\frac{\Delta V}{V}\right)^2 = \left(\frac{1}{Bh}\frac{Q}{V}\frac{\Delta Q}{Q}\right)^2 + \left(\frac{Q}{B^2 h}\frac{B}{V}\frac{\Delta B}{B}\right)^2 + \left(\frac{Q}{Bh^2}\frac{h}{V}\frac{\Delta h}{h}\right)^2, \tag{3.14}$$

and is shown graphically in **Figure 3-26**.

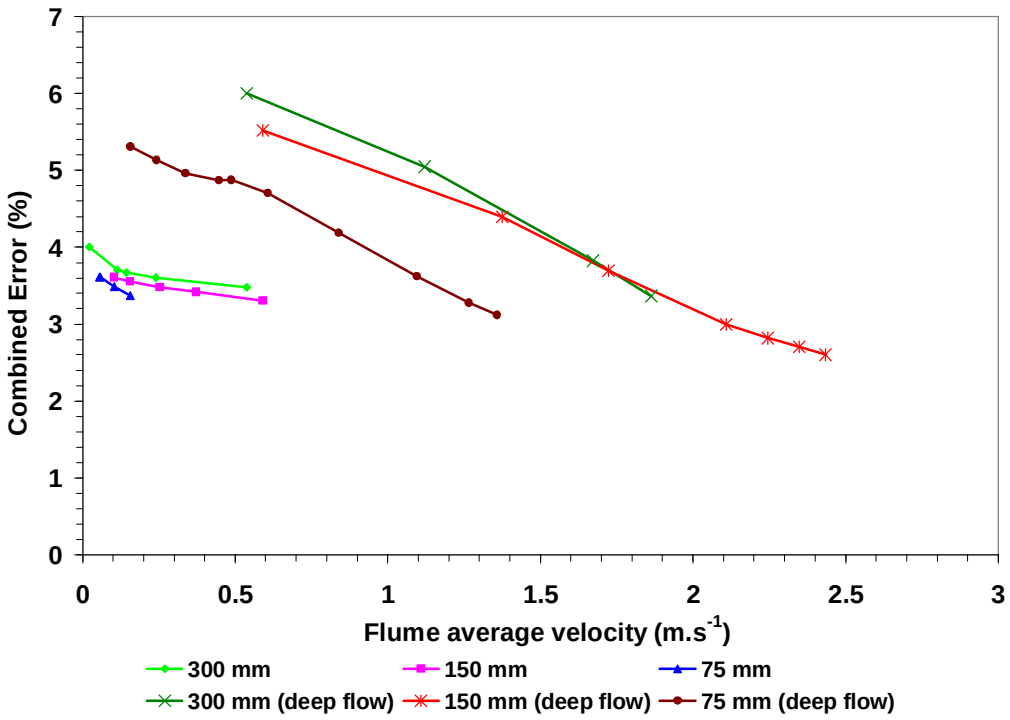

Figure 3-26 Combined errors for flume average velocity

The combined error when calculating flume average velocity is better than 5%. The jump that occurs with increased velocity occurs because the accuracy of measuring the surface level decreases when the surface becomes uneven.

3.5.5 Flume flow depth

The digital depth gauges are accurate to a 0,1 mm. The problem is measuring the flow level of the fluid in the flume especially when the flow is turbulent. It is estimated that the accuracy of flow depth measurement when the flow is laminar and viscous is better than 0,5 mm and when the flow is turbulent and less viscous better than 1 mm. For a flow depth of 20 mm in laminar flow, the accuracy would be 2,5%. If the flow depth is then 50 mm in turbulent flow the accuracy would be 2%. It is very difficult to precisely predict the accuracy of flow depth measurements.

3.6 EXPERIMENTAL PROCEDURES

In this section the experimental procedure pertaining to the tube viscometer rig and the flume rig is presented.

3.6.1 Tube viscometer rig

The procedure that is followed to establish a range of values of Δp and V is as follows. The procedure is the same for all three the tube diameters.

- Before any slurry is tested, the flow meters and the differential pressure transducers are calibrated.
- Water tests are then conducted in all three tubes and the values compared with the Colebrook-White equation.

- About 2 000 litres of slurry are mixed in the main mixing tank until the slurry is well mixed.
- A representative sample is taken and the relative density is calculated. If the required concentration is not achieved, more solids are added and mixed.
- During the mixing process the slurry is circulated through all three tubes so that any water in the system is mixed in the slurry and will not afterwards influence the concentration.
- The pods that prevent solids from entering the differential pressure transducers (**Figure 3-3**) are connected to the pressure tappings. The lines linking the tappings and DPTs are flushed with water. This sometimes has to be repeated during tests when solids start entering the system. The amount of fluid in the system is more than 2000 litres and the volume for flushing is very small. As the rheology was checked on-line, the minute effect of flushing water on overall concentration was not a problem.
- The flow rate is regulated by means of a series of valves, and as the pump cannot achieve the low flow rates, the excess flow is diverted through a by-pass line back into the mixing tank. This helps ensure that the slurry is well mixed.
- The data logger is switched on and the visual basic programme on the PC is activated. The data is exported to an Excel spreadsheet.
- When the correct flow rate is set, the data-logger is triggered and the programme samples flow rates and differential pressures over a preset time interval.
- The average flow rate and differential pressure are exported to the spreadsheet and are visually displayed on a graph plotting wall shear stress against pseudo shear rate.

- This is repeated with a range of flow rates until sufficient data points are available for the pseudo shear diagram.
- The process is repeated for the 13 mm, 28 mm and 80 mm tubes.
- All three sets of data are plotted on one graph, which enables one to see whether there are any obvious errors in the data sets. If the laminar flow data of all three tubes form one line, this also indicates that there is no slip occurring in the lines.

During the flume tests the in-line tube viscometer was used to see whether the rheology changed. This was very important as the tests often took a day to complete.

3.6.2 The flume rig

The procedure that is followed to establish a range of values of flow rate (Q) and fluid depth (h) is as follows. The procedure is the same for all the three flume sizes.

- The flume slope is adjusted to the correct slope with the hydraulic ram for the large flume and with the mechanical screw mechanism of the small flume.
- The slurry is diverted to the flume and is now circulating through the tube viscometer rig and the flume rig. This is to enable one to check whether the rheology of the slurry has changed during the flume test at regular intervals.
- The data logger is switched on and the visual basic programme on the PC is activated. The data is exported to an Excel spreadsheet.
- The two depth verniers are fitted to the flume and connected to the data logger.
- The depth verniers are zeroed on the bottom of the flume.
- When the correct flow rate is set, the depth gauges are manually lowered to the fluid surface.

- The data-logger is triggered and the program samples flow rates over the set time interval.
- The average flow rate and the fluid height recorded by the two depth verniers are exported to the spreadsheet.
- The procedure is repeated for a range of flow rates, as well as for different slopes.
- The spreadsheet contains a Moody diagram and the Reynolds numbers and friction factors are plotted directly on the diagram.
- This enables one to make sure that the range of data points is covered sufficiently.

3.7 MATERIALS TESTED

The materials used in this thesis were selected to represent a wide range of rheological properties. For calibration purposes water was selected and to test laminar flow of Newtonian fluids a sucrose solution was used. The power law fluid selected was Carboxymethyl Cellulose (CMC), which is generally regarded as an ideal solution for experimental work. Bentonite was selected as the Bingham plastic suspension. The yield pseudoplastic suspension selected was kaolin. This material has been used in the Flow Process Research Centre over a very long period and is reasonably stable. Only limited tests were done with another yield pseudoplastic suspension, namely Carbopol.

3.7.1 Water

For calibration purposes ordinary municipal tap water was used. As large volumes of water were used, that was the only option. The properties of tap water are typically the

following: a pH of 9 with a total alkalinity of 35 mg/l as $CaCO_3$, with total Calcium of 35 mg/l as $CaCO_3$ and an ionic strength of less than 0.001 (molar scale) (Loewenthal, 2003). This reflects a fluid which is chemically reasonably stable.

3.7.2 Sucrose solution (sugar)

A 55% per volume sugar solution was made up to obtain a viscous Newtonian liquid. This solution proved very difficult to test as the pump induced a lot of air bubbles which made the test work very difficult. The results were not satisfactory at all.

3.7.3 Carboxymethyl Cellulose (CMC)

Several solutions of CMC, a polymer solution which is an industrial thickening agent, were prepared. The polymer was mixed with water to produce a pseudoplastic solution. At one stage in the test programme a bactericide was used to prevent bacterial action but this influenced the rheology drastically and therefore it was not used again. The CMC was replaced when any bacterial action was noticed. All the concentrations were tested in the pipe viscometer and the rheometer to obtain the rheological parameters and then tested in the flumes.

3.7.4 Bentonite

Bentonite powder was used to prepare different concentration bentonite:water suspensions. The concentrations varied from 3-6% per volume. The particle size distribution is depicted in **Figure 3-19**. All the concentrations were tested in the pipe viscometer and the rheometer to obtain the rheological parameters and then tested in the flumes.

3.7.5 Kaolin

Dry kaolin powder was used to prepare the kaolin:water suspensions. The kaolin was obtained from one source. Different concentrations were prepared ranging from 3-10% per volume. The particle size distribution is depicted in **Figure 3-18**. All the concentrations were tested in the pipe viscometer and the rheometer to obtain the rheological parameters and then tested in the flumes.

3.7.6 Carbopol Solution

Carbopol® is a registered trademark for a family of polymers that are used as thickeners, suspending agents and stabilisers. They are utilised in a wide variety of personal care products, pharmaceuticals and household cleaners. Most Carbopol polymers are high molecular weight acrylic acid chains, usually cross-linked, and are available as powders or liquids (http://www.admix.com/carbopol.htm). (Admix. 2002).

Carbopol is a polymer and mixed with water becomes an aqueous solution. A 1% concentration was prepared and tested in the small flume as part of a pilot study. Carbopol solution is a yield pseudoplastic fluid and because it very expensive and entrains air when mixed, was difficult to test. For these reasons it was only used in the initial tests. Only a few test results will be shown.

3.8 RESULTS AND DISCUSSION

The flume data is presented in Appendix D. The flow rate, flow depth and slope as well as the rheological parameters are presented in tabular form for all the tests.

The results are also presented in Appendix A in two sections.

Section A.1 contains tables with all the relevant fluids properties, as well as the rheograms. An example of the fluid properties of one concentration is given in **Table 3-3** below.

Table 3-3 Slurry properties of 5.4% kaolin

SLURRY PROPERTIES	**5.4% KAOLIN**
Solids Relative Density	2.65
Slurry Relative Density	1.090
Volumetric Concentration	5.4%
Yield Stress	4.985 Pa
Fluid Consistency Index	0.0297 $Pa.s^n$
Flow Behaviour Index	0.717
Apparent viscosity (100 s^{-1})	0.058 Pa.s
Apparent viscosity (500 1^{-1})	0.015 Pa.s

An example of a rheogram for 5.4% kaolin is given in **Figure 3-27**.

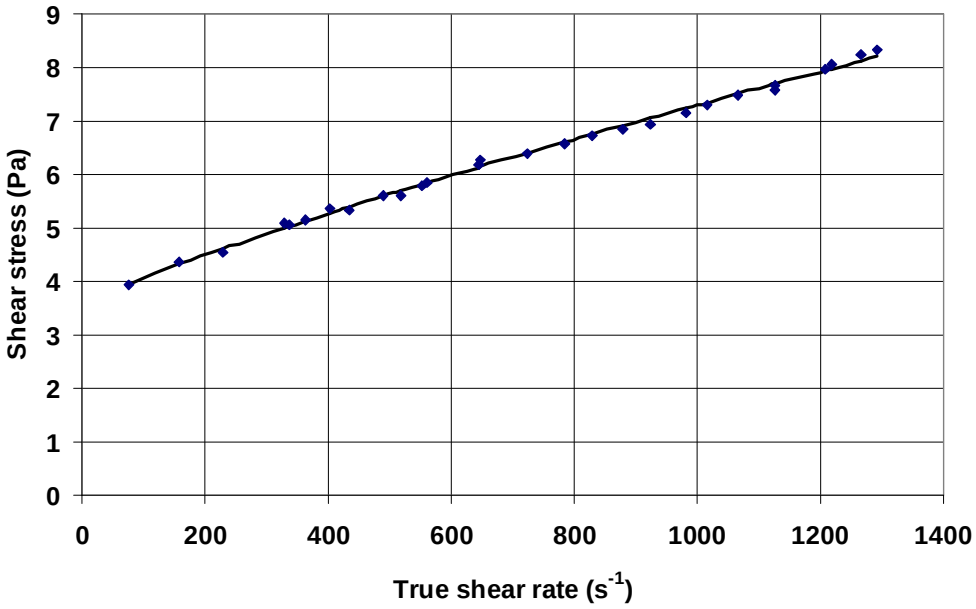

Figure 3-27 Rheogram of 5.4% kaolin

Section A.2 contains the Moody diagrams for all the fluids tested.

An example of the Moody diagram is given in **Figure 3-28**.

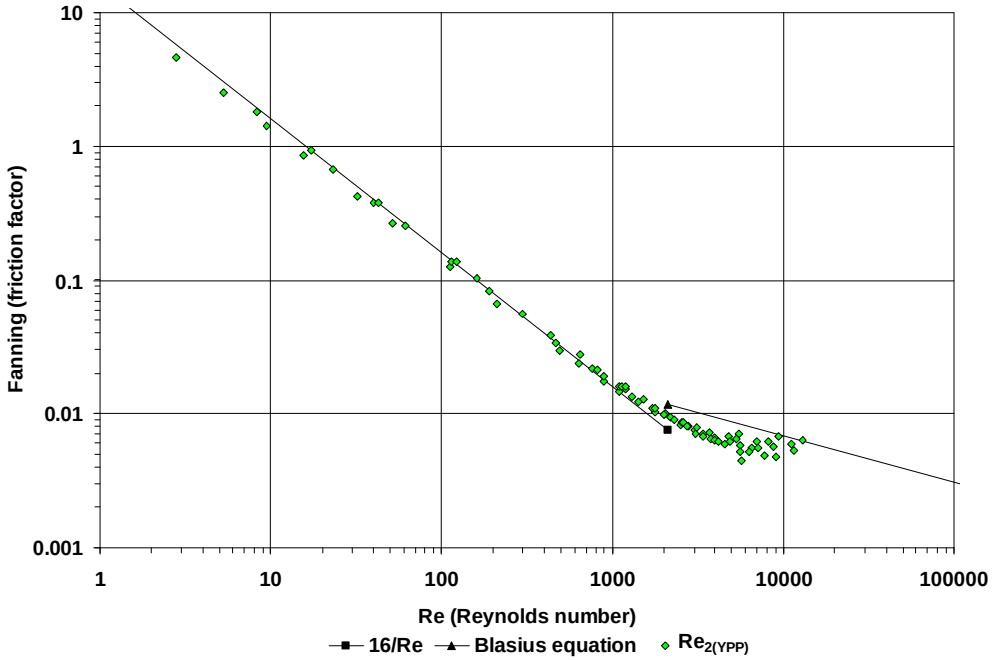

Figure 3-28 Moody diagram of 5.4% kaolin in 150 mm flume

The Moody diagram presents the Fanning friction factor plotted against the Re_2 Reynolds number indicating the laminar flow region depicted by the 16/Re line and the turbulent water line predicted by the Blasius equation.

3.9 GENERAL OBSERVATIONS

The following empirical flow characteristics were observed during the experimental phase of this research project.

3.9.1 Flow behaviour

From the outset it was the intention to depict the flow regions on the Moody diagram as it is well known and has been successfully used for Newtonian open channel flow.

The problem with non-Newtonian open channel flow is that the rheological classification of a fluid can involve three rheological parameters, which makes the non-Newtonian Reynolds number more complicated than the Newtonian one.

- In laminar flow the 16/Re line was used to collapse the different laminar flow data by using the hydraulic radius instead of the diameter as for pipe flow (see **Figure 3-28**).
- For the less viscous concentrations the traditional jump in friction factor in the transition region of Re =2 000-3 000 was observed similar to that of water (see **Figure 3-35**). This jump was difficult to establish as there were intermittent turbulent puffs occurring which created an irregular surface. As the frequency of these irregularities on the surface increased with an increase in flow rate, a point

was reached where the flow height was measured on top of the irregularities, which then signalled the jump to full turbulence.

- The difference between pipe flow and open channel flow became very obvious when a deviation from the 16/Re lines was observed for more viscous fluids at lower Reynolds numbers than the traditional transition region around Re = 2 000 (see **Figure 3-33**).
- The more viscous the fluid became, the smoother the transition region became, and the lower the Reynolds number was where the deviation from the 16/Re line occurred. See **Figure 5-1**.
- It seemed from observations that the critical Reynolds number could not be fixed to a small region but occurred over a wide region of Reynolds numbers depending on the viscous characteristics of the fluid. See **Figure 3-35**, **Figure 3-37** and **Figure 5-1.**
- This phenomenon was the same for three very different rheologically classified fluids, namely CMC, bentonite and kaolin. The first is a pseudoplastic and the latter two are both fluids with a so-called yield stress.
- Transition could not be accurately determined from the Moody diagram. A more useful plot was when the Reynolds number was set against Froude number. The following empirical behaviour could be noticed. There was a clear laminar flow region. The point of inflection indicated the onset of transition. The maximum value of the Froude number indicated the onset of another flow region which seemed to indicate full turbulence. This behaviour was noticed for all the different slopes and fluids. An example is presented in **Figure 3-29**.

- For less viscous fluids in turbulent flow the liquid surface displayed typical surface irregularities, whereas for the very viscous fluids the surface stayed smooth.
- The viscous fluids also did not follow the slope of the Blasius equation in the turbulent region but remained more on a constant friction factor (see **Figure 3-30**).
- The critical Froude number, Fr=1, which for water indicates an unstable region, did not seem to have the same implication for the more viscous fluids.
- In turbulence there seems to be an increase in friction factor with increase in viscosity. This can be observed for different concentrations kaolin in the 150 mm flume all at a 5 degree slope shown in **Figure 3-30**. This could be the particle roughness effect as described by Slatter (1994) for pipe flow and incorporated in his roughness Reynolds number.

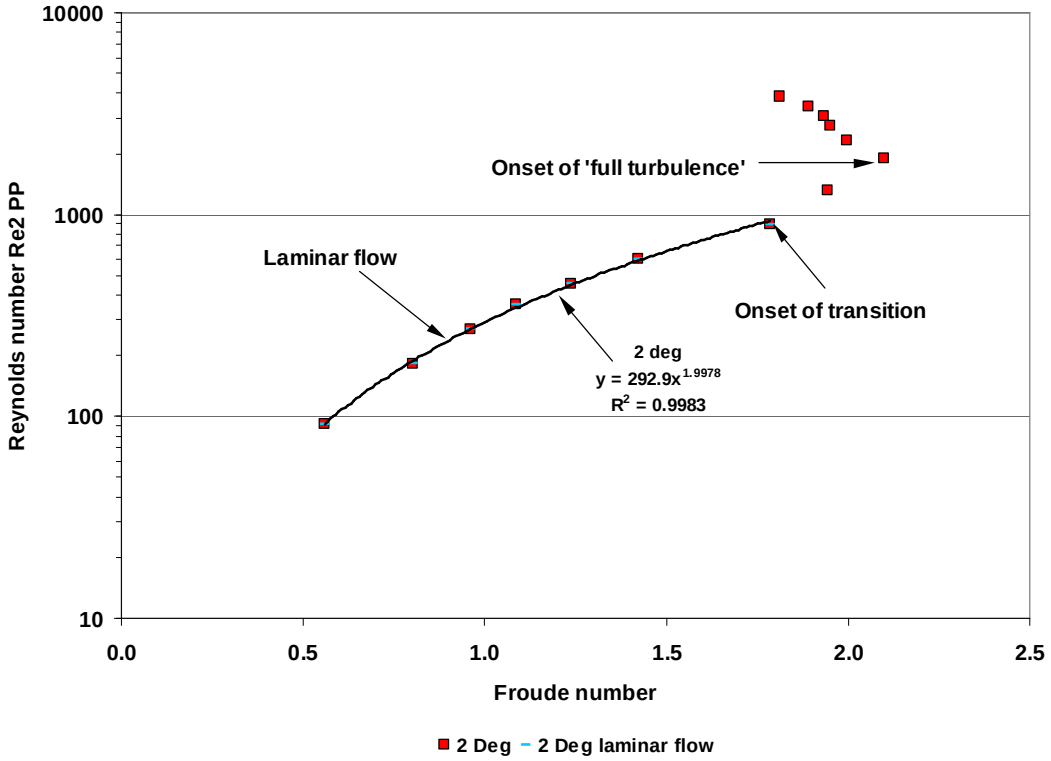

Figure 3-29 Empirical behaviour of 2.8% CMC in 150 mm flume

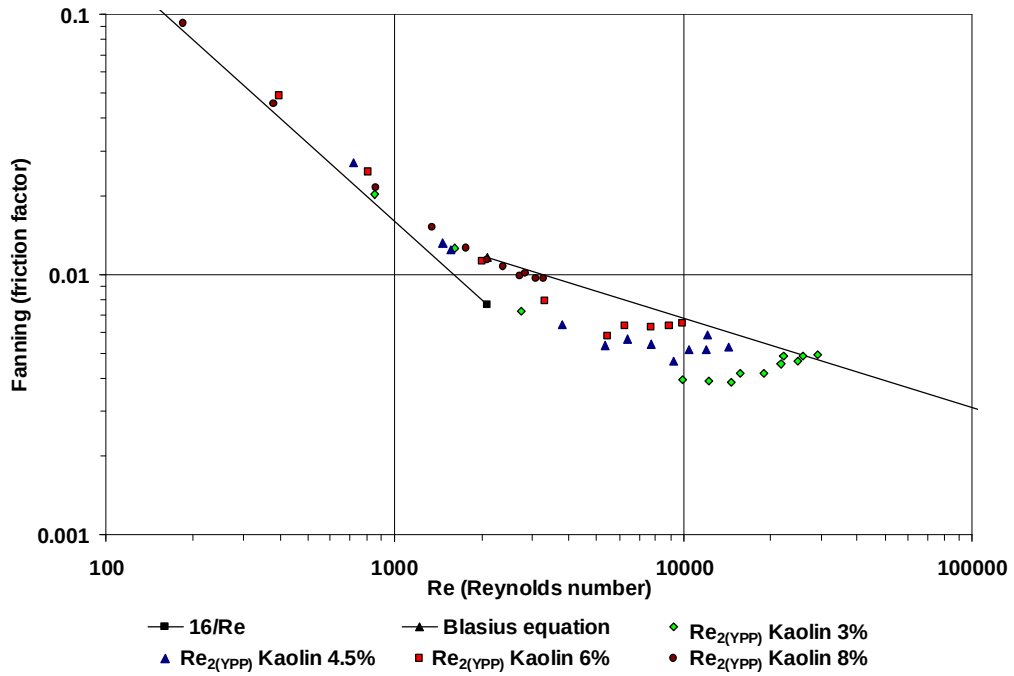

Figure 3-30 Different kaolin concentrations in 150 mm flume at 5 degree slope

3.9.2 Rheological behaviour

The fluids tested were very different from a rheological characterisation point of view. Although they were very different, they displayed similar viscous behaviour in the flume as described above. This is not so unusual if one looks at the following graph, **Figure 3-31**, where the apparent viscosity is plotted against shear rate. At certain shear rates the apparent viscosities for three very different materials are very similar. An example is the apparent viscosity of 1.8% CMC, 4.5% bentonite and 5.4% kaolin at a shear rate of about 260 s^{-1}. This position is indicated by point A on **Figure 3-31**. At that shear rate the apparent viscosity of the three different fluids is within 10% of each other. This ought to indicate similar behaviour of the materials at this specific shear rate.

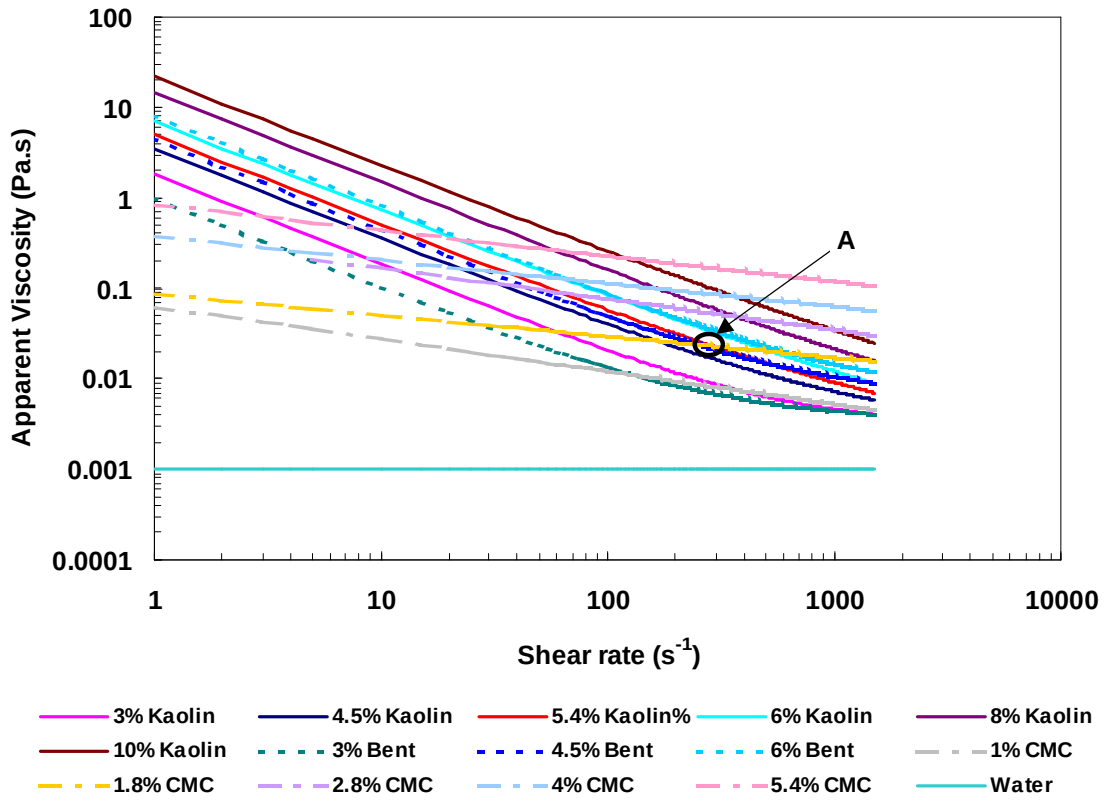

Figure 3-31 Apparent viscosity against shear rate of all the fluids tested

In the following **Figure 3-32**, the fluids with the highest apparent viscosities, namely the 10% kaolin and the 5.4% CMC, are plotted against shear rate together with water. It can be seen that the apparent viscosities between the maximum values at shear rate 100 s^{-1} are vastly different to the viscosity of water. The apparent viscosity of the 5.4% CMC and the 10% kaolin at the same shear rate is very close even though they are very different materials.

A similar behaviour can be noted if the flume data of the two materials are plotted on a Moody diagram. **Figure 3-33** shows that the transition of the two fluids occurs at roughly the same Reynolds number.

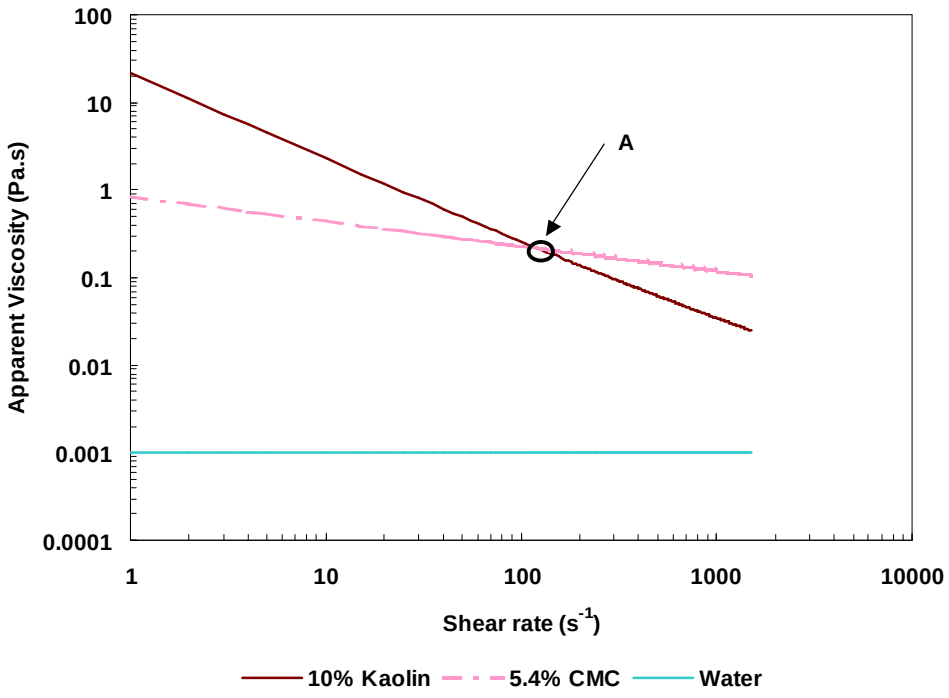

Figure 3-32 Apparent viscosity against shear rate for 10% kaolin, 5.4% CMC and water

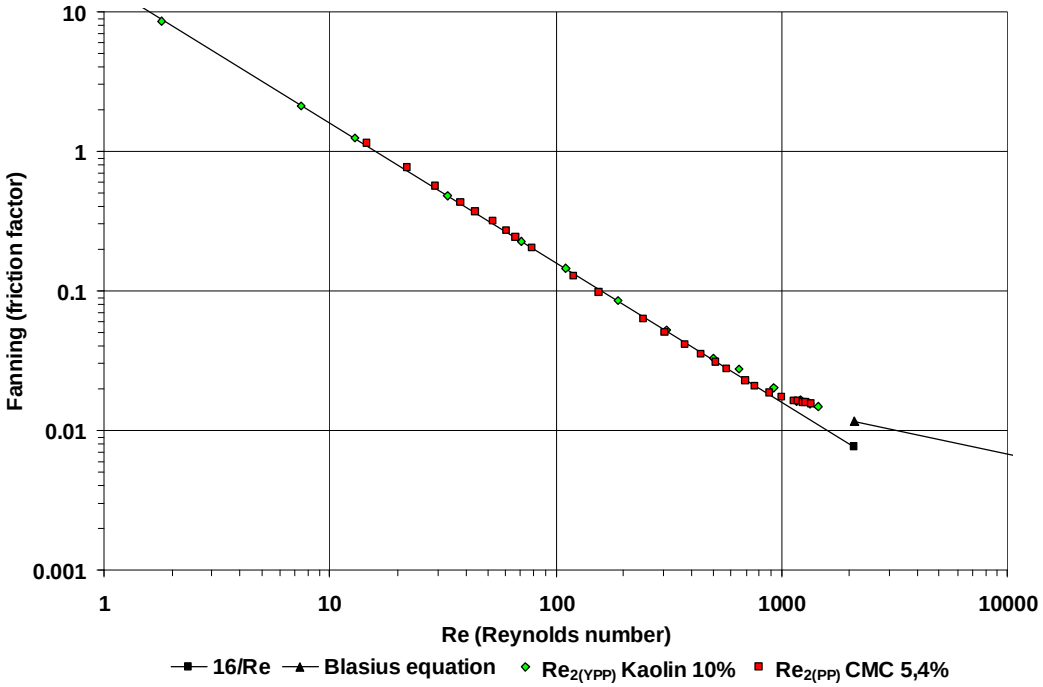

Figure 3-33 Moody diagram: 10% kaolin and 5.4% CMC in 150 mm flume at 5°

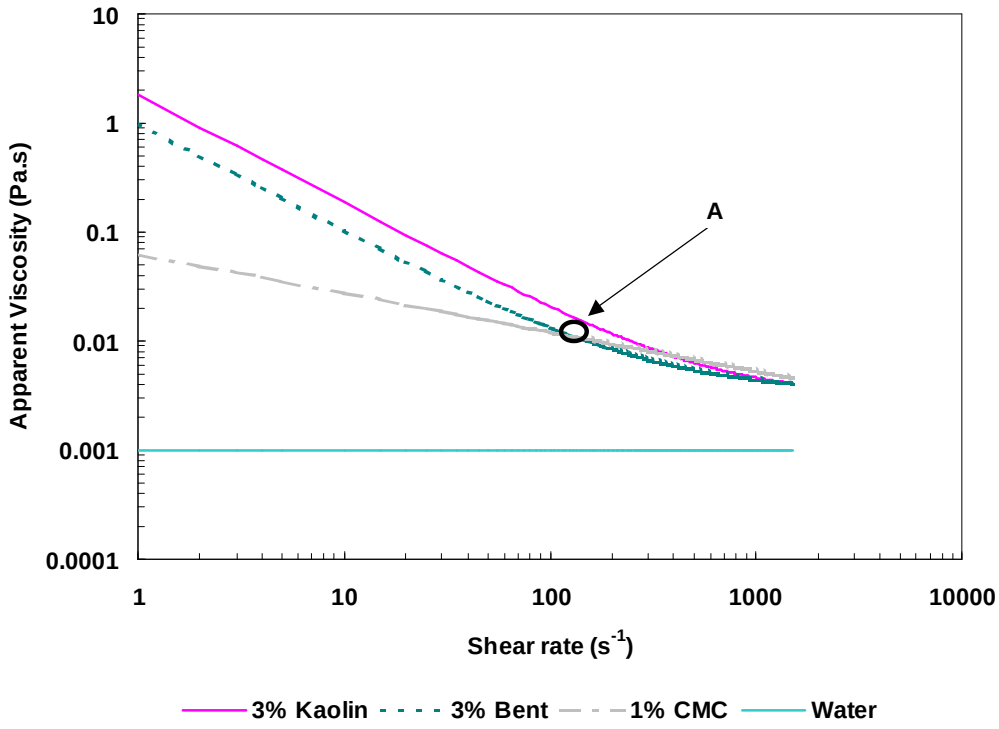

Figure 3-34 Apparent viscosity against shear rate for 3% kaolin, 3% bentonite and 1% CMC

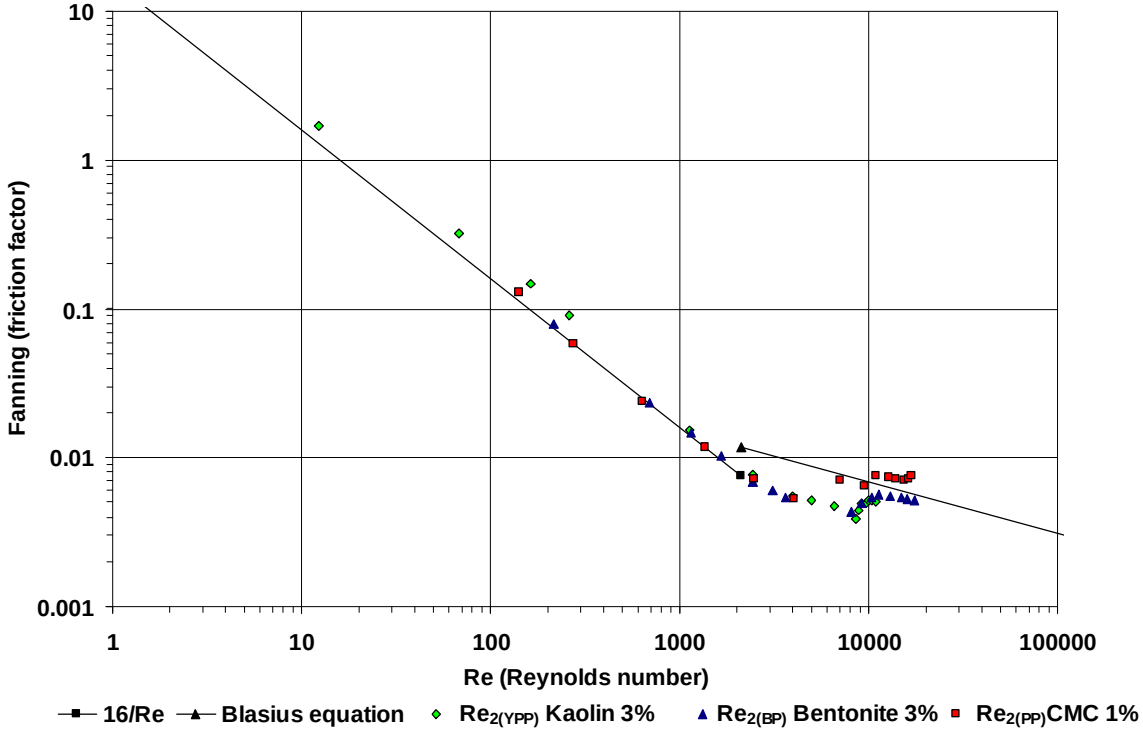

Figure 3-35 Moody diagram: 3% kaolin, 3% bentonite and 1% CMC in 150 mm flume at 3°

Figure 3-34 shows the apparent viscosity against the shear rate for the fluids with the lowest apparent viscosities and again at a shear rate of 100 s^{-1}, the apparent viscosity is very similar.

If one considers **Figure 3-35**, the Moody diagram depicting the flow of three different fluids, namely 3% kaolin, 3% bentonite and 1% CMC at the same slope of 3 degrees and in the 150 mm flume, the flow behaviour is again very similar. The transition is very similar to that of water. This is because the fluids are not very viscous, and therefore very nearly Newtonian in behaviour.

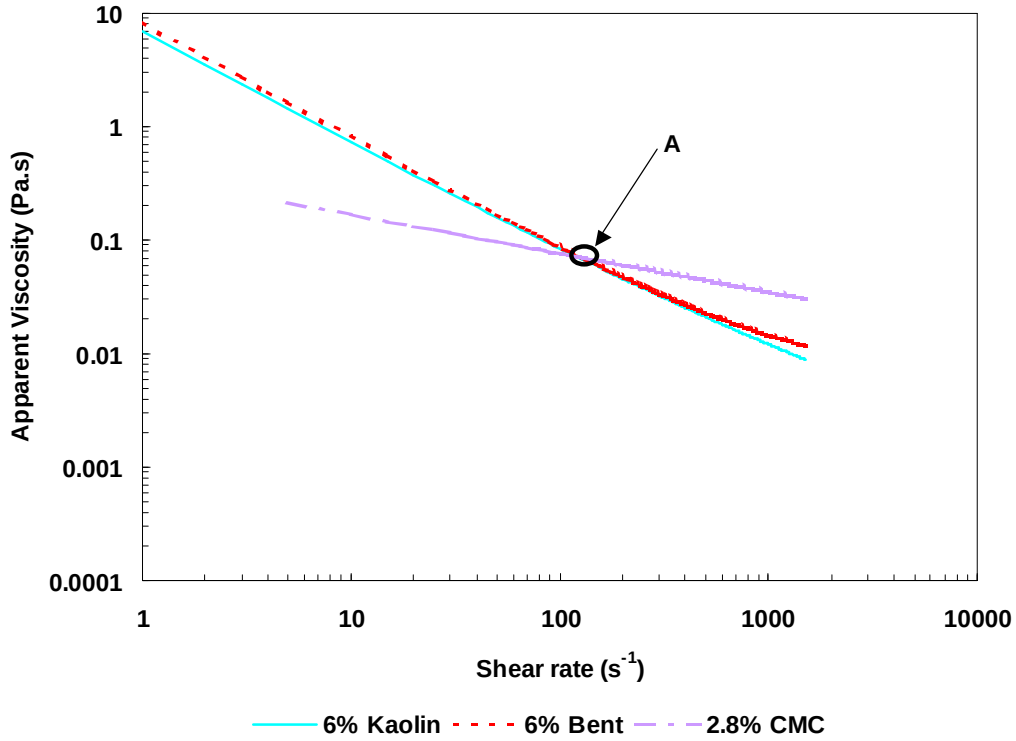

Figure 3-36 Apparent viscosity against shear rate for 6% kaolin, 6% bentonite and 2.8% CMC

Figure 3-36 depicts the apparent viscosity against shear rate of 6% kaolin, 6% bentonite and 2.8% CMC. At a shear rate of 100 s^{-1} it can be seen that the fluids again have similar apparent viscosities.

The Moody diagram in **Figure 3-37** again shows that for the 6% kaolin, 6% bentonite and 2.8% CMC in the 150 mm flume at 2 degrees, the laminar and transitional flow behaviour is very similar.

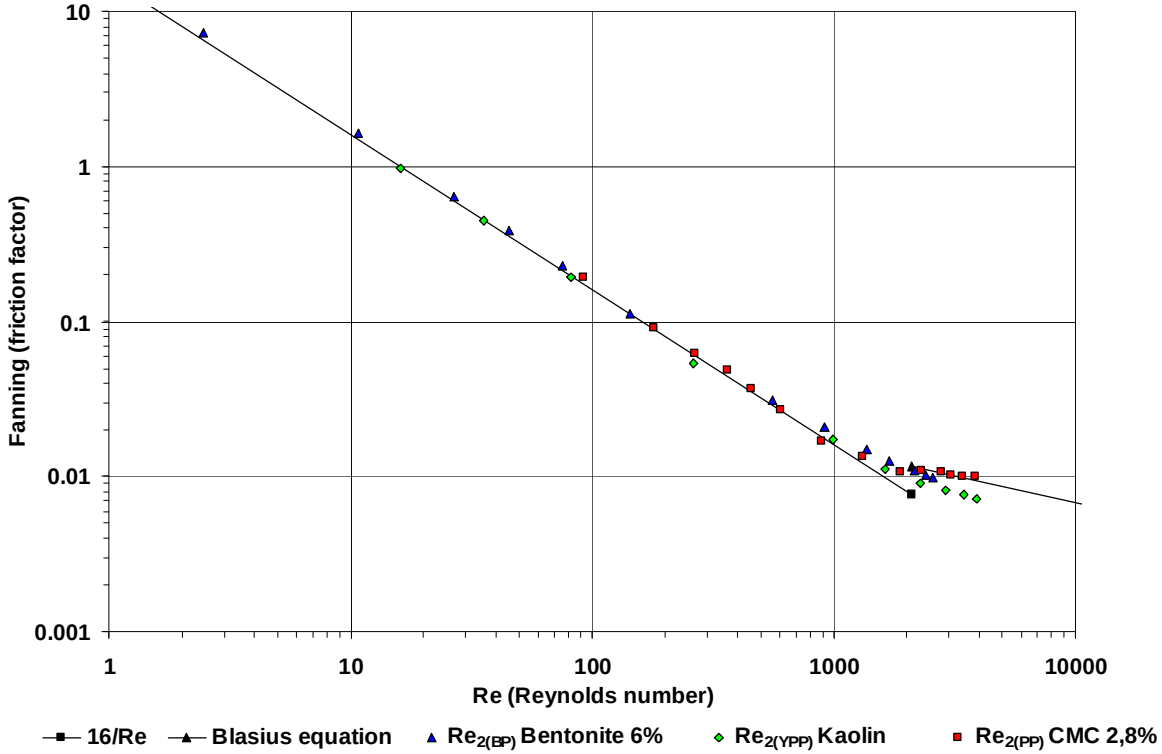

Figure 3-37 Moody diagram: 6% kaolin, 6% bentonite and 2.8% CMC in 150 mm flume at 3˚ slope

All the data presented in **Figure 3-32** to **Figure 3-37** indicate that although the materials tested are rheologically very different, they have similar apparent viscosities at certain shear rates and that these fluids show similar open channel flow behaviour especially in laminar flow and in the transitional region. The transitional behaviour is not the same: for the less viscous materials, more Newtonian-like behaviour is seen and for the highly viscous materials, the transition occurs earlier and is much smoother.

3.10 CONCLUSIONS

3.10.1 Flow behaviour observations

Most of the observations pertaining to the test work are described in Section 3.9.

In conclusion the following needs to be added:

- **Empirical behaviour**

The difference between pipe and open channel flow behaviour was very noticeable. The behaviour of more viscous fluids especially in the transition region was very different to that of the more Newtonian fluids.

The effect of the slope on the onset of transition was also noted.
When the Reynolds number was plotted against the Froude number the effect was even more noticeable (see **Figure 5-7**).

When the Froude number is one, Newtonian open channel flow is described as critical. For the higher concentrations the viscous forces seemed to be so dominant that the significance of Fr=1 did not seem to be relevant. For these concentrations the surface during transition stayed smooth.

3.10.2 Experimental equipment and procedures

All the equipment discussed in this thesis was designed and built for this project with the exception of the existing 75 mm flume, which was only modified.
The equipment includes a tube viscometer with 3 diameter tubes linked to a 300 mm tilting flume as well as a 75 mm tilting flume. The 300 mm flume was designed to be partitioned to form a 150 mm wide flume.

A unique feature of this experimental facility is that the pipe viscometer is in-line in series with the flumes.

The equipment was equipped with all the necessary instrumentation to measure flow rates, differential pressure, temperatures and flow depths.
Software was developed to sample the data and log it in spreadsheets where the results were displayed in graphical format for user-friendly interface between operator and test rig.

The equipment was commissioned with clear water tests.

Calibration and test procedures were developed to accurately produce pipe flow data to establish relevant rheological parameters of all the suspensions and polymer solutions tested.

In addition flume data was obtained over a wide range of flow rates and slopes in three different size flumes.

The experimental errors pertaining to the tube viscometer and the flumes have been analysed and discussed and are deemed to be within acceptable limits.

Several concentrations of bentonite and kaolin suspensions and polymer solutions CMC and Carbopol were used for the tests. This yielded a wide range of rheological properties.

The database compiled was used to evaluate the limited models available in literature and these are presented in Chapter 4. The database was also used to develop, test and

present the new design procedure developed in this thesis. This is presented in Chapters 5 and 6.

CHAPTER 4

ANALYSIS OF RESULTS USING MODELS FROM THE LITERATURE

4.1 Introduction

This chapter will evaluate appropriate models found in the literature using the database compiled for this thesis. It will be shown that as far as can be ascertained, nobody has used materials with such a variation in rheological characteristics, and over such a wide range of slopes and flow rates covering laminar and transitional flow, as well as turbulence, as has been presented in this thesis.

In this chapter the three flow regions will be examined in separate sections namely:

- laminar flow
- the transition from laminar to turbulent flow
- turbulent flow.

The flow of non-Newtonian slurries in open channels can be divided into three flow regimes: laminar flow, turbulent flow and the transition zone in between the two regimes. These flow regimes have been presented by many authors, for both pipe and open channel flow on the standard Moody diagram where the friction factor is plotted against the Reynolds number on logarithmic scales.

4.2 ERROR PRESENTATIONS

When comparing models in laminar flow, the friction factor deviation will be used because the 16/Re line is at a steep slope on the Moody diagram. In turbulence the predicted velocity will be compared to the experimentally measured velocity. This is because the friction factor slope is very flat in this flow region.

To present an objective measure of comparison between two models, the log standard error will be used. The log standard error, LSE, was found to be useful to compare models by Lazarus and Nielson (1978), and is defined as follows:

$$\mathrm{LSE} = \frac{\sqrt{\sum \left(\log(V_{obs}) - \log(V_{calc})\right)^2}}{N-1}. \qquad 4.1$$

In addition to the LSE, the average percentage deviation as well as maximum and minimum deviations will be presented. This will help to present and quantify certain trends.

4.3 LAMINAR FLOW

There are a number of authors who have presented work in the laminar region for open channel flow. Most of them have concluded, without experimental verification, that one should be able to use pipe analysis and translate that by means of the equivalent diameter to open channel analysis (Chow, 1959). For laminar flow there seems to be some evidence that this may be true.

4.3.1 Work done by Kozicki and Tiu

The study of shape effect is not really part of this thesis as only rectangular shaped

flumes are used, but as Kozicki and Tiu (1967) did produce Reynolds numbers for rectangular shaped flumes for Bingham and power law fluids, it was decided to evaluate them.

4.3.1.1 Shape factors

The shape factors a and b they propose to account for the side wall effects are defined as follows:

$$a = 0{,}5\left(\frac{\lambda}{1+\lambda}\right)^2\left(1-\frac{32}{\pi^3}\sum_0^{\infty}\left(\frac{(-1)^n}{(2n+1)^3}\left(\frac{1}{\cosh\frac{(2n+1)}{2}\pi\lambda}\right)\right)\right)^{-1} \qquad 2.82$$

with:

$$\lambda = {}^{B}\!/_{h} \qquad 2.83$$

and:

$$b = a(3\varphi - 1) \qquad 2.84$$

$$\varphi = \frac{\left(1-\frac{32}{\pi^3}\sum_0^{\infty}\left(\frac{(-1)^n}{(2n+1)^3}\left(\frac{1}{\cosh\left(\frac{(2n+1)}{2}\pi\lambda\right)}\right)\right)\right)}{\left(1-\frac{192}{\pi^5}\frac{1}{\lambda}\sum_0^{\infty}\left(\frac{1}{(2n+1)^5}\right)\tanh\left(\frac{(2n+1)}{2}\pi\lambda\right)\right)} \; . \qquad 2.85$$

4.3.1.2 Reynolds number for pseudoplastic or power law fluids

The Reynolds number that Kozicki and Tiu (1967) propose for a power law fluid in a rectangular flume is as follows:

$$Re_{K\&Tiu\,(PP)} = \frac{\rho V^{(2-n)} R_h^n}{2^{n-3} K\left(\frac{a+bn}{n}\right)^n} \quad . \qquad 2.85$$

The power law fluid that was used in this thesis was CMC and various concentrations were tested in the three flumes.

The results were plotted on the Moody diagram and were compared with the Reynolds number used in this thesis without taking the effect of shape into account. This Reynolds number is derived in Chapter 5 (Section 5.2).

$Re_{2(PP)}$ for a power law fluid is as follows:

$$Re_{2(PP)} = \frac{8\rho V^2}{K\left(\frac{2V}{R_h}\right)^n} . \qquad 5.8$$

The deviation from the 16/Re line, which depicts laminar flow, was calculated for each point and compared. The frequency depicted on the y-axis is the number of data points. Over the range of concentrations, slopes, flow rates and flumes tested, $Re_{2(PP)}$ was more accurate than the Reynolds number proposed by Kozicki and Tiu (1967).

The following Figure 4-1, Figure 4-2 and Figure 4-3 depict three sets of CMC data in three different size flumes and indicate the trend described in the previous paragraph.

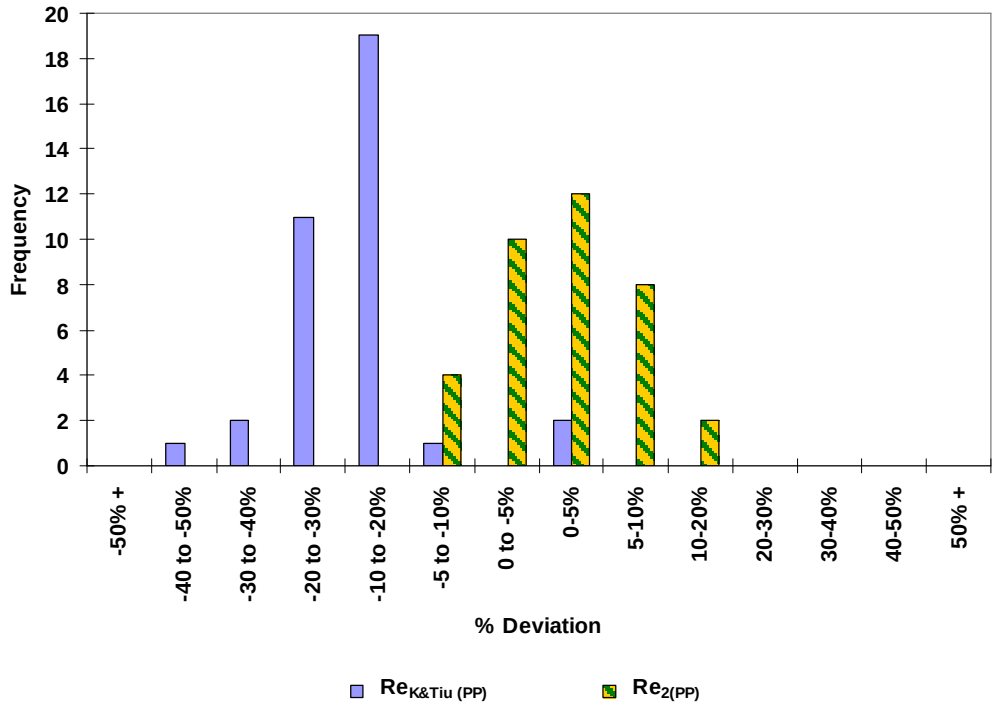

Figure 4-1 Laminar flow of 2.8% CMC in 150 mm flume: shape effect comparison

Table 4-1 Friction factor shape effect comparison. CMC 2.8% in 150 mm flume

Model	T_y	K	n	max % Dev	min % Dev	ave % Dev	LSE
K&T		5.626	0.0293	1.27%	-40.67%	19.14%	0.0139
Re_2		5.626	0.0293	11.32%	-8.86%	4.43%	0.0042

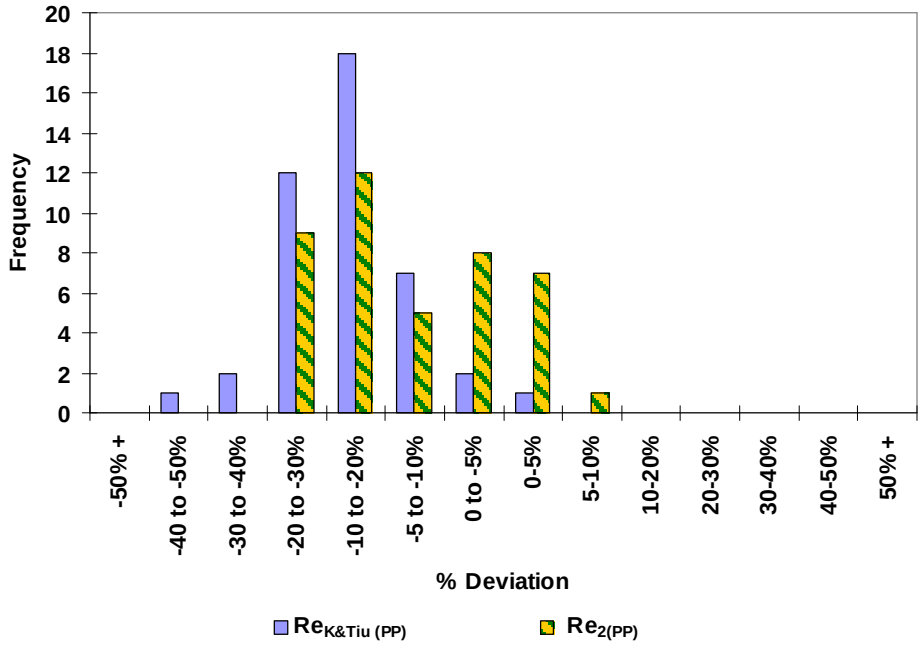

Figure 4-2 Laminar flow of 3.8% CMC in 75 mm flume: shape effect comparison

Table 4-2 Friction factor shape effect comparison. CMC 3.8% in 75 mm flume

Model	T_y	K	n	max % Dev	min % Dev	ave % Dev	LSE
K&T		9.1205	0.0604	1.78%	-38.22%	16.72%	0.0113
Re_2		9.1205	0.0604	7.85%	-29.36%	11.78%	0.0091

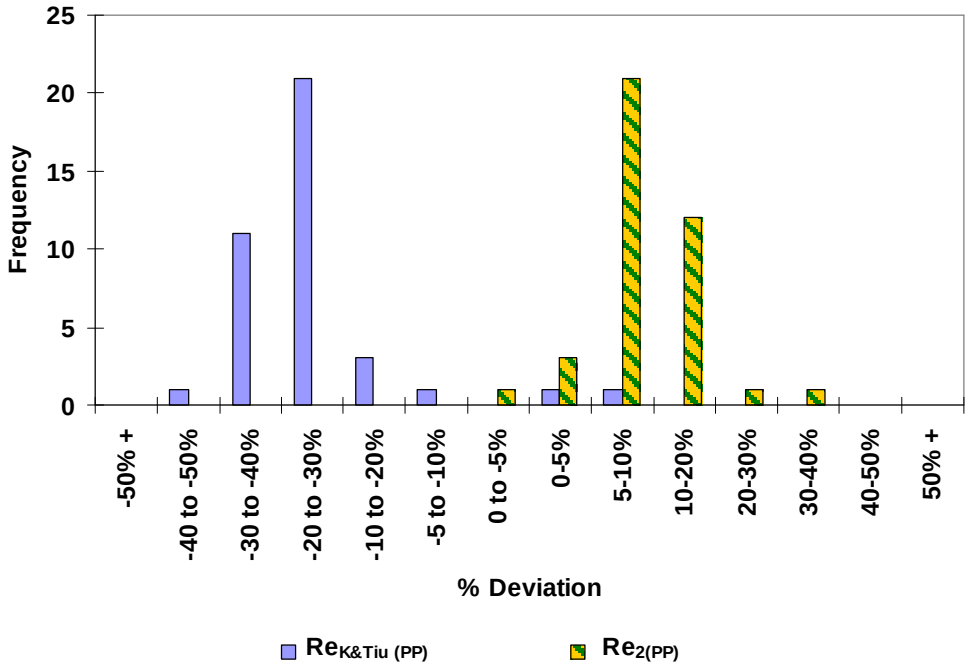

Figure 4-3 Laminar flow of 1.5% CMC in 300 mm flume: shape effect comparison

Table 4-3 Friction factor shape effect comparison. CMC 1.5% in 300 mm flume

Model	T_y	K	n	max % Dev	min % Dev	ave % Dev	LSE
K&T		0.1407	0.0129	5.28%	-46.02%	26.73%	0.0174
Re_2		0.1407	0.0129	32.29%	-1.95%	10.13%	0.0073

From the above **Figure 4-1, Figure 4-2** and **Figure 4-3**, and **Table 4-1, Table 4-2**, and **Table 4-3**, one can conclude that the effect of shape incorporated in the Reynolds number for pseudoplastic fluids as proposed by Kozicki and Tiu is no better than the Reynolds number Re_2 proposed in this thesis. In almost all the data sets, Re_2 performs better than the Kozicki and Tiu Reynolds number. Re_2 is also much less complicated to use, as it does not contain the shape effect calculations.

4.3.1.3 Bingham fluids

For Bingham fluids, Kozicki & Tiu (1967) propose a different Reynolds number, which is as follows:

$$Re_{K\&Tiu(BP)} = \frac{4VR_h\rho}{K}\left[\frac{1}{a+b} - \frac{1}{b}\left(\frac{\tau_y}{\tau_{ave}}\right) + \frac{a}{b(a+b)}\left(\frac{\tau_y}{\tau_{ave}}\right)^{\left(1+\frac{b}{a}\right)}\right] \qquad 2.87$$

with $\tau_W = R_h\rho g \sin\alpha$. 2.50

The Bingham fluid that was used in this thesis was a Bentonite suspension with four different concentrations. Again the Reynolds number proposed was compared to the Reynolds number used in this thesis $Re_{2(BP)}$.

$$Re_{2(BP)} = \frac{8\rho V^2}{\tau_y + K\left(\frac{2V}{R_h}\right)}. \qquad 5.9$$

The results are depicted in Figure 4-4, Figure 4-5 and Figure 4-6, this time on the Moody diagram since the difference in accuracy is very obvious.

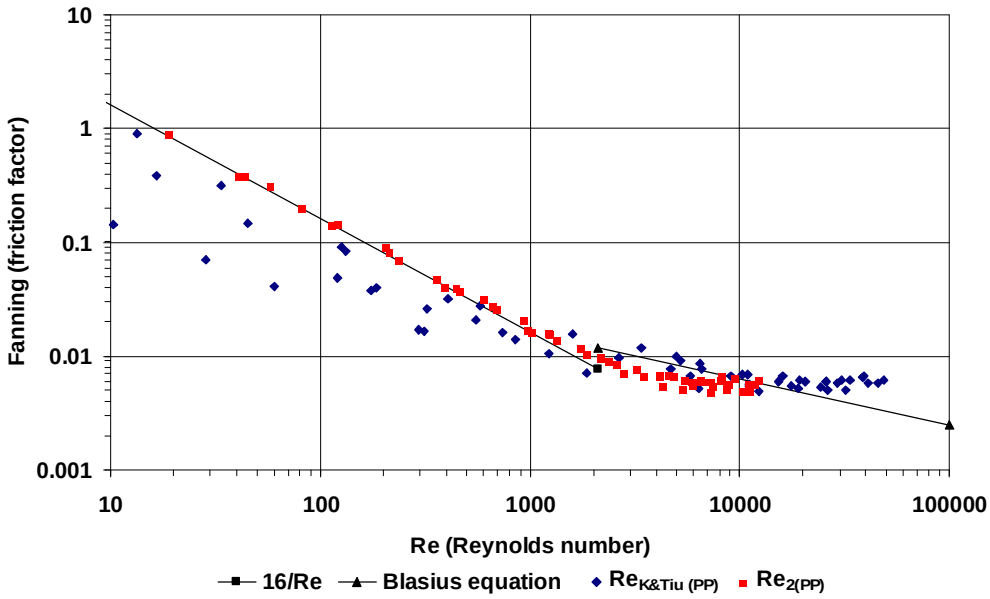

Figure 4-4 Bentonite 4.5% in 150 mm flume (Kozicki & Tiu Reynolds number vs Re_2)

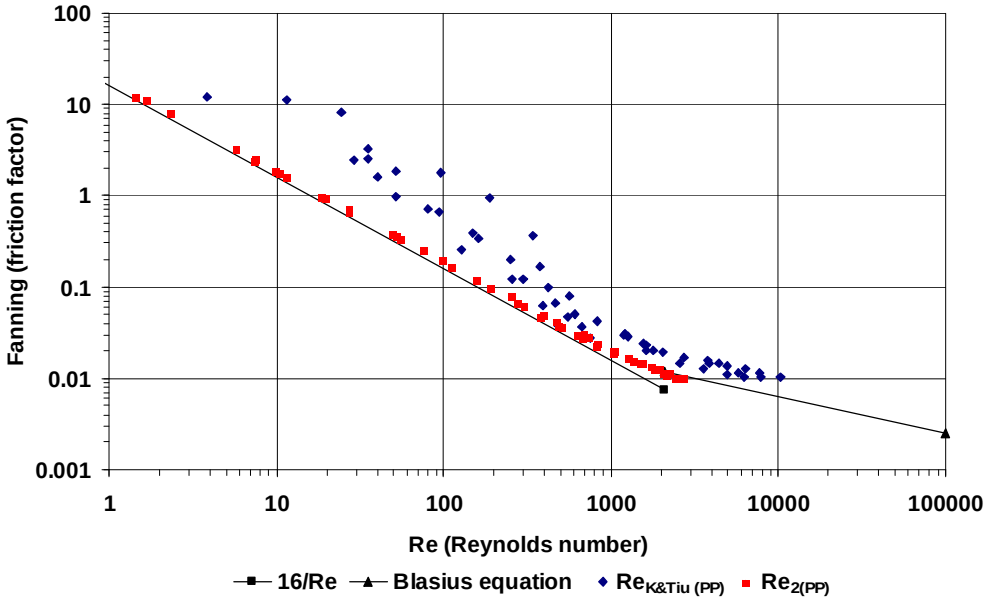

Figure 4-5 Bentonite 6% in 300 mm flume (Kozicki & Tiu Reynolds number vs Re_2)

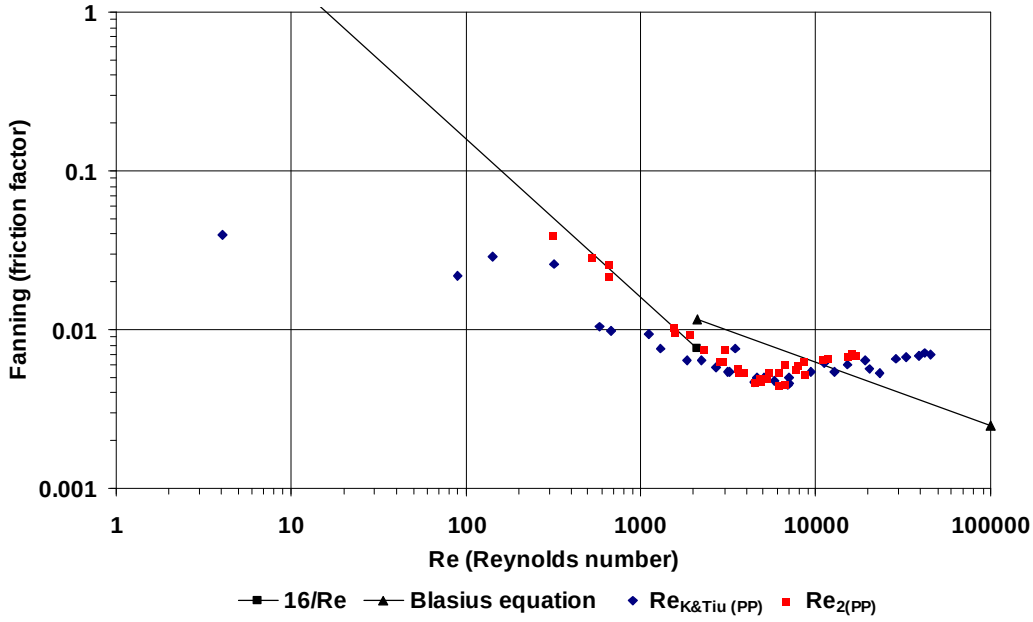

Figure 4-6 Bentonite 3% in 75 mm flume (Kozicki & Tiu Reynolds number vs Re_2)

From the three data sets depicted **Figure 4-4**, **Figure 4-5** and **Figure 4-6**, it can be clearly seen that the Reynolds number proposed by Kozicki and Tiu (1967) for Bingham fluids which incorporates the shape factors, does not fit the data used in this thesis well.

4.3.2 Hyperconcentration flow Research By Zhang And Ren

The laminar flow equation developed by Zhang and Ren (1982), is similar to $Re_{2(BP)}$. The Reynolds number is valid for Bingham fluids and is given as:

$$Re_{Zhang} = \frac{4R_h V}{K + \frac{\tau_y R_h}{2V}} . \qquad 2.88$$

The friction factor was defined as:

$$f = \frac{2gR_h \sin\alpha}{V^2} . \qquad 2.89$$

This Reynolds number is written in a different format than $Re_{2(BP)}$ (Bingham plastic) but when transformed it will be the same.

For the Bentonite tested, which is a Bingham plastic fluid, this Reynolds number works well.

4.3.3 Concentrated mud suspension flow research by Coussot

The design protocol presented by Coussot (1994) is described in Chapter 2. The kaolin suspensions that he used were characterised as a Herschel-Bulkley or yield pseudoplastic fluid. He simplified the fit by fixing n to 0.333.

The database for kaolin suspensions was used to test this design procedure. The values obtained for the velocity were compared to the actual velocities measured. The average difference was 80% with a maximum deviation of 500%. The LSE of the velocity for the kaolin data was 0.0656.

Although Coussot does not use a Moody diagram in his work, the Reynolds number and friction factors were calculated using the velocities obtained from his model. These Reynolds numbers calculated from the predicted velocity using the Coussot model are compared with the Reynolds numbers calculated from the measured velocities and this is presented in **Figure 4-7** below.

The 10% Kaolin suspension tested in the 300 mm flume was used for this comparison.

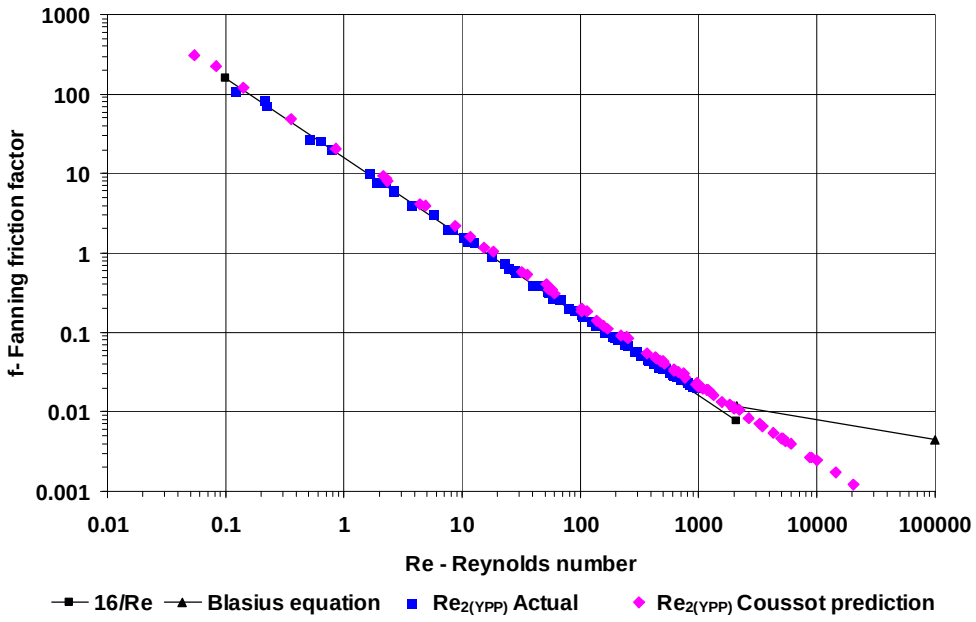

Figure 4-7 Comparison of Coussot prediction with actual for 10% kaolin in 300 mm flume

As can be seen from **Figure 4-7**, the Reynolds number Re_2, calculated from the velocity obtained by the Coussot model, predicts the data over a much larger range of Reynolds numbers entering the turbulent region. The Coussot model over-predicts at higher velocities into a region where turbulence could be expected. In the case of the 10% kaolin in the 300 mm flume, the fluid was so viscous that turbulence was not probable. It is highly improbable that the highest Reynolds number predicted could have been 20 000 as shown.

The data set published by Coussot (1994) was then used to check the design procedure. Coussot mentioned that the predicted values were within 30% of the actual data.

The actual velocity was compared with the calculated velocity using the Coussot model and plotted on the graph in **Figure 4-8** below.

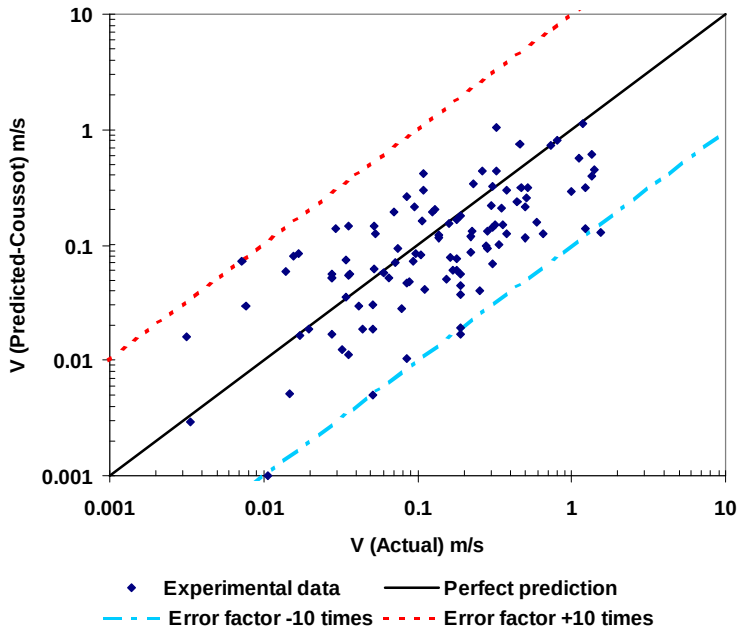

Figure 4-8 Coussot data and model: actual versus predicted velocity for a yield pseudoplastic suspension

The LSE of the velocities prediction of the Coussot data set presented in **Figure 4-9** is 0.0495.

The data shown in **Figure 4-8** shows a rather large scatter, which is far outside the 30% deviation mentioned by Coussot. It seems as though the effect of the shape factor influences the fluctuation, because if Coussot's data is plotted on a Moody diagram using $Re_{2\ (YPP)}$, the scatter and fit is much better and the flow is also in a Reynolds number range which one would expect seeing that the maximum flow rate was only about 8 l/s. Re_2 does not contain any shape factor. The Moody diagram depicting Coussot's data is shown below in **Figure 4-9** and it shows that the Coussot experimental data is very good.

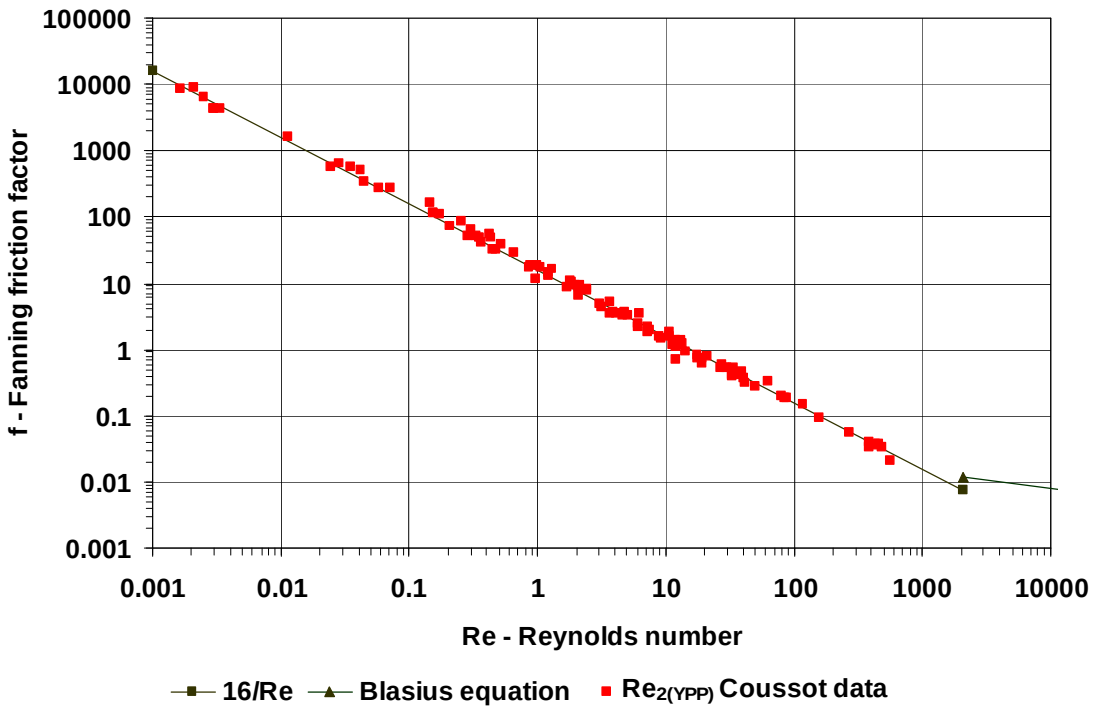

Figure 4-9 Moody diagram $Re_{2\ (YPP)}$ using Coussot's data

If the 10% kaolin data set of this thesis is tested using the Coussot model, the velocity comparison is as follows:

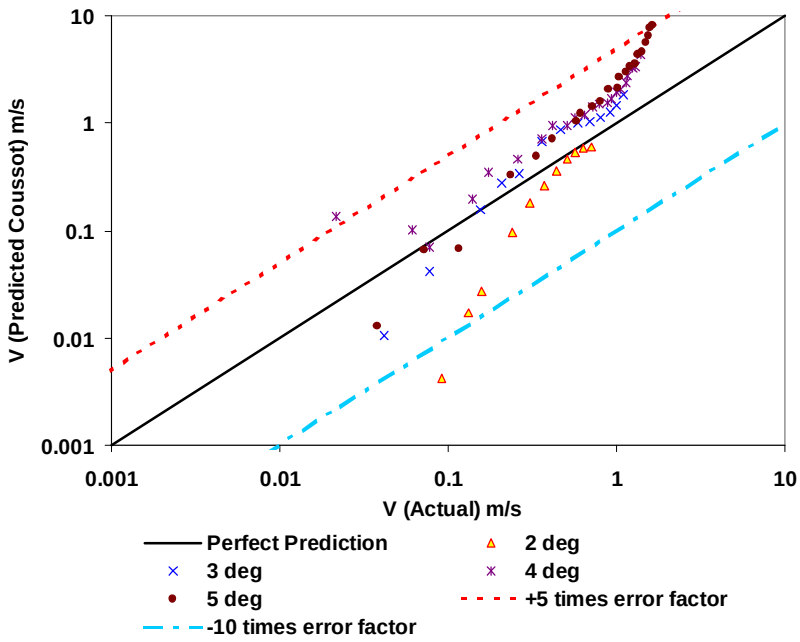

Figure 4-10 10% kaolin in 300 mm flume. V predicted (Coussot) versus V actual.

From the data depicted in **Figure 4-10**, it seems as though there is a slope effect. There is no explanation at this stage for this. The LSE for the 10% kaolin data set is 0.0656, which is similar to the Coussot data set where the LSE was 0.0495.

The following **Figure 4-11** shows the same velocity comparison but this time for 6% kaolin in a 150 mm wide flume.

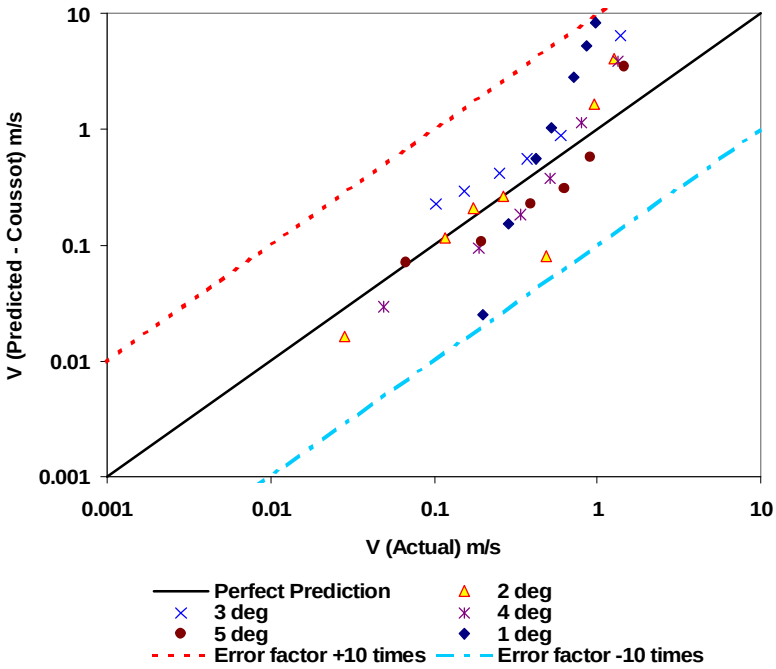

Figure 4-11 6% kaolin in 150 mm Flume. V predicted (Coussot) against V actual.

The relationship between actual and predicted velocities is again not good and although the slope effect is not as clear, this can be attributed to the fact that the data sets are smaller and the viscous effects much less than for the 10% kaolin. The material and the flume size are very different. The LSE for the velocities of the 6% kaolin data set in the 150 mm flume is 0.0851.

One oversimplification used by Coussot is that he fixes the n value to 0.3333 which seems to work reasonably well for the data set used by him but which could be an over-simplification to apply to all yield pseudoplastic suspensions and fluids. It is also not clear that the shape effect that he uses is correct, as it is not valid over the range of depth/width ratios it is supposed to be effective over. This was discussed in Chapter 2 (Section 2.7.3).

4.3.4 Yield pseudoplastic fluids on an inclined plane

De Kee, Chhabra, Powley and Roy (1990) developed flow prediction formulae for viscoplastic fluids including one for yield-pseudoplastic fluids like the kaolin used in this thesis. The formulae are only relevant for sheet flow. The average wall shear stress is ρghsinα. The average velocity that they propose is as follows.

$$V = \frac{nK}{(2n+1)\rho g \sin\alpha}\left(\frac{\tau_0}{K}\right)^{\left(\frac{n+1}{n}\right)}\left(1-\frac{\tau_y}{\tau_0}\right)^{\left(\frac{n+1}{n}\right)}\left(1+\left(\frac{n}{n+1}\right)\frac{\tau_y}{\tau_0}\right). \qquad 4.2$$

Out of interest, some of the data points taken in the 300 mm flume for the 8% kaolin with depth to width ratios of less than 0.1 (Coussot, 1997) were collated. The Reynolds numbers were kept to less than 2000 as the model is only for laminar flow. The actual velocity is compared with the velocity calculated by using Equation 4-1.

The results are depicted on **Figure 4-12**.

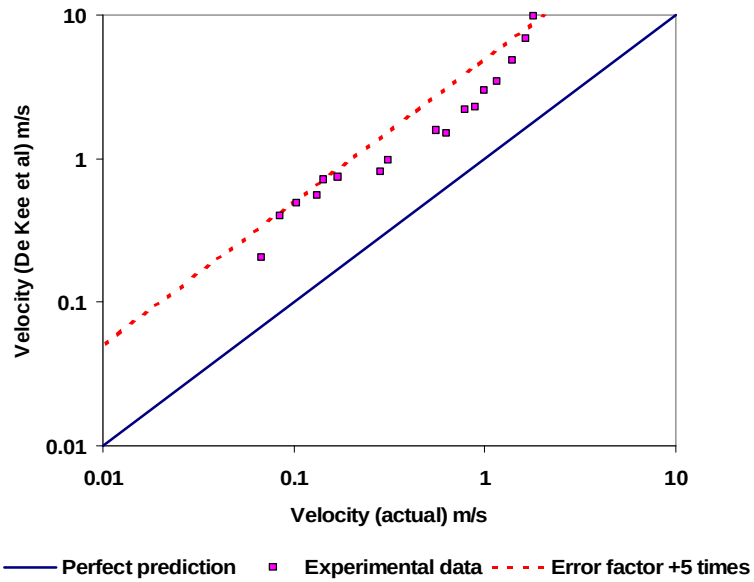

Figure 4-12 Actual versus predicted velocity (De Kee *et al.*) for 8 % kaolin in 300 mm flume

The results shown in **Figure 4-12** indicate that the velocity is significantly over-predicted. The LSE of the velocities of the 8% kaolin data set in the 300 mm flume is 0.1336.

Another set of data, this time 6% kaolin in the 300 mm wide flume, was used and the results are presented in Figure 4-13. The LSE of the velocities of the 6% kaolin data set in the 300 mm flume is 0.0974 which is slightly better than for the 8% Kaolin.

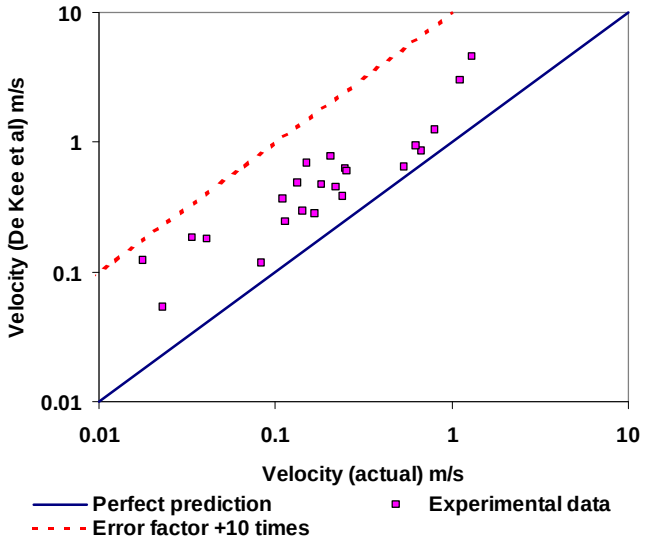

Figure 4-13 Predicted velocity (De Kee *et al.*) versus actual velocity for 6% kaolin in 300 mm flume

The same trend as seen for the laminar flow of kaolin can be observed for bentonite as shown in the following two data sets, **Figure 4-14** and **Figure 4-15**.

The LSE for the 4.5% bentonite velocities in the 300 mm flume is 0.1684 and the LSE for the 6% bentonite velocities in the 300 mm flume is 0.2246. This is worse than for the kaolin data sets presented.

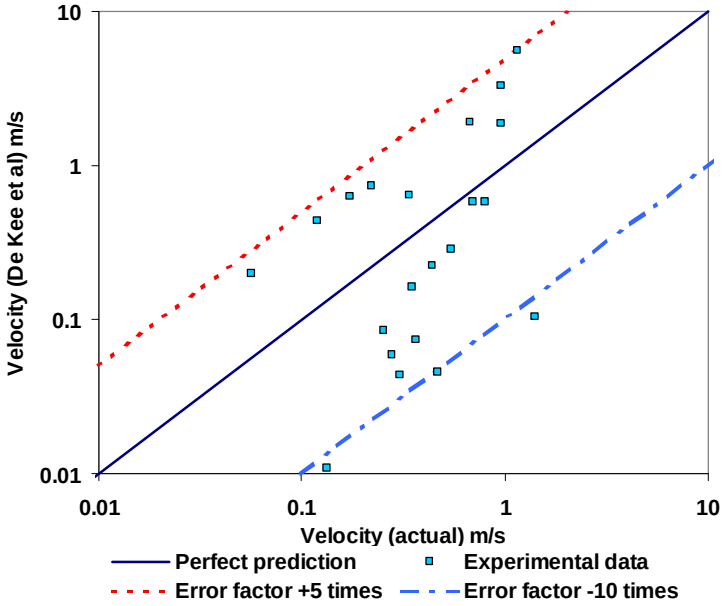

Figure 4-14 Predicted velocity (De Kee *et al.*) versus actual velocity for 4.5% bentonite in 300 mm flume

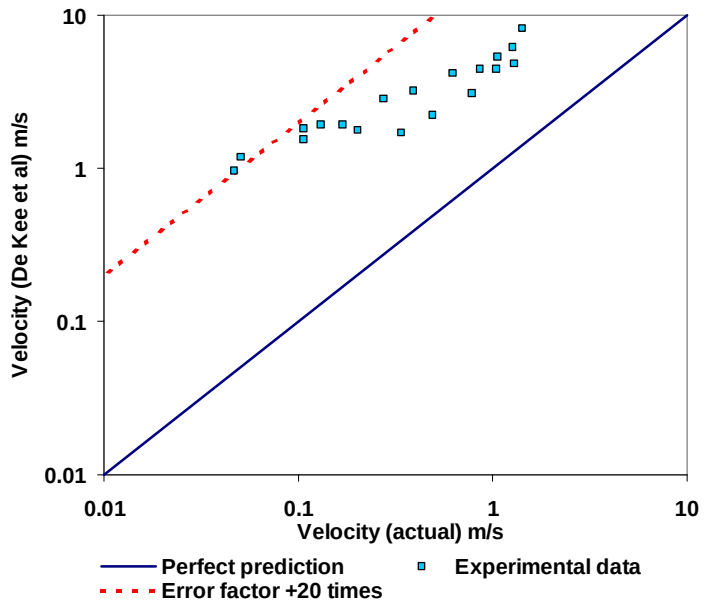

Figure 4-15 Predicted velocity (De Kee *et al.*) versus actual velocity for 6% bentonite in 300 mm flume

The following are laminar flow data sets for different concentrations CMC and these are depicted in **Figure 4-16**, **Figure 4-17**, **Figure 4-18** and **Figure 4-19**.

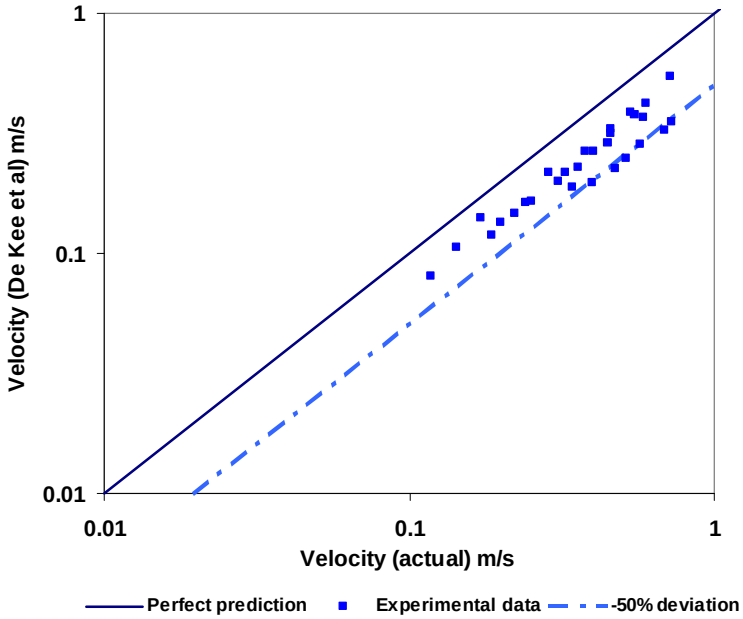

Figure 4-16 Predicted velocity (De Kee *et al.*) versus actual velocity for 1.8% CMC in 300 mm flume

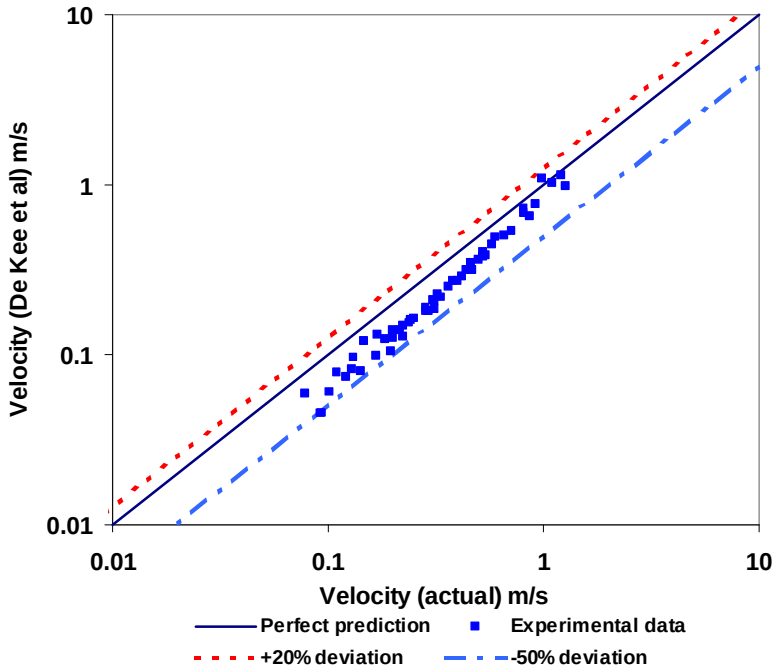

Figure 4-17 Predicted velocity (De Kee *et al.*) versus actual velocity for 2.8% CMC in 300 mm flume

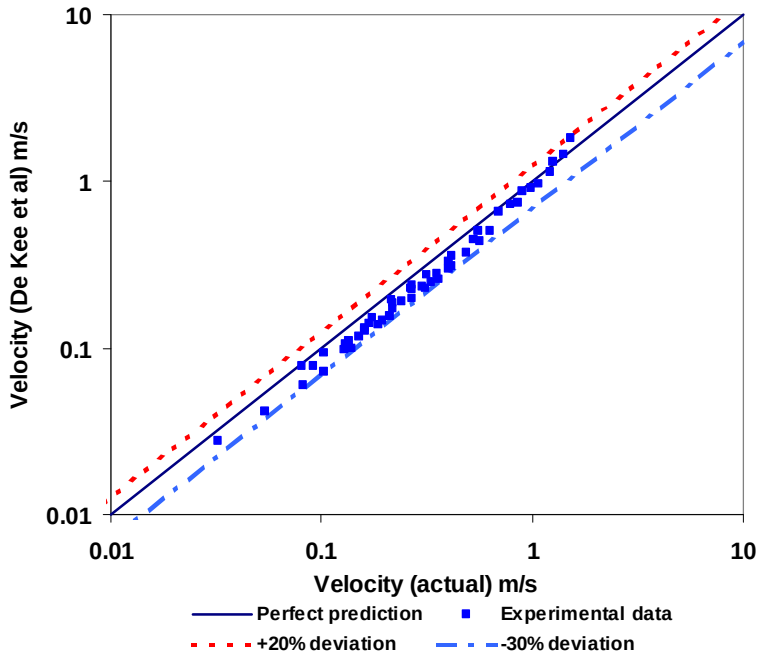

Figure 4-18 Predicted velocity (De Kee *et al.*) versus actual velocity for 3.8% CMC in 300 mm flume

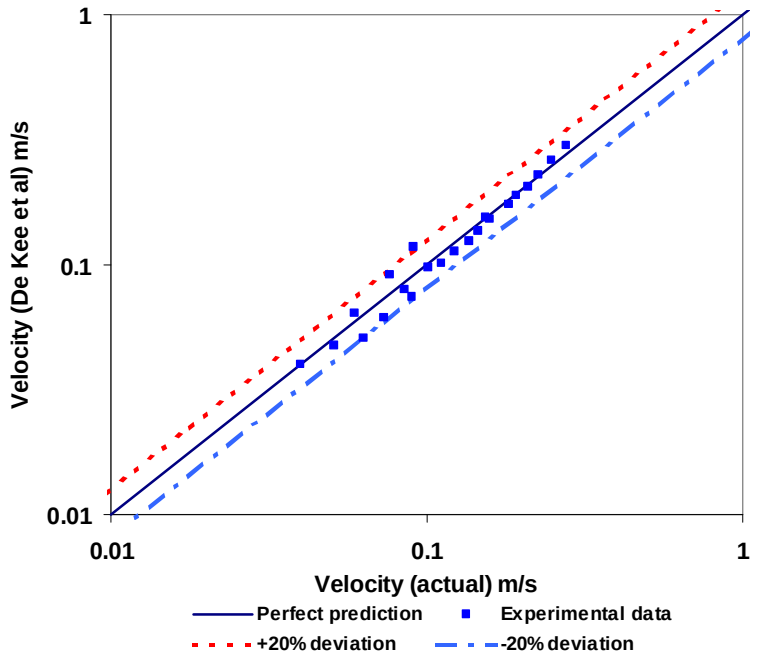

Figure 4-19 Predicted velocity (De Kee *et al.*) versus actual velocity for 5.4% CMC in 300 mm flume

The LSE for the 1.8% CMC velocities in the 300 mm flume is 0.0389, for the 2.8% CMC it is 0.024, for the 3.8% CMC it is 0.0139 and for the 5.4% CMC it is 0.0099, which is significantly better than for the kaolin or the bentonite. There is also an improvement in the fit with increase in concentration.

The results shown from **Figure 4-12** to **Figure 4-15** for kaolin and bentonite, which are both yield stress fluids, indicate that the velocity predicted is significantly different to the actual velocity. This indicates that for the data presented in this thesis, the model cannot be used for the yield stress fluids, even when the aspect ratio is limited to less than 0.1.

For the CMC the predictions are very good as shown in **Figure 4-16** to **Figure 4-19**. The predictions are within 30% of the actual, which is within experimental error range.

It is not clear why this model (Equation 4.2) is not able to predict the velocity for the yield stress fluids, as this is a mathematically and physically rigorous prediction.

Perhaps the effect of the yield stress requires a smaller aspect ratio to be sheet flow. This was tested in **Figure 4-20**, where the aspect ratio was plotted on the secondary axis. The aspect ratios are all less than 0.1 in this figure. It can be seen that the aspect ratio does not seem to be linked to the deviation. There are errors over the range of velocities regardless of whether the aspect ratio is high or low. Points A and B both are well predicted with A having a relatively high aspect ratio and B a low aspect ratio.

Points C and D are poorly predicted, and again the two points have very different aspect ratios. One can therefore not link the error to the aspect ratios.

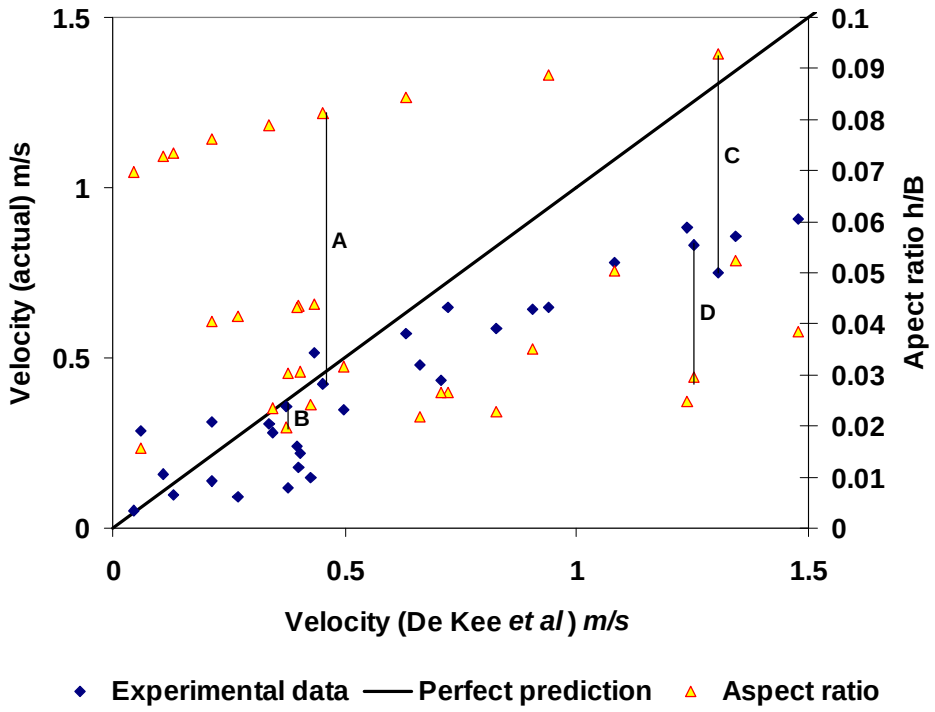

Figure 4-20 Actual versus predicted velocity (De Kee *et al.*) for 4.5% kaolin in 300 mm flume

For the database used in this thesis this model, which was developed for thin film flow, cannot be used for the yield stress fluids kaolin and bentonite, but it predicts the flow of CMC adequately as long as the aspect ratio is less than 0.1. This indicates that for yield stress fluids the sidewall has a significant effect, even with small aspect ratios.

4.3.5 Newtonian Reynolds number used by Naik

In his doctoral thesis, Naik (1983) presents a Newtonian Reynolds number for the kaolin that he tested. He publishes some of his turbulence data in his thesis. The data range is presented in **Table 4-4** as follows:

Table 4-4 Data presented by Naik (1983)

	Unit	From	To
Slope		1:50	1:150
Relative density		1.15	1.36
Plastic viscosity	Pa.s	0.00258	0.01317
Bingham yield stress	Pa	0.4	5.03
Flow rate	l/s	2.8	41.6
Flow depth	m	0.0604	0.0128

Some comments about his range of material properties:

- The density of the kaolin suspensions that he uses is very high. The 10% kaolin that is used in this thesis has a density of only about 1160 kg/m^3.
- The plastic viscosity and yield stresses are both low if the densities are taken into consideration. Both these parameters are calculated by means of a process, where the particle size distribution, reduced volume fractions, particle shape and porosity are all taken into account. No standard rheological measurements, either by using a tube or rotary viscometer, are used to calculate the rheological parameters.
- The flow depths are also reasonably low substantiating the fact that the yield stress was relatively low.

Naik uses a Bingham Reynolds number, which is a Newtonian Reynolds number. This does not take the yield stress into account at all. The implications are not so great if the yield stress is low, but for higher yield stress fluids it could be quite different.

The Bingham Reynolds number used is:

$$Re_{(Naik)} = \frac{\rho V 4 R_h}{K}. \qquad 4.3$$

The friction factor used is the Fanning friction factor adapted for open channels as used in this thesis and is as follows:

$$f = \frac{2\rho g R_h}{V^2}. \qquad 4.4$$

As Naik classifies the kaolin tested in his thesis as a Bingham fluid, the bentonite used in this thesis was used to compare the Reynolds number that Naik proposes with $Re_{2\,(BP)}$ in laminar flow.

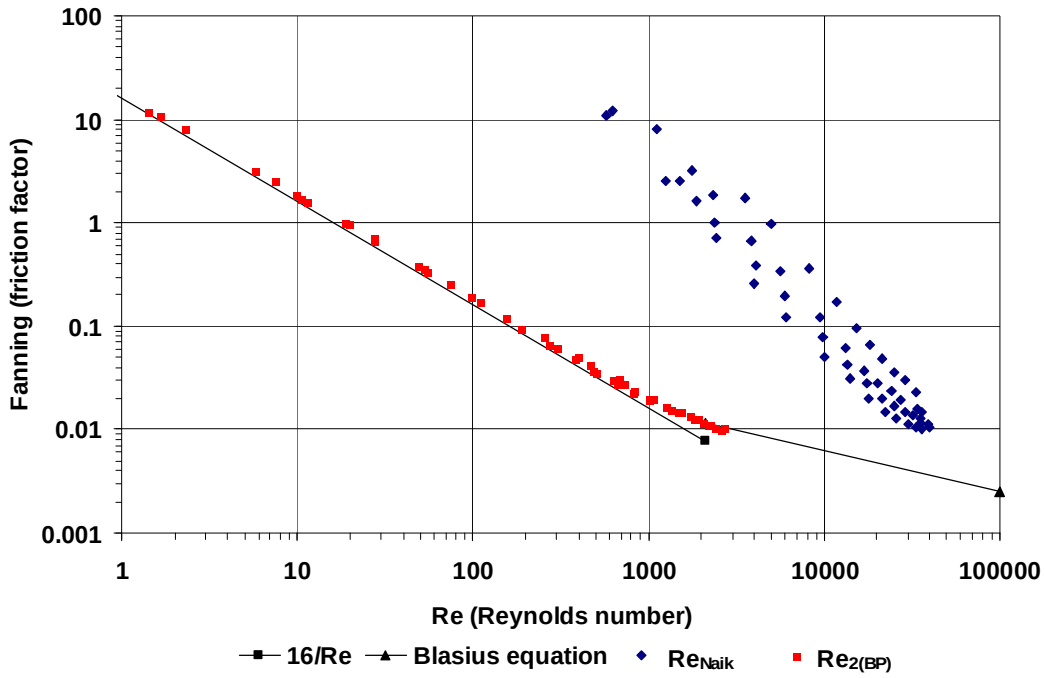

Figure 4-21 6% bentonite in 300 mm flume: Re_{Naik} compared with $Re_{2\,(BP)}$

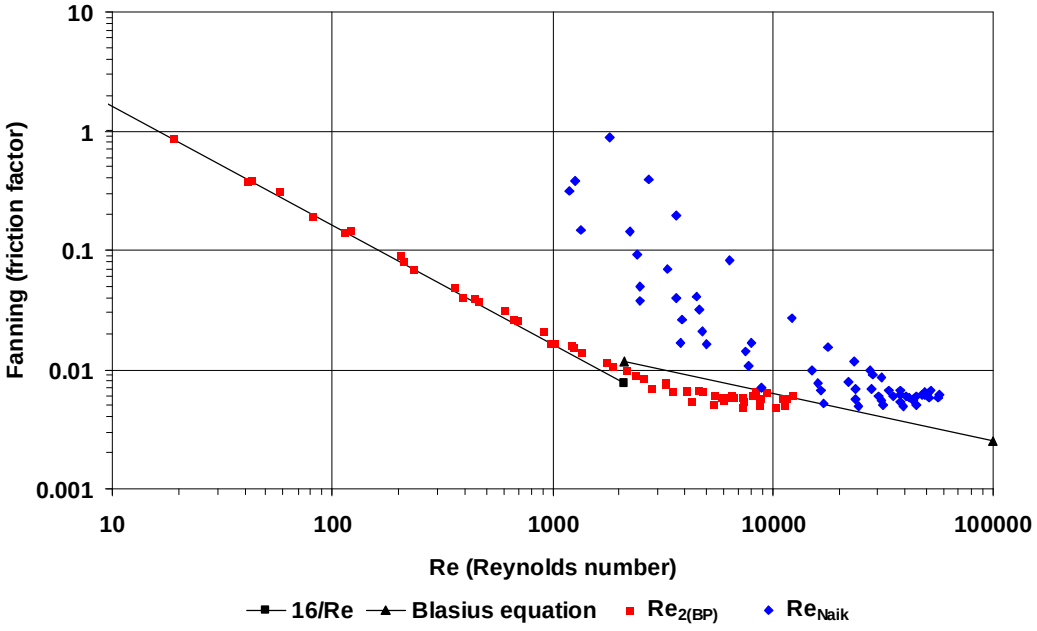

Figure 4-22 4.5% bentonite in 150 mm flume: Re_{Naik} compared with $Re_{2\ BP}$

Both **Figure 4-21** and **Figure 4-22** clearly indicate that the Newtonian type Reynolds number does not predict the laminar flow adequately. The yield stress is not accounted for and does play a role in the flow behaviour. In both figures the slope effect can be seen as they form different lines. To emphasise this, the different slopes are plotted separately in **Figure 4-23**. Naik may not have picked this up, as he only tested up to 2.5 degrees slope.

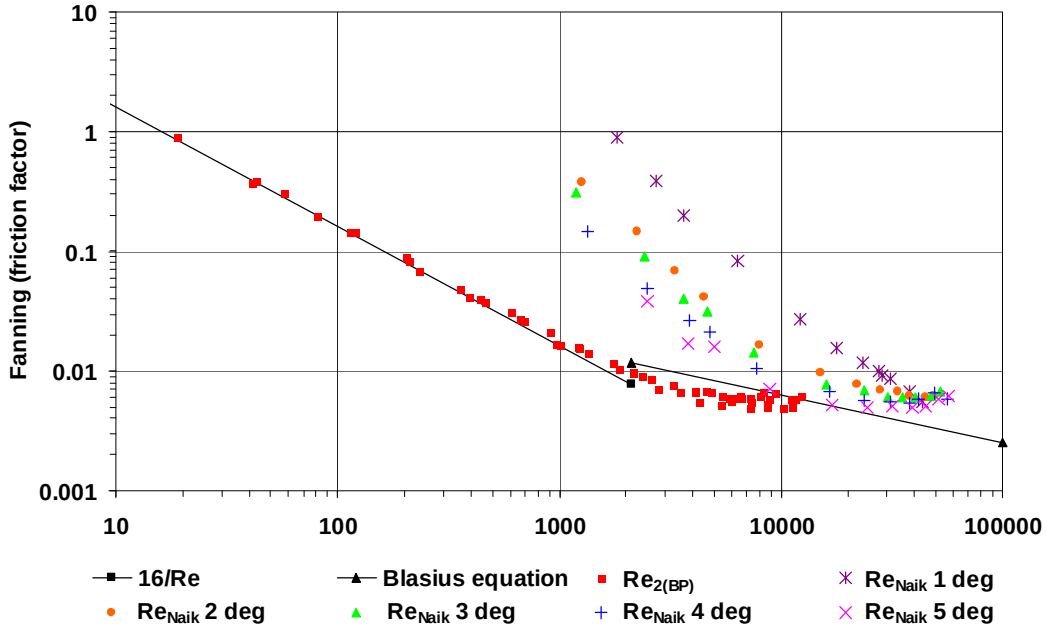

Figure 4-23 4.5% bentonite in 150 mm flume: Re_{Naik} compared with $Re_{2\,(BP)}$ showing the slope effect

4.4 LAMINAR TURBULENT TRANSITION

For laminar turbulent transition prediction of slurries in pipes there are a number of methods described in the literature. The same cannot be said for open channel flow.

The transition of open channel flow is as complex or more complex than that of pipe flow.

There is not much reference to transitional flow of open channels in the literature. What one finds, is that authors speculate that the methods used in pipe flow should work for open channel flow too (Coussot, 1997; Wilson, 1991).

To be able to predict transition accurately is essential when open channels are designed because when the laminar flow models are used for too high Reynolds numbers, they will under-predict the friction factor significantly.

4.2.1 Work by Straub *et al.* (1958)

Straub *et al.* (1958) suggest that transition occurs between 2 000 and 3 000 for water in smooth open channels, and that it depends to some extent on channel shape. Their research was on water and therefore it is not really applicable to non-Newtonian slurries. They derived the shape factors used by Kozicki and Tiu (1967).

4.2.2 Hedström number approach

The approach followed by Naik (1983) in his PhD thesis to predict the onset of transition using the Hedström number is described in Chapter 2.

This method is only valid for Bingham fluids and is derived from pipe flow.

Slatter and Wasp (2000) present three correlations between Re_c and He for non-Newtonian pipe flow data. This is described in Chapter 2 (Section 2.6.3.4).

The data in the thesis for the bentonite and kaolin transitions were used in the following graph. The kaolin was characterised as a Bingham fluid and the Bingham viscosity and yield stress calculated to determine the Hedström number at the transition Reynolds number obtained from the normal adherence function graph. This graph is a plot of f.Re/16 against Re and the deviation from NAF (normalized adherence function) =1, the point of transition, was visually observed (Slatter, 1999).

The Reynolds number at transition versus the Hedström number is presented below in **Figure 4-23**.

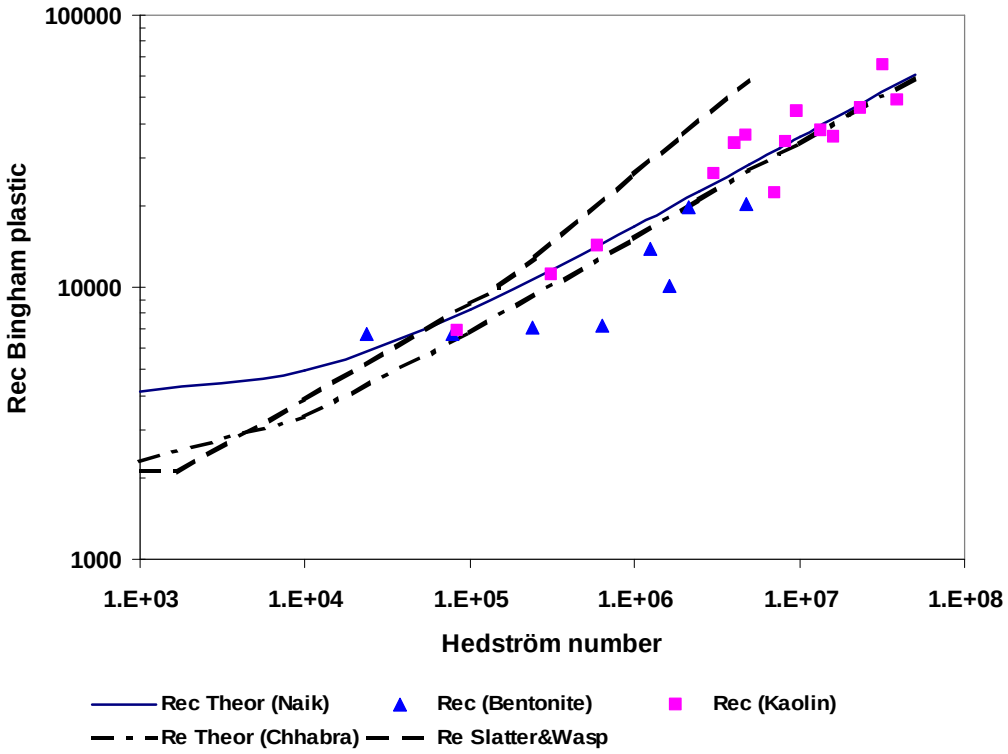

Figure 4-24 Re_{crit} vs Hedström number

From **Figure 4-24** above, it can be seen that there is a relationship between Bingham Re_{crit} and the Hedström number as described in the literature. The relationship as described by Chabbra and Richardson (1999) is the best fit. The Slatter and Wasp (2002) relationship for pipe flow and adjusted for open channel flow does not fit well.

The problem with using the Hedström number to predict transition is that unlike for a pipe, in open channel flow you always have slope and depth of flow as additional variables, which makes it very difficult to calculate the transition. Furthermore, the constant used in the formula is not fixed, but varies from 16 800 to 96 000. As can be seen from the data the fit is not very good.

Coussot (1997) uses the Hanks criteria to derive a formula to predict the onset of turbulence for mudflow which he rheologically characterises as a yield pseudoplastic suspension.

He suggests that the flow becomes turbulent when the depth of flow is larger than:

$$h = \frac{1}{\rho g \sin\alpha}\left[\tau_y + K\left(\frac{404(m+1)\rho(g\sin\alpha)^2}{Kv}\right)^{\left(\frac{1}{2m+1}\right)}\right] \qquad 2.103$$

with:

m=1/n

and

$$v = \left[\left(\frac{m}{2m+1}\right)^{\left(\frac{m}{m+1}\right)} - \left(\frac{m}{2m+1}\right)^{\left(\frac{2m+1}{m+1}\right)}\right]. \qquad 2.104$$

This was tested, by using a set of 6% kaolin data in the 150 mm flume.

The depth values were calculated for slopes from 1-5 degrees using the formula presented by Coussot (1997). The closest depth in the data set was then taken and the actual velocity and Reynolds number for that height extracted. This point was then compared to the depth velocity and Reynolds number at transition points visually selected from the Moody diagram for the same slope. The results are tabulated below in **Table 4-5**.

Table 4-5 Transition (Coussot) compared to actual

$h_{c\ (Coussot)}$	$h_{c\ (actual)}$	$Re_{c\ (Coussot)}$	$Re_{c\ (actual)}$	$V_{c\ (Coussot)}$	$V_{c\ (actual)}$	Slope (deg)
		398				5
0.0146	0.0176	280	1753	0.5143	1.345	4
		153				3
0.027	0.039	36	1642	0.174	1.255	2
0.053	0.147	17	1328	0.12	1.092	1

It can be seen from the data in **Table 4-5** that the prediction of the onset of turbulence is not good at all and very sensitive to the slope of the channel. If the depth variation between calculated Re_{crit} and actual Re_{crit} is calculated at 1 degree, it is 66%. The Coussot equation under-predicts the depth by 66%.

4.5 TURBULENT FLOW

Turbulent flow in pipes and open channels is still not well understood. McComb (1995), states that ”turbulence is the subject of much phenomenological study by those who cannot wait for the fundamental questions to be answered”. Even in pipelines there are a variety of models available, which vary significantly. For open channel flow it is as difficult, and again authors have suggested that models for pipeline turbulence can just be used in open channels. Very little work has been done to verify this experimentally.

In this section appropriate models will be tested with actual data.

4.5.1 Blasius turbulence model (Chow, 1959).

The Blasius equation for open channel flow is:

$$f = \frac{0.079}{\mathrm{Re}^{0.25}}. \qquad 2.51$$

As the Blasius equation was developed for turbulent water flow, it was not really to be expected to work for non-Newtonian open channel flow. Over the range of data tested, the turbulent data generally did not fit the simple relationship as described by the Blasius formula.

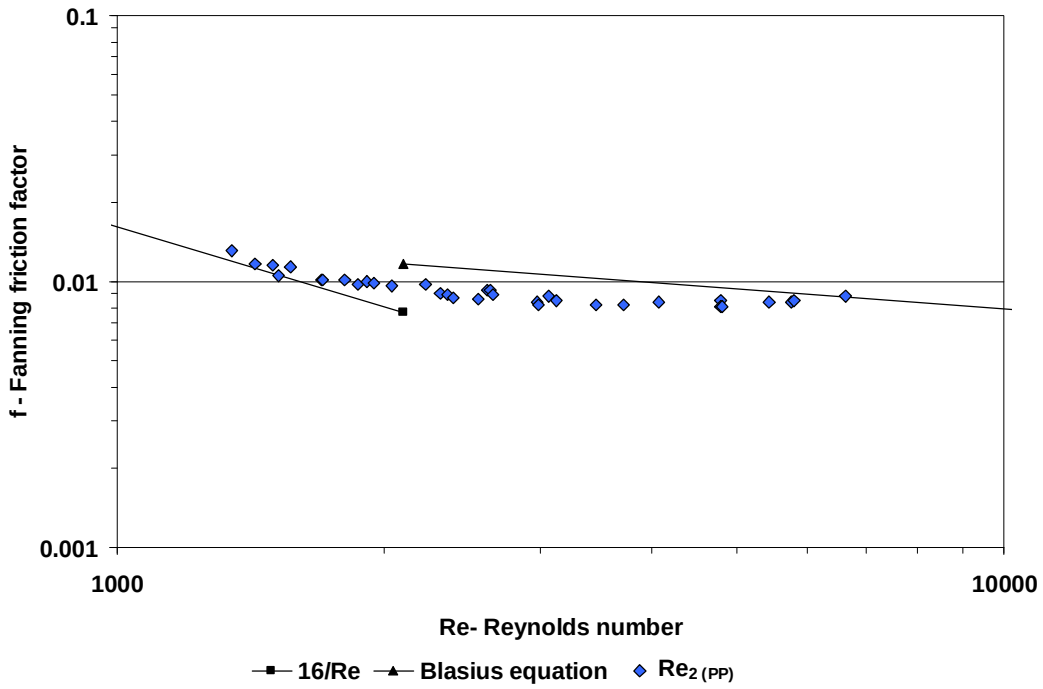

Figure 4-25 Blasius model – 3% CMC in 150 mm flume

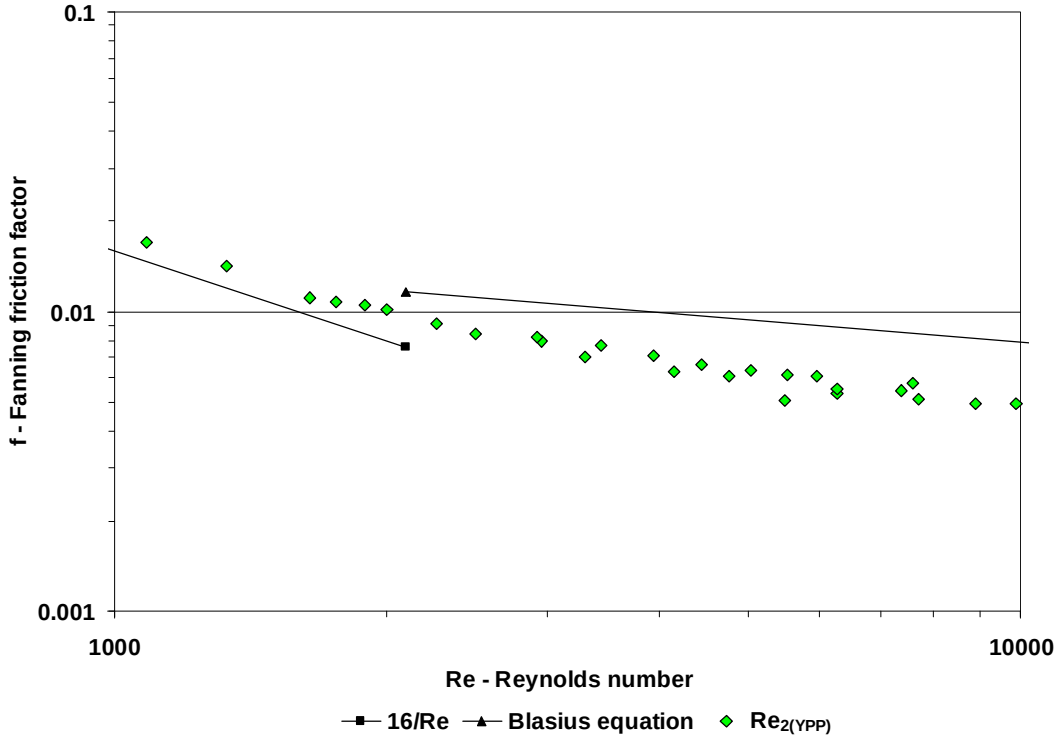

Figure 4-26 Blasius model – 6% kaolin in 150 mm flume

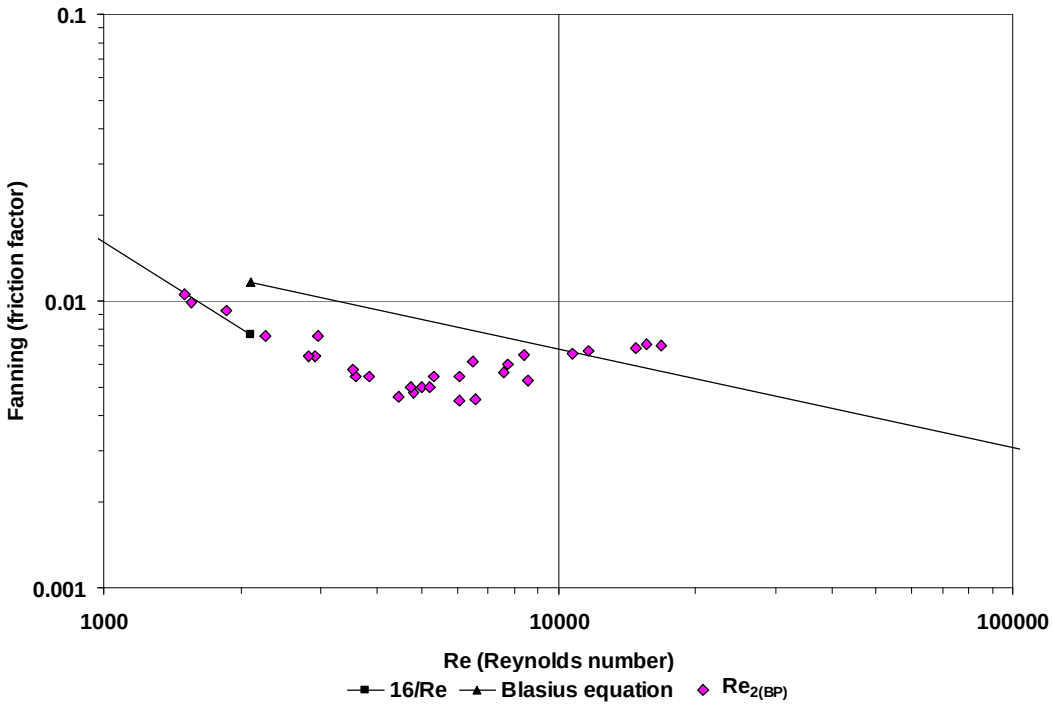

Figure 4-27 Blasius model – 3% bentonite in 75 mm flume

From the above **Figure 4-25**, **Figure 4-26** and **Figure 4-27**, it can be seen that the Blasius equation is not adequate to predict non-Newtonian turbulent flow.

4.5.2 Torrance turbulence model

Torrance (1963) developed a turbulent flow model for non-Newtonian slurries in pipes. His model uses the Herschel-Bulkley or yield pseudoplastic rheological model and is derived from the Newtonian turbulent model.

The Von Karman constant used in the formula is 0.36n, which means it depends on the viscous characteristics of the fluid.

$$\frac{V}{V_*} = \frac{3.8}{n} + \frac{2.78}{n}\ln\left(1-\frac{\tau_y}{\tau_0}\right) + \frac{2.78}{n}\ln\left(\frac{V_*^{2-n}\rho(R)^n}{K}\right) - 4.17 \quad . \qquad 2.62$$

For open channel flow the diameter is substituted by the hydraulic radius as follows:

$$R = D/2 = 4R_h/2 = 2R_h .$$

Therefore for open channel flow the average turbulent velocity is:

$$\frac{V}{V_*} = \frac{3.8}{n} + \frac{2.78}{n}\ln\left(1-\frac{\tau_y}{\tau_0}\right) + \frac{2.78}{n}\ln\left(\frac{V_*^{2-n}\rho(2Rh)^n}{K}\right) - 4.17 . \qquad 4.5$$

4.5.3 Slatter turbulence model

Slatter (1994) developed a new turbulence model that can be interpreted in terms of a particle roughness effect. The roughness Reynolds number formulated takes the complete rheology and the representative particle size of the solids into account.

$$V = V_*\left(2.5\ln\left(\frac{R}{d_{85}}\right) + 2.5\ln Re_r + 1.75\right). \qquad 2.64$$

If the hydraulic radius replaces the radius, the open channel flow equation will be:

$$V = V_* \left(2.5 \ln \left(\frac{2R_h}{d_{85}} \right) + 2.5 \ln Re_r + 1.75 \right). \qquad 4.6$$

The roughness Reynolds number is presented as follows:

$$Re_r = \frac{8\rho(V_*)^2}{\tau_y + K\left(\frac{8V_*}{d_x}\right)^n}. \qquad 4.7$$

4.5.4 Wilson and Thomas turbulence model

The model developed by Wilson and Thomas (1985) for turbulent pipe flow, predicts the thickening of the laminar sub-layer by an area ratio factor A_r. The model is described in Chapter 2.

Equation 2.72 below has to be adapted to open channel flow.

$$V_N = V_* \left(2.5 \ln \left(\frac{\rho V_* R}{\mu} \right) + 1.75 \right). \qquad 2.72$$

This can be done, by substituting the pipe radius with the equivalent hydraulic radius of the open channel yielding:

$$V_N = V_* \left(2.5 \ln \left(\frac{\rho V_* 2R_h}{\mu'} \right) + 1.75 \right). \qquad 4.8$$

The secant viscosity μ' is from the yield pseudoplastic rheogram.

The mean velocity according to Wilson and Thomas is:

$$V = V_* \left(\frac{V_N}{V_*} + 11.6(A_r - 1) - 2{,}5 \ln A_r - \Omega \right). \qquad 2.71$$

4.5.5 The Naik turbulence model

Naik (1983) presents the following formula for the mean velocity of a Bingham fluid for rough wall turbulent flow in an open channel based on previous work by Chow (1959).

$$V = 2.5V_*\left(1-\frac{\tau_y}{\tau_0}\right)^{0.5}\left(A_0+\ln\left(\frac{R_h}{k}\right)\right), \qquad 2.94$$

where:

$$A_0 = \ln\left(\left(\frac{30h}{R_h}\right)^{\left(-1-\left(\frac{\left(\frac{B}{h}+2\right)h^2}{4A}\right)\right)}\right). \qquad 2.95$$

4.5.6 Turbulence models compared

The following three figures show the Torrance, Wilson and Thomas, Slatter, and Naik models with the actual data. For each model the predicted velocity is calculated. The Reynolds number Re_2 and friction factor using the predicted velocity are then calculated and plotted on the Moody diagram.

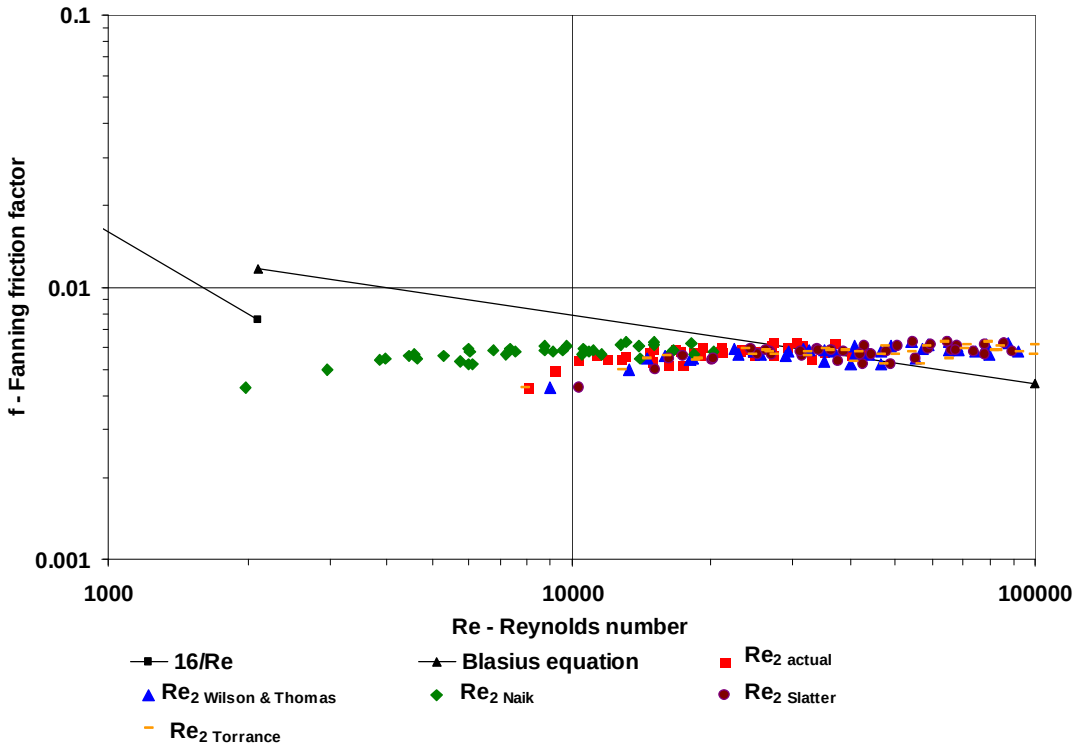

Figure 4-28 Turbulence model predictions versus actual: 3% bentonite in 150 mm flume

The Moody diagram does not clearly show the deviation and therefore predicted velocities were compared with the measured velocities for all the models. The deviations are plotted in the following **Figure 4-29, Figure 4-30, Figure 4-31 and Figure 4-32**.

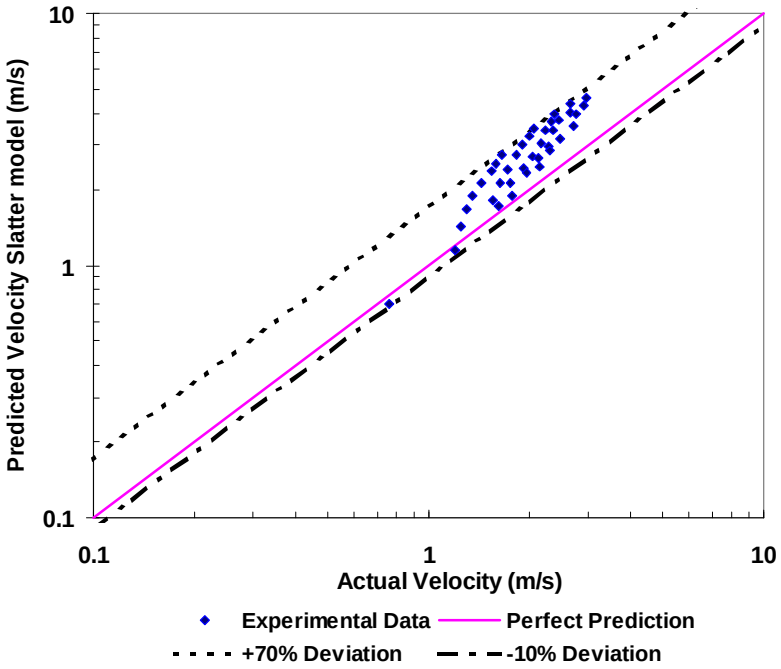

Figure 4-29 Slatter turbulence model

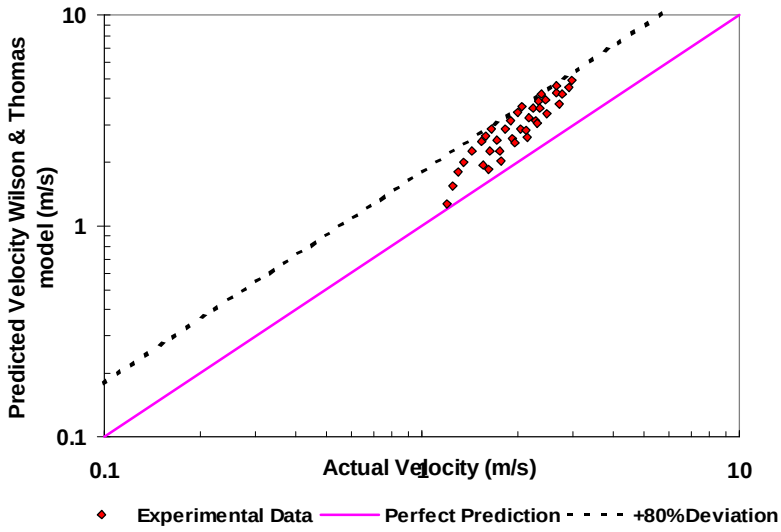

Figure 4-30 Wilson and Thomas turbulence model

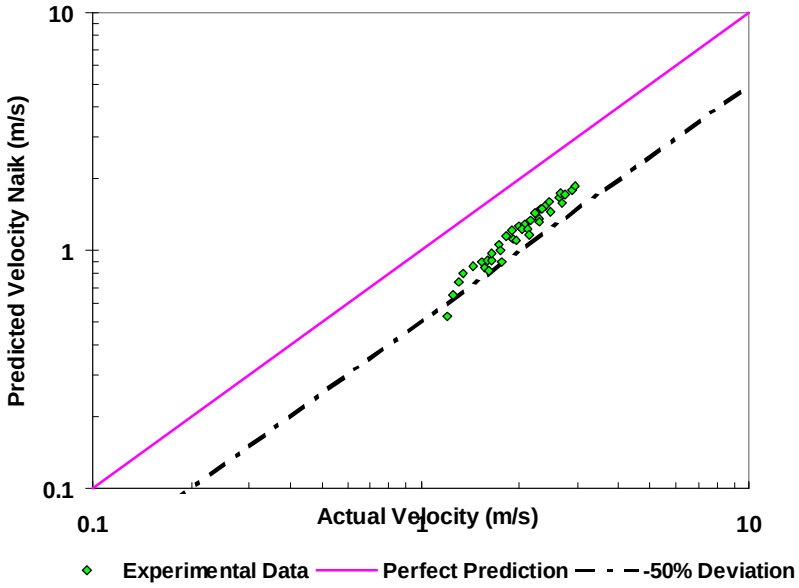

Figure 4-31 Naik turbulence model

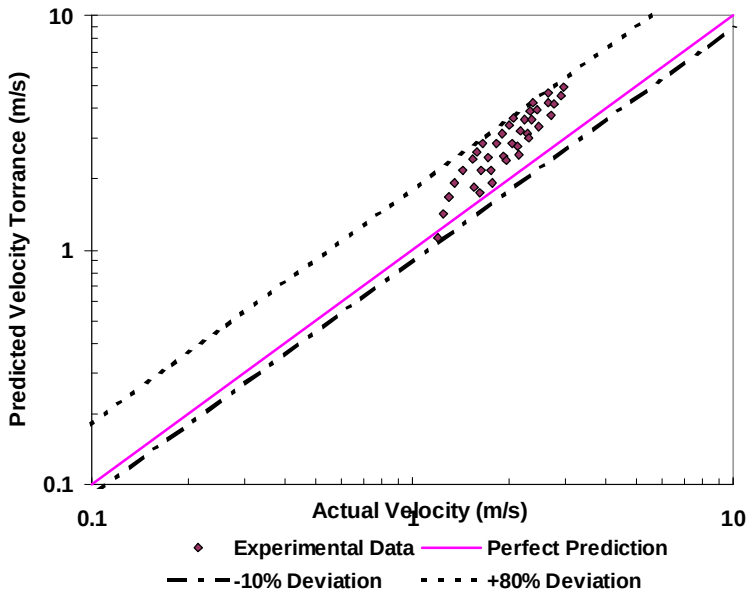

Figure 4-32 Torrance turbulence model

Examining **Table 4-6** gives a summary of the deviations of the velocity predictions for the various models.

Examining the results in **Table 4-6** it seems that although the Slatter model is slightly better than the other models, not one of them predicts the velocities well.

Table 4-6 Turbulence model predictions 3% bentonite in 150 mm flume

		Torrance	Slatter	Wilson&Thomas	Naik
3% bentonite In 150 mm flume	Deviation from actual velocity.	+80%	+70%	+80%	
		-10%	-10%		-60%
	LSE	0.0276	0.0199	0.0287	0.0393

The turbulent data of the 3% kaolin results in the 150 mm flume are presented next in **Figure 4-33**

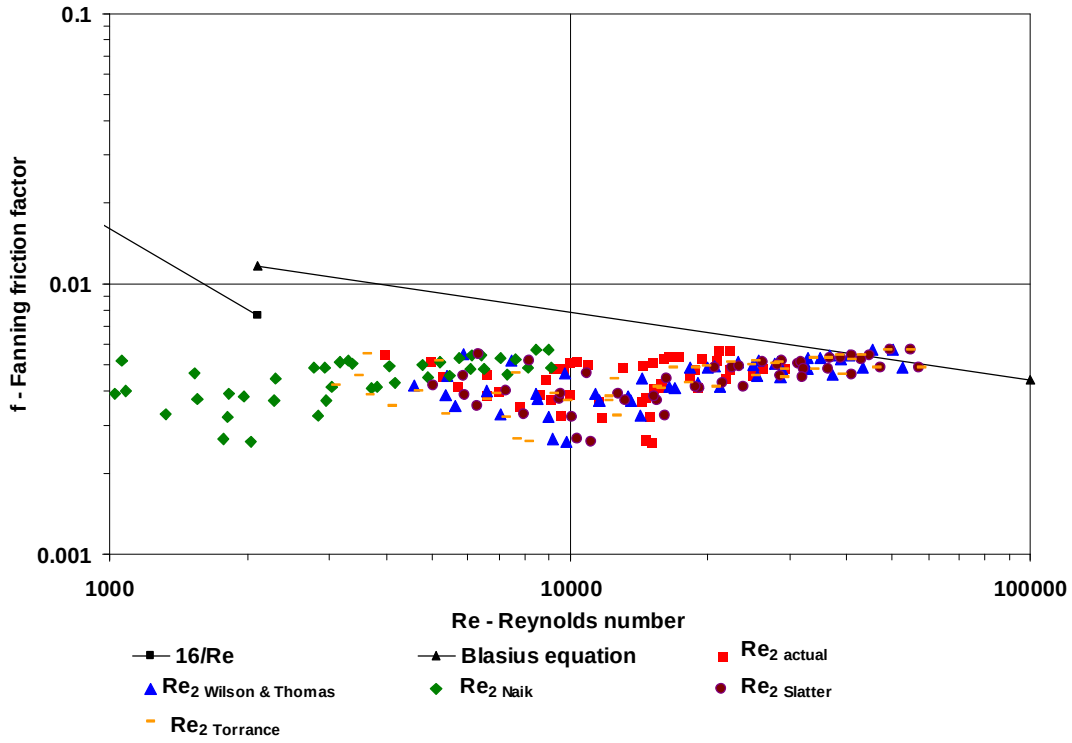

Figure 4-33 Turbulence model predictions versus actual: 3% kaolin in 150 mm flume

When the predicted velocities are compared to the measured, the deviations are summed up in **Table 4-7** below.

Table 4-7 Turbulence model predictions 3% kaolin in 150 mm flume

		Torrance	Slatter	Wilson&Thomas	Naik
3% kaolin In 150 mm flume	Deviation from actual velocity.	+60%	+60%	+60%	
		-40%	-30%	-30%	-70%
	LSE	0.233	0.0225	0.0268	0.0535

The Slatter, Torrance, and Wilson and Thomas models all have similar predictions with the Naik model under-predicting the velocities.

The following test set is the 3% kaolin in the 300 mm wide flume.

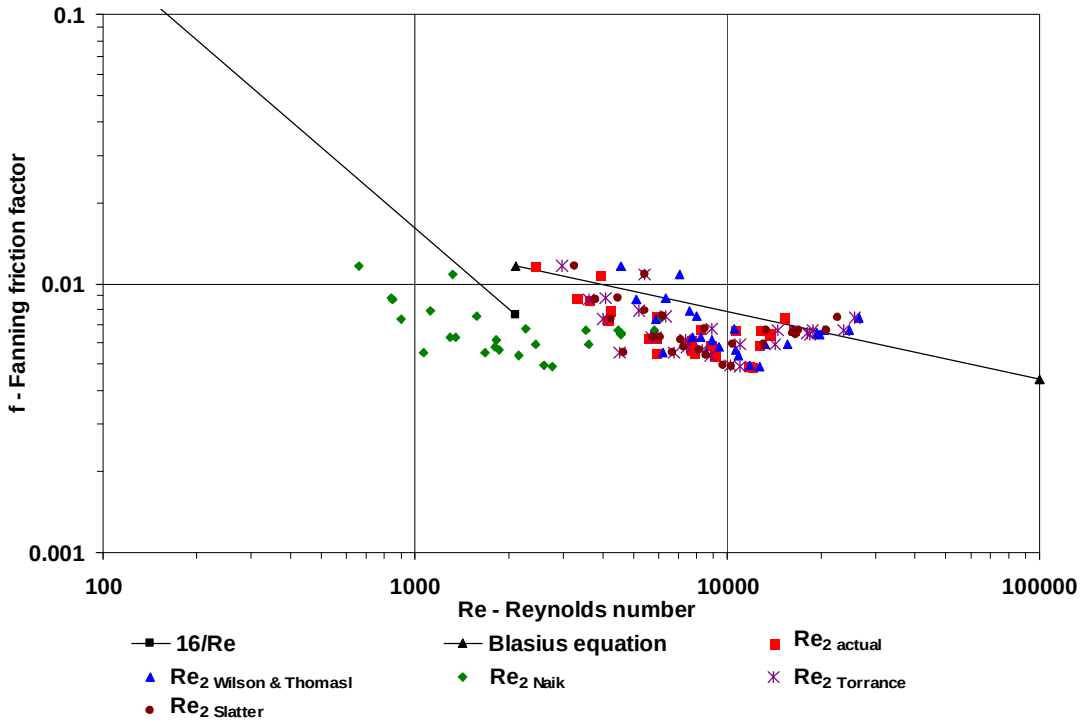

Figure 4-34 Turbulence model predictions versus actual: 3% kaolin in 300 mm flume

Figure 4-34 again shows that the Naik model under-predicts the flow and the other models are difficult to evaluate from the Moody diagram. When the predicted velocities are compared to the measured, the deviations are summed up in **Table 4-8** below. Both Torrance and Slatter models predict this data set well. This is not so obvious when one looks at the Moody-diagram.

Table 4-8 Turbulence model predictions 3% Kaolin in 300 mm flume.

		Torrance	**Slatter**	**Wilson&Thomas**	**Naik**
3% kaolin In 300 mm flume	Deviation from actual velocity.	+30%	+20%	+50%	
		-20%	-20%		-60%
	LSE	0.0103	0.0098	0.0191	0.0654

To give an idea of the deviations, some more test results are depicted in **Table 4-9**.

Table 4-9

Table 4-9 Turbulence model predictions compared

		Torrance	Slatter	Wilson&Thomas	Naik
4.5% kaolin In 150 mm flume	Deviation from actual velocity.	+35%	+10%	+50%	
		-15%	-25%		-70%
	LSE	0.0228	0.0174	0.0303	0.0408
4.5% bentonite in 150 mm flume	Deviation from actual velocity.	+30%	+30%	+50%	
		-20%	-20%		-70%
	LSE	0.0366	0.0294	0.0369	0.0524
1% CMC in 150 mm flume	Deviation from actual velocity.	+100%	+150%	+100%	
		-40%	-10%	-30%	-70%
	LSE	0.0302	0.0476	0.0326	0.0275
1.8% CMC in 150 mm flume	Deviation from actual velocity.	+80%	+70%	+80%	
		-20%	-10%	-10%	-40%
	LSE	0.0242	0.0255	0.0266	0.0253
1.8% CMC in 300 mm flume	Deviation from actual velocity.	+40%	+40%	+50%	
		-10%	-10%	-10%	-40%
	LSE	0.0114	0.0111	0.0162	0.0249
2.8% CMC in 150 mm flume	Deviation from actual velocity.	+80%	+100%	+100%	
					-25%
	LSE	0.0352	0.0372	0.0385	0.0170

4.5.7 Naik's Bingham Reynolds number in turbulent flow

The Newtonian-type Reynolds number that Naik (1983) uses has been described in 4.1.5.

Naik publishes some kaolin turbulent data in a 300 mm flume, which is characterised as a Bingham fluid. The data is presented on a Moody diagram in **Figure 4-35**, and compared with the Reynolds number $Re_{2\,(BP)}$ in this thesis.

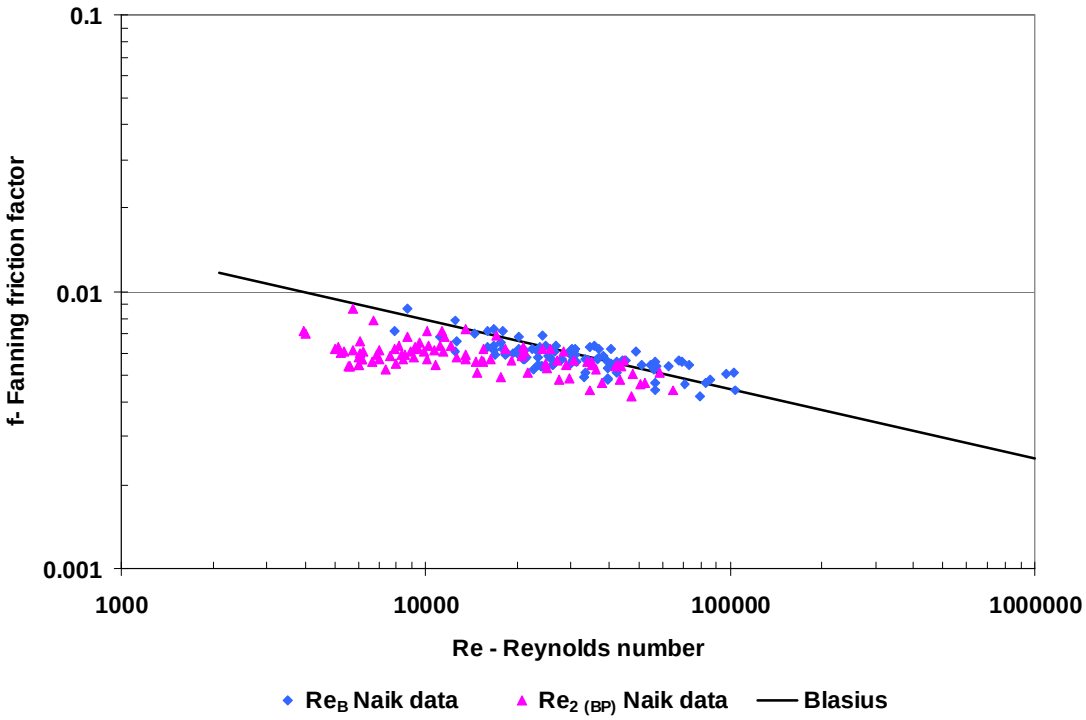

Figure 4-35 Moody diagram of Naik's data comparing Re_2 with Re_B

When comparing the Reynolds number with Re_2, the following can be observed:

- The Bingham Reynolds number varies with $Re_{2(BP)}$ between 25% and 370% with the high deviation occurring with the points with the highest yield stress.
- The Bingham Reynolds number follows the water line indicated by the Blasius equation, whereas $Re_{2(BP)}$ shows at the lower end of the data more of a 'transition range'.

4.5.8 Naik's Bingham Reynolds number applied to own data

The bentonite used in this thesis was also treated as a Bingham fluid. The following **Figure 4-36** displays the turbulent data of 4.5% Bentonite tested in the 150 mm flume. The $Re_{2\,(BP)}$ Reynolds number is compared to the Naik Bingham Reynolds number Re_B .

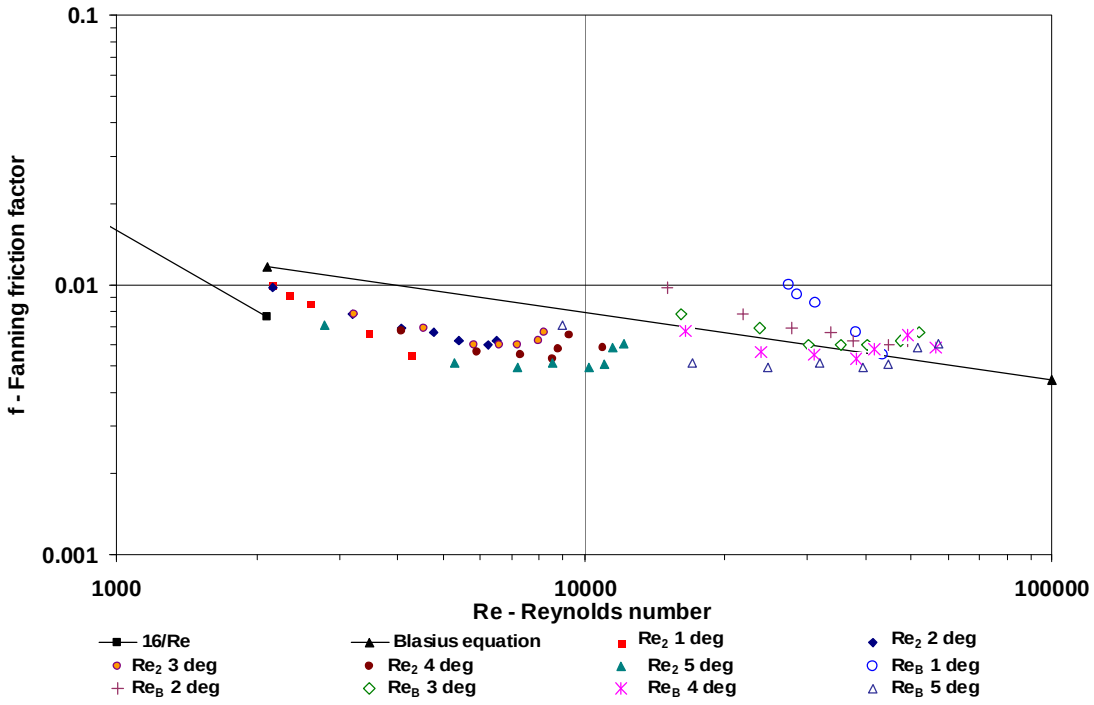

Figure 4-36 4.5% bentonite tested in 150 mm flume – testing Naik's Reynolds number

From **Figure 4-36** it can be seen that the Newtonian-type Reynolds number that is used by Naik (Re_B) and which does not take the yield stress into account, gives much higher Reynolds numbers. There is also a significant slope effect visible. This is true for both but more clearly present in the Bingham Reynolds number. Naik tested only to a slope of 2.3 degrees, so he would not have seen the effect if it had manifested.

4.5.9 Manning and Chezy

If one talks about open channel flow design for Newtonian fluids, the Manning and Chezy formulae come to mind. These were some of the earliest equations used for Newtonian open channel flow design.

4.5.9.1 Chezy

The Chezy equation is defined as follows (Chanson 1999):

$$V = C_{Chezy}\sqrt{R_h \sin\alpha}\,. \qquad 2.51$$

To find out whether the Chezy equation could be used for non-Newtonian open channel design purposes, the turbulent data sets were used to plot the average flow velocity (V) against the values of: $\sqrt{R_h \sin\alpha}$.

A linear equation through the origin was then fitted through the data and the slope of the equation would then be C_{Chezy}.

For water in all three flumes the data is presented in **Figure 4-37**. The C-value for the 75 mm flume was 54, for the 150 mm flume 61 and for the 300 mm flume 60. The 150 and the 300 mm flumes are the same flume just partitioned and the 75 mm is a different flume. For the Manning n the 75 mm flume value was also slightly less.

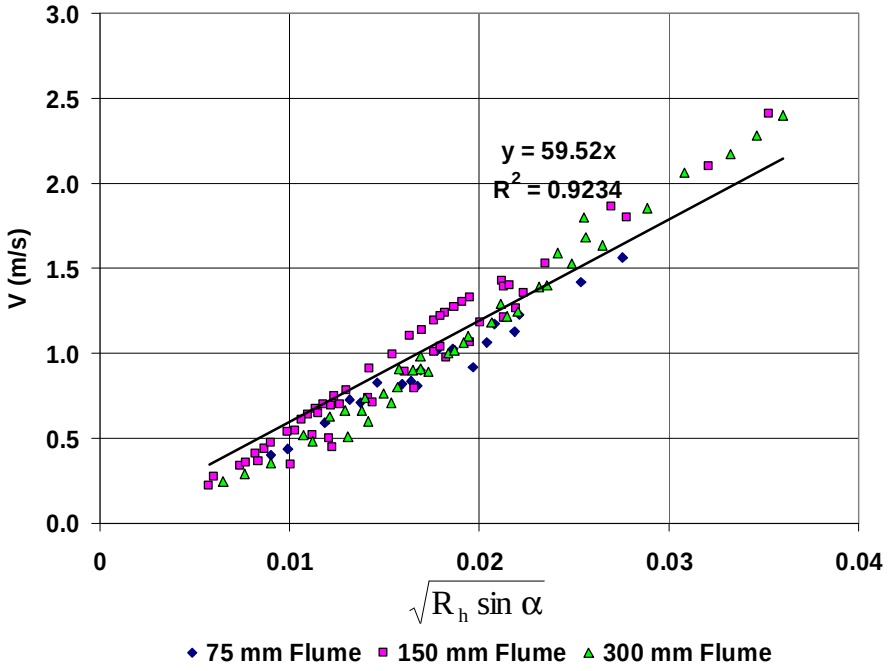

Figure 4-37 Water tests in 75 mm 150 mm and 300 mm flumes. Chezy Equation

An example of a non-Newtonian fluid is presented in **Figure 4-38**. This was for 3% kaolin in the 150 mm flume.

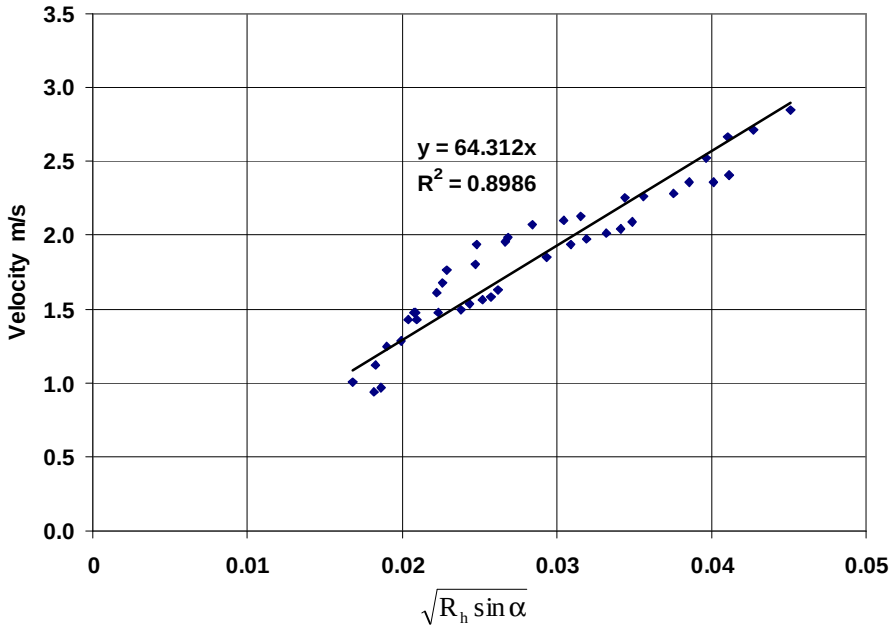

Figure 4-38 Chezy constant for 3% kaolin in 150 mm flume

The Chezy constant in this instance was 64. This value is close to the value obtained for water. This is not unusual as 3% kaolin is very Newtonian in behaviour.

This was repeated for all the test sets and the values of n were plotted against concentration. This is shown in **Figure 4-39**, **Figure 4-40** and **Figure 4-41**.

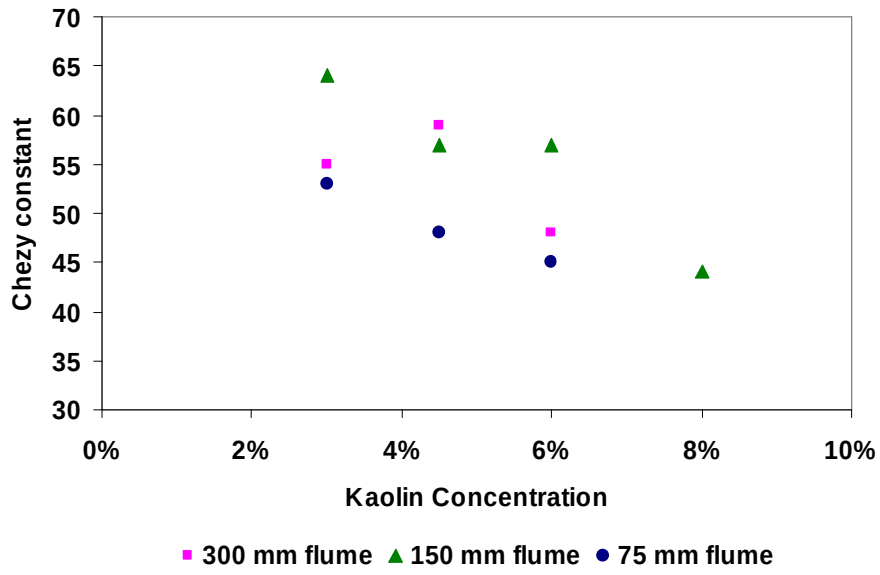

Figure 4-39 Chezy constant against kaolin concentration

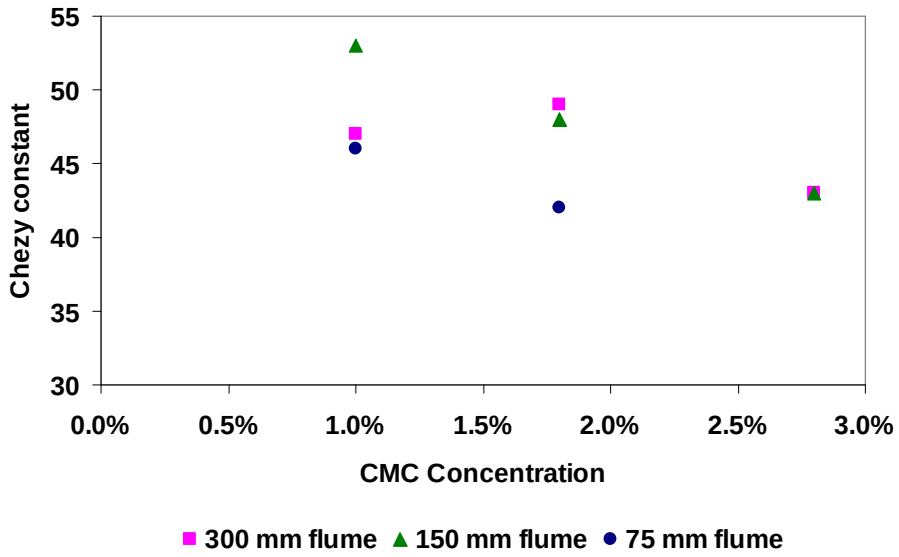

Figure 4-40 Chezy constant against CMC concentration

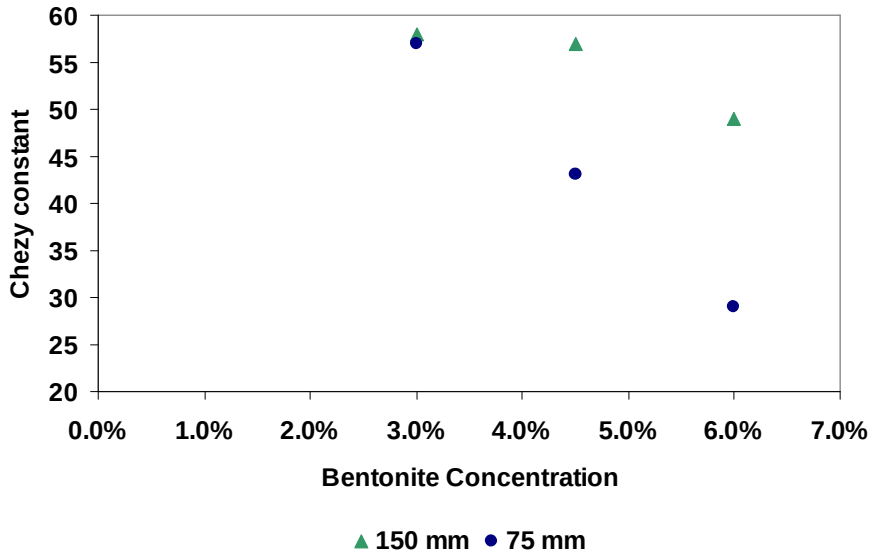

Figure 4-41 Chezy constant against bentonite concentration

The results presented in **Figure 4-39**, **Figure 4-40** and **Figure 4-41** indicate that the concentration and therefore the viscous characteristics of the fluids tested influence the value of the Chezy constant. This equation can therefore not be used for non-Newtonian open channel flow design.

4.5.9.2 Manning

The Manning equation is defined as follows by Chanson (Chanson, 1999).

$$V = \frac{1}{n_{Manning}} \left(R_h\right)^{\frac{2}{3}} \sqrt{\sin \alpha} \,. \qquad 2.53$$

The turbulent data of the database in this thesis was used to try to establish whether the Manning n-value was a constant. This would mean that a simple, well-known design equation could be used.

To establish this, each data set was used separately and the velocity (V) was plotted against the following: $R_h^{2/3}\sqrt{\sin\alpha}$.

A linear equation was fitted through the data points and the slope of the equation established. From the slope the n value was calculated to be: $n_{(Manning)}$ = 1/slope.

To establish whether this method will yield realistic results water tests were used and displayed in **Figure 4-42**.

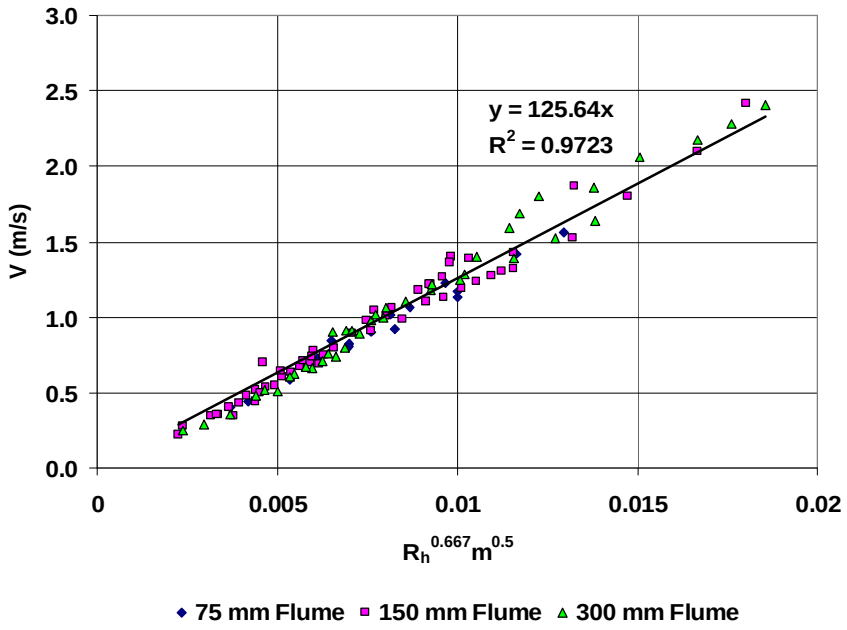

Figure 4-42 Manning n for water in the 75 mm, 150 mm and 300 mm flumes

The manning n value for the channel is 1/126 = 0.008 which is close to the value of 0.009 presented by Chow (1959) for smooth channels.

Another example is presented in **Figure 4-43** for 3% kaolin tested in the 150 mm flume.

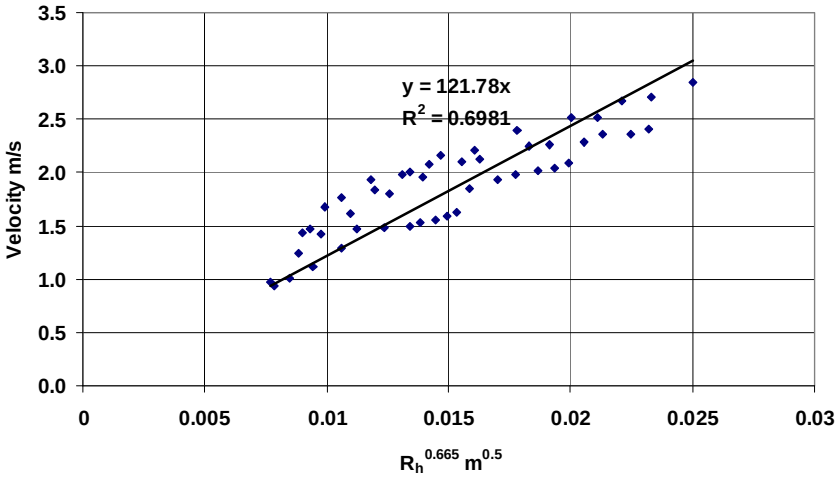

Figure 4-43 Manning n for 3% kaolin in 150 mm flume

The value of $n_{Mannimg}$ is equal to: 1/122 = 0.081. This is very similar to the value obtained for water but then one must realise that 3% kaolin is very Newtonian in behaviour.

All the turbulent data sets were used to establish the Manning n values. These were plotted against the concentrations of the fluids tested and the results are presented in **Figure 4-44**, **Figure 4-45** and **Figure 4-46**.

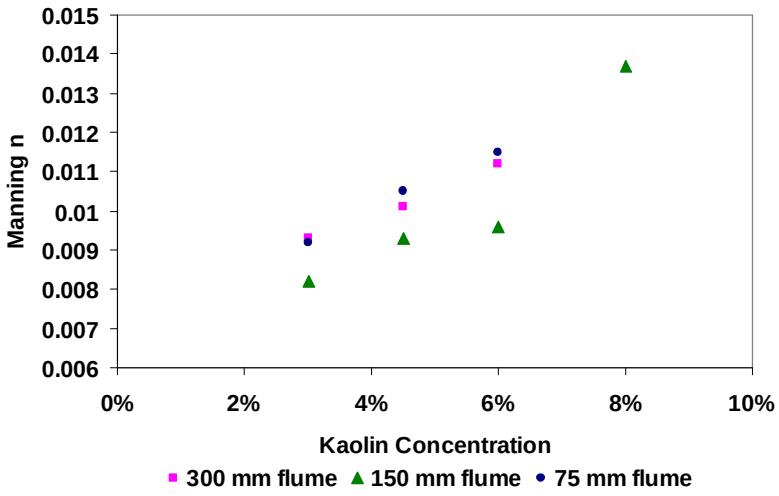

Figure 4-44 Manning n against kaolin concentration.

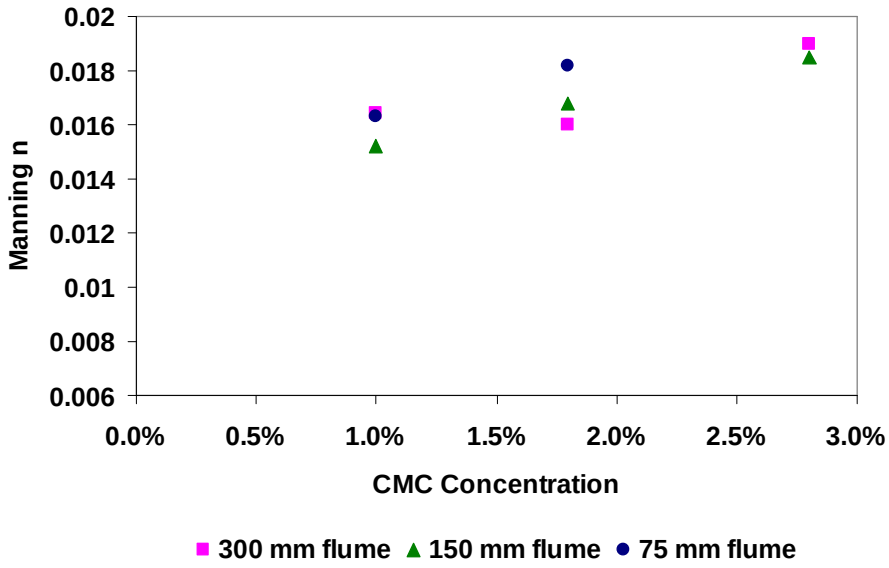

Figure 4-45 Manning n against CMC concentration

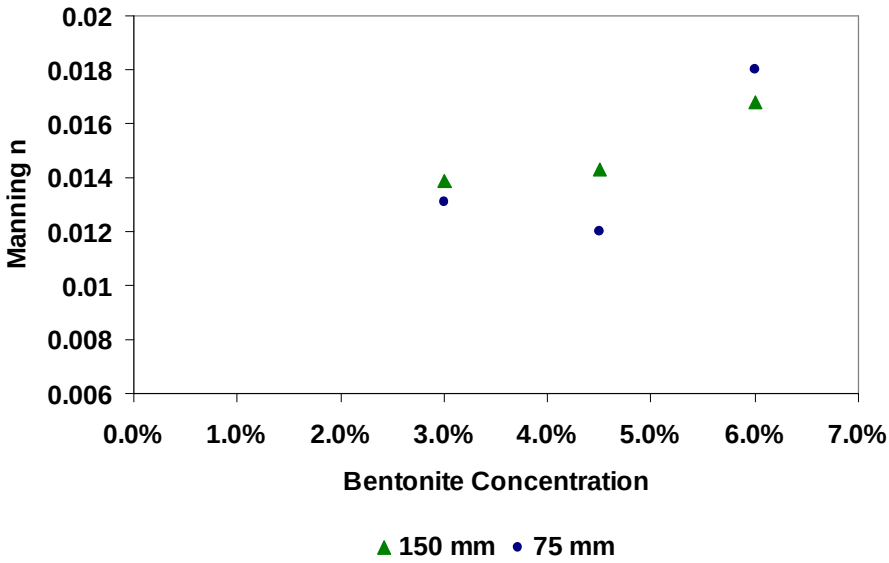

Figure 4-46 Manning n against bentonite concentration

As could be seen earlier for the Chezy C, the trend in **Figure 4-44**, **Figure 4-45** and **Figure 4-46** also indicates that the Manning n values are not constant but vary with concentration. The n-value increases as the fluids become more viscous. The Manning formula therefore also cannot be used for non-Newtonian open channel flow design.

4.6 CONCLUSIONS

The models presented in this chapter found in the literature were all developed either for pipe flow and converted to open channel flow without being tested, or they were developed specifically for either Newtonian, Bingham or yield pseudoplastic fluids. None of these models accommodate the effect of the channel slope.

- **Laminar flow**

In laminar flow, the only Reynolds number that fitted the bentonite data (Bingham model), is the one presented by **Z**hang and Ren (1982).

The fundamentally mathematically and physically rigorous sheet flow model presented by De Kee *et al.* (1990) was shown to predict velocities well for a pseudoplastic fluid like CMC, but it was not useful to predict the yield stress fluids like kaolin and bentonite. This was a disappointment as the model is fundamentally correct and mathematically rigorous. It is not clear why this is so except that it could be that the sidewall effect for the yield stress fluids is more prominent. It could also be that the so-called yield stress, which was derived from the curve fitting of the pipe-flow data, is very sensitive for this model. The indications are also there that the sidewall effect could be significant for these yield stress fluids even if the aspect ratios are small.

The Reynolds numbers presented by Kozicki and Tiu (1967), which includes shape factor coefficients, fitted the experimental data reasonably well for pseudoplastic fluids, but the Bingham Reynolds number did not predict the experimental data well.

- **Transition**

Only the method proposed by Hanks' (1963a; 1963b) method using the Hedström number, which was modified by Coussot (1997) and Naik (1983) for pipe flow was found in the literature.

This model, which is adapted from pipe flow and seems to indicate some transition for open channel flow, does not adequately predict the transition.
The transition depth that Coussot (1997) deduced from the Hanks method does seem to take the slope adequately into account and therefore could not predict the transition accurately.

- **Turbulence**

No turbulent models were found for pseudoplastic fluids.

To evaluate the experimental data of this thesis, the Slatter (1994), Torrance (1963) and Wilson and Thomas (1985) models, which were all developed for pipe flow, were adapted for open channel flow. None of these models adequately predicted flow over the range of materials, slopes and sizes tested in this thesis.

The model presented by Naik (1983), based on work previously done by Chow (1959) for rough turbulent open channel flow of Bingham fluids, also did not predict the flow well for all the data presented in this thesis. It was very sensitive to channel roughness. If the channel was considered to be very smooth, the model predicted the velocities much better. It is not clear why this should be so.

The Manning and Chezy formula developed for Newtonian pipe flow and converted for Newtonian open channel flow also cannot be used. It was shown that the Manning n and Chezy C constants vary with fluid concentration. This means they are sensitive to the fluid rheology.

- **General**

The database has proven its usefulness for evaluating flow models, and will be useful for the development of new models.

The conclusion that can be drawn at the end of this chapter is that there is ample scope to develop competent design criteria for non-Newtonian open channel flow. These design criteria should cover a wide range of flow conditions and fluid properties. This will be attempted in Chapter 5, where the new models will be introduced.

CHAPTER 5

NEW OPEN CHANNEL FLOW MODELS

5.1 INTRODUCTION

One of the principal objectives of this work is to develop relationships for predicting laminar, transitional and turbulent flow in open channels for design engineers. In the absence of a workable approach being developed from a fundamental physical basis McComb (1994), the approach used in this thesis has been to develop models which are empirical correlations between Reynolds number, Froude number and friction factors.

This chapter will outline the way in which these new models and design procedures were developed to predict the different flow regimes:

- laminar flow
- the onset of transition from laminar to turbulent flow
- the onset of 'full turbulence'
- turbulent flow.

Before the new work is introduced, the following points arising from the previous chapters need to be mentioned to set the trend for the approach taken in this chapter. From the experimental work done and explained in Chapter 3, as well as the analysis of the results with models found in the literature review in Chapter 4, the following comments can be made.

§ Observing the flow of viscous fluids in flume did not follow the trends expected from the knowledge of Newtonian open channel flow and pipe flow.

§ The shear stress distribution is indeterminate with the available knowledge. This makes it impossible to develop fundamental flow formula as for pipe flow.

- Even mathematically and physically rigorous approaches for laminar sheet flow of non-Newtonian fluids (de Kee *et al*, 1994) have been shown not to be very useful for prediction of flow velocities, except for power-law fluids.
- The transition zone appears to be over a range of Reynolds numbers with the more viscous fluids displaying an earlier deviation from the laminar flow line.
- The viscous materials have a smoother transition than the less viscous fluids, which display the typical water transition with a sudden jump in friction factor at transition.
- The viscous characteristics of some of the fluids, although they have been rheologically classified with different models, have similar apparent viscosities at specific shear rates. These groups of fluids with similar apparent viscosities also display similar transitional behaviour when the flume data is plotted on the Moody diagram.
- The flume slope also influence the onset of transition with the higher slopes entering transition at higher Reynolds numbers. This was observed much clearer when Reynolds number was plotted against Froude number.
- The turbulent data sets are more horizontal on the Moody diagram with increase in Reynolds number than the Blasius prediction for water.

From the above it is clear that a more empirical approach will have to be adopted to predict the various flow regimes for the database compiled for this thesis which comprises such a varied range of materials concentrations, slopes, flume sizes and flow rates.

5.2 LAMINAR FLOW

The Reynolds number used in this thesis is derived from the assumption made by Osborne Reynolds that:

$$\mathrm{Re} \propto \frac{\text{inertial forces}}{\text{viscous forces}} . \qquad 5.1$$

This dimensionless group can be formulated as (Featherstone & Nalluri, 1995):

$$\mathrm{Re} \propto \frac{\rho D^2 V^2}{\tau_{visc} D^2} . \qquad 5.2$$

Slatter (1994) shows that the representative viscous stress across a pipe if the representative shear rate is 8V/D can be expressed for a yield pseudoplastic fluid as:

$$\tau_{visc} = \tau_y + K\left(\frac{8V}{D}\right)^n \qquad 5.3$$

which results in the viscous force being:

$$\text{Viscous force} \propto D^2\left(\tau_y + K\left(\frac{8V}{D}\right)^n\right). \qquad 5.4$$

The pipe Reynolds number is:

$$\mathrm{Re}_2 \propto \frac{\rho V^2}{\tau_y + K\left(\frac{8V}{D}\right)^n} . \qquad 5.5$$

When the proportionality constant is taken as 8, the Reynolds number in Equation 5.5 reduces to the Newtonian Reynolds number under Newtonian conditions, which results in the final form of Re_2 in Equation 5.6.

$$\mathrm{Re}_2 = \frac{8\rho V^2}{\tau_y + K\left(\frac{8V}{D}\right)^n} . \qquad 5.6$$

When one uses the hydraulic radius instead of the Diameter ($D_e=4R_h$), the open channel

Reynolds number becomes:

$$Re_{2(YPP)} = \frac{8\rho V^2}{\tau_y + K\left(\frac{2V}{R_h}\right)^n}. \qquad 5.7$$

The advantage of this Reynolds number is that it can be used for a yield pseudoplastic fluid as it is presented (see also Appendix E).

For a pseudoplastic fluid it becomes:

$$Re_{2(PP)} = \frac{8\rho V^2}{K\left(\frac{2V}{R_h}\right)^n} \qquad 5.8$$

and for a Bingham fluid it becomes:

$$Re_{2(BP)} = \frac{8\rho V^2}{\tau_y + K\left(\frac{2V}{R_h}\right)}. \qquad 5.9$$

In its simplest form it reverts to the Newtonian Reynolds number:

$$Re_{Newt} = \frac{\rho V 4R_h}{\mu}. \qquad 5.10$$

The Re_2 Reynolds number has been published in Haldenwang, Slatter and Chhabra (2000), as well as Haldenwang, Slatter and Chhabra (2002).

This Reynolds number fitted the experimental data well for all the fluids tested in laminar flow. In Chapter 6 (section 1-5) the laminar flow data is discussed and evaluated and all the data sets are shown in Appendix A.

5.3 FROUDE NUMBER EFFECT

The Froude number is the ratio between inertial and gravity forces.

For a rectangular open channel the Froude number is:

$$Fr = \frac{V}{\sqrt{gh}}. \qquad 2.4$$

The Reynolds number, as well as the Froude number, describes flow behaviour.

The Moody diagram where friction factor is plotted against Reynolds number is the standard way of presenting pipe and open channel flow data.

From the first flow results involving more viscous slurries, it could be seen that the behaviour of the more viscous slurries was fundamentally different from the low viscosity (eg, water) results. The viscous slurries yielded transitional behaviour at lower Reynolds numbers. This can be seen for the two concentrations CMC in the 150 mm flume as depicted in **Figure 5-1**.

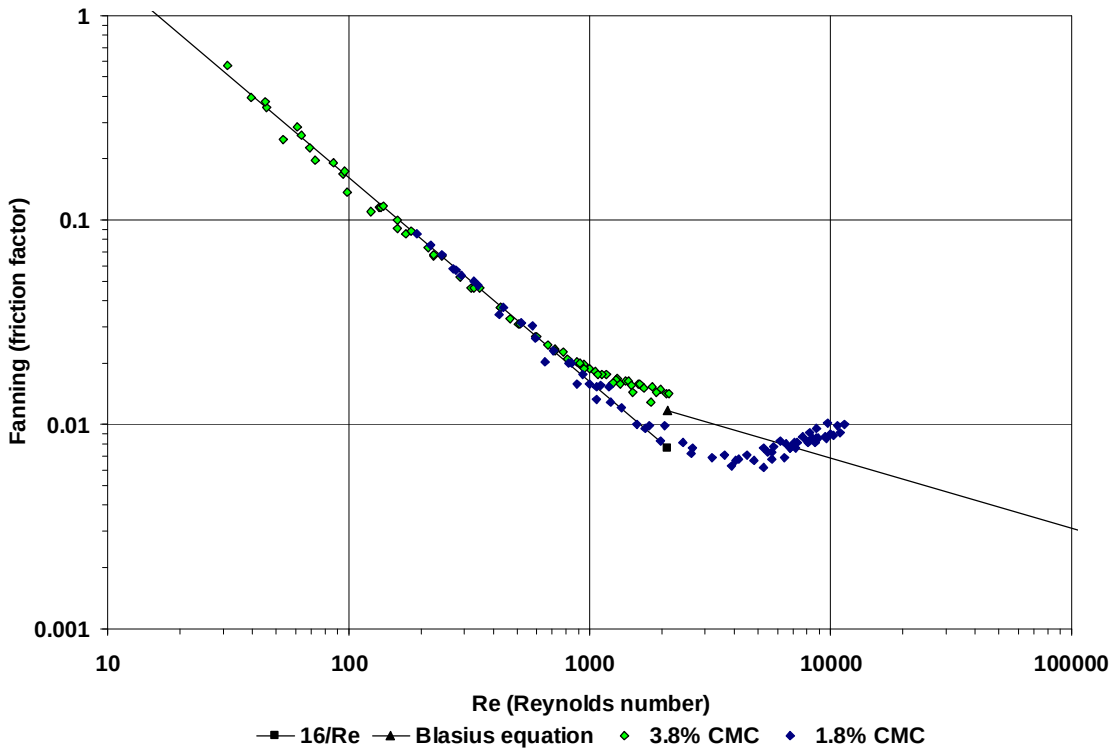

Figure 5-1 Transitional behaviour for two concentrations CMC in 150 mm flume

It also seemed that the slope of the flume had an influence on the onset of transition with the steeper slopes resulting in a later onset of transition than the shallower slopes. When the Froude number was plotted against the Reynolds number it could be observed that the slope definitely seemed to play a role.

When the Reynolds number was plotted against the Froude number with the Reynolds number being in log scale and the Froude number in linear scale, it was observed that the flow could be divided into different flow regions. It also seemed as though the laminar region followed a power law relationship. After generating plots of all the data sets, a similar trend could be observed.

After this very consistent behaviour the curvature changed into a transitional region until it veered off drastically into the 'turbulent region'.
The following three figures will show this for CMC in **Figure 5-2**, Bentonite in **Figure 5-3** and Kaolin in **Figure 5-4**:

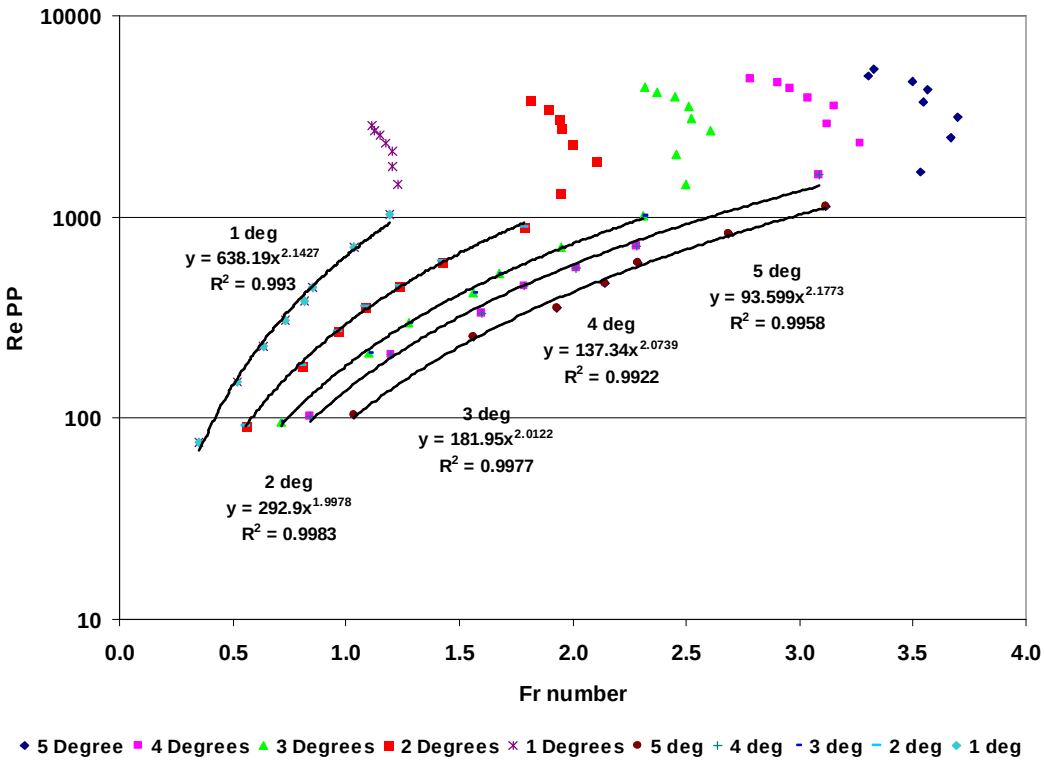

Figure 5-2 2.8% CMC in 150 mm flume

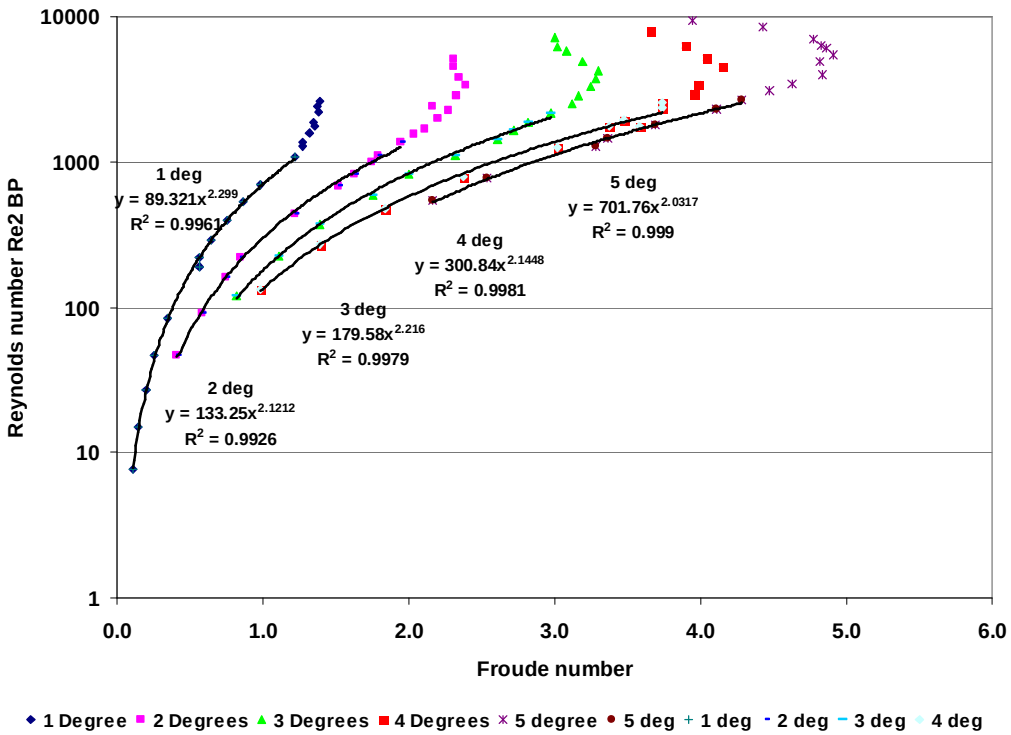

Figure 5-3 4.6% bentonite in 150 mm flume

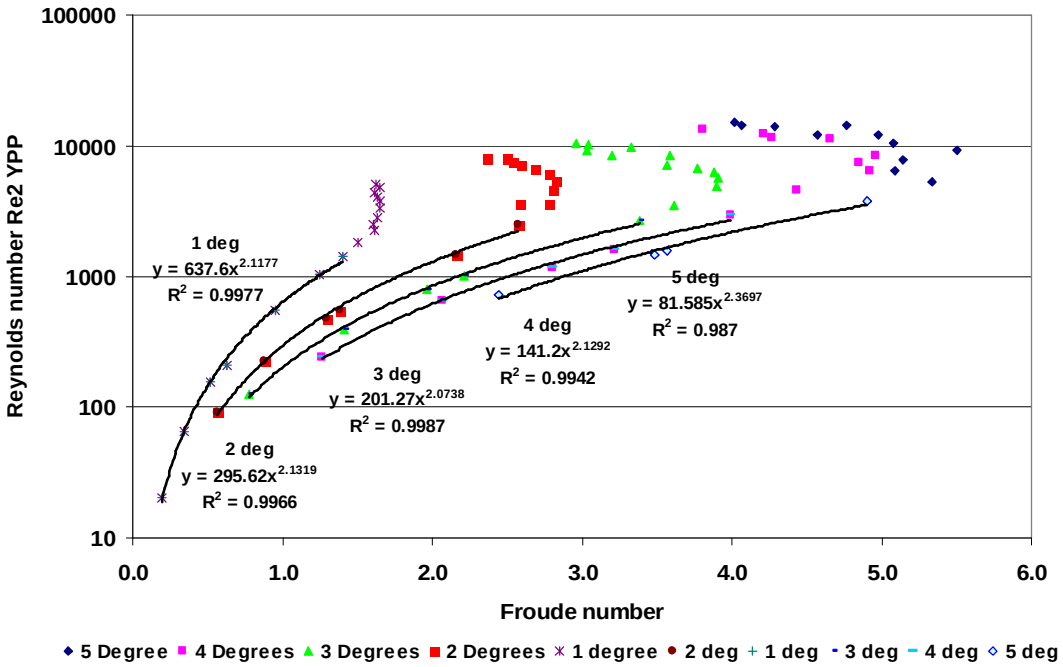

Figure 5-4 4.5% kaolin in 150 mm flume

A Moody diagram was then constructed with the Froude number on a secondary vertical axis. This indicated that the same behaviour could be observed from both relationships indicating the same regions of flow behaviour. The 2.8% CMC concentration in the 150 mm flume is shown below in **Figure 5-5** to demonstrate this trend.

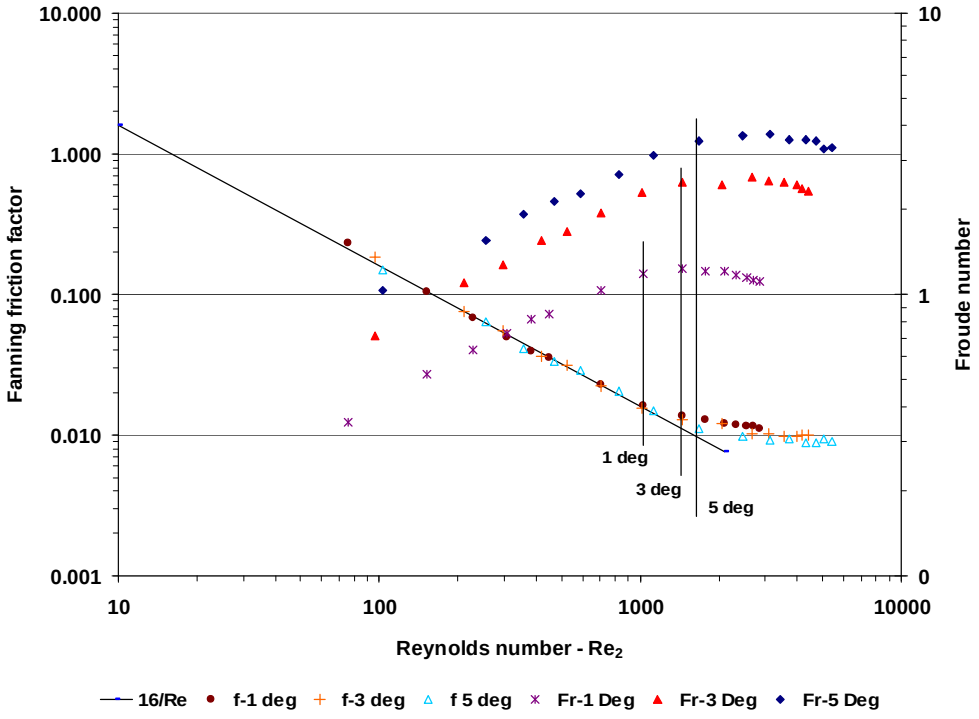

Figure 5-5 Moody diagram for 2.8% CMC in 150 mm flume

5.4 ONSET OF TRANSITION

It is a well known fact that the Froude and Reynolds numbers are critically important parameters for describing and analysing open channel flow behaviour (Chow, 1959).

The Moody diagram was initially used to try to find a relationship between Reynolds number and the rheological parameters of the fluids tested. The slope effect was very difficult to see and the rheological parameters made it just about impossible to establish a relationship that included all the parameters. If the test results of the materials were separated, there were trends between the onset of transition and the yield stress for kaolin and bentonite, but the yield stress on its own was not sufficient to fully describe the viscous properties of the fluid, and all the fluids were not yield stress fluids.

5.5 APPARENT VISCOSITY

The next idea was to establish one rheological parameter that could somehow sufficiently characterise the three very different slurries. In Chapter 3, Section 3.9.2, it was shown that all the data presented in **Figure 3-31** to **Figure 3-36** indicate that although the materials tested are rheologically very different, they have similar apparent viscosities at certain shear rates and that these fluids show similar open channel flow behaviour especially in laminar flow and in the transitional region. The transitional behaviour is not the same: for the less viscous materials, more Newtonian-like behaviour is seen and for the highly viscous materials, the transition occurs earlier and is much smoother.

When the rheogram or flow curve for a fluid is compiled and a shear rate is selected, the apparent viscosity for that material can be calculated easily by obtaining the shear stress at that shear rate, and dividing the shear stress by the shear rate. The apparent viscosity of all the materials tested, was calculated at shear rates of 50, 100, 200 and 500 s^{-1}.

The graph in **Figure 5-6** shows how the apparent viscosity for 2.8 % CMC, 4.5% bentonite and 4.5% kaolin, which are rheologically different materials, can be calculated and compared at different shear rates.

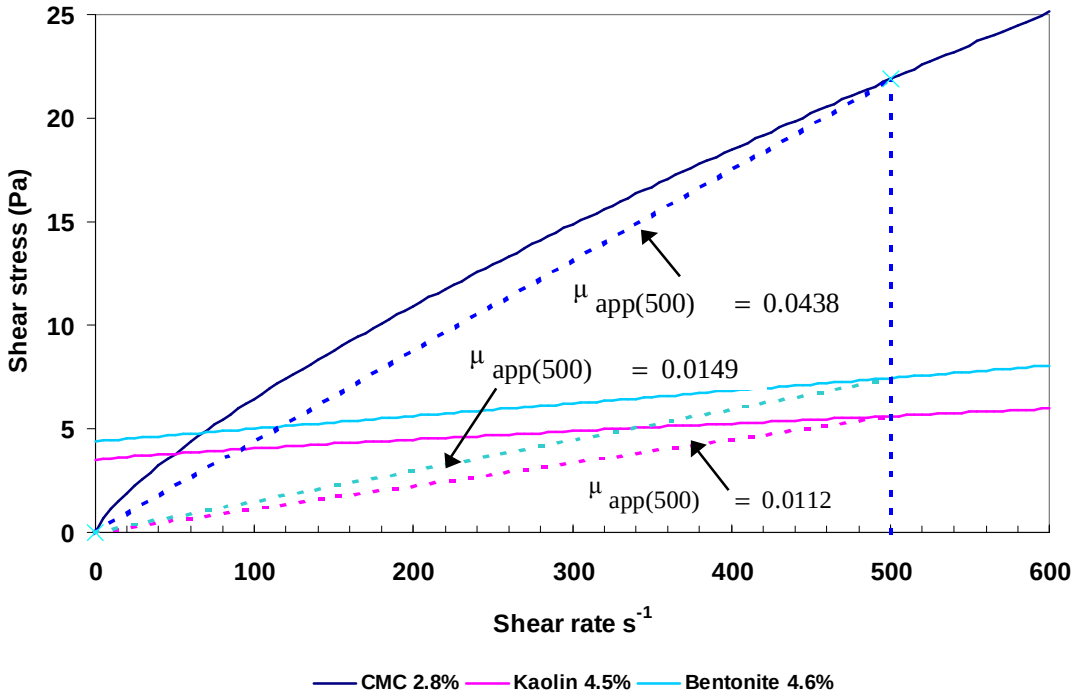

Figure 5-6 Rheogram CMC 2.8%, kaolin 4.5% and bentonite 4.6%

This apparent viscosity is therefore a single parameter that can describe the slurry at a specific shear rate.

A summary of the rheological parameters of the three slurries is presented in **Table 5-1** below.

Table 5-1 Rheological parameters of three tested fluids

150 mm Slurry	Flume Conc.	Ty	K	n	App visc 500 s^{-1}	App visc 200 s^{-1}	App visc 100 s^{-1}	App visc 50 s^{-1}
CMC	2.80%	0	0.197	0.7579	0.043757	0.054624	0.064605	0.076409
Kaolin	4.50%	3.51	0.0117	0.836	0.011242	0.022457	0.040598	0.07636
Bentonite	4.50%	4.402	0.0061	1	0.014904	0.02811	0.05012	0.09414

The next step was to establish a relationship between the apparent viscosities of a specific slurry and the Froude number as observed from the plot of Reynolds number

and Froude number for each slope. The start of transition was deemed to be the point of inflection, as this point corresponds in all cases with the deviation from the 16/Re line on the Moody diagram. The points of inflection were connected and the linear relationship was established between these points to establish a transition locus for a given fluid as shown in **Figure 5-7**. This was done for all the data sets. The following figures will show some examples of the how this was done, again for CMC 2.8% in **Figure 5-7**, kaolin 4.5% in **Figure 5-8** and bentonite 4.6% in **Figure 5-9**.

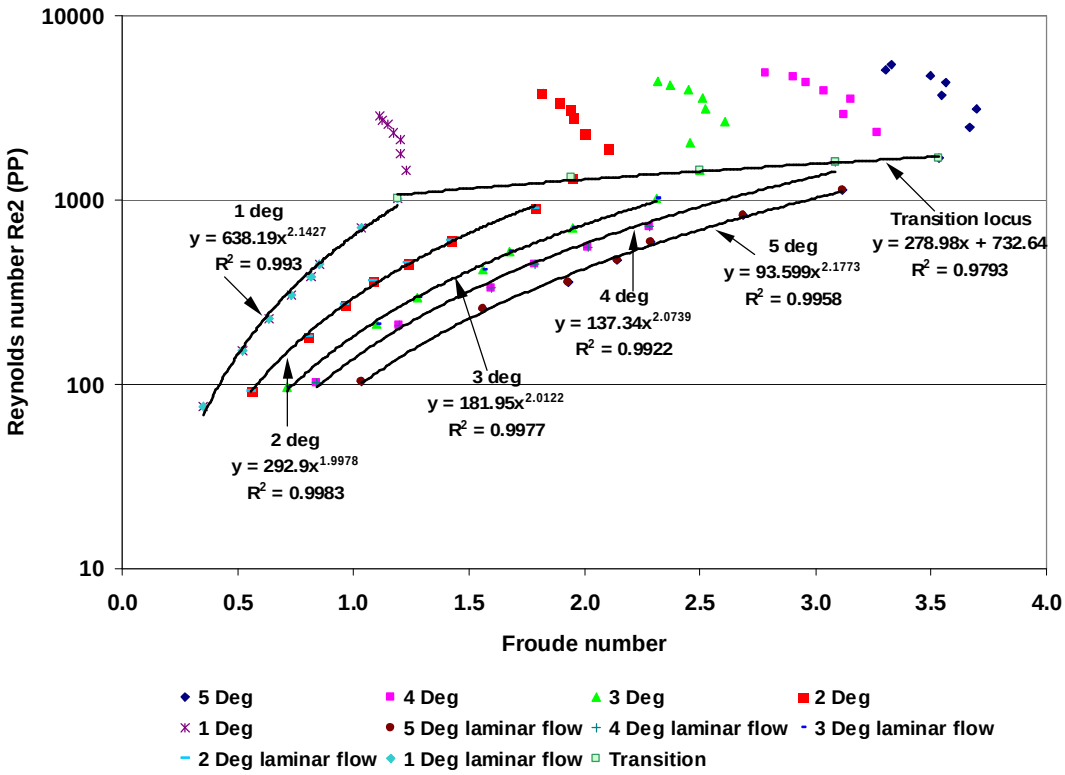

Figure 5-7 Onset of transition locus for 2.8% CMC in 150 mm flume

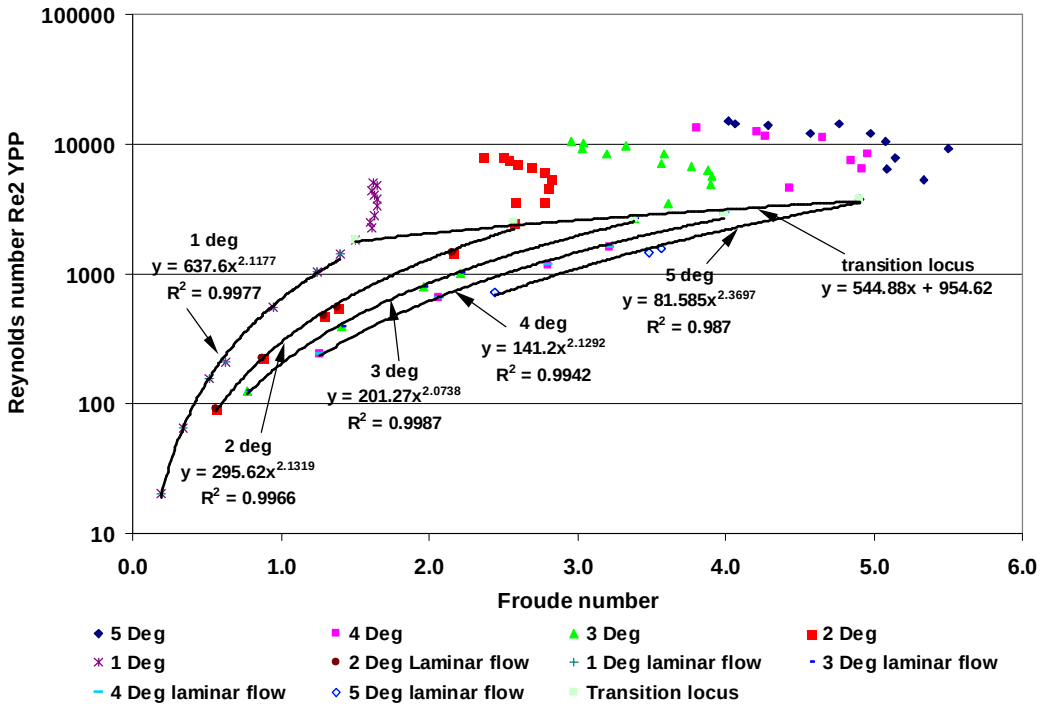

Figure 5-8. Onset of transition locus for 4.5% kaolin in 150 mm flume

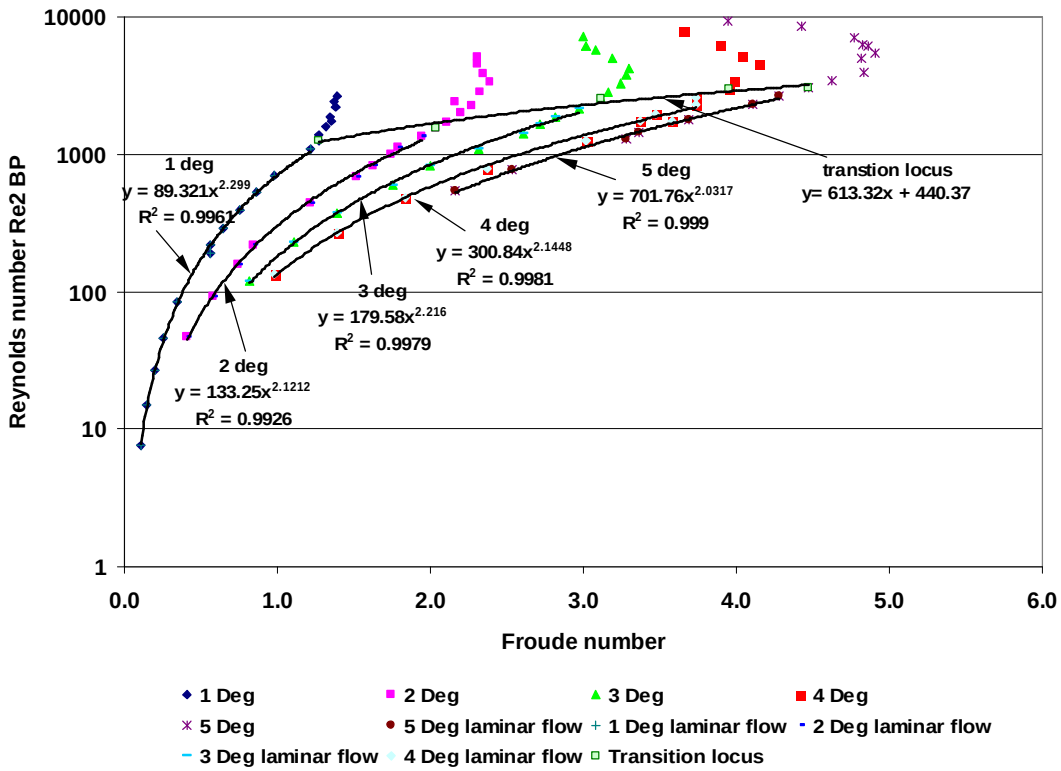

Figure 5-9 Onset of transition locus for 4.6% bentonite in 150 mm flume

The linear relationships were calculated for all the data sets and then the slope and y-intersect for each relationship was plotted against the apparent viscosities at shear rates 50, 100 and 200 s^{-1}. It was reasoned that the onset of transition would be in the lower shear rate region. The apparent viscosity shear rate diagrams in Chapter 3, Section 3.9.2, **Figure 3-32** to **Figure 3-37** indicated that at the shear rate of 100 s^{-1} the apparent viscosity was very similar for certain data sets.

From this a trend was established between the slope (m) and the y-intercept (c) values, with the apparent viscosities.

The best relationship was for the apparent viscosity at a shear rate of 100 s^{-1}.

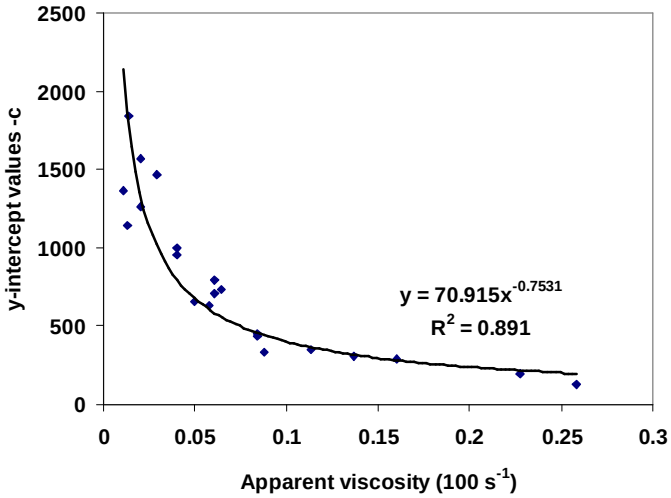

Figure 5-10 Onset of transition locus – relationship of c-values with apparent viscosity at 100 s^{-1} for all fluids

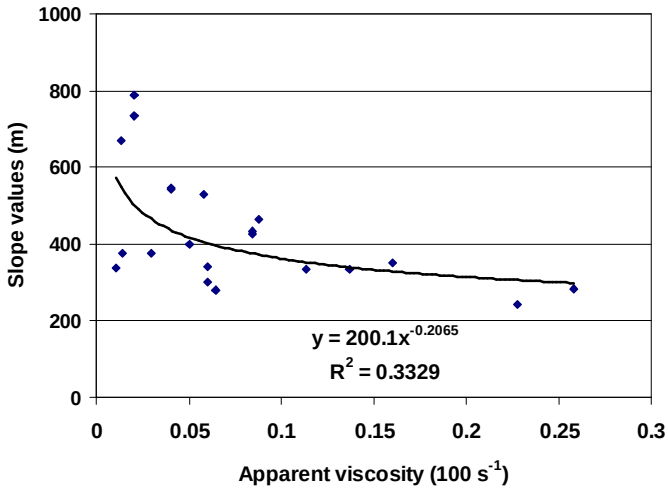

Figure 5-11. Onset of transition locus – relationship of m-values with apparent viscosity at 100 s^{-1} for all fluids

From the above two relationships a critical Reynolds number for predicting the onset of transitional flow could be established using the Froude number.

The relationship between the critical Reynolds number at the onset of transition and the Froude number was established to be a linear relationship for an apparent viscosity of 100 s^{-1}, with the slope being the relationship established in **Figure 5-11** and the y-intercept value the relationship shown in **Figure 5-10**.

The value of the critical Reynolds number at the onset of transition is:

$$\mathrm{Re}_c = \frac{200}{\left(\mu_{app(100s^{-1}}\right)^{0.21}}\mathrm{Fr} + \frac{71}{\left(\mu_{app(100s^{-1}}\right)^{0.75}}. \qquad 5.11$$

The constant 200 has a unit of $Pa.s^{0.21}$ and the constant 71, a unit of $Pa.s^{0.75}$.

The same procedure was followed with the apparent viscosities at 50 and 200 s^{-1}. All the sets of data were tested and the onset of transition was compared visually on the various Moody diagrams. The Reynolds number using the 100 s^{-1} apparent viscosity

relationship fitted the best over the whole range of data sets. The mathematical relationships were also the best at the shear rate of 100 s^{-1}.

This Reynolds number does not have a single value, but is a relationship between Reynolds number and Froude number for the specific apparent viscosity. The position of the onset of transition is where the Re_c (Equation 5.11) intersects with the 16/Re line. This is an optimisation process where the depth is optimised to satisfy both equations until the Reynolds numbers are the same.

This process is depicted in a flow chart format (see **Figure 5-12**).

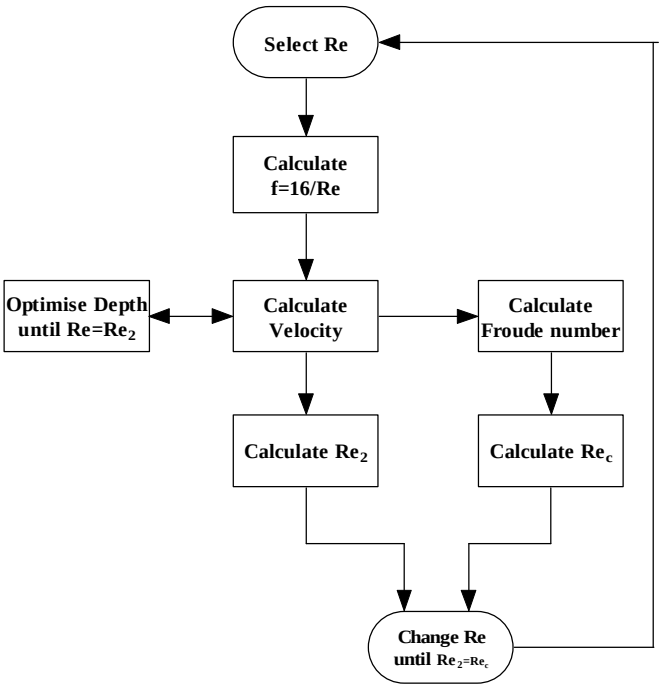

Figure 5-12 Flow chart: onset of transition calculation

An example is graphically displayed in **Figure 5-13**, and a worked example is given in Appendix C.

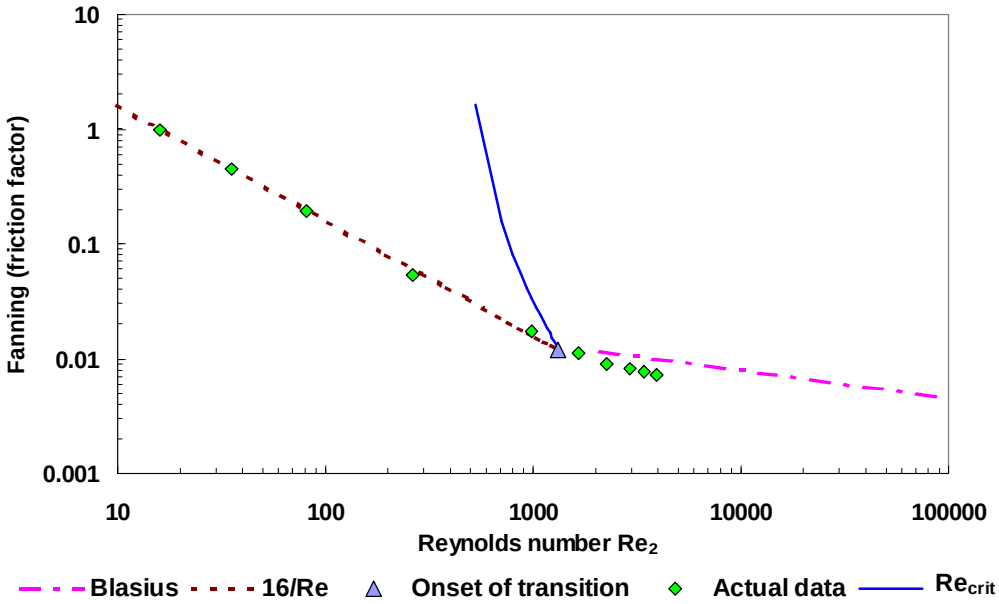

Figure 5-13 Example of the onset of transition. 6% kaolin in 150 mm flume, slope 3 degrees

This model is not perfect, but it is the only model that takes the viscous properties of the slurry as well as the slope of the flume into consideration.

5.6 ONSET OF 'FULL TURBULENCE'

From the trends established in **Figure 5-2**, **Figure 5-3** and **Figure 5-4**, it could be seen that at certain Reynolds numbers, depending on the slope and viscous properties of the slurry, the Froude number changed sharply when reaching a maximum value, which again seemed to indicate a change in flow behaviour.

Like for the onset of transition, the next step was to try to establish a relationship between the apparent viscosities of a specific fluid and the Froude number as observed from the plot of Reynolds number and Froude number for each slope. The points where the Froude number was a maximum, were connected and a linear relationship was

established. This was done for all the sets of data.

The following figures will show some examples of how this was done again for CMC 2.8% in **Figure 5-14**, kaolin 4.5% in **Figure 5-15** and bentonite 4.6% in **Figure 5-16**.

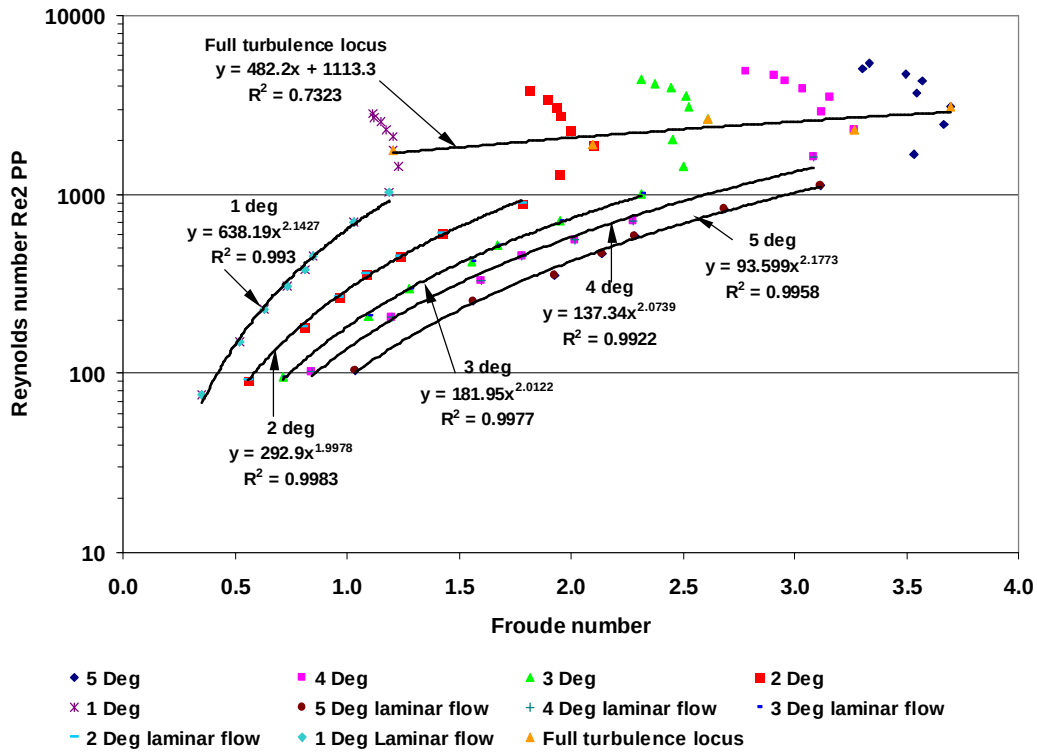

Figure 5-14 Onset of "full turbulence" 2.8% CMC in 150 mm flume

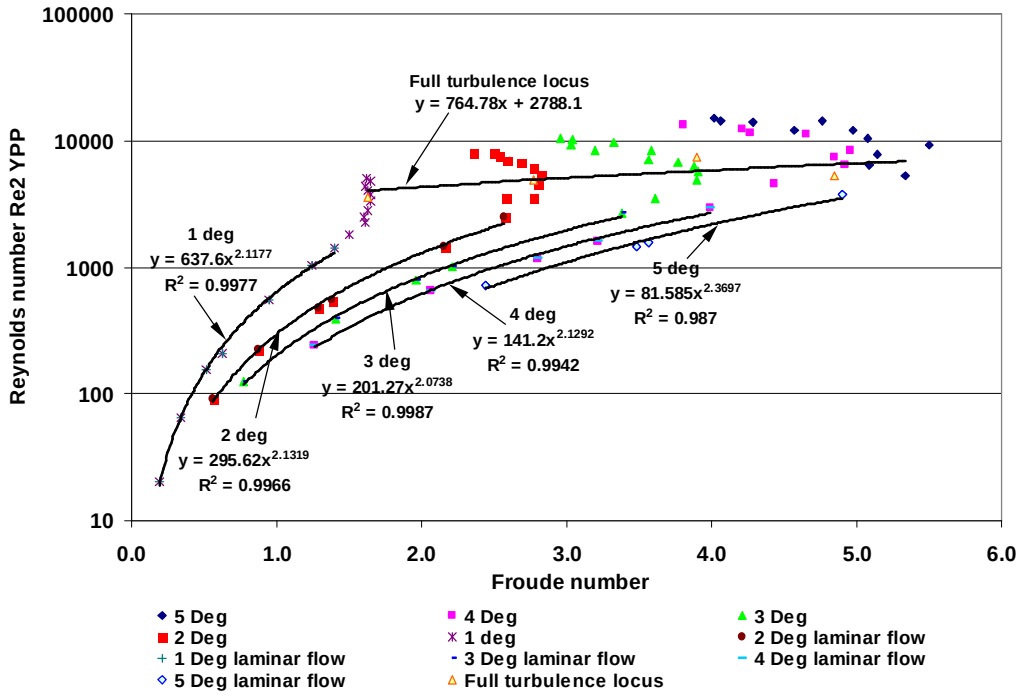

Figure 5-15 Onset of "full turbulence" 4.5% kaolin in 150 mm flume

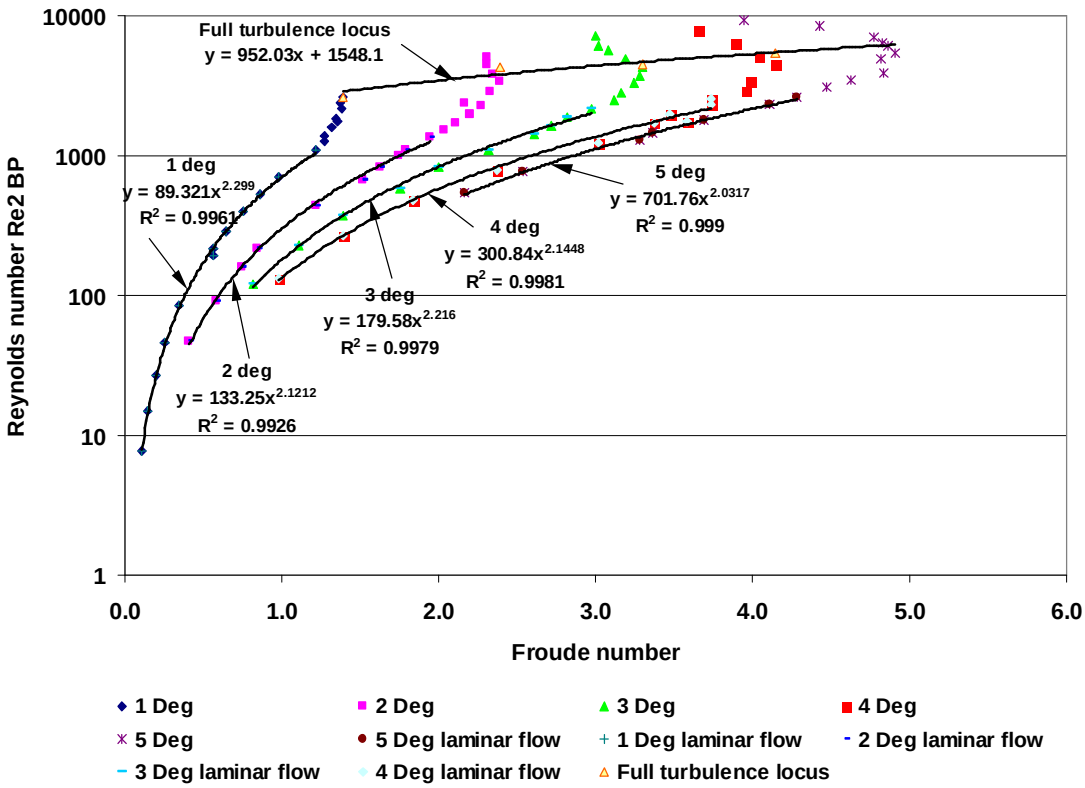

Figure 5-16 Onset of 'full turbulence' 4.6% bentonite in 150 mm flume

The linear relationships were calculated for all the data sets and then the slope and y-intercept for each relationship was plotted against the apparent viscosities at 100, 200 and 500 s^{-1}. It was reasoned that the onset of 'full turbulence' would be in the higher shear rate region, at least higher than 100 s^{-1}. From this a trend was established between the slope (m) and the y-intercept (c) values, and the apparent viscosity.

The best relationship was for the apparent viscosity at a shear rate of 500 s^{-1}.

The relationships are presented graphically below in **Figure 5-17** and **Figure 5-18**.

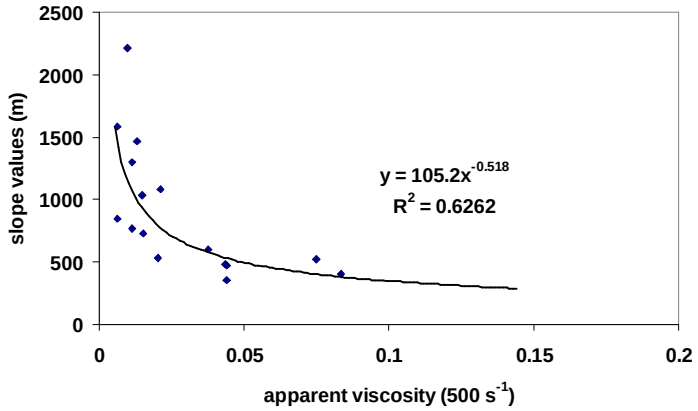

Figure 5-17 Onset of 'full turbulence' locus –relationship of m-values with apparent μ at 500 s^{-1} for all fluids

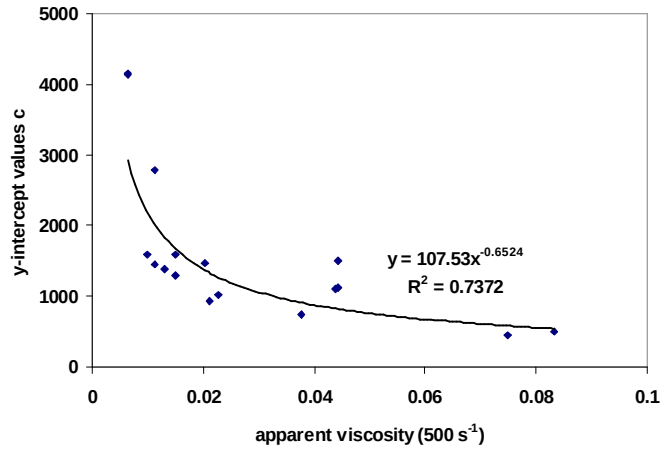

Figure 5-18 Onset of 'full turbulence' locus – relationship of c-values with apparent μ at 500 s^{-1} for all fluids

From the two relationships in **Figure 5-17** and **Figure 5-18**, a critical Reynolds number for predicting the onset of 'full turbulence' flow could be established using the Froude number at a shear rate of 500 s^{-1}.

The relationship between the critical Reynolds number at 'full turbulence' and the Froude number was established to be a linear relationship for an apparent viscosity of 500 s^{-1}, with the slope being the relationship established in **Figure 5-17** and the y-intercept value the relationship shown in **Figure 5-18**.

The value of the critical Reynolds number at the onset of 'full turbulence' or end of transition is:

$$Re_{c(turb)} = \frac{105}{\left(\mu_{app(500s^{-1})}\right)^{0.52}} Fr + \frac{108}{\left(\mu_{app(500s^{-1})}\right)^{0.65}}. \qquad 5.12$$

The constant 105 has a unit of $Pa.s^{0.52}$ and the constant 108 a unit of $Pa.s^{0.65}$.

To calculate this point is again an iterative process. The calculation starts with selecting the depth of flow calculated at the onset of transition. The turbulence velocity is then calculated using Equation 5.17. Both Re_2 and $Re_{c(turb)}$ are calculated. The depth is then increased until the two Reynolds numbers are the same. This process is shown by the flow process in **Figure 5-19**, depicted graphically in **Figure 5-20**, and a worked-out example is given in Appendix C.

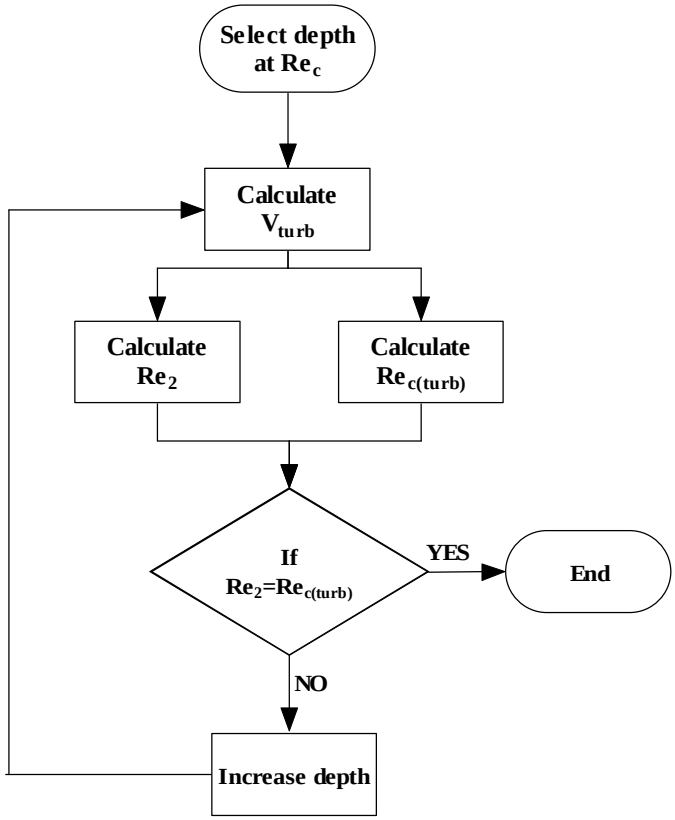

Figure 5-19 Flow chart: calculation of onset of 'full turbulence'

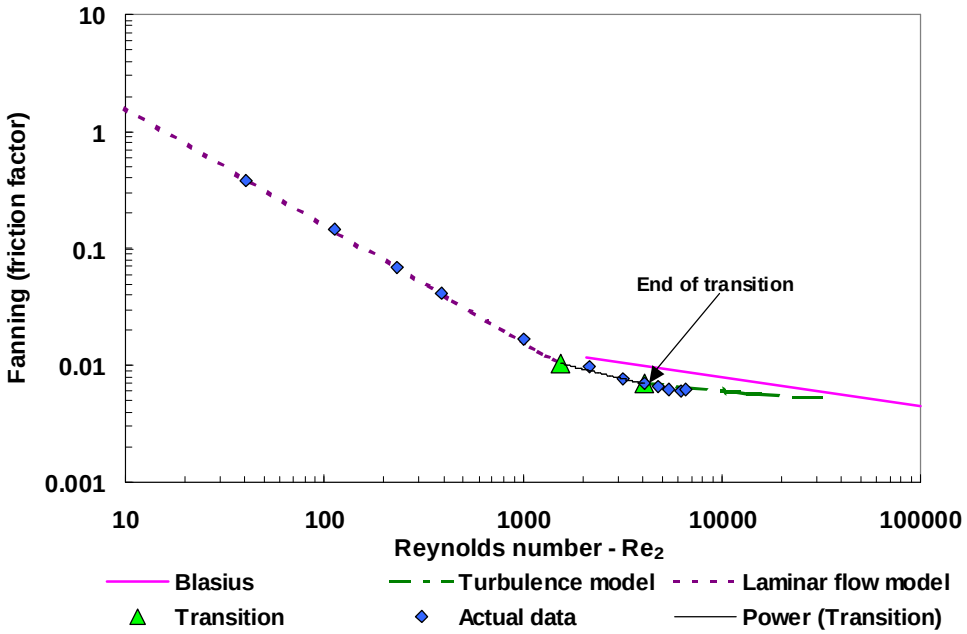

Figure 5-20 Onset of 'full turbulence' 4.5% bentonite in 150mm flume, slope 2 deg

As for the onset of transition, this Reynolds number is not perfect, but it is the only model that takes the viscous properties of the slurry as well as the slope of the flume into consideration to predict the onset of 'full turbulence' or end of transition.

5.7 TURBULENCE MODEL

In Chapter 4, various turbulent models were tested with the available turbulent test data and none of the models seem to be able to predict the turbulent data of the three different fluids adequately. Over the whole range, the Slatter model seemed to perform the best.

5.7.1 Roughness function B

The objective here was to establish a roughness function B for all the test data as Slatter (1994) did for his turbulence model for pipe flow. This, however, did not work, as there was a flume slope effect. This can be seen from the data displayed in **Figure 5-21**, **Figure 5-22** and **Figure 5-23**. The roughness Reynolds number is:

$$Re_r = \frac{8\rho V^*}{\tau_y + K - \left(\frac{8V^*}{d_x}\right)^n}. \qquad 5.13$$

The roughness function B is used by Slatter (1994) for pipe flow when he takes the effect of particle size roughness of the slurry into account by including the solids particle effect $d_x = d_{85}$. The average velocity is defined as:

$$\frac{V}{V_*} = \frac{1}{\chi}\ln\left(\frac{R}{d_{85}}\right) + B - 3.75. \qquad 5.14$$

This reverts to the following equation for open channel flow when the diameter is substituted by the hydraulic radius:

$$\frac{V}{V_*} = \frac{1}{\chi}\ln\left(\frac{2R_h}{d_{85}}\right) + B - 3.75. \qquad 5.15$$

From equation 6.19, B is equal to:

$$B = \frac{V}{V_*} - \frac{1}{\chi}\ln\left(\frac{2R_h}{d_{85}}\right) + 3.75. \qquad 5.16$$

The roughness function B was plotted versus the roughness Reynolds number as shown below for CMC 2.8% in **Figure 5-21**, kaolin 4.5% in **Figure 5-22** and bentonite 4.6% in **Figure 5-23**, all in the 150 mm flume.

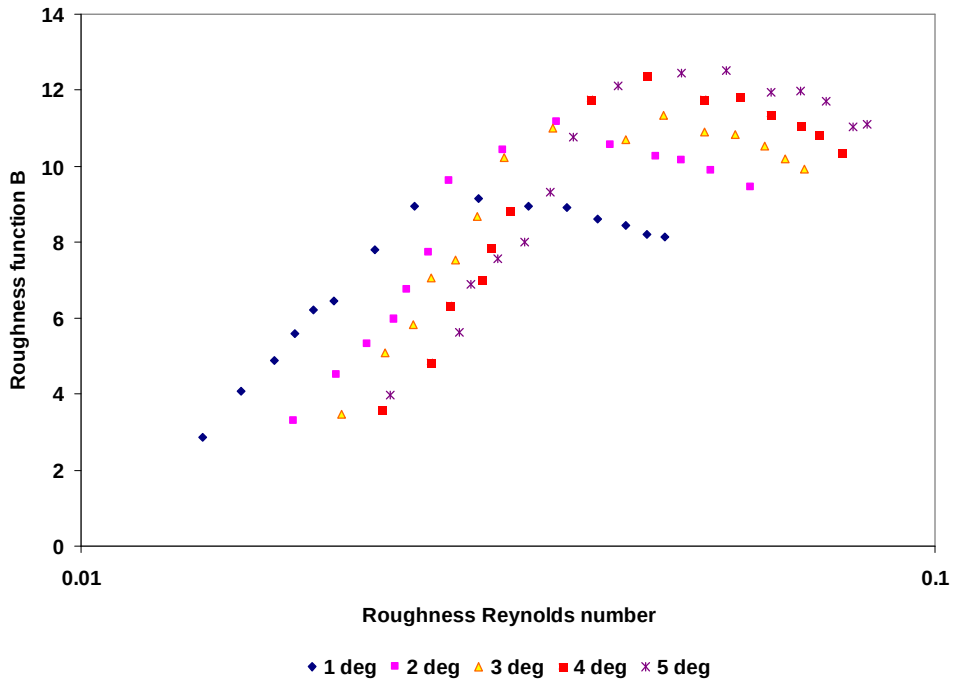

Figure 5-21 Roughness function B for 2.8% CMC in 150 mm flume

For the CMC the representative particle size becomes the flume roughness.

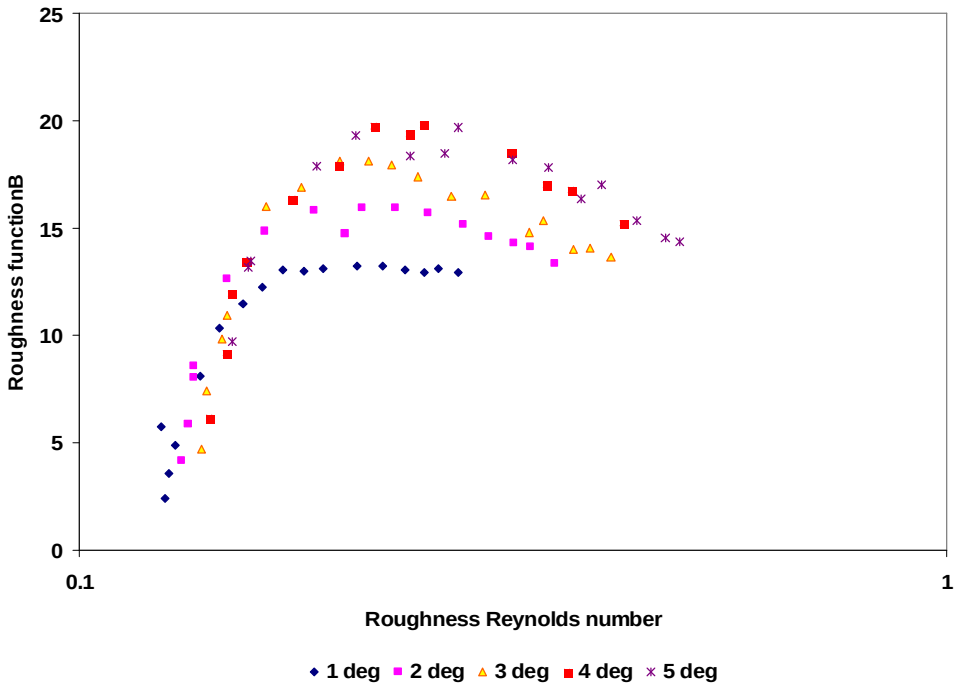

Figure 5-22 Roughness function B for 4.5% kaolin in 150 mm flume

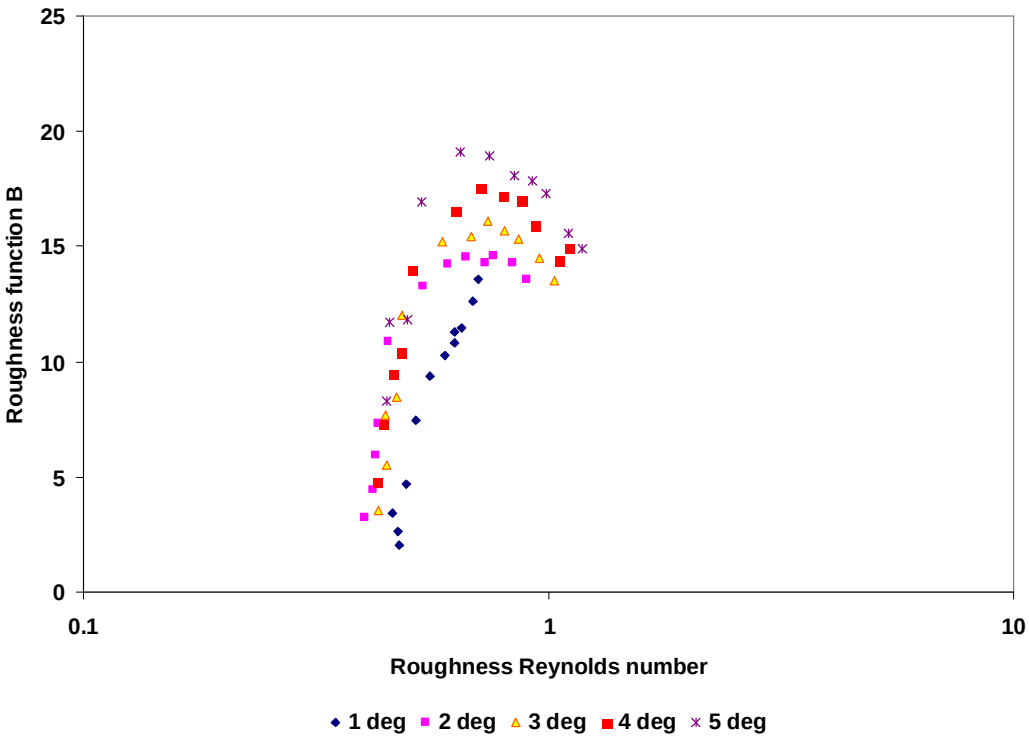

Figure 5-23 Roughness function B for 4.5% bentonite in 150 mm flume

When using the various values for B obtained from the graphs displayed typically in **Figure 5-21**, **Figure 5-22** and **Figure 5-23**, and taking the particle roughness into consideration, the turbulent model prediction did not fit the actual data well. There seemed to be an over-prediction of Reynolds number value and an under-prediction of friction factor, and a slope effect was also clearly visible.

It seemed as though some viscous effect needed to be taken into account even in the turbulent flow regime. This was already very visible when the more viscous concentrations showed no surface disturbance, even at reasonably high Reynolds numbers, indicating that some viscous effects were still present.

5.8 NEW TURBULENCE MODEL

All the turbulent data sets were again analysed by visually optimising the value of B-3.75 in Equation 5.15, as well as the constant by which the friction factor had to be adjusted to align the predicted values with the actual data.

The values of B-3.75 and friction factor adjustment constant are plotted versus the apparent viscosity at shear rate 500 s^{-1}, and displayed below in **Figure 5-24** and **Figure 5-25**.

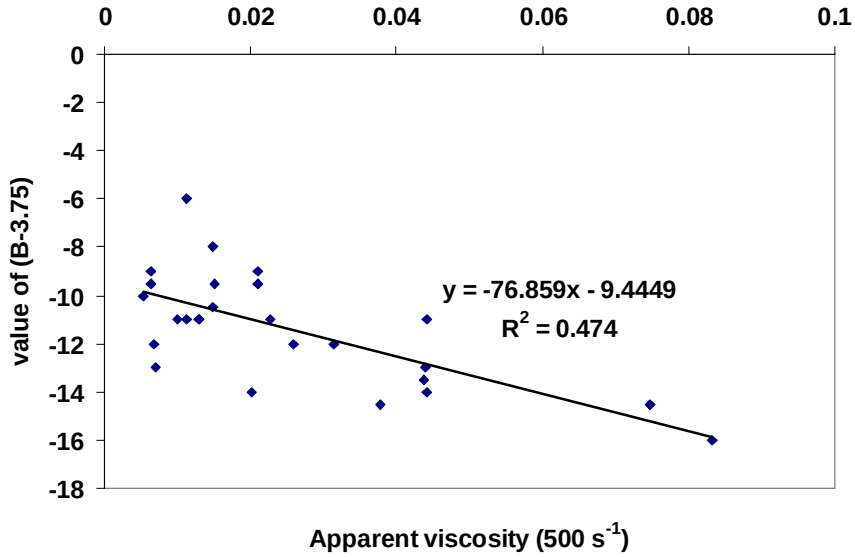

Figure 5-24 Turbulent data (values of B-3.75) against apparent viscosity of 500 s^{-1}

The relationship between the B-3.75 versus the apparent viscosity at shear rate 500 s^{-1} is not a very good fit but a linear relationship as shown in **Figure 5-24** was the best that could be established with the available turbulent data.

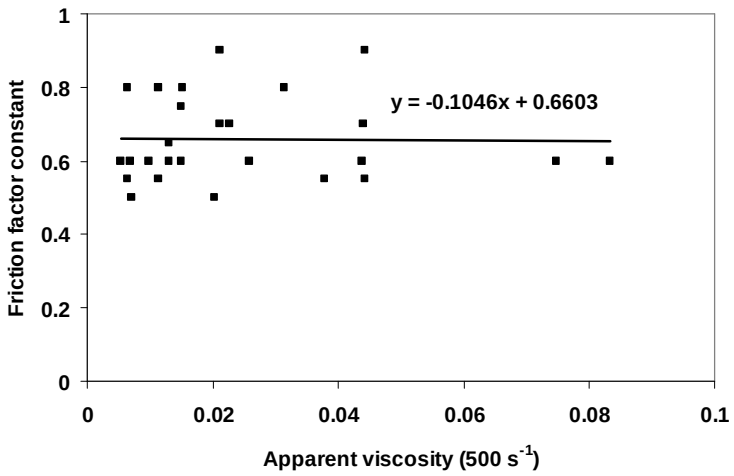

Figure 5-25 Turbulent data: friction factor constant against apparent viscosity (500 s^{-1})

The slope of the relationship between the constant for the friction factor and the apparent viscosity is very small and therefore the constant was taken to be 0.66.

The average velocity for turbulence taking is therefore:

$$V_{turb} = \sqrt{ghsin\alpha}\left(2.5\ln\frac{2R_h}{k} - 76.86\mu_{app(500)} - 9.45\right). \qquad 5.17$$

With this velocity the depth of flow can be calculated by substituting depth and width of the flume instead of the hydraulic radius.

Although **Figure 5-24** and **Figure 5-25** show significant scatter, the velocities as calculated from equation 5.17 will be show much lower errors. See Section 6.8.3 in Chapter 6.

The friction factor in turbulent flow is:

$$f = \frac{0.66\left(2ghsin\alpha\right)}{\left(V_{turb}\right)^2}. \qquad 5.18$$

5.9 TRANSITION RANGE

To estimate the values of the friction factor in the range between the onset of transition and full turbulence, a power law curve was fitted between the two points. For the experimental database contained in this thesis, this adequately estimated the values in this range for the friction factor.

The full design procedure is described in Annexure C.

5.10 EXAMPLES

The following six figures from **Figure 5-26** to **Figure 5-31** show a few selected typical

examples of experimental data with the models fitted using all three slurries, three size flumes and different slopes from 1 to 5 degrees.

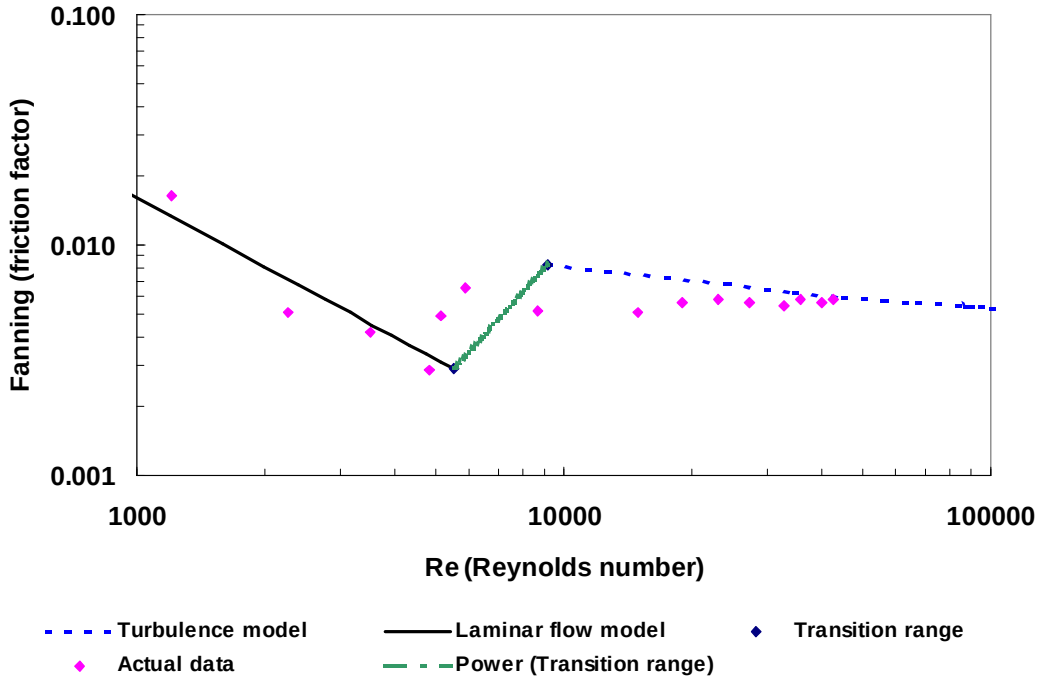

Figure 5-26 Moody diagram 3% bentonite in 150 mm flume with 5 deg slope

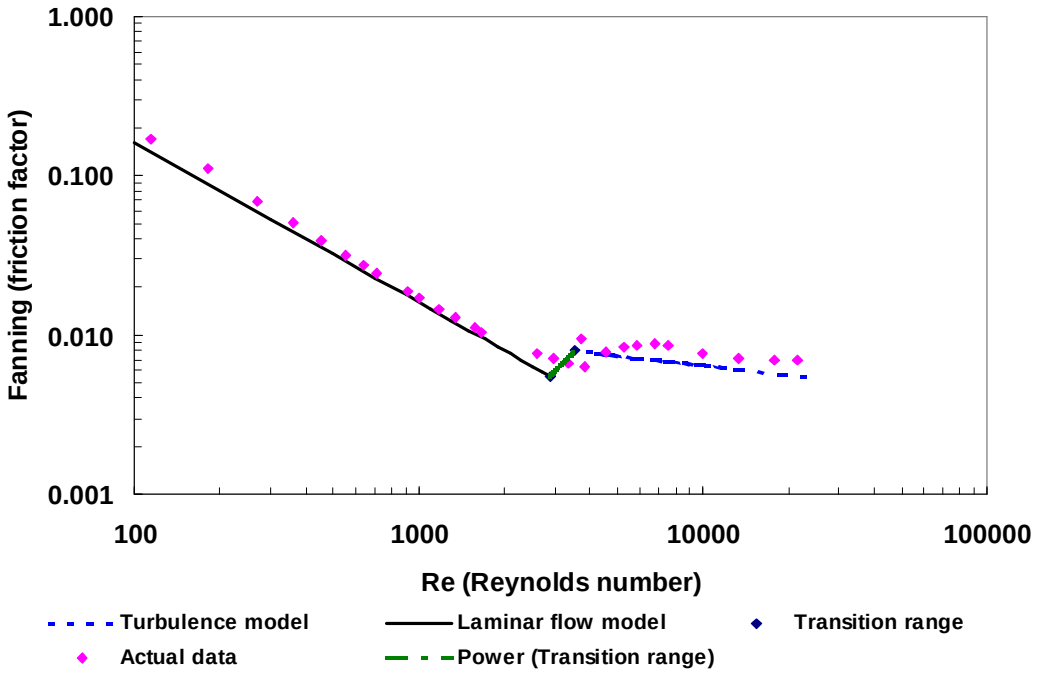

Figure 5-27 Moody diagram 1.5% CMC in 300 mm flume with 1 deg slope

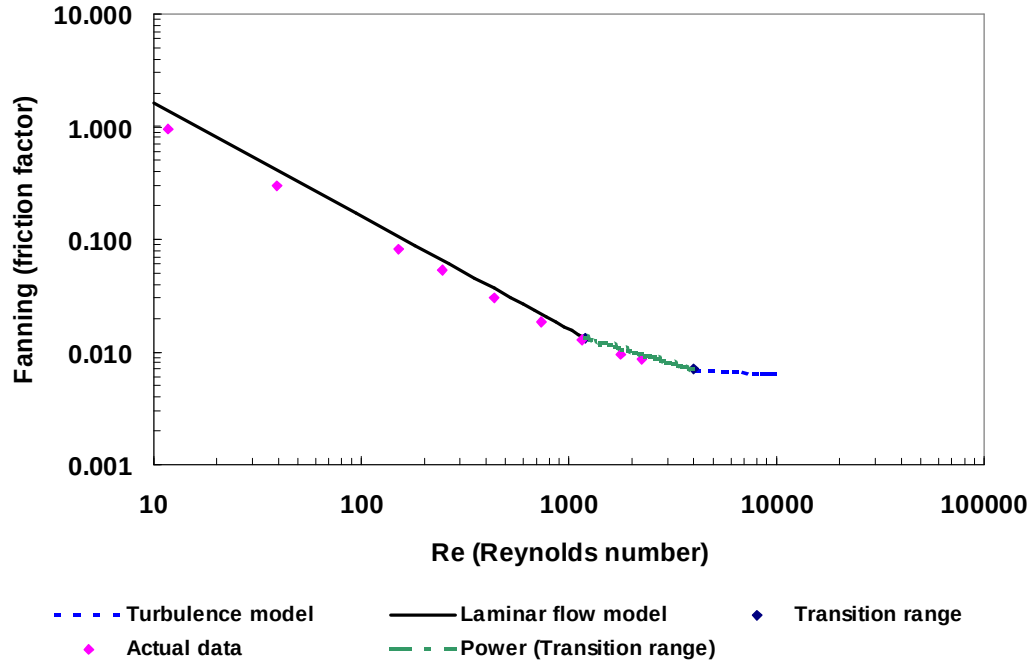

Figure 5-28 Moody diagram 4.5% kaolin in 75 mm flume with 1 deg slope

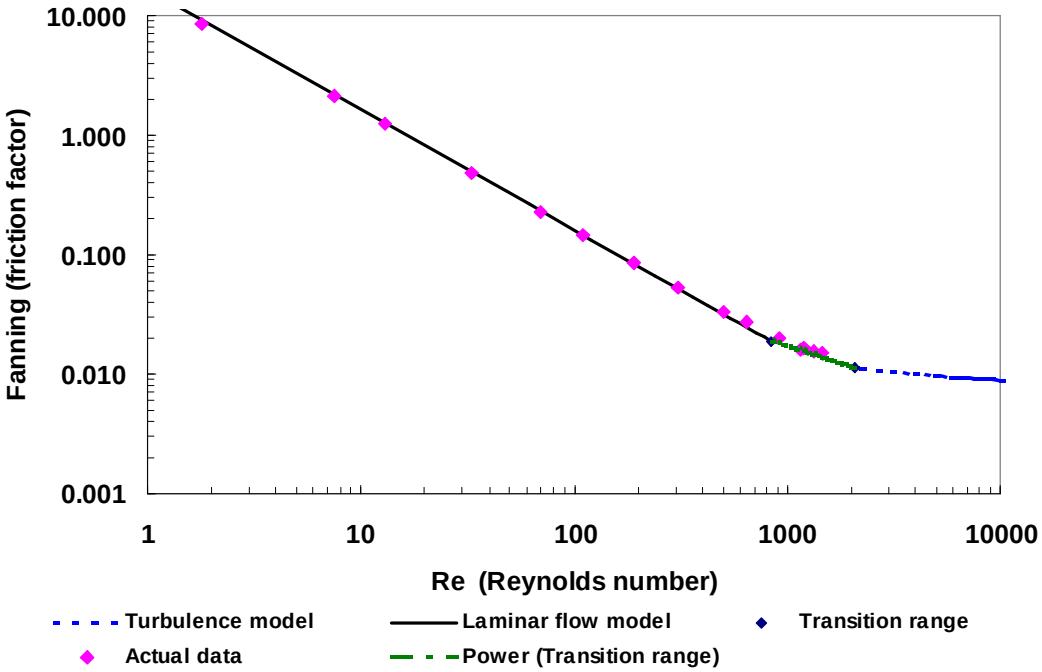

Figure 5-29 Moody diagram 10% kaolin in 150 mm flume with 5 deg slope

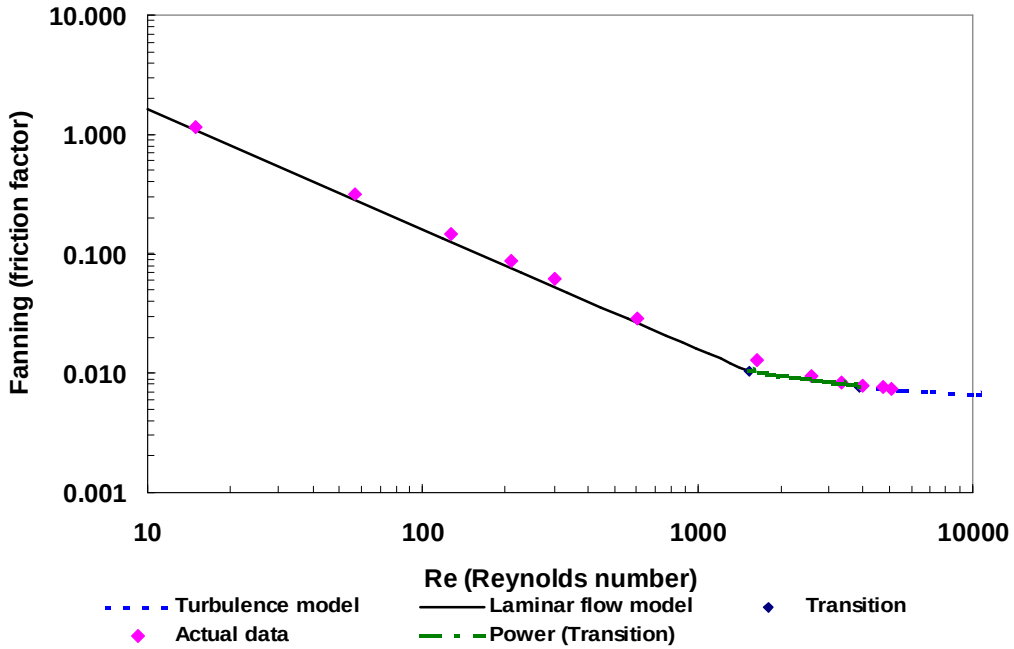

Figure 5-30 Moody diagram 6% bentonite in 150 mm flume with 4 deg slope

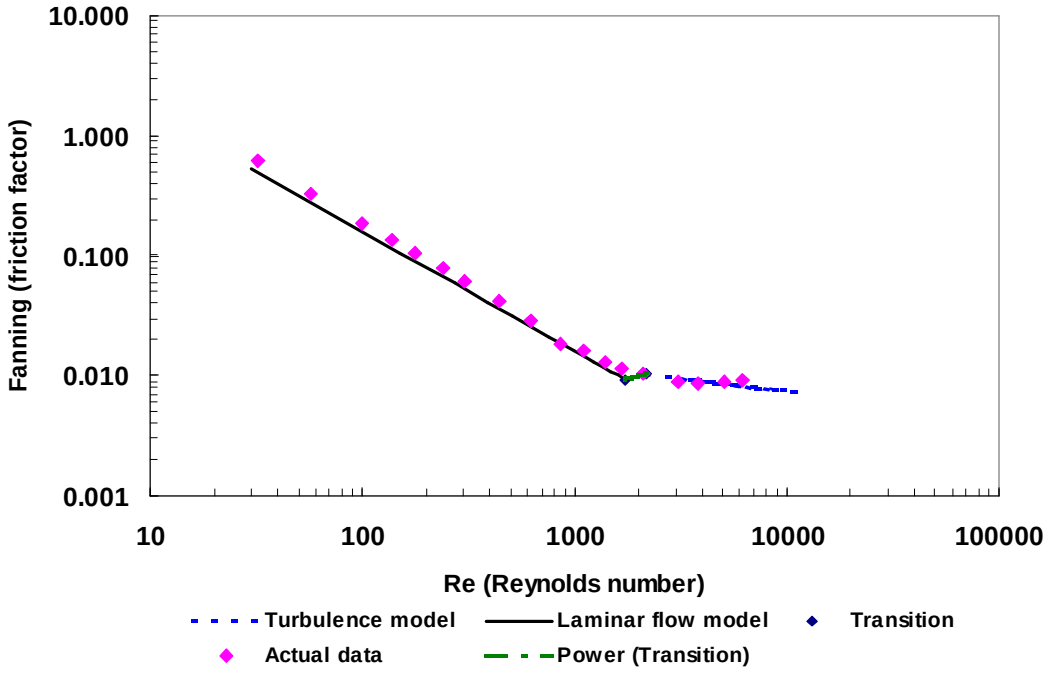

Figure 5-31 Moody diagram 3% CMC in 300 mm flume with 3 deg slope

5.11 CONCLUSIONS

The previous six figures from **Figure 5-26** to **Figure 5-31** show that the Moody diagram is a suitable format on which the open channel flow regimes can be displayed for the non-Newtonian fluids tested in this thesis. The data presented also predicts the flow over the range of data presented in this thesis adequately.

The following new models have been presented:

- **Laminar Flow**

A laminar flow Reynolds number, which suitably predicts the flow of all three materials namely CMC, kaolin and bentonite over a range of concentrations and over slopes varying from one to five degrees and in three rectangular flumes 75, 150 and 300 mm in width. The slurries presented are classified rheologically as pseudoplastic, yield pseudoplastic and Bingham fluids. The Reynolds number reverts to the Newtonian Reynolds number in its simplest form.

The laminar flow data has been presented on the Moody diagram and all the laminar flow data available can be collapsed on the 16/Re line. This is very convenient when calculating the friction factor, because it is a simple relationship.

- **Transition Zone**

From the experimental work it was observed that the transition for the less viscous fluids was water-like, but the more viscous fluids displayed a very different transition. The transition occurred at much lower Reynolds numbers and the transition was also much smoother.

It was also observed that viscous characteristics of very different fluids were very similar at certain shear rates when the apparent viscosity was plotted against the shear rate. Some fluid concentrations could be grouped together. One such zone occurred at 100 s^{-1}. The fluids with these similar apparent viscosities also displayed similar transitional behaviour.

The Froude number effect on the more viscous fluids also did not seem to be critical. The fluid surface in the transition zone was very smooth, indicating the strength of the viscous forces at the free surface. When Reynolds number was plotted against Froude number, the transition zone was more visible than on the Moody diagram.

A transition criterion in the form of a new Reynolds number is presented which is expressed in terms of the Froude number and which uses the apparent viscosity of the slurry at a shear rate of 100 s^{-1} to take represent the viscous behaviour of the fluid.

A new Reynolds number to predict the onset of 'full turbulence' is presented also in terms of the Froude number. The apparent viscosity at shear rate 500 s^{-1} represents the viscous behaviour of the fluid in this Reynolds number.

For the transition range a power law curve is fitted between the point of onset of transition and the onset of full turbulence.

- **Turbulence**

The experiments showed that the friction factor had a much flatter slope on the Moody diagram for the more viscous fluids than a Newtonian model like the Blasius equation indicated.

For turbulence a new model is presented based on the turbulence model of Slatter (1994), which does not take particle roughness into account but uses a relationship for the roughness number B and the apparent viscosity of the slurry at a shear rate of 500 s^{-1}.

It is believed that this is the first time that a procedure has been developed to predict non-Newtonian rectangular open channel flow over a wide range of slopes, flow rates and slurry types.

CHAPTER 6

EVALUATION OF NEW MODELS

6.1 INTRODUCTION

In this chapter, the new models developed in this thesis that were described in Chapter 5 will be evaluated. The following will be discussed.

- The Reynolds number developed.
- The effect of different rheological models on the friction factor in laminar flow.
- The effect that the different rheological characterisation approaches have on the friction factor in laminar flow.
- The average wall shear stress approach.
- The transition zone.
- The turbulence model.

6.2 NEW REYNOLDS NUMBER

The development of the new Reynolds number is described in Chapter 5. The advantage of this Reynolds number is that it can be used for any non-Newtonian fluid that can be rheologically classified as either a pseudoplastic, yield pseudoplastic or Bingham fluid. The Reynolds number in its simplest form will revert to the Newtonian Reynolds number.

6.3 THE EFFECT OF THE RHEOLOGICAL MODEL USED ON LAMINAR FLOW

When characterising a non-Newtonian fluid, it is generally accepted that it is important to make sure that the correct model is fitted to the rheogram.

The Reynolds number used in this thesis, Re_2, uses the rheological parameters τ_y , K and n to characterise the fluid. The tube viscometer data is plotted on a pseudo shear diagram and then the Rabinowitsch-Mooney transformation is applied to the data. The pseudo shear diagram is therefore transformed into a rheogram. By means of curve fitting, the data is then classified as either a Bingham, pseudoplastic or yield pseudoplastic fluid. The pseudoplastic model is also called the power-law model and the yield pseudoplastic model the Herschel-Bulkley model. The question now arises whether it matters if a so-called Bingham fluid is classified as a yield pseudoplastic or a pseudoplastic. In the literature this is often found, for example, when for the sake of simplicity a yield pseudoplastic is classified as a Bingham fluid. An example of this is Naik (1983) and Slatter and Wasp (2000), who classified kaolin as a Bingham fluid.

In this thesis, kaolin was classified as a yield pseudoplastic, CMC as a pseudoplastic and bentonite as a Bingham fluid. Each concentration was then also rheologically classified as a yield pseudoplastic, pseudoplastic and a Bingham fluid to determine if this would have an effect on the results.

All the laminar data of all the fluid concentrations were extracted. The Reynolds number $Re_{2(YPP)}$, $Re_{2(PP)}$ and $Re_{2(BP)}$, were calculated for all the data sets. The deviation

of the friction factor from the 16/Re line was then calculated and compared for the different rheological models. The reason for this was to establish whether the model really played a significant role. When one just looks at the Moody diagram, one can already see a variation, even though the diagram uses log values on both axes.

6.3.1 Bentonite 4.5% in 150 mm flume

The following is an example of 4.5% bentonite in the 150 mm flume, applying the three rheological models to the same data set. The Moody diagram already indicates that the best fit is the Bingham model. This is shown in **Figure 6-1**.

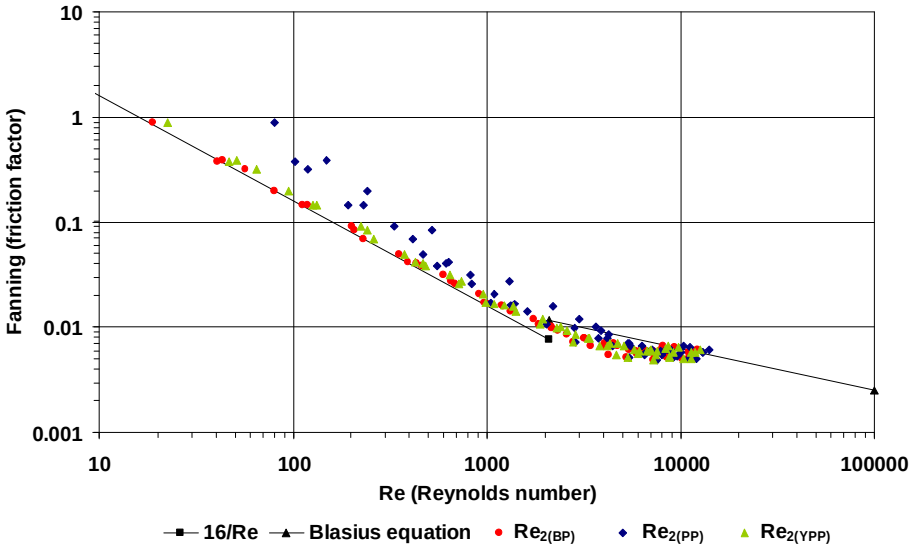

Figure 6-1 4.5 % bentonite in a 150 mm flume. Different rheological models

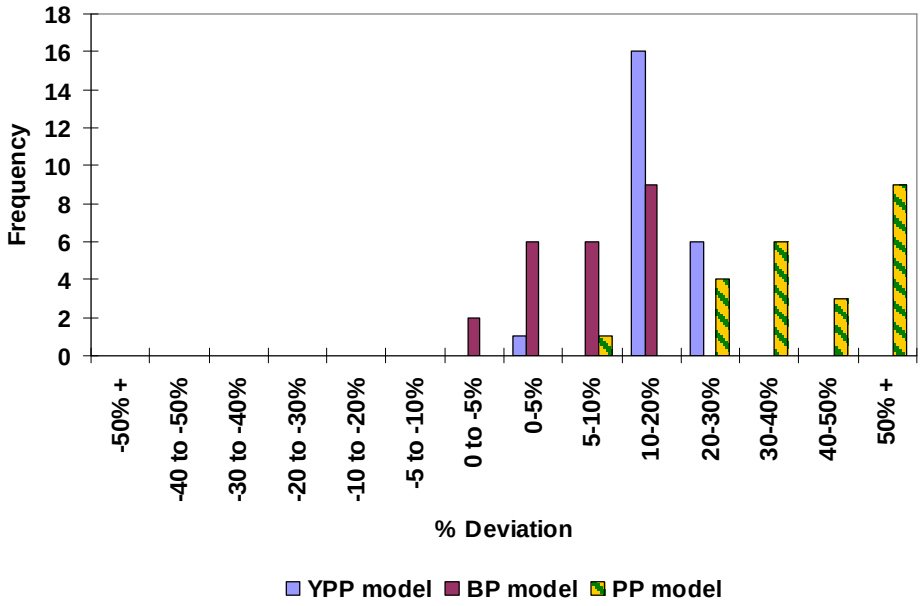

Figure 6-2 Friction factor deviation in laminar flow. Different rheological models for 4.5 % bentonite in 150 mm flume

In **Figure 6-2**, the frequency of deviation from the 16/Re line is plotted versus the percentage deviation.

Figure 6-2 shows clearly that bentonite is a Bingham fluid as the deviation is the least. It also shows that the pseudoplastic fit is the worst. The yield pseudoplastic model is a reasonable fit but not as good as the Bingham model. This is substantiated by the data presented in **Table 6-1**.

Table 6-1 Bentonite 4.5% in 150 mm flume. Different Rheological models

Model	T_y	K	n	max % Dev	min % Dev	ave % Dev	LSE
$Re_{2(YPP)}$	11.774	0.018	0.867	19.07%	8.05%	12.71%	0.0140
$Re_{2(BP)}$	12.698	0.006		15.07%	2.39%	7.63%	0.0088
$Re_{2(PP)}$		2.4612	0.2971	59.57%	33.76%	45.92%	0.0634

6.3.2 Bentonite 6% in 75 mm flume

The next data set is also for bentonite but this time for a 6% concentration in a 75 mm flume.

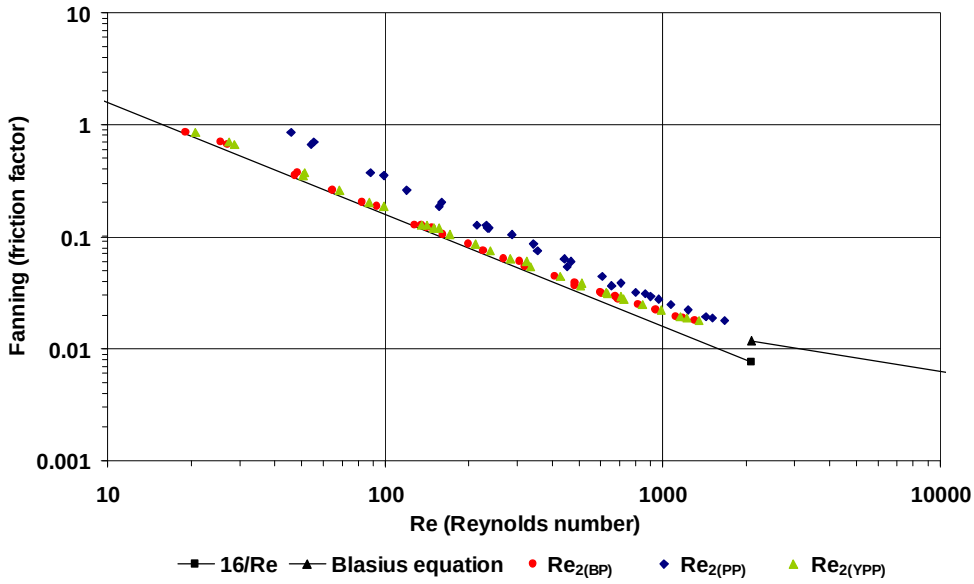

Figure 6-3 6 % bentonite in a 75 mm flume. Different rheological models

The Moody diagram in Figure 6-3 and the friction factor deviation in Figure 6-4 again indicate clearly that Bentonite is a Bingham fluid and cannot be classified as a pseudoplastic fluid. In this case the yield pseudoplastic model does not fit badly but is still not as good as the Bingham model. This is also substantiated by the data presented in **Table 6-2**.

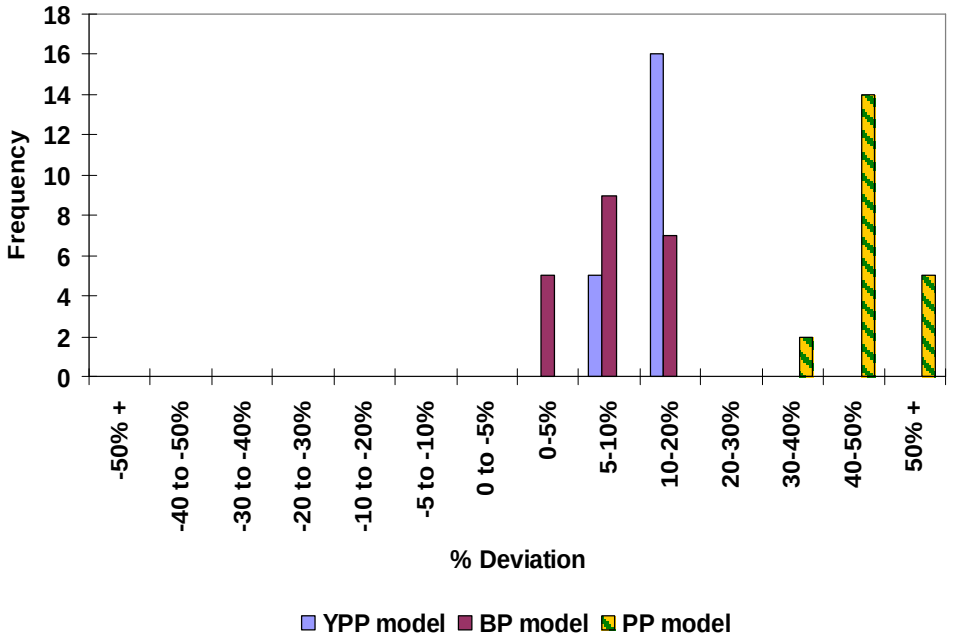

Figure 6-4 Friction factor deviation in laminar flow. Different rheological models for 6 % bentonite in 75 mm flume

Table 6-2 Bentonite 6% in 75 mm flume. Different rheological models

Model	T_y	K	n	max % Dev	min % Dev	ave % Dev	LSE
$Re_{2(YPP)}$	11.774	0.018	0.867	19.07%	8.05%	12.71%	0.0140
$Re_{2(BP)}$	12.698	0.006		15.07%	2.39%	7.63%	0.0088
$Re_{2(PP)}$		2.4612	0.2971	59.57%	33.76%	45.92%	0.0634

6.3.3 CMC 2.8% in 75 mm flume

The next set of data is for 2.8% CMC tested in a 75 mm flume. CMC is usually classified as a pseudoplastic or power-law fluid. The Moody diagram in **Figure 6-5** shows that the CMC is not a Bingham fluid and that the pseudoplastic and yield pseudoplastic models give similar values. The reason for this is that when you fit these models to the data they are similar. The yield pseudoplastic model only has a small yield stress, which does not significantly influence the data.

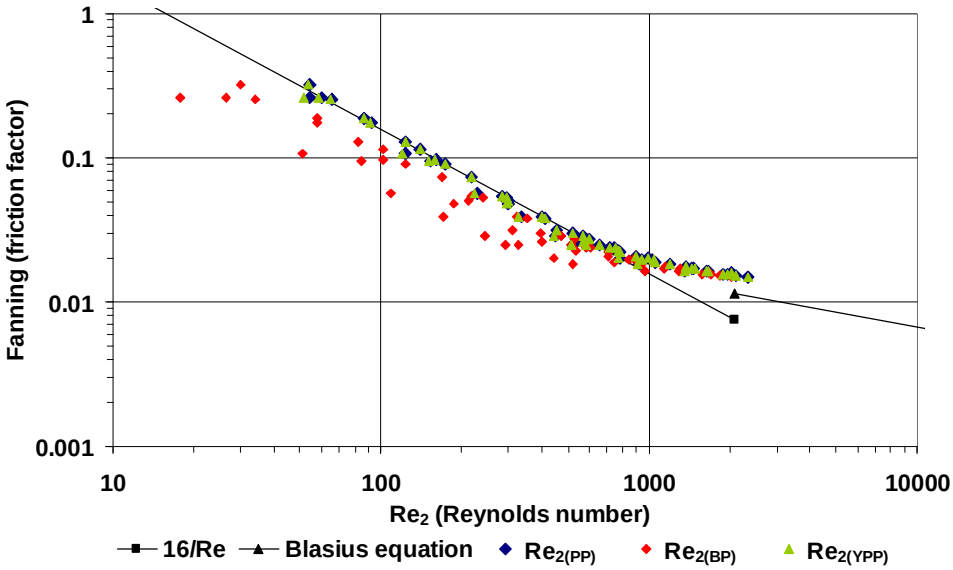

Figure 6-5 Moody diagram 2.8% CMC in 75 mm flume. Different rheological models

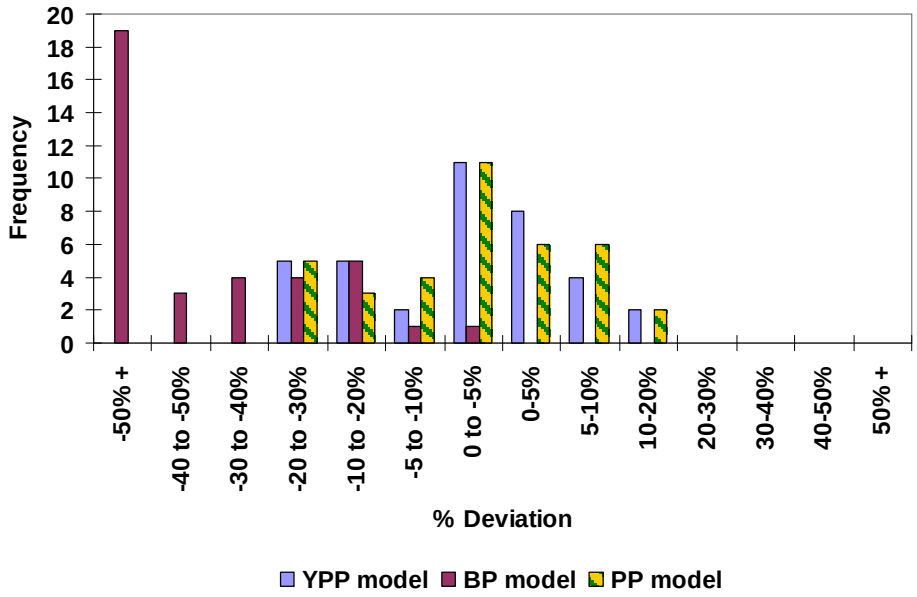

Figure 6-6 Friction factor deviation in laminar flow. Different rheological models for 2.8% CMC in the 75 mm flume

Figure 6-6 shows the same trend as described for **Figure 6-5** and is substantiated by the data presented in **Table 6-3**.

Table 6-3 CMC 2.8% in 75 mm flume. Different rheological models

Model	T_y	K	n	max % Dev	min % Dev	ave % Dev	LSE
$Re_{2(YPP)}$	0.202	0.182	0.769	15.00%	-26.04%	8.17%	0.0077
$Re_{2(BP)}$	5.626	0.0293		-3.31%	-241.49%	65.56%	0.0398
$Re_{2(PP)}$		0.197	0.7579	14.96%	-24.27%	7.53%	0.0071

6.3.4 CMC 3.8% in 300 mm Flume

The following data set is for 3.8% CMC in the 300 mm flume. CMC is generally classified as a pseudoplastic fluid. The Moody diagram in **Figure 6-7** and the friction factor deviation in **Figure 6-8** as well as **Table 6-4**, show that the Bingham plastic rheological model is the worst fit. This is the same trend as described for the 2.8% CMC in the 75 mm flume.

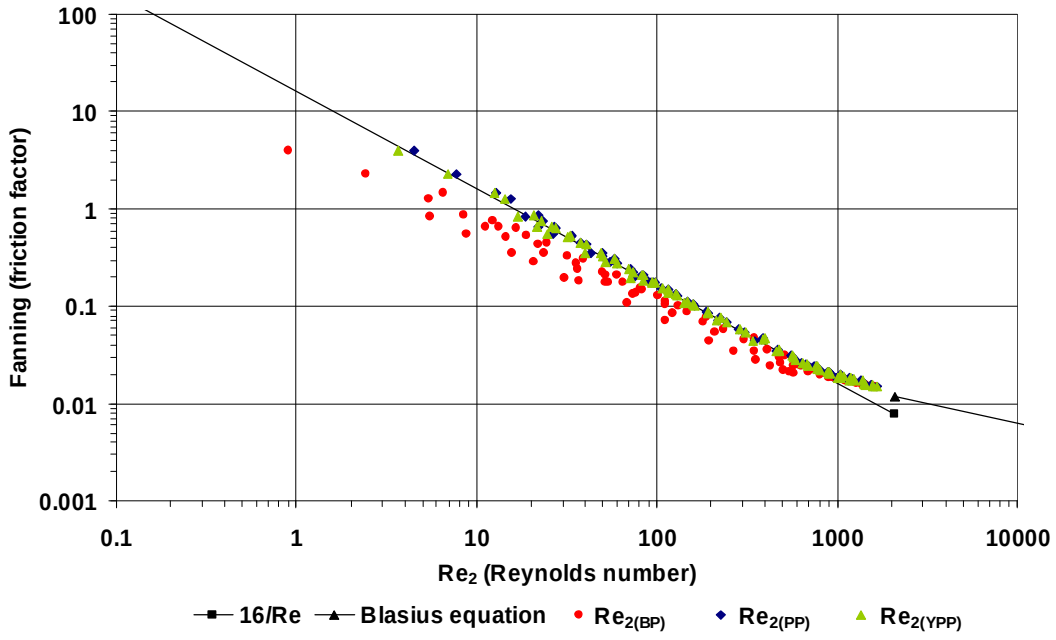

Figure 6-7 Moody diagram 3.8% CMC in 300 mm Flume. Different rheological models

The reason why the yield pseudoplastic model number fits reasonably well is because with the curve fitting a small yield stress results, which is then very close to a pseudoplastic fit.

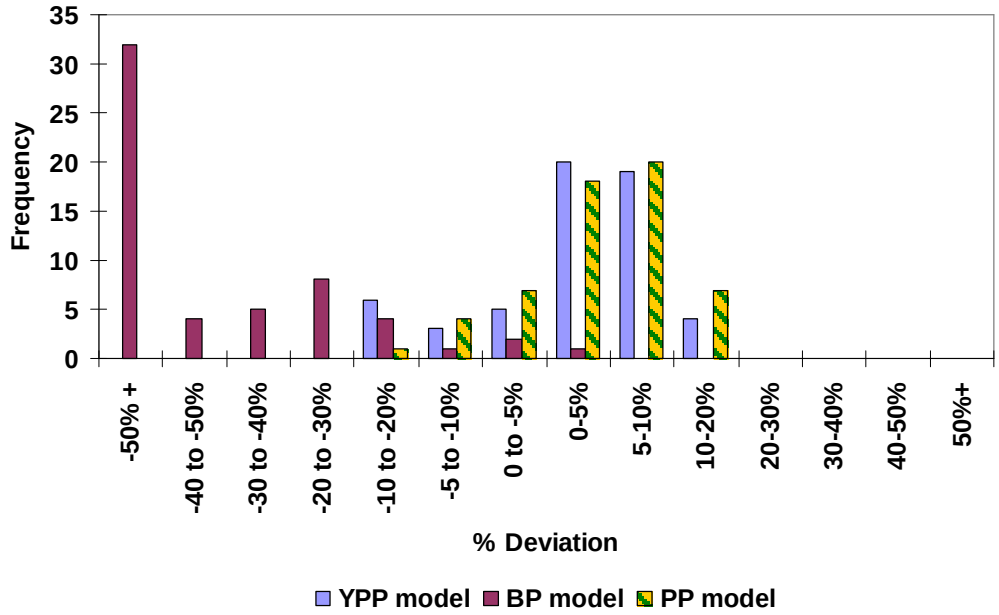

Figure 6-8 Friction factor deviation in laminar flow. Different rheological models for 3.8% CMC in the 300 mm flume

Table 6-4 CMC 3.8% in 300 mm flume. Different rheological models

Model	T_y	K	n	max % Dev	min % Dev	ave % Dev	LSE
$Re_{2(YPP)}$	0.815	0.453	0.724	20.00%	-16.90%	6.62%	0.0046
$Re_{2(BP)}$	9.1205	0.0604		1.36%	-342.30%	60.35%	0.0348
$Re_{2(PP)}$		0.6063	0.6776	18.05%	-11.45%	5.97%	0.0044

6.3.5 Kaolin 8% in 300 mm flume

The next set of data is the 8% Kaolin data tested in the 300 mm flume.

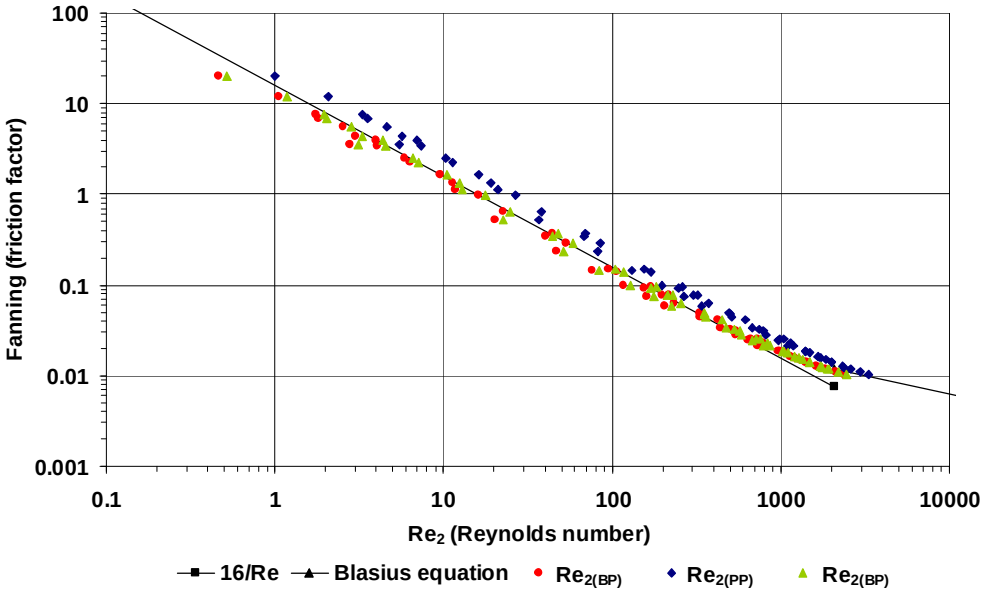

Figure 6-9 Moody Diagram. 8% kaolin in 300 mm Flume. Different rheological models

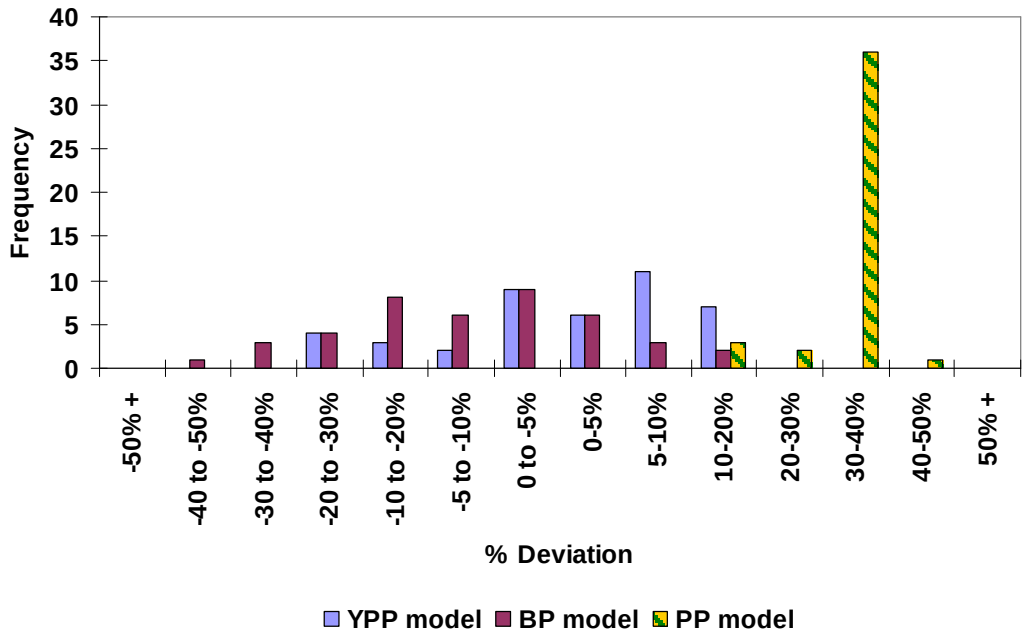

Figure 6-10 Friction factor deviation in laminar flow. Different rheological models for 8 % kaolin in 300 mm flume

Table 6-5 Kaolin 8% in 300 mm flume. Different rheological models

Model	T_y	K	n	max % Dev	min % Dev	ave % Dev	LSE
$Re_{2(YPP)}$	14.630	0.057	0.694	16.39%	-29.29%	8.38%	0.0068
$Re_{2(BP)}$	16.44	0.0046		12.24%	-42.60%	11.38%	0.0091
$Re_{2(PP)}$		7.5506	0.0953	40.26%	16.97%	33.37%	0.0272

This time it is evident from **Figure 6-9**, **Figure 6-10** and **Figure 6-11**, that the kaolin is a yield pseudoplastic fluid. The pseudoplastic model does not fit the kaolin data well. The Bingham model fits reasonably well but not as well as the yield pseudoplastic model. The difference will become more evident, the higher the concentration gets and with it the n value which defines the curvature of the rheological model.

6.3.6 Kaolin 6% in 150 mm flume

The next set of data is the 6% kaolin data tested in the 150 mm flume. From **Figure 6-11**, **Figure 6-12** and **Table 6-6**, it can be seen that kaolin is again best characterised by the yield pseudoplastic model although the pseudoplastic and Bingham models are not that far off.

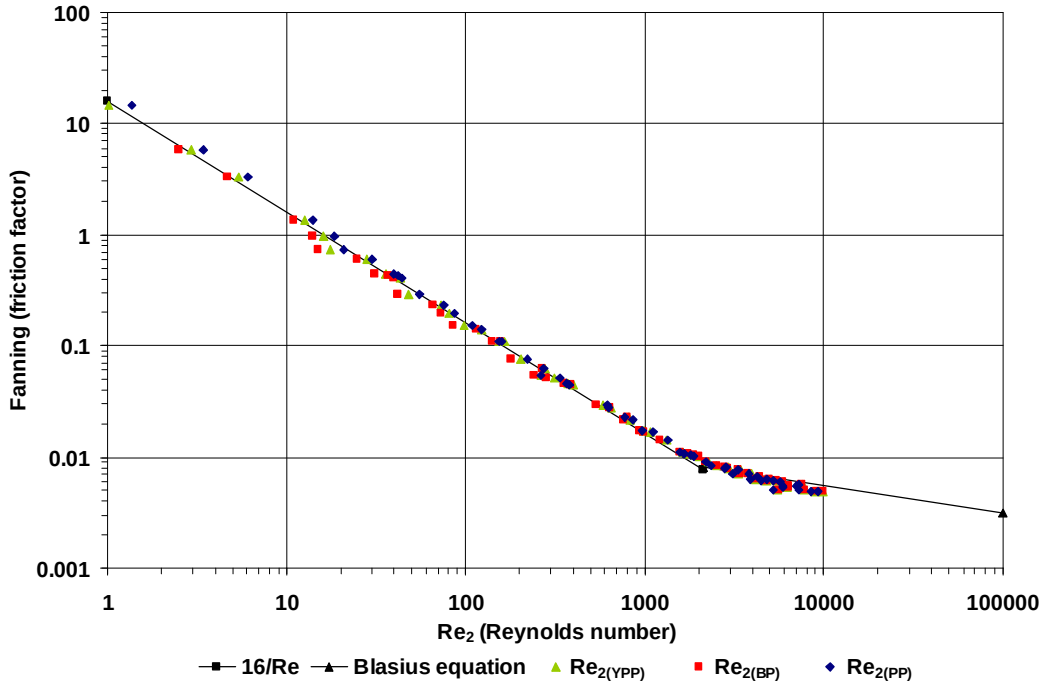

Figure 6-11 Moody Diagram. 6% kaolin in 150 mm Flume. Different rheological models

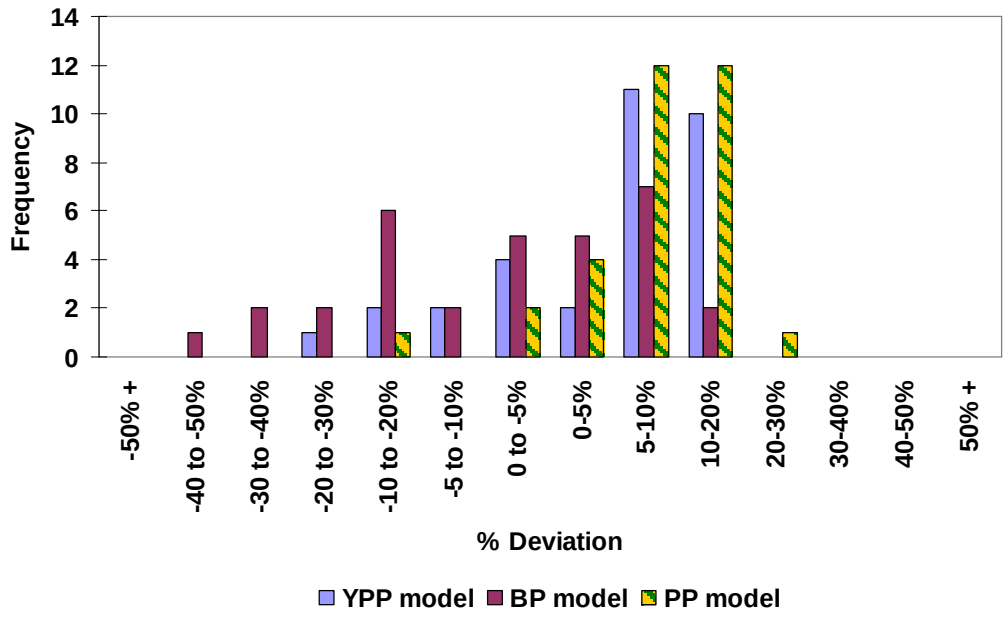

Figure 6-12 Friction factor deviation in laminar flow. Different rheological models for 6 % kaolin in 150 mm flume

Table 6-6 Kaolin 8% in 150 mm flume. Different rheological models

Model	Ty	K	n	max % Dev	min % Dev	ave % Dev	LSE
$Re_{2(YPP)}$	6.840	0.148	0.517	15.47%	-24.11%	8.90%	0.0083
$Re_{2(BP)}$	8.461	0.0032		15.48%	-44.92%	11.11%	0.0108
$Re_{2(PP)}$		4.47915	0.1452	20.58%	-13.19%	9.72%	0.0092

6.3.7 Conclusions

It can be deduced from the data presented in the previous section that for the data presented in this thesis there is enough evidence to conclude that the rheological model used plays a significant role in predicting the friction factor for laminar flow in open channels.

The importance of using the correct rheological model has been demonstrated. It is evident from the data presented that kaolin behaves like a yield pseudoplastic, CMC like a pseudoplastic and bentonite like a Bingham fluid.

The advantage of Re_2 is that it can predict laminar flow of three very different fluids so long as the rheological parameters are available and the fluid is classified correctly.

If the correct Reynolds number is chosen the prediction is better than +/-30% from the actual.

6.4 IMPACT OF USING DIFFERENT METHODS TO ESTABLISH THE RHEOLOGICAL PARAMETERS AND THE EFFECT THEY HAVE ON THE FRICTION FACTOR

The on-line tube viscometer data was used to establish the rheological constants for this thesis. This was done in various ways.

In Chapter 2, the Rabinowitsch-Mooney transformation process, the Tikhonov regularization, as well as the Slatter method to derive rheological constants were described. In the Rabinowitsch-Mooney transformation one can use any number of polynomial fits to the data, eg, first, second, third and fourth order, to establish the rheogram. So for each order fit one can obtain a different set of rheological constants. Which one does one use?

The data obtained from the rotary viscometer was also used to establish rheological constants. As the shear rate is true shear rate, no transformation is required and the model can be fitted directly to the data. This was also compared to the pipe viscometer data.

In the following section the effect of these six different sets of rheological constants on the Reynolds number and friction factor is tested.

6.4.1 Kaolin 6% in 150 mm flume

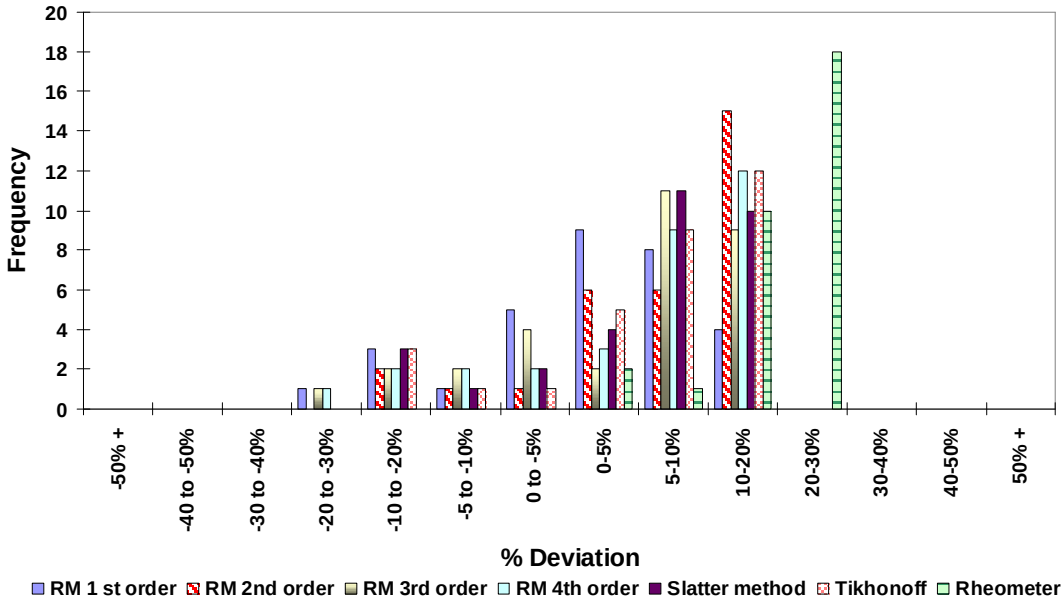

Figure 6-13 Friction factor deviation. Effect of rheological fitting method. 6% kaolin in 150 mm flume

The data represented in **Figure 6-13** shows that the 1st order Rabinowitsch-Mooney transformation seems to be the best fit, but when one looks at **Table 6-7**, the difference is not really significant except in the case of the rheometer results. Even with the rheometer data, the error is still within 30%. The rheological constants of the 6% kaolin are summarised in **Table 6-7** below. The % errors in the table substantiate the results depicted in **Figure 6-13**. The LSE indicates that the 1st order Rabinowitsch-Mooney constants are the best.

Table 6-7 Summary of rheological constants and errors. 6% kaolin in 150 mm flume

Model	Ty	K	n	max % Dev.	min % Dev.	LSE
RM 1 st order	6.61	0.33	0.39	13.40	-25.59	0.0075
RM 2 nd order	5.74	0.46	0.38	17.65	-15.21	0.0089
RM 3 rd order	6.84	0.15	0.52	15.47	-24.11	0.0082
RM 4th order	6.74	0.13	0.55	16.86	-21.86	0.0087
Slatter	6.18	0.34	0.42	16.36	-18.96	0.0082
Tikhonoff	6.45	0.21	0.48	17.09	-19.63	0.0087
Rheometer	5.00	0.27	0.48	28.65	19.57	0.0187

6.4.2 CMC 2.8% in 150 mm flume

The next data set presented is the 2.8% CMC tested in the 150 mm flume. The results in **Figure 6-14** indicate that in this specific case the effect of choosing the correct fit is even less significant except for the rheometer data. The rheometer data is better than for Kaolin but still significantly less accurate. **Table 6-8** substantiates this fact.

So for this case it did not matter which fit was chosen.

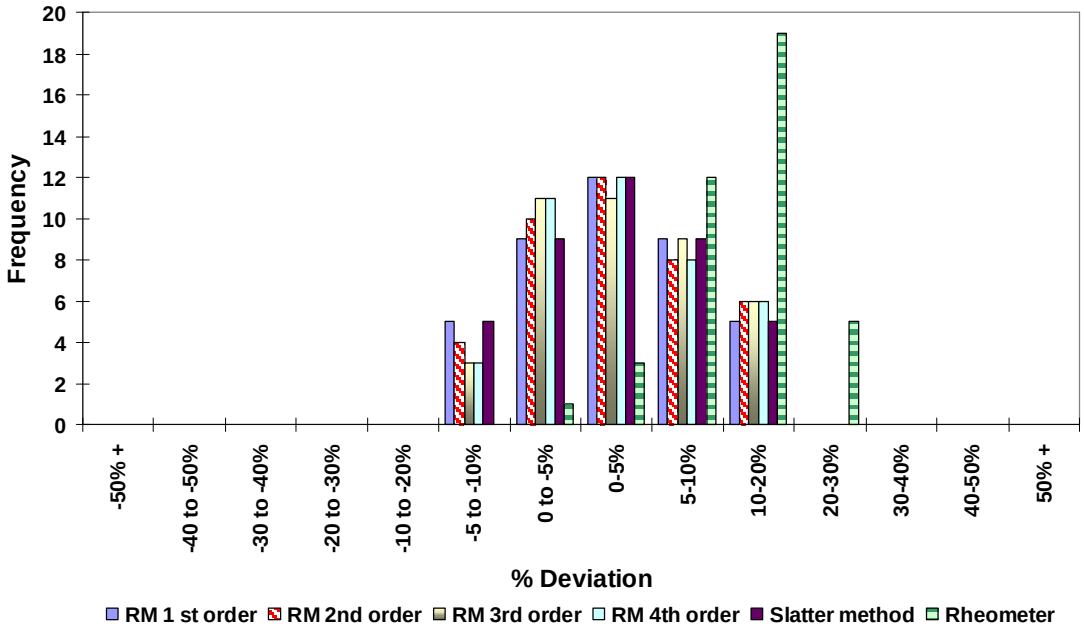

Figure 6-14 Friction factor deviation. Effect of rheological fitting method 2.8% CMC in 150 mm flume

Table 6-8 Summary of rheological constants and errors 2.8% CMC in 150 mm flume

Model	K	n	max % Dev.	min % Dev.	LSE
RM 1 st order	0.199	0.7562	19.365	-9.05	0.0052
RM 2 nd order	0.197	0.7579	19.62	-8.86	0.0053
RM 3 rd order	0.1973	0.7574	19.66	-8.76	0.0053
RM 4th order	0.1941	0.761	19.87	-8.91	0.0054
Slatter	0.199	0.756	19.43	-8.95	0.0053
Rheometer	0.1335	0.8237	28.9	-2.01	0.0108

6.4.3 Bentonite 4.5% in 150 mm flume

The bentonite that was used does not make a very stable suspension. It is time dependent or thixotropic. The bentonite was sheared over a long time before the tests and then it behaved reasonably well. The results of the 4.5% bentonite tested in the 150 mm flume are depicted in **Figure 6-15** below. It can be seen that there is not much difference between the various methods except for the rheometer results. The rheometry of the bentonite was not done correctly as time dependency was not taken into consideration.

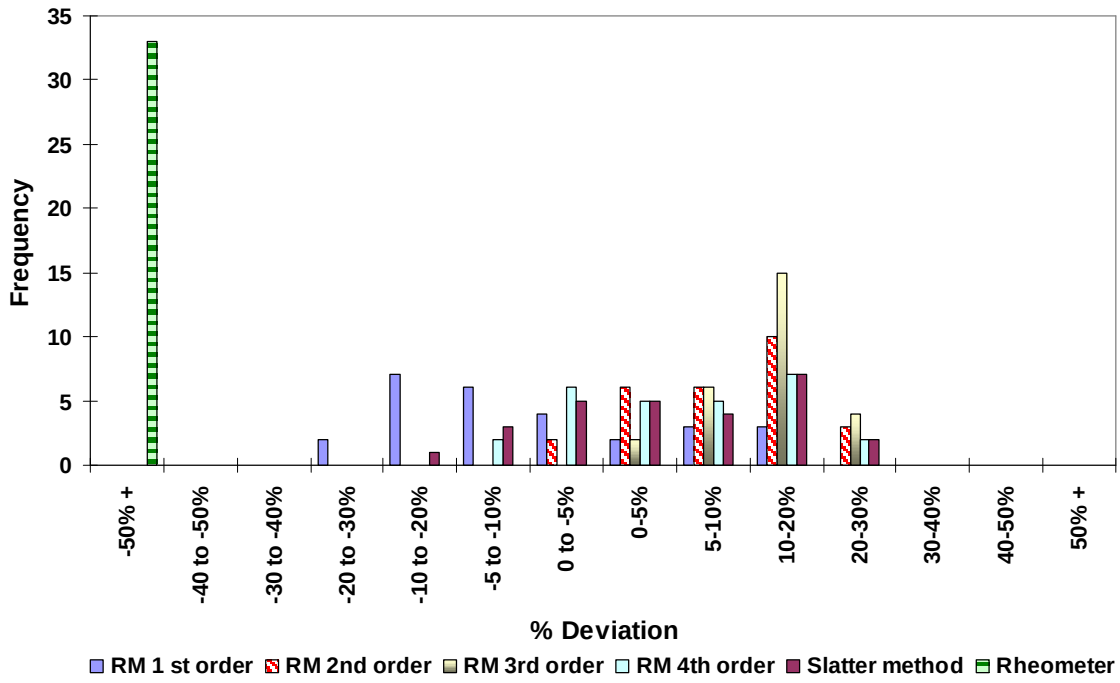

Figure 6-15 Friction factor deviation. Effect of rheological fitting method 4.5% bentonite in 150 mm flume

The rheological constants and % errors are summarised in **Table 6-9**. In this case the LSE indicate that the RM 4th order and the Slatter method were the best fits.

Table 6-9 Summary of rheological constants and errors
4.5% bentonite in 150 mm flume

Model	Ty	K	max % Dev.	min % Dev.	LSE
RM 1 st order	5.41	0.0041	12.745	-25.717	0.0109
RM 2 nd order	4.402	0.0061	25.392	-3.808	0.0121
RM 3 rd order	4.152	0.0061	28.818	1.623	0.0150
RM 4th order	4.676	0.0057	21.496	-9.842	0.0094
Slatter	4.721	0.0054	21.102	-10.693	0.0094
Rheometer	10.849	0.0119	-80.871	-154.124	0.0673

6.4.4 Kaolin 10% in 300 mm flume

The following set is for 10% kaolin in the 300 mm wide flume. This was the highest concentration kaolin tested. The graphical represention is shown in **Figure 6-16**.

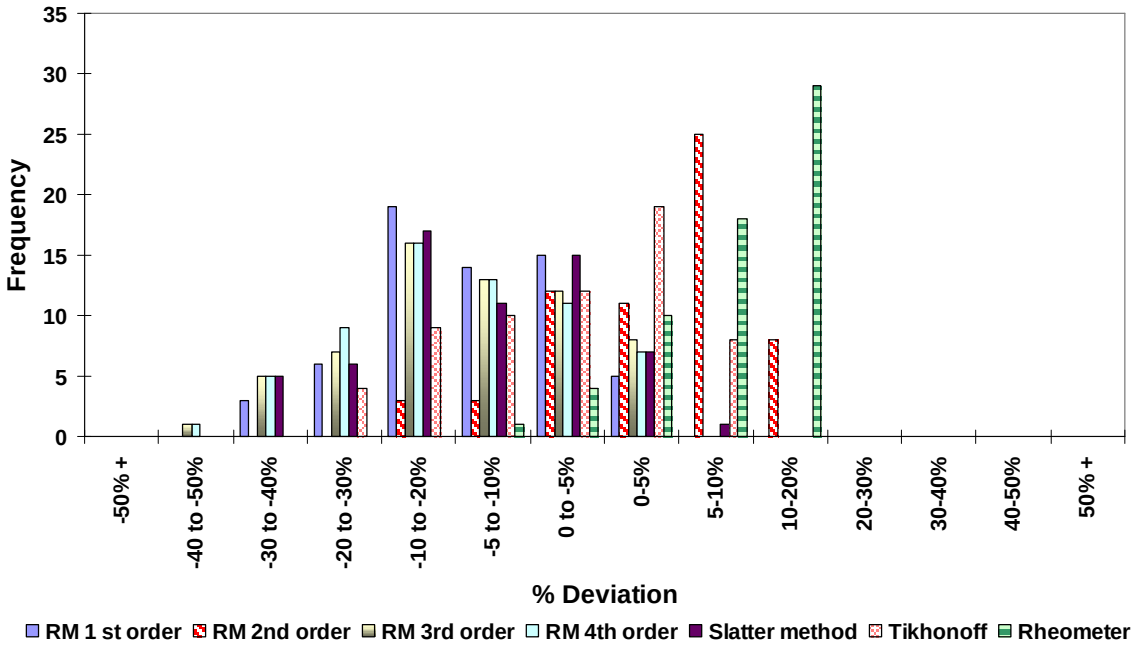

Figure 6-16 Friction factor deviation. Effect of rheological fitting method
10% kaolin in 300 mm flume

Table 6-10 it can be seen that the 2nd order Rabinowitsch-Mooney transformation provided the best fit followed by the Tikhonov transformation, and then the rheometer data. This is significant as in all the other sets of data the rheometer results were the worst. It could possibly mean that if the rheometer tests were done correctly, they could

be accurate enough to accurately predict the rheological parameters. A few of the points that deviate between 30% and 40% were very low Reynolds numbers where the flow height measurement is very sensitive owing to the thin film thickness. It is interesting to note that if the model is changed the deviation becomes less than 30%.

Table 6-10 Summary of rheological constants and errors
10% kaolin in 300 mm flume

Model	Ty	K	n	max % Dev.	min % Dev.	LSE
RM 1 st order	26.06	0.2450	0.518	2.96	-36.65	0.0073
RM 2 nd order	21.31	0.5240	0.468	13.09	-14.31	0.0042
RM 3 rd order	27.07	0.0320	0.784	4.33	-40.12	0.0080
RM 4th order	27.37	0.0210	0.834	3.92	-41.56	0.0083
Slatter	26.89	0.0238	0.827	5.33	-39.08	0.0076
Tikhonoff	24.44	0.1460	0.613	9.23	-27.53	0.0049
Rheometer	19.50	0.8000	0.433	14.87	-7.00	0.0056

6.4.5 CMC 3.8% in 300 mm flume

The next data set is of 3.8% CMC tested in the 300 mm flume. The results are graphically depicted in Figure 6-17, and the rheological parameters and errors in **Table 6-11**. The results are very close, with only the rheometer results being significantly different.

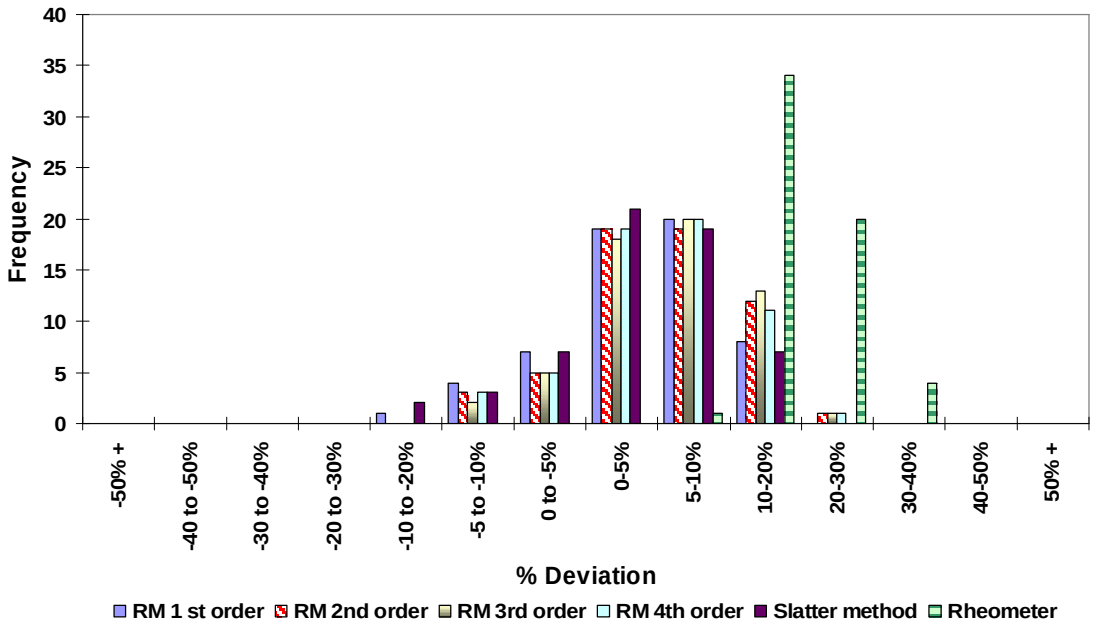

Figure 6-17 Friction factor deviation. Effect of rheological fitting method 3.8% CMC in 300 mm flume

Table 6-11 Summary of rheological constants and errors 3.8% CMC in 300 mm flume

Model	K	n	max % Dev.	min % Dev.	LSE
RM 1 st order	0.603	0.678	18.05	-11.45	0.0044
RM 2 nd order	0.575	0.688	20.16	-9.33	0.0049
RM 3 rd order	0.561	0.693	21.09	-8.42	0.0052
RM 4th order	0.572	0.690	20.16	-9.47	0.0049
Slatter	0.791	0.459	17.68	-11.91	0.0042
Rheometer	0.400	0.744	35.80	8.75	0.0135

6.4.6 Bentonite 4.5% in 75 mm flume

The data in Figure 6-18 is for 4.5% bentonite tested in the 75 mm flume. The LSA values in Table 6-12 indicate that the R-M 1st order is the best fit. The R-M 4th order and the Slatter method are next.

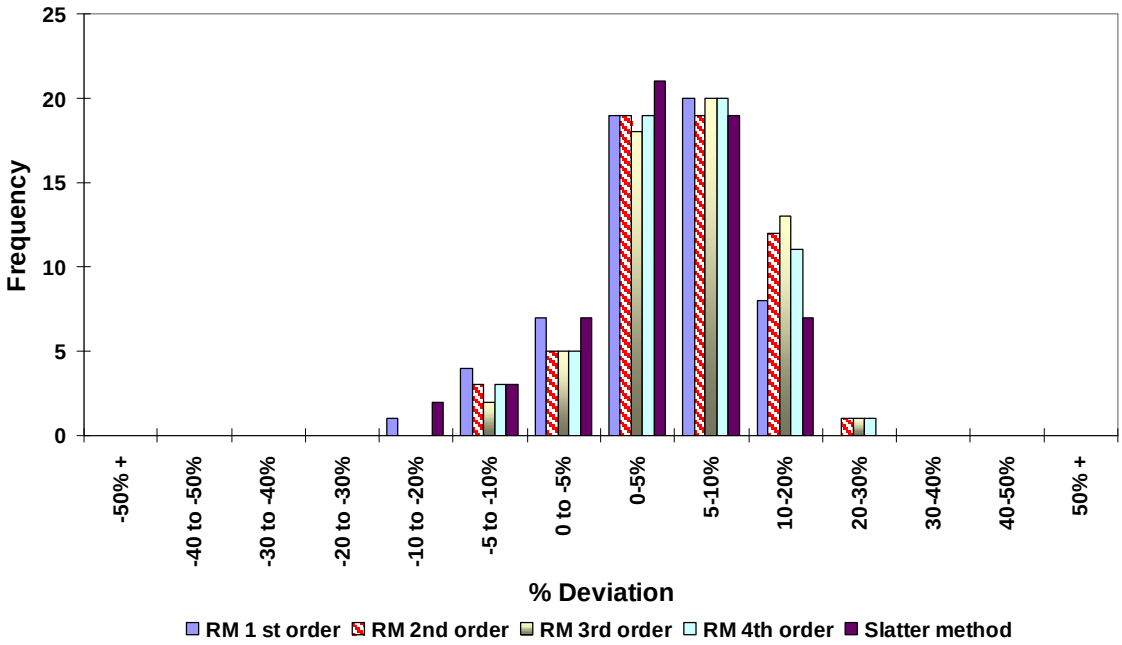

Figure 6-18 Friction factor deviation. Effect of rheological fitting method 4.5% bentonite in 75 mm flume

Table 6-12 Summary of rheological constants 4.5% bentonite in 75 mm flume

Model	Ty	K	max % Dev.	min % Dev.	LSE
RM 1 st order	5.41	0.0041	20.47	-35.99	0.0114
RM 2 nd order	4.40	0.0061	29.41	-12.45	0.0148
RM 3 rd order	4.15	0.0066	31.61	-6.62	0.0174
RM 4th order	4.68	0.0057	26.69	-18.92	0.0124
Slatter	4.72	0.0054	26.76	-19.84	0.0124

6.4.7 Conclusion

It can be seen from the above examples that the difference is not very significant when one looks at the graphical display of the data between the different methods used to establish the rheological parameters of the fluid. Only the rotary viscometer data is in most cases significantly different. The reason for this is that at the time of testing the rotary viscometer had just been purchased and test procedures had not been properly established. From recent tests done it seems that with proper test procedures, and using

the correct geometries, this difference could be significantly less. If one looks more closely at the LSE differences they are quite significant and vary up to about 75%. This is not evident when establishing the rheological parameters. The question may now be asked how one decides which of the methods to use?

Using $Re_{2,}$ most of the friction factors are within 20% of the predicted values over the laminar flow range. There are a few points, either at very low flow rates where the flow depth is very small or at the higher flow rates where the flow could already be starting in the transitional range, which show larger errors.

6.5 TESTING Re_2 IN LAMINAR FLOW WITH INDEPENDENT DATA

Coussot (1994) published some laminar flow data. He tested kaolin in a rectangular flume and used various concentrations, slopes and widths. The kaolin was also characterised as a yield pseudoplastic fluid. The range of data is summarised in **Table 6-13** and compared to the data used in this thesis. What should be noticed is that the data complements the data presented in this thesis for the following reasons:

- The maximum channel width used is double that used in this thesis.
- The maximum slope is 11 times steeper than the slope that could be reached by our flume.
- The maximum concentration of the kaolin suspension tested by Coussot was 20% versus the 10% used in this thesis. This resulted in a maximum yield stress of 53 Pa while the 10% kaolin suspension used in this thesis had a yield stress of 21 Pa.

This Reynolds number could therefore be validated over a wider range of widths, slopes, densities and yield stresses.

The test data presented by Coussot is compared to the data presented in this thesis in **Table 6-13** below.

Table 6-13 Coussot data compared with thesis data for kaolin

	Minimum Coussot	Maximum Coussot	Minimum Thesis	Maximum Thesis
Slope (degrees)	1.7	56	1	5
Width (mm)	80	600	75	300
Density kg/m	1328	1434	1049	1165
Concentration % (volumetric)	20	27	4.5	10
τ_y (Pa)	13.7	52.8	1.84	21.3

The actual values were used and Re_2 was used to establish the Reynolds number for each data point. The friction factor was then established from the 16/Re relationship for laminar flow.

For each value of actual flow depth the predicted value of average flow velocity was then calculated and compared with the actual velocity. The maximum deviation was less than 20%, which is similar to the error that was obtained with the data of this thesis.

A plot of actual versus predicted velocities is depicted in **Figure 6-19**.

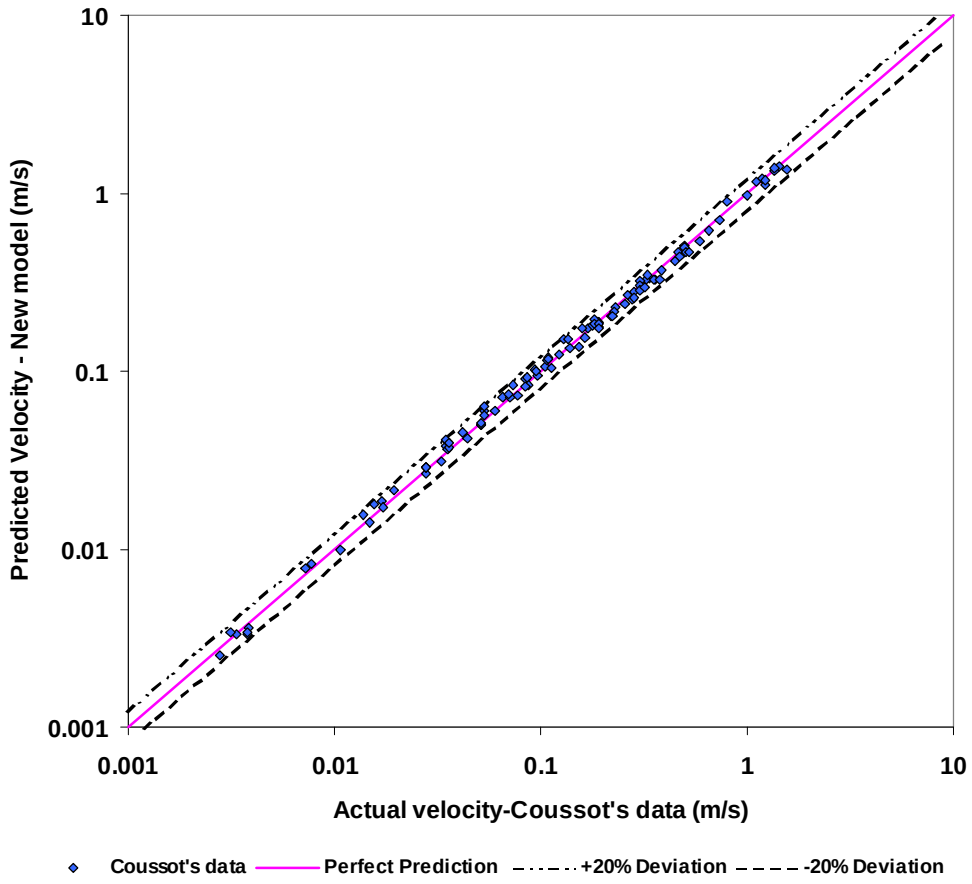

Figure 6-19 Coussot data – actual versus predicted velocity using Re_2

The data presented in **Figure 6-19** clearly demonstrates that Re_2 predicts the Coussot data well over a wide range of velocities (three orders of magnitude). The LSE for the data set is 0.0031 and the average deviation is 6.1%.

6.6 THE AVERAGE WALL SHEAR STRESS

In pipe flow the wall shear stress distribution is well known and can be used to develop the velocity distribution and from that the flow rate. The shear stress distribution is a linear relationship with the maximum at the wall and the minimum in the centreline of the pipe.

For open channel flow the shear stress distribution is much more complex.

Often the sheet flow approach is adopted and the shear stress distribution is then taken to be linear from 0 at the surface to a maximum at the bottom of the flume. This is correct if the width of the flume is infinitely wide. De Kee *et al.* (1990) use this in their sheet flow model evaluated in Chapter 4. The maximum value is then:

$$\tau_{0(\text{wide flume})} = \rho g h \sin\alpha \,. \qquad 4.2$$

This is, however, not correct when the height of the flow increases for a narrow flume. The sidewall effects then play a role. The effect is then compensated for, by using the hydraulic radius instead of the depth. The wall shear stress then becomes:

$$\tau_0 = \rho g R_h \sin\alpha \,. \qquad 2.50$$

The use of the hydraulic radius is generally accepted to be the average wall shear stress but this is also only an approximation. Kozicki and Tiu (1967) used this in the definition of the Fanning friction factor. This approach is also used in this thesis.

A third approach was investigated. If one assumes that the shear stress at the bottom of the flume remains constant over the width of the flume as in the thin film approach and one then assumes that the value of the shear stress varies from a maximum at the bottom on the side-walls to zero at the fluid surface, the average wall shear stress is as follows:

$$\tau_{0(\text{average})} = \rho g h \sin\alpha \left(\frac{B + 2.\frac{1}{2}h}{B + 2h} \right). \qquad 6.1$$

Figure 6-20 demonstrates the effect of using the different wall shear stress approaches. When using the wall shear stress for a wide flume or the average wall shear stress

approach, the data does not collapse on the 16/Re line. If the data is scrutinised more closely the effect of flume slope can also be seen clearly. This example is for 6% kaolin in the 150 mm flume.

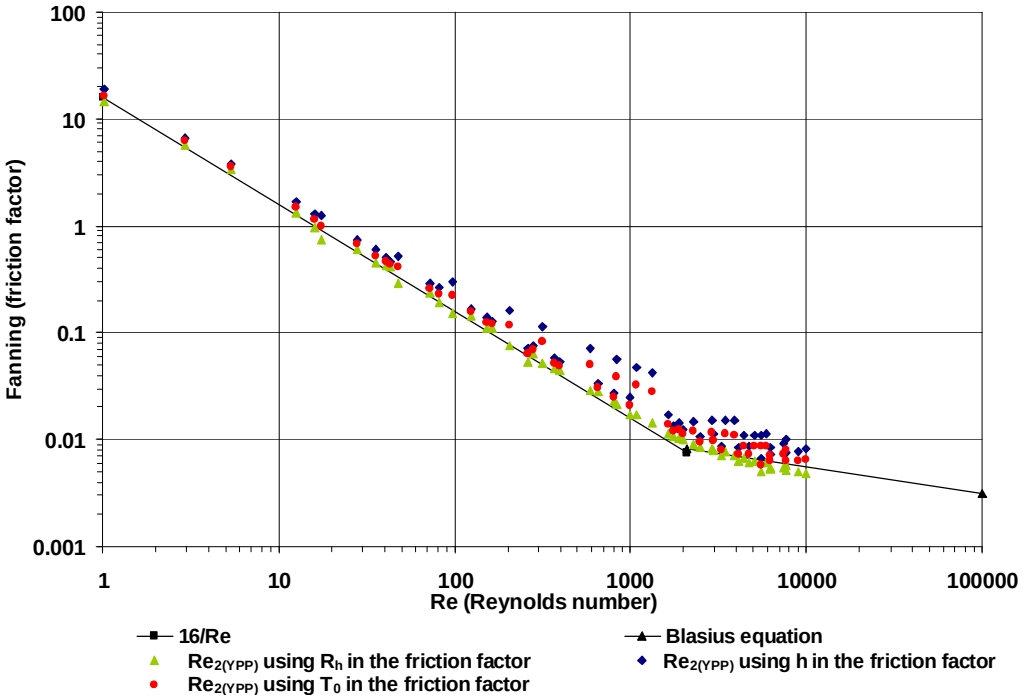

Figure 6-20 Effect of using different wall shear stress models on the friction factor for 6% kaolin in 150 mm flume

Figure 6-21 shows the same effect for 2.8% CMC in the 150 mm flume.

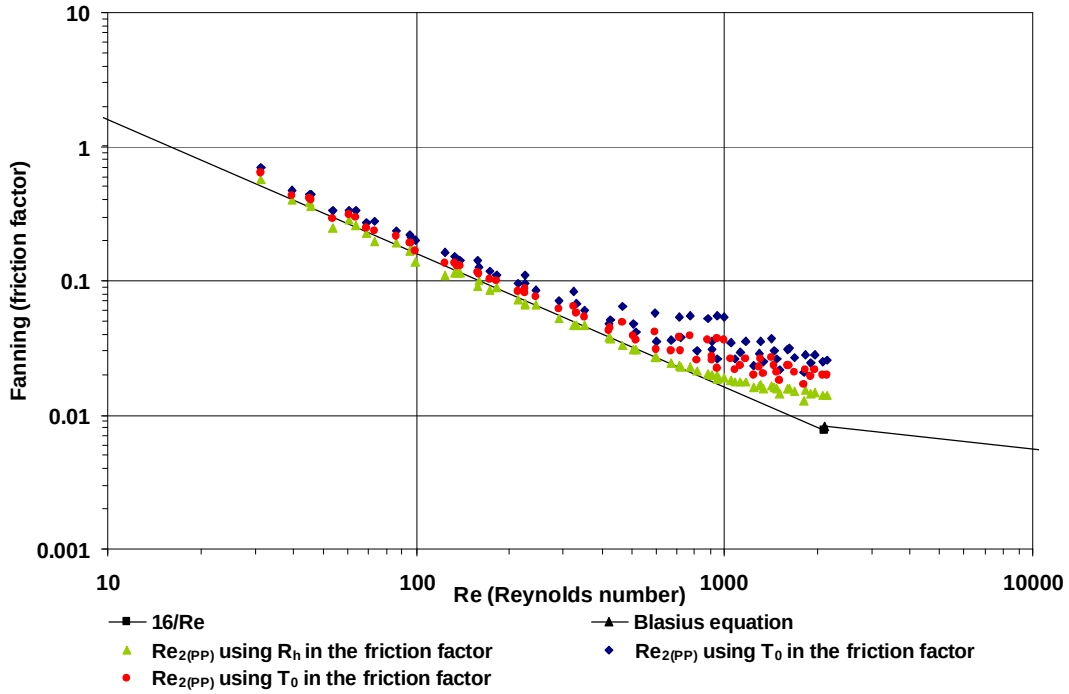

Figure 6-21 Effect of different wall shear stress models on the friction factor for 3.8% CMC in 150 mm flume

Even though using the hydraulic diameter in the friction factor is an approximation, one can see that for the data presented it seems to be adequate. To find the true average shear stress of the cross-section of a rectangular flume seems to be a very difficult problem which up to now has not been solved.

6.7 TRANSITIONAL FLOW

The transitional region is and will always be a complex region to deal with. This holds for pipe and open channel flow. The reason for this is that in this region the flow is neither laminar nor turbulent, but a combination of both.

6.7.1 Existing Approaches

There are only two types of approaches found in literature to predict transition and they are either to adopt the same approach as for Newtonian open channel flow where the transition occurs over a range between 2 000 and 3 000 with an abrupt jump from laminar to turbulence, or the Hanks approach which is linked to the Hedström number. This was discussed in Chapter 4 and it was shown that it does not predict the transition region adequately for the data in this thesis.

6.7.2 New approach using Froude number

In Chapter 5, the new approach to predict the transition zone is described. This approach uses the relationship between Reynolds number and Froude number to indicate the change in flow behaviour. This approach has never been used as far as can be ascertained. The Froude number shows the onset of transition better than the friction factor and also shows up the effect of channel slope. Why it does show up the change in flow behaviour is not clear, except that one could argue that both Reynolds number and Froude number describe flow behaviour.

Another criticism to the approach could be to question the use of apparent viscosity as the non-Newtonian fluid indicator.

When trying to find a relationship between the onset of transition and any of the rheological parameters, relationships could be found with any of the parameters τ_y , K and n. The problem is that except for flow depth, width and slope, one then still has to contend with three rheological constants, which makes the problem considerably more

complex. By combining the three rheological constants of a fluid into the apparent viscosity, a relationship could be established between the onset of transition and the apparent viscosity at a shear rate of 100 s^{-1}. The apparent viscosity at other shear rates was also tested, both lower and higher than 100 s^{-1}. Over the data range of this thesis they did not fit the transition better.

The data presented at the end of Chapter 3, Section 3.9.2, seems to indicate that different fluids at shear rate 100 s^{-1} have similar apparent viscosities and that for those fluid concentrations that were similar, transition occurred over the same Reynolds number ranges.

It should be stated that this was not so easy to determine. Lower and higher shear rates were used and the Reynolds number calculated for each. Every set of data was then visually inspected to see whether the onset of transition was closer or further away from where transition was perceived to occur.

The new Reynolds number for establishing the onset of transition works reasonably well for the data tested in this thesis.

The fact that three vastly different fluids were used over a wide range of slopes and flow rates complicated the matter considerably.

6.8 TURBULENCE

6.8.1 Introduction

It must be stated from the outset that for high yield stress fluids, fully turbulent flow (whichever way one would describe such flow) is not possible in a flume such as has been used in this thesis. The depth of flow, especially at low slopes, will increase so quickly that the flume will overflow before high enough flow rates and velocities are achieved. For example, with the 10% kaolin in the 150 mm wide channel with a slope of 2 degrees, at a flow depth of 160 mm, the Reynolds number is only 161 and the velocity 0.5 m/s. This means that the flow will always be laminar even with an increase in flow rate, because the flow level will increase so quickly that the flume will overflow without a significant increase in Reynolds number. This phenomenon is presented in **Figure 6-22**.

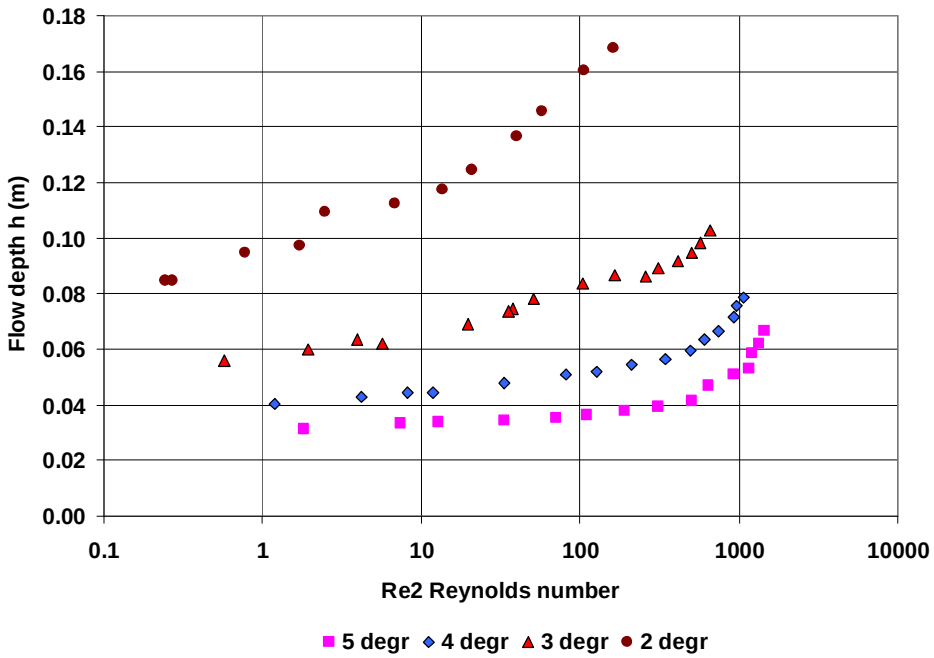

Figure 6-22 Increase in flow depth with Reynolds number 10% kaolin in 150 mm flume

This example illustrates that it is very difficult to obtain any turbulent data with viscous non-Newtonian fluids. That is why the data published by Coussot (1994) which had high concentrations was all in laminar flow, and the data published by Naik (1983) which did not seem to have high yield stresses again was more in the turbulent region.

The intention of this thesis was to obtain a database with laminar and turbulent data for three totally different fluids over a range of concentrations. Obviously, as explained, the high concentrations will be mainly in laminar flow and the lower concentrations mainly in turbulent flow.

The lower concentration fluids exhibited a typically Newtonian behaviour where the transition occurred between 2 000 and 4 000 with a sudden jump into full turbulence. This jump was not so easy to pinpoint, as puffs of turbulence occurred at intervals. As the flow rates increased, the intervals became shorter, and at some stage the fluid depth had to be measured on top of the irregular surface. That would then indicate where the jump occurred.

With the more viscous fluids the transition occurred at much lower Reynolds numbers and the transition zone was a smooth one. No sudden increase in friction factor occurred and the surface stayed smooth.

6.8.2 The New Turbulence Model

When the transition zone was analysed using the Froude number, in all the plots where Froude number was plotted against Reynolds number, there seemed to be a second

change in flow behaviour that was very abrupt. This seemed to correspond with 'turbulent behaviour'. Whether this is full turbulence is debatable, and will have to be established with pressure transducer profiles to see whether full turbulence has developed through the whole cross-sectional profile. For the scope of this thesis, the sudden change in flow behaviour was deemed to be 'turbulence'.

The model is described in Chapter 5. None of the existing models available seemed to fit the data well. This was described in Chapter 4.

The model does take into account that there is some non-Newtonian effect in the turbulent zone. As before, the non-Newtonian flow parameters are combined into one rheological parameter to classify the fluid, this time as the apparent viscosity at a shear rate of 500 s^{-1}. The apparent viscosity at lower and higher shear rates was also evaluated.

6.8.3 Evaluating the new turbulent model with own data

The following sets of turbulent data show a number of different concentrations and materials.

The data in **Figure 6-23** depicts 3%, 4.5% and 6% kaolin in the 150 mm flume. All the predicted velocities are within 30% of the actual. The LSE is 0.0072 and the average percentage deviation is 12,8%.

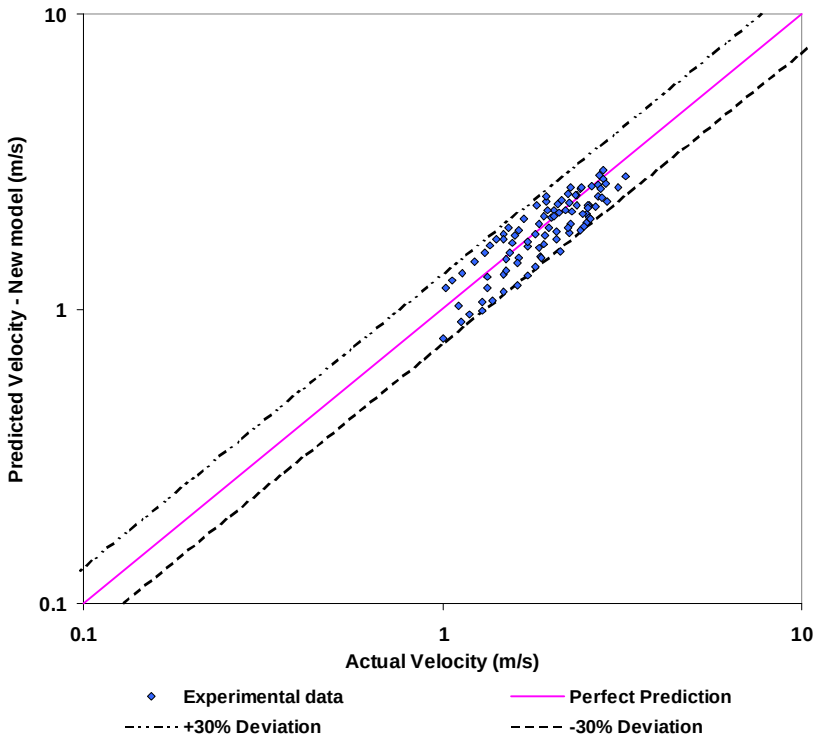

Figure 6-23 Turbulent data of three concentrations kaolin in 150 mm flume

The following data in **Figure 6-24** is for three concentrations CMC in the 300 mm flume.

The predicted velocity is within 30% of the actual velocity. The LSE is 0.0059, and the average percentage deviation is 11.9%.

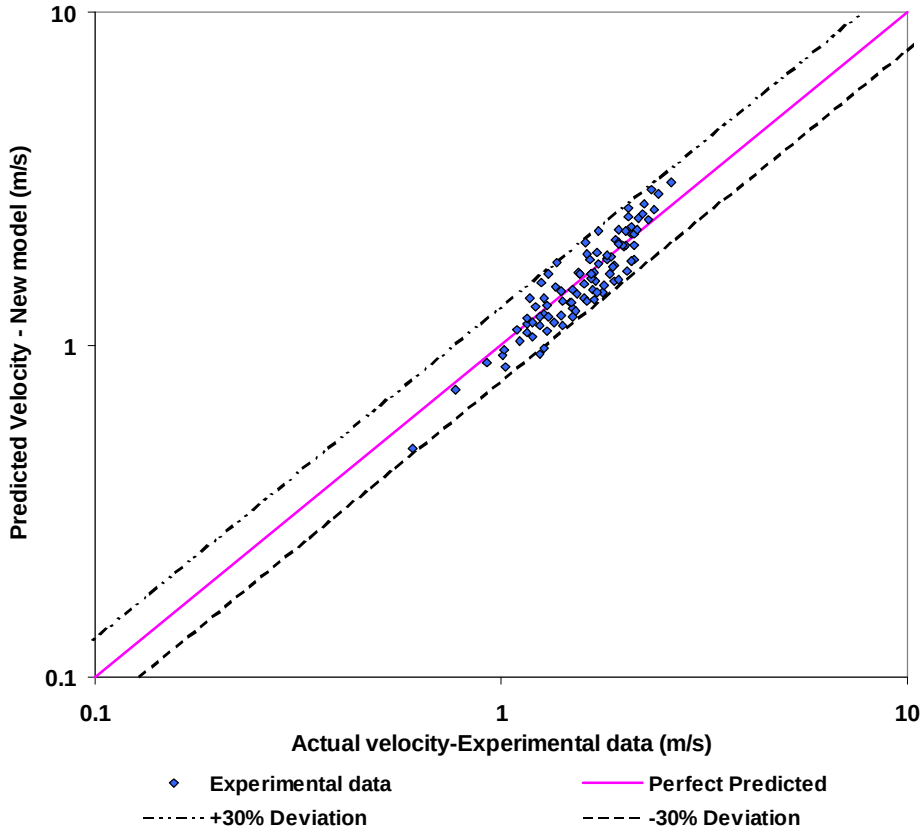

Figure 6-24 Turbulent data of three concentrations CMC in 300 mm flume

The following turbulent data is from tests conducted with bentonite 3% and 4.5% concentrations in the 75 mm and 150 mm flumes. The LSE is 0.0074 and the average percentage deviation is 10.6%.

The predicted values again are within 30 % of the measured experimental values. The data is presented in **Figure 6-25**.

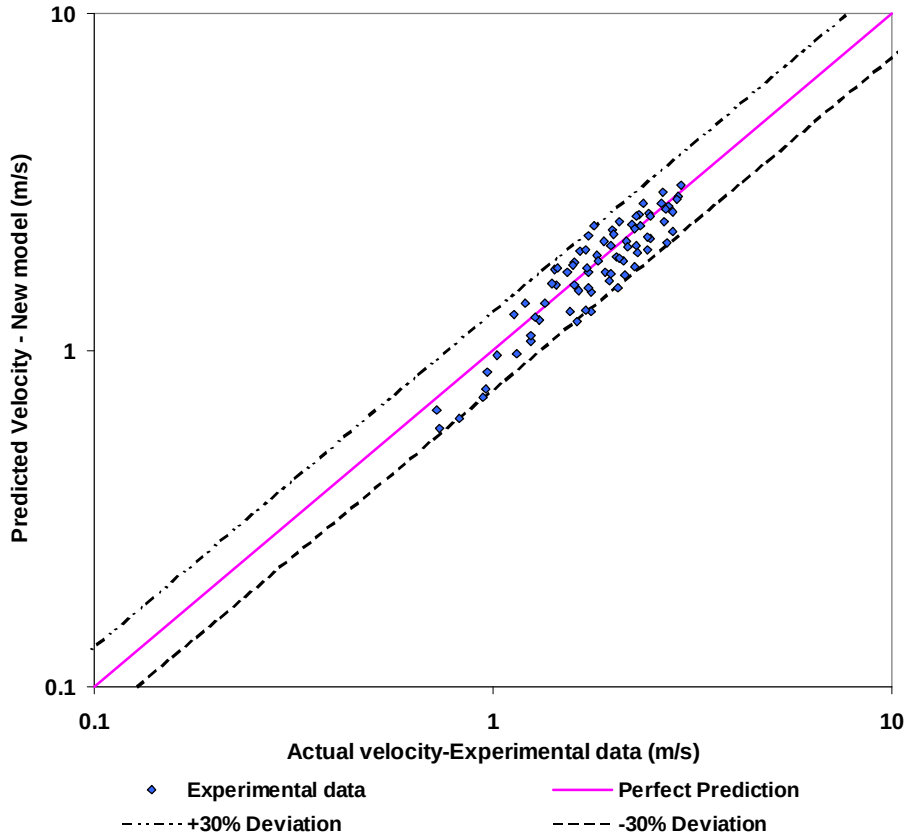

Figure 6-25 Turbulent data of three concentrations bentonite in 75 and 150 mm flume

Even though the range of turbulent data presented in this thesis is limited, the new model predicts the experimental data better than 30%. A summary of turbulence LSE values for the different models is presented in **Table 6-14**.

Table 6-14 LSE values for turbulence models

		Torrance	Slatter	Wilson& Thomas	Naik	New Model
3% Kaolin in 150 mm flume	LSE	0.0233	0.0225	0.0268	0.0535	0.014
3% Kaolin in 300 mm flume	LSE	0.0103	0.0098	0.0191	0.0654	0.02
4.5% Kaolin in 150 mm flume	LSE	0.0228	0.0174	0.0303	0.0408	0.0118
3% Bentonite in 150 mm flume	LSE	0.0276	0.0199	0.0287	0.0393	0.0106
4.5% Bentonite in 150 mm flume	LSE	0.366	0.0294	0.0369	0.0524	0.013
1% CMC in 150 mm flume	LSE	0.0302	0.0476	0.0326	0.0275	0.0112
1.8% CMC in 150 mm flume	LSE	0.0114	0.0111	0.0162	0.0249	0.012
1.8% CMC in 300 mm flume	LSE	0.0242	0.0255	0.0266	0.0253	0.013
2.8% CMC in 150 mm flume	LSE	0.0352	0.0372	0.0385	0.017	0.0155

The new model does better for most of the sets except for the 3% kaolin in the 300 mm flume.

The LSE and average percentage deviation is also very similar for the three different fluids tested. Due to the fact that the maximum flow rates were limited some of the data points could well not have been fully turbulent, which would have had an influence on the deviation percentages.

6.9 EVALUATING NEW TURBULENCE MODEL AGAINST INDEPENDENT DATA

The only turbulent data that could be obtained was that published by Naik (1983) in his PhD dissertation. He only published 95 data points all of which were in turbulent flow. The slurry was a kaolin suspension. The kaolin was characterised as a Bingham fluid. The fluid parameters, together with physical aspects of the test, are shown in **Table 6-15**.

Table 6-15 Fluid and test parameters of the Naik Data

	Unit	From	To
Slope		1:50	1:150
Relative density		1.15	1.36
Plastic viscosity	Pa.s	0.00258	0.01317
Bingham yield stress	Pa	0.4	5.03
Flow rate	l/s	2.8	41.6
Flow depth	m	0.0604	0.0128

The flume that Naik used had a smooth painted steel floor and glass sides. This should give a very smooth surface. For the calculations, a roughness of 2 micron was used. This is similar to the roughness established for the flume used in this thesis (3 micron).

For each of the data points the predicted velocity was calculated using the new turbulence model. The actual data was plotted against the predicted velocities and presented in **Figure 6-26**. The new model under-predicts the Naik data by a maximum of 18 %. If the roughness is changed to 3 micron, the maximum deviation is less than 24%, and if the roughness is 1 micron, the deviation is less than 10%.

When the roughness is 3 micron the LSE is 0.004 and the average deviation is 7.11%.

The turbulent range obtained by Naik is over a much higher Reynolds number range than the data presented in this thesis. Considering the difficulty of obtaining accurate turbulent data in an open channel and the difference in material properties, the model predicts the data reasonably well.

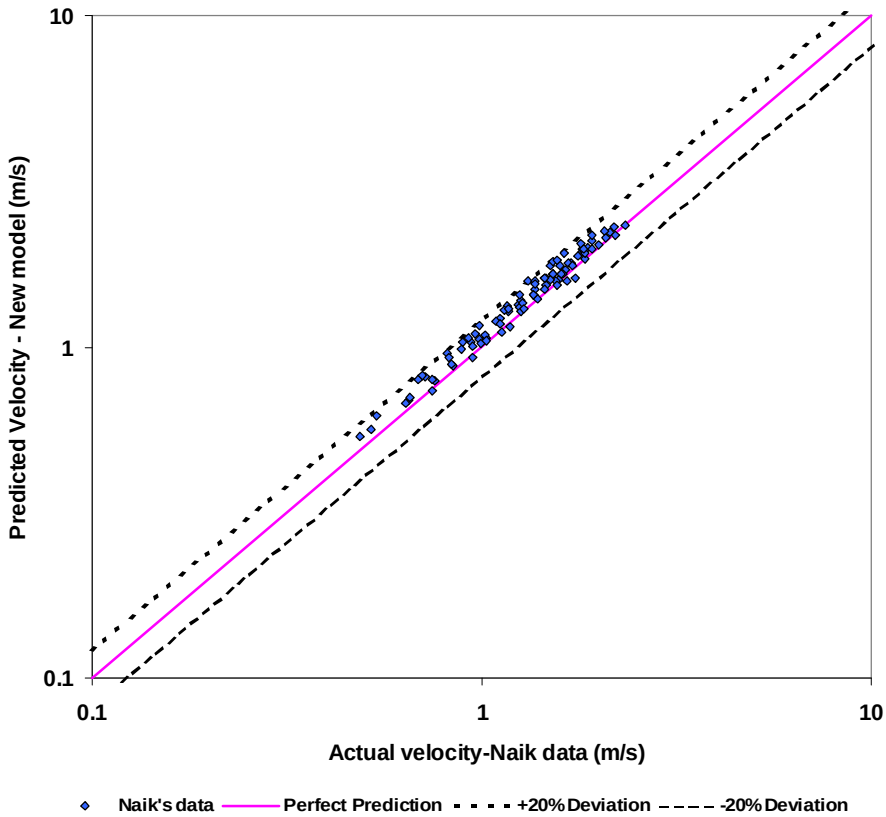

Figure 6-26 New turbulence model tested with Naik data.

From the own turbulent data presented as well as the independent data from the work by Naik (1983), the new turbulence model predicts the velocity better than 30% of the actual velocity.

The data presented by Naik was in a much higher Reynolds number range, which means that the turbulence was well developed. Therefore the new model predicted the values even better than for the own data, ie, to within 20% of the actual.

6.10 DISCUSSION OF NEW MODELS

At the start of this thesis, there was very little data available. Only two published sets could be found, one by Coussot (1994) for laminar flow, and one by Naik (1983) for turbulent flow. No transition data could be found. Very few theoretical models are available. As far as can be ascertained, no one has ever studied the Froude–Reynolds number relationship. There was no coherent model available covering laminar, transitional and turbulent flow in open channels for non-Newtonian fluids.

- **Laminar flow**

For laminar flow, the new Reynolds number, Re_2, includes the three rheological parameters τ_y, K and n which makes it suitable to define a wide range of non-Newtonian fluids including yield stress and power law fluids. In it most basic form it reverts back to the Newtonian Reynolds number. The fact that all the laminar flow data can be collapsed on the 16/Re line also simplifies the design process. Because the start of transition for the more viscous concentrations occurred at lower Reynolds numbers than

for the more Newtonian concentrations necessitates a method to predict the onset of transition other than the standard idea that it will occur around Re=2 000.

- **Transition**

Transition is a difficult region to predict. As there seemed to be a relationship between Froude and Reynolds number indicating the change in behaviour clearly and over all the materials tested, prompted the further investigation of this phenomenon. Apparent viscosity was used to combine the three rheological parameters, τ_y, K and n into one parameter. The use of a shear rate to determine which apparent viscosity to use was determined empirically. At shear rate 100 s^{-1}, however, there seemed to be a shear rate where different fluids exhibited similar apparent viscosities. (This was shown in Chapter 3.)

This approach could be challenged. However, there is no other method available that can predict transition, especially as it has been found that this occurs over a wide region and also varies with increase in viscosity. For lower viscosities the transition occurs at higher Reynolds numbers with the traditional jump, but for higher concentrations the transition is smooth and starts at much lower Reynolds numbers.

- **Turbulence**

The turbulent data in this thesis exhibited a much flatter slope than the Newtonian models like Colebrook-White and Blasius.

The new turbulence model developed is based on the Slatter turbulence model (Slatter, 1994). The new model also includes the effect of the viscous forces by incorporating the apparent viscosity at a shear rate of 500 s^{-1}. The model fits the data presented in this thesis reasonably well.

The new models have been tested against independent data from Coussot (1994) and Naik (1983), to cover a wider range of flow and fluid conditions.

6.11 CONCLUSIONS

The new models described in Chapter 5 have been evaluated and tested both with experimental data used in this thesis and also with data found in the literature.

The following conclusions can be made:

- For laminar flow it has been found that the new Reynolds number Re_2 predicts flow well over a wide range of concentrations, channel widths and slopes.
- By plotting the data on the Moody diagram where two dimensionless groups, the Reynolds number and the Fanning friction are used, and collapsing the data on one line, dynamic similarity within acceptable limits of all the data sets is achieved.
- The effect of choosing the correct rheological model has been shown to be very important. It has been shown that kaolin must be characterised as a yield pseudoplastic fluid, bentonite as a Bingham fluid and CMC as a pseudoplastic fluid. If the wrong rheological parameters are used, large errors can be induced.
- It has been shown that the way that the rheological parameters are obtained from pipe flow data by various methods like the Rabinowitsch-Mooney transformation

with first, second, third or fourth order curve fitting, or the Tikhonov regularisation method, does not effect the friction factor values obtained in laminar flow adversely in most cases. Some cases have shown that selecting the wrong method could have a significant effect. This is not possible to predict.

- An independent laminar data set by Coussot (1994), was used to validate the laminar flow model and the model predicted the actual flow velocities to within 20% accuracy.
- The effect of the use of the hydraulic radius instead of the fluid height or the average wall shear stress has been compared and it has been shown that using the hydraulic radius for determining the shear stress is adequate for establishing the friction factor for the data presented in this thesis. No fundamental theoretical approach is available to determine the wall shear stress in a flume.
- The laminar-turbulent transition is a complex phenomenon and the new model using the Froude number is able to predict this region adequately for the data presented in this thesis. There is no independent data available to test this model. Even when testing the model with the data in this thesis it is not easy to quantify the accuracy, as it is very difficult to say where transition actually occurs. The only way is to visually look at the Moody diagrams presented in Chapter 5 and see the predicted and actual values for a specific data set.
- For turbulent flow the new model is able to predict the turbulent flow velocity of the data presented in this thesis to within 30% accuracy.
- The model was also tested with an independent set of turbulent data presented by Naik (1983) and was able to predict the flow velocity with better than 20% accuracy.

All appropriate data available to the author has been analysed and it has been shown that this analysis is accurate to +/- 30%. Furthermore, this analysis covers laminar, transition and turbulent flow over a wide range of rheological properties and flow conditions. The new models also accurately describe the slope effect which has been observed.

CHAPTER 7

SUMMARY, CONTRIBUTIONS, RECOMMENDATIONS AND CONCLUSIONS

7.1 INTRODUCTION

This thesis reports on an investigation into the flow behaviour of non-Newtonian fluids in rectangular open channels.

A single Reynolds number was developed to predict laminar flow of all the slurries that included pseudoplastic, yield pseudoplastic and Bingham fluids. The research has shown that a shape factor for the rectangular flume is not required.

The research has produced a new model to predict the onset of transitional flow and the onset of 'full turbulence'. No model was found in the literature to adequately predict the transition zone.

A new turbulent model was produced which was able to adequately predict the flow of all the fluids tested.

Existing turbulence models were not able to adequately describe turbulence of the slurries tested.

The models were tested with two sets of data found in the literature, one set for laminar flow and the other for turbulent flow. The models performed well in both regions.

7.2 SUMMARY

The flow of Non-Newtonian slurries in open channels has significant implications in the mining field where high concentration slurries have to be transported to tailings dams. Water restrictions, as well as the new water law in South Africa, are forcing the industry to transport slurries at higher concentrations. The design of open channels or flumes transporting slurries is not well understood. It is not just a simple matter of using pipe design formulae and adapting them for open channel flow. Open channels are also used in chemical engineering plants and in civil engineering where partially full sewer pipes are also open channels.

The aim of this thesis has been to develop a design procedure for open channels transporting non-Newtonian fluids in both the laminar region and through the transition zone into full turbulence.

In laminar flow, some research has been done by Coussot (1994), Naik (1983), and Zhang and Ren (1982). Coussot (1994) tested a Kaolin suspension and classified it as a yield pseudoplastic material, Naik (1983) and Zhang and Ren (1982) classified and modelled the same slurry as a Bingham fluid.

The rheological characterisation done by Coussot (1994) was with a rotary viscometer while Zhang and Ren used a capillary viscometer. Naik (1983) derived the Bingham parameters from the particle size distribution and reduced volume fraction of the solids.

Naik (1983) uses the Hedström number as a prediction for the onset of transition. This

was shown, in this thesis, not to take into account the effect of slope sufficiently.

Coussot (1994) refers to the work of Naik (1983) and also suggests the Hedström number as the only way to predict the onset of transition.

Zhang and Ren (1982) describe transition but do not model this adequately. Their flume was only at one slope and they would not have been able to study the effect of slope.

Naik (1983) and Zhang and Ren (1982) both present turbulence models but these models did not adequately predict the flow of the various materials tested in this thesis.

For the thesis a new test facility was designed and constructed. It consists of a 5 m long by 75 mm wide and a 10 m long by 300 mm wide rectangular tilting flumes linked to a online pipe viscometer with three nominal bore diameter tubes, namely 13 mm, 28 mm and 80 mm. The 300 mm flume could be partitioned centrally to make up a 150 mm by 10 m flume. Test procedures were developed to determine the rheological parameters and flow data of three different fluids with concentrations from 0% - 10%, slurry relative densities of 1.02 –1.16, and flows from 0.05 to 45 l/s.

This test facility was used to compile a database that was used to evaluate existing models as well as testing the new models.

The accurate rheological characterisation of the slurries was found to be extremely important to the successful modelling of the flume data. The on-line pipe viscometer

was accurate and very sensitive to the changes in rheology. It was very difficult to establish a correlation with the rotary viscometer. This problem has been adequately described by Coussot (1994). The pipe viscometer is deemed to be a more suitable instrument to rheologically characterise these slurries than the rotary viscometer (Slatter, 1994).

The new analysis is presented in three parts. The laminar flow data is modelled using a Reynolds number developed for a yield pseudoplastic fluid but which can also model pseudoplastic and Bingham fluids successfully.

The onset of turbulence is modelled using a new critical Reynolds number that is related to the Froude number and the apparent viscosity at 100 s^{-1}. This Reynolds number is sensitive to the rheology of the material as well as the slope of the flume.

The onset of turbulence is modelled similarly and related to the Froude number and the apparent viscosity at 500 s^{-1}.

The turbulence model is based on the Reynolds number developed by Slatter (1994) which includes the particle size roughness. This did not adequately predict the data and the roughness function B was not constant when plotted against the roughness Reynolds number.

7.3 NEW CONTRIBUTIONS

A new design procedure for the flow of pseudo-homogeneous non-Newtonian slurries

in rectangular open channels has been developed. The work has been tested by an extensive experimental database using different types of slurries. The analysis can be divided into three sections, namely laminar, transitional and turbulent flow.

7.3.1 Laminar flow

It has been established that in laminar flow it is of paramount importance that the correct rheological model is chosen. The Reynolds number that has been used can accommodate a yield pseudoplastic, pseudoplastic and Bingham fluid, and can revert to the Newtonian Reynolds number. The most accurate predictions occurred when the correct model was used, ie, bentonite was characterised as a Bingham fluid, CMC as a pseudoplastic and kaolin as a yield pseudoplastic fluid.

All the laminar flow data could be collapsed on the 16/Re line of the standard Moody Diagram. This makes laminar flow predictions much simpler.

It was also shown that the method used to characterise the fluid rheologically could significantly influence the accuracy of the prediction in certain cases, although in many data sets the effect was not significant. There is no way in which this can be predicted. Sound engineering care needs to be taken.

The Reynolds number developed by Kozicki and Tiu (1967) for pseudoplastic fluids and which includes an elaborate shape factor did not yield more accurate results than our Reynolds number. From this it could be concluded that for a rectangular flume it is not necessary to include a shape factor.

The Bingham Reynolds number proposed by Kozicki and Tiu (1967), which also includes shape factors, was evaluated with the bentonite data sets of this thesis and did not perform well.

The thin film approach of De Kee et al. (1990) worked well for the pseudoplastic fluids but not for the yield stress fluids. This was disappointing as the method is mathematically and physically rigorous.

7.3.2 Transitional flow

The prediction of the onset of transition has been established by developing a new critical Reynolds number that includes the Froude number and the apparent viscosity at 100 s^{-1}.

For the onset of 'full turbulence', a similar Reynolds number was developed related to the Froude number and the apparent viscosity at 500 s^{-1}.

The relationship of apparent viscosity against shear rate for the different fluids indicated that different fluids at certain concentrations could be grouped together and had similar apparent viscosities at, for example, 100 s^{-1}. When the transitional behaviour of these sets of data were compared, they were very similar.

The transitional behaviour of the more viscous concentrations was very different from the more Newtonian fluids. At higher concentrations the transition occurred at lower Reynolds numbers and were much smoother. The lower concentrations displayed a

more Newtonian behaviour similar to that of water with a sudden increase in friction factor at a much higher Reynolds number.

It was shown that the transition zone is not only sensitive to the rheology of the material but that the slope of the flume also has an influence on the onset of transition as well as the onset of full turbulence.

7.3.3 Turbulent flow

The turbulent behaviour of the more viscous fluids yielded friction factors with a much flatter slope than that predicted by Newtonian models like the Blasius equation.

The Manning and Chezy turbulent models were evaluated and it was shown that the constants of both equations changed with increase in concentrations and could therefore not be used for non-Newtonian open channel flow predictions.

A new model to predict turbulent flow was developed where the roughness Reynolds number was related to the apparent viscosity at 500 s^{-1}. The roughness function B was not found to be constant. The particle roughness was not used but only the flume hydraulic roughness.

7.3.4 Design Protocol

In Appendix C, a design protocol is set out with a worked out example to show how the new models can be used to predict non-Newtonian open channel flow.

7.4 RECOMMENDATIONS FOR FUTURE RESEARCH

The following aspects not covered in this thesis should be investigated.

- The effect of the cross-sectional shape of the flume on the flow of non-Newtonian slurries on laminar flow, the onset of transition as well as turbulent flow.
- The effect of roughness, as the flumes that were used were nearly smooth, and this is not always true of flumes found in industry.
- Velocity profiles and pressure fluctuations in laminar flow and transition to verify the onset of transition should be investigated.
- The highest flow rate obtained was only about 45 l/s and the size and design of the flume also limited higher flow rates and deeper flows. The turbulence model should be tested in a larger flume.
- A large database has been compiled for this thesis and it will be interesting to use this to calibrate computational fluid dynamics (CFD) software and extend the scope of the work done in this thesis.

7.5 CONCLUSIONS

The following final conclusions can be made:

For the three different non-Newtonian fluids tested at eleven concentrations in three different size smooth rectangular flumes with slopes varying from 1-5 degrees and flow rates from 0.01 – 45 l/s:

- Laminar flow can be predicted using one Reynolds number that can cater for the various fluid types, provided that the rheological parameters have been accurately established.

- New criteria have been developed to predict the onset of transition and to predict the onset of 'full turbulence'. As far as can be established this has not been done before.
- A new turbulent model has been developed with a varying roughness function B, which varies with the apparent viscosity at 500 s^{-1}.
- The transition range can also be predicted for the database used.
- All these models were tested using an extensive experimental database that was compiled.
- The models were also tested with data found in the literature both in laminar and in turbulent flow.
- These models take the effect of channel slope into consideration.
- The new open channel design procedure is presented in Appendix C.

The work presented in this thesis is fundamentally empirical in nature and will always be open to challenges of a more analytical nature. It is important in the absence of more rigorous fundamentals to produce competent design procedures. It is envisaged that this work will be seen as part of an ongoing debate which will eventually realise a more rigorous basis.

REFERENCES

ASTARITA, G., MARUCCI, G. & PALUMBA, G. 1964**.** Non-Newtonian flow along inclined plane surfaces. *I & EC fundamentals*, (3) 4: 333-339.

ALI, K. H. M. & GIOGIADIS, K. 1991. Laminar motion of fluid mud. *Proc. Instn. Civil Eng.* Part 2. paper 9801: 795-821.

BARNES WALTERS 1997 The yield stress myth.

BARR, G. 1931. *A Monograph of Viscometry.* Oxford University Press. London.

BRINKWORTH, B.J. 1968. *An Introduction to experimentation*. English University Press. London.

CAMP, T. R. 1942. Minimum velocities for sewers. *Journal of the Boston Society of Civil Engineers,* (29).

CHANSON, H. 1999. *The Hydraulics of Open Channel Flow.* Arnold. London.

CHHABRA, R.P. & RICHARDSON, J.F. 1999. *Non-Newtonian Flow in the Process Industries.* Butterworth Heineman. Oxford.

COUSSOT, P. 1994. Steady laminar flow of concentrated mud suspensions in open channels. *Journal of hydraulic research*. (32) 4: 535-558.

COUSSOT, P. 1997. *Mudflow Rheology and Dynamics.* A.A.Balkema. Rotterdam.

CHOW, VEN T. 1959. *Open Channel Hydraulics.* New York: McGraw-Hill.

DE KEE, D., CHHABRA, R. P., POWLEY, M.B. & ROY, S. 1990. Flow of viscoplastic fluids on an inclined plane: evaluation of yield stress, *Chem. Eng. Comm.* (96): 229-239.

DE KEE, D. & TURCOTTE, G. 1980. Chem. Eng. Comm**.**, (6): 273.

DODGE, D. W., & METZNER, A. B. 1959. Turbulent flow of non-Newtonian systems**.** *AIChE Journal*. (5)2: 189-204.

DOUGLASS, J. F., GASIOREK, J.M., SWAFFIELD, J. A. 1985. *Fluid Mechanics.* Longman Scientific and Technical. Essex. England.

FADDICK, R. R. 1986. Slurry flume design. *10th Int. Conf. On the hydraulic transport of of solids in pipes, Hydrotransport.* 10: 143-147.

FEATHERSTONE, R. E., & NALLURI, C. 1995. *Civil Engineering Hydraulics*. Oxford: Blackwell Science.

GREEN, H. R., LAMB, D. M. & Taylor, A. D. 1978. A new launder design procedure. *Society of mining engineering.* 1210-1216.

GOVIER, G.W. & AZIZ, K. 1972. *The flow of Complex mixtures in pipes.* Van Nostrand Reinhold Co. Florida USA.

HANKS, R.W. 1963a. The laminar-turbulent transition for flow in pipes, concentric annuli, and parallel plates. *AIChE Journal*. 9: 45-48.

HANKS, R.W. 1963b. The laminar-turbulent transition for fluids with a yield stress. *AIChE Journal*. 9: 306-309.

HANKS, R.W. 1979. Course notes. Hydraulic design for flow of complex fluids., *1981 Richard Hanks Associates, Inc. Orem, Utah. USA.*

HEYWOOD, N.I, MEHTA, K.B, and POPLAR, D. 1993, Evaluation of seven commercially available electromagnetic flow meters with Newtonian and non-Newtonian china clay slurry in pipeflow, *12th Int. Conf. on slurry handling and pipeline transport, Hydrotransport 12, BHR group*, p353.

IRELAND, J.W. 1971. *Mechanics of Fluids.* Butterworth & Co Publishers Ltd. London.

KLINE, S.J. and Mc.CLINTOCK, F.A. 1953. Describing uncertanties in single sample experiments. Mechanical Engineering, Vol 75, No. 1, (3-8).

KOZICKI, W. & TIU, C. 1967. Non-Newtonian flow through open channels. *The Canadian journal of chemical engineering*, (45): 127-134.

KOZICKI, W. & TIU, C. 1988. Parametric modelling of flow geometries in non-Newtonian flows. Chapter 8. *Encyclopedia of fluid mechanics. Vol 7. Rheology and non-Newtonian flows.* Editor: N.P. Cheremisinof. Housten: Gulf Publishing company.

LAU, H. H. 1979. A literature study on slurry transport by flumes. BHRA project no 13195: 1-11.

LAZARUS, J.H. 1982. A short course on hydraulics transport of solids in pipelines**.** Chapter 3. Hydrotransport 8. Johannesburg. South Africa.

LAZARUS, J.H. & NIELSON, I.D. 1978, A generalised correlation for friction head losses of settling mixtures in horizontal smooth pipelines, 5th Int. conf. On the hydraulic transport of solids in pipes, Hydrotransport 5, Paper B1.

LOEWENTHAL, R.E. 1994, Private Communication, University of Cape Town.

MACOSKO, C.W. 1994. *Rheology: Principles, Measurements and Applications.* VCH Publishers. New York.

McComb, W.D, 1995, Theory of turbulence. Rep. Prog. Phys., 58, 1117-1206.

METZGER, T. 1998. A little course in Rheology Part 1. Physica, Messtechnik GmbH, Stuttgart, Germany. 49-53

METZNER, A.B. & REED, J.C. 1955. Flow of non-Newtonian fluids – correlation of the laminar, transition and turbulent flow regions. *American institute of chemical engineers journa*l, (1) 4: 434-440

MUN, R. 1988. Turbulent pipe flow of yield stress fluids. M Eng Sci Thesis. University of Melbourne.

NAIK, B. 1983. Mechanics of mudflow treated as the flow of a Bingham fluid. Unpublished PhD thesis. Washington State University.

NGUYEN, Q.D. & BOGER, D.V. 1983. Yield stress Measurement for Concentrated Suspensions. *Journal of Rheology* 27 (4): 321-349.

NGUYEN, Q.D. & BOGER, D.V. 1985 Direct Yield stress Measurement with the Vane method. *Journal of Rheology* 27 (4): 321-349.

NGUYEN, Q.D. VU, T.D. WONG, Y.L. YEOW, Y.L. 1999 Solving the inverse problem of capillary viscometry by Tikhonov regularisation. *Journal of Non-Newtonian Fluid Mechanics* 87: 103-116.

SANDERS, R.S., Schaan, J., Gillies, R.G., McKibben, M.J., Sun, R. & Shook. C.A. 2002. Solids transport in laminar, open-channel flow of non-Newtonian slurries. Hydrotransport 15, Bannf, Canada.

SCHLICHTING, H. 1960. *Boundary layer theory.* New York: 4 th edition, McGraw-Hill: 475-479.

SHOOK, C.A. and ROCO, M.C. 1991. *Slurry flow: principles and practice,* Butterworth and Heinemann.

SLATTER, P.T. 1986. The Rheological characterisation of non-Newtonian slurries using a novel Balanced Beam Tube Viscometer. Unpublished MSc thesis. University of Cape Town. Cape Town.

SLATTER, P.T. & LAZERUS, J.H. 1988. The application of viscometry to the hydraulic transport and backfill material. Conf. Backfill in South African mines. *SAIMM*. 263-285.

SLATTER P T and LAZARUS J H (1993); Critical flow in slurry pipelines; British Hydromechanics Research Group 12th International Conference on Slurry Handling and Pipeline Transport HYDROTRANSPORT 12; Brugge, Belgium: 28-30 September, 1993. ISBN 0 85298 874 5 pp 639 - 654.

SLATTER, P.T. 1994. Transitional and Turbulent flow of non-Newtonian slurries in pipes. Unpublished PhD thesis. University of Cape Town. Cape Town.

SLATTER P.T. 1999. A New Friction Factor for Yield Stress Fluids; British Hydromechanics Research Group 14th International Conference on Slurry Handling and Pipeline Transport HYDROTRANSPORT 12. Maastricht, Netherlands. 255-265.

SLATTER, P.T. & WASP, E.J. 2000. The laminar/turbulent transition in large pipes. *10th Int. Conf. On Transport and sedimentation of solid particles.* Wrocÿaw: 4-7 September, 2000. Poland. 389-399.

SOZANSKI, M. M., KEMPA, E. S., GROCHOLSKI, K., BIEN, J. 1997. The Rheological experiment in sludge properties research. International Workshop on Rheology of Sludges Bari Italy. 148-162.

STRAUB, L.G., SILBERMAN, E., NELSON, H.C. 1958. Open channel flow at small Reynolds numbers. American Society of Civil Engineers. (123) 685-713.

STREETER, V.L. 1971. *Fluid Mechanics.* 5th Edition. New York. McGraw-Hill inc.

THOMAS, A.D., & WILSON, K.C. 1987. A new analysis of non-Newtonian flow- yield- power-law fluids. *Canadian Journal Chemical Engineering*. (65): 335-338.

THOMAS, D.G. 1965. Transport characteristics of supensions:VIII A note on the viscosity of Newtonian suspensions of uniform spherical particles. *Journal of colloid science*, (20): 267-277.

TORRANCE, B. McK. 1963. Friction factors for turbulent non-Newtonian flow in circular pipes. *S.A. Mechanical Engineer* (13)

US ARMY ENGINEERS. 1964. Hydraulic design criteria. Waterways Experiment Station, Vicksburg, Miss.

VANONI, V. 1946. Transportation of suspended sediment by water. *Trans Am. Soc. Civil Engineers,* (III).

WAN, Z. & WANG, Z. 1994. *Hyperconcentrated Flow.* AA Balkema. Rotterdam.

WILSON, K.C., & THOMAS, A.D. 1985. A new analysis of the turbulent flow of non-Newtonian fluids**.** *Canadian Journal Chem. Eng.* (63): 539-546.

WILSON, K.C. 1986. Modelling the effects of slurry flows with a free surface. In *Proc. Hydrotransport 10.* Insbruck. Austria. 123-132.

WILSON, K.C. 1988. Effect of non-Newtonian slurry properties on drag reduction and course particle suspension**.** In *Proceedings of the 10th international congress on rheology,* Sydney, Australia.

WILSON, K.C. 1991. Slurry transport in flumes. Chapter 8 *Slurry handling: Design of solid-liquid systems.* Eds. Brown, N.P. & Heywood, N.I., London: Elsevier Science Publishers LTD. 167-180.

WILSON, K.C., ADDIE, G.R., SELGREN, A & CLIFT, R. 1996. *Slurry transport using centrifugal pumps*. 2nd Edition. London, Blackie Academic & Professional (Chapman & Hall).

ZHANG, H., & Ren, Z. 1982. Discussion of resistance of Hyperconcentrated Flow in Open channels. *Scientia Sinica (Series A).* (25.12) 1332-1342.

APPENDIX A

EXPERIMENTAL RESULTS

In this appendix the following is depicted:

- The fluid properties and rheological parameters are given in section A.1
- The experimental data obtained from the tube viscometers are depicted in the form of rheograms in section A.1
- The flume data is depicted in the form of Moody diagrams in section A.2.

A.1 RHEOGRAMS OF MATERIALS USED

Kaolin 3-10% by volume

Bentonite 3-6%

CMC 1-5.3%

Carbopol 1%

A.2 FLUME DATA

Kaolin 3-10% in 75 mm 150 mm and 300 mm flumes

Bentonite 3-6% in 75 mm 150 mm and 300 mm flumes

CMC 1-5.3% in 75 mm 150 mm and 300 mm flumes

Carbopol 1% in 75 mm flume.

A.1 RHEOGRAMS

3% KAOLIN

SLURRY PROPERTIES	
Solids Relative Density	2.65
Slurry Relative Density	1.049
Volumetric Concentration	3%
Yield Stress	1.843 Pa
Fluid Consistency Index	0.0018 Pa.s^n
Flow Behaviour Index	1.062
Apparent viscosity (100 s^{-1})	0.021 Pa.s
Apparent viscosity (500 s^{-1})	0.0063 Pa.s

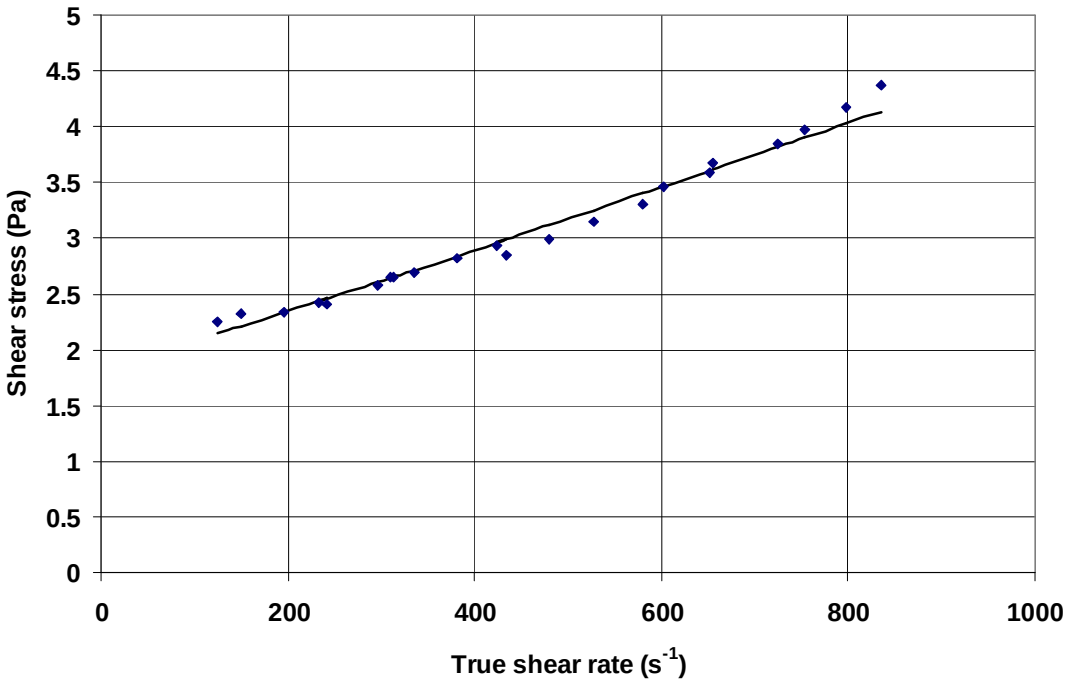

Rheogram -3% kaolin

4.5% KAOLIN

SLURRY PROPERTIES	
Solids Relative Density	2.65
Slurry Relative Density	1.075
Volumetric Concentration	4.5%
Yield Stress	3.51 Pa
Fluid Consistency Index	0.0117 Pa.s^n
Flow Behaviour Index	0.836
Apparent viscosity (100 s^{-1})	0.041 Pa.s
Apparent viscosity (500 s^{-1})	0.0076 Pa.s

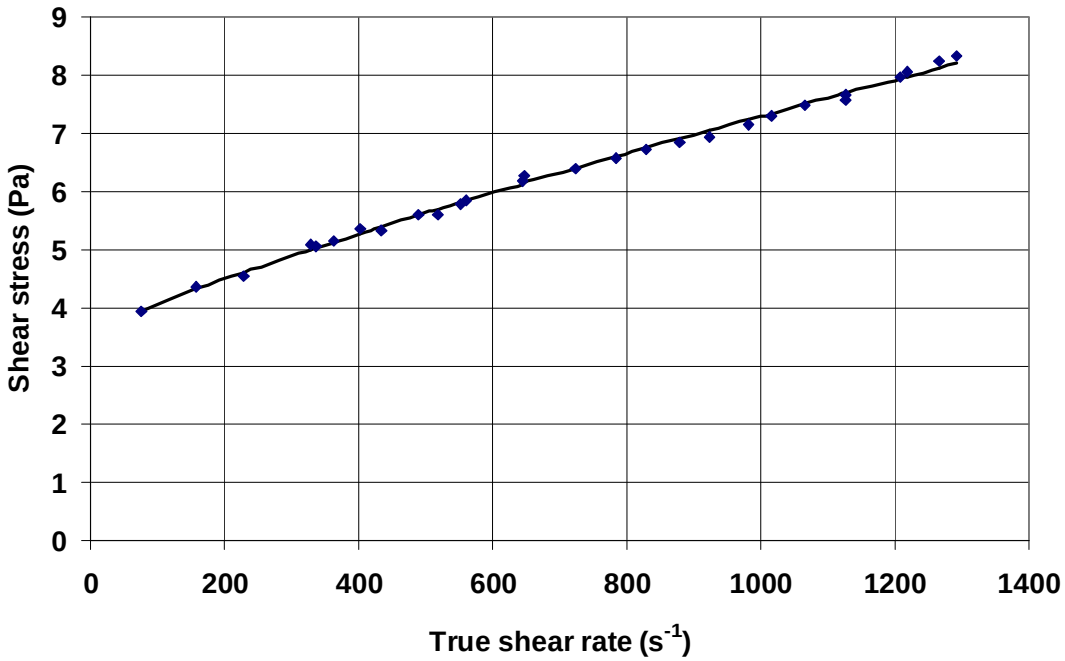

Rheogram 4.5% kaolin

5.4% KAOLIN

SLURRY PROPERTIES	
Solids Relative Density	2.65
Slurry Relative Density	1.090
Volumetric Concentration	5.4%
Yield Stress	4.985 Pa
Fluid Consistency Index	0.0297 Pa.s^n
Flow Behaviour Index	0.717
Apparent viscosity (100 s^{-1})	0.058 Pa.s
Apparent viscosity (500 s^{-1})	0.015 Pa.s

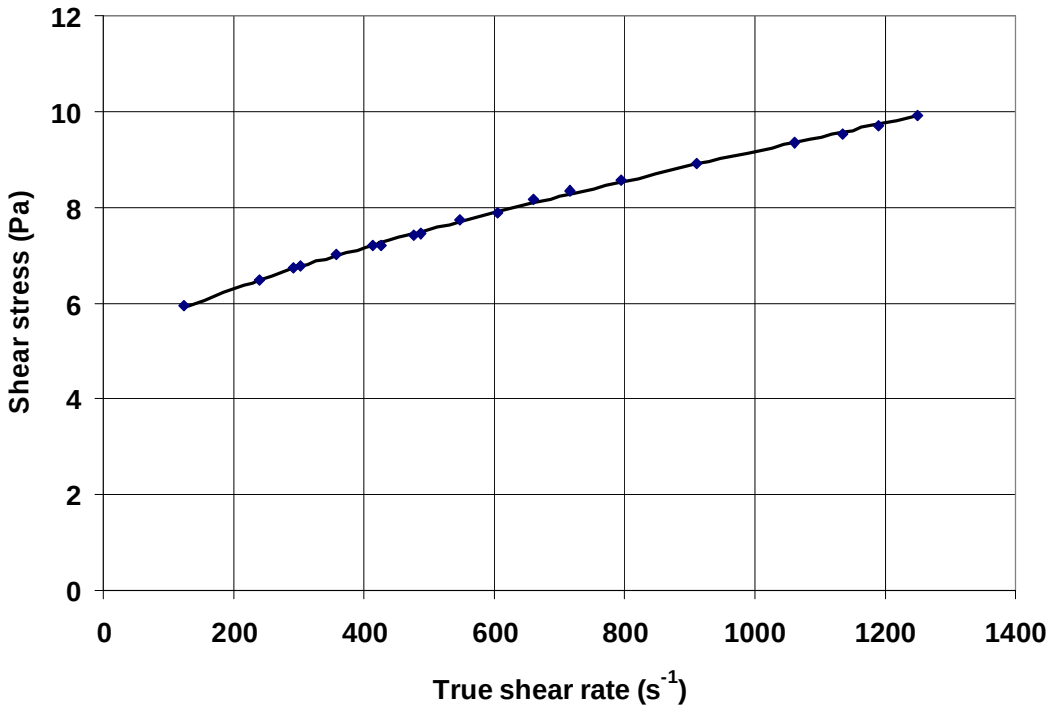

Rheogram Kaolin 5.4%

6% KAOLIN

SLURRY PROPERTIES	
Solids Relative Density	2.65
Slurry Relative Density	1.099
Volumetric Concentration	6%
Yield Stress	4.78 Pa
Fluid Consistency Index	0.0986 Pa.s^n
Flow Behaviour Index	0.583
Apparent viscosity (100 s^{-1})	0.084 Pa.s
Apparent viscosity (500 s^{-1})	0.021 Pa.s

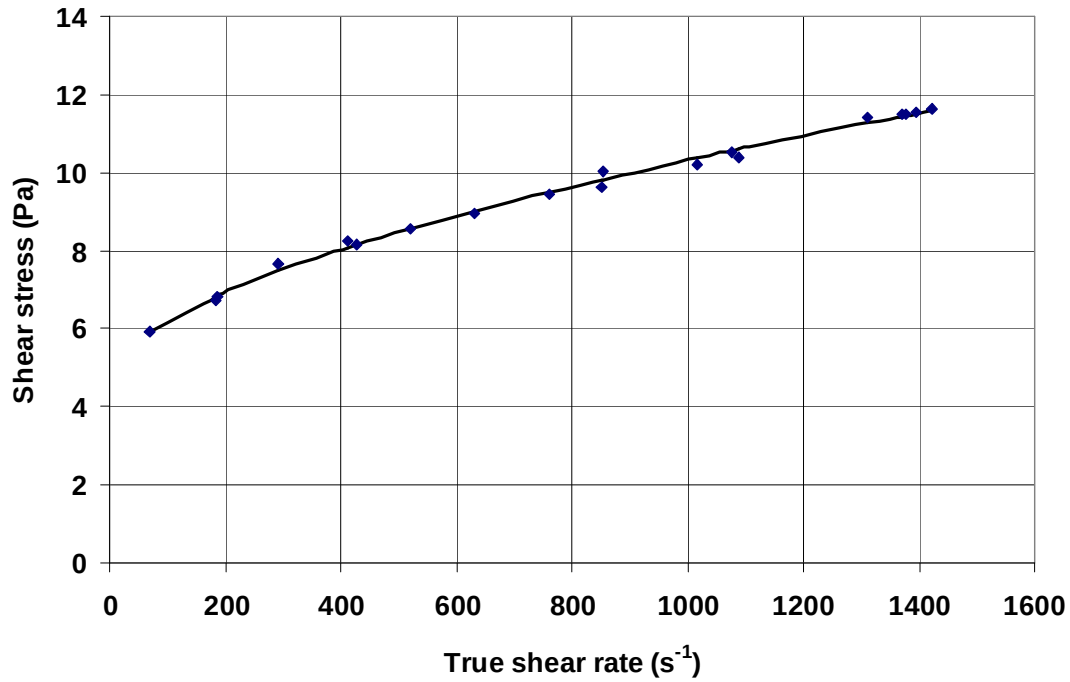

Rheogram 6% kaolin

7.1% KAOLIN

SLURRY PROPERTIES	
Solids Relative Density	2.65
Slurry Relative Density	1.1183
Volumetric Concentration	7.1%
Yield Stress	9.431 Pa
Fluid Consistency Index	0.625 Pa.s^n
Flow Behaviour Index	0.388
Apparent viscosity (100 s^{-1})	0.132 Pa.s
Apparent viscosity (500 s^{-1})	0.033 Pa.s

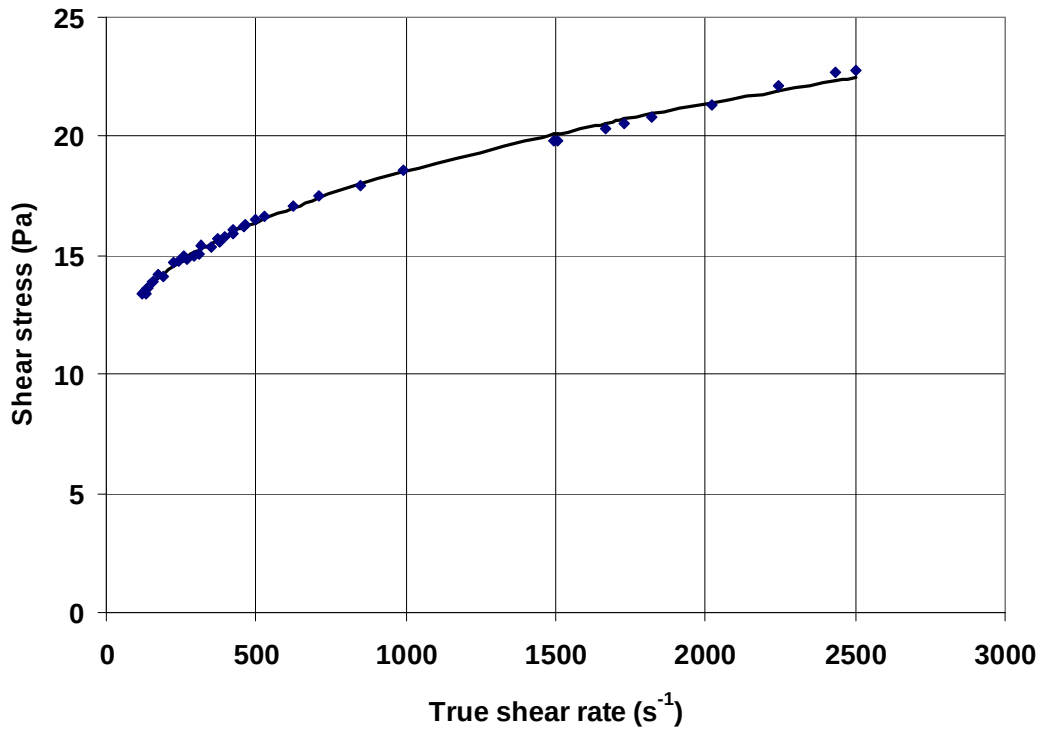

Rheogram 7.1% kaolin

8% K AOLIN

SLURRY PROPERTIES	
Solids Relative Density	2.65
Slurry Relative Density	1.133
Volumetric Concentration	8%
Yield Stress	14.63 Pa
Fluid Consistency Index	0.0569 Pa.s^{n}
Flow Behaviour Index	0.694
Apparent viscosity (100 s^{-1})	0.16 Pa.s
Apparent viscosity (500 s^{-1})	0.038 Pa.s

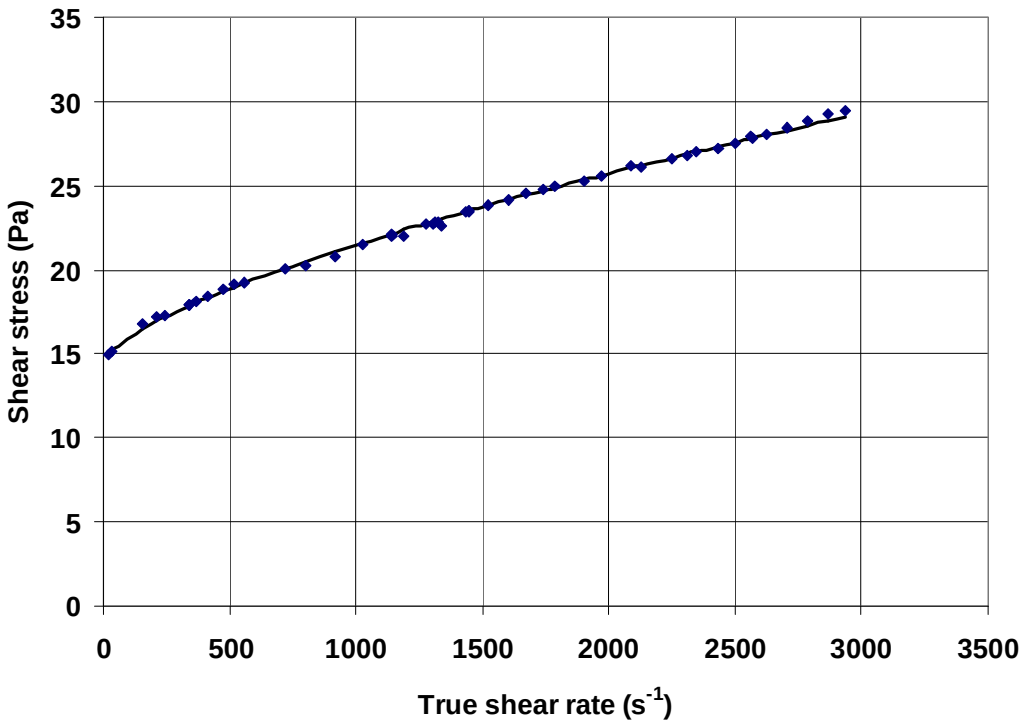

Rheogram 8% kaolin

9% KAOLIN

SLURRY PROPERTIES	
Solids Relative Density	2.65
Slurry Relative Density	1.1494
Volumetric Concentration	9%
Yield Stress	20.45 Pa
Fluid Consistency Index	0.267 Pa.s^n
Flow Behaviour Index	0.535
Apparent viscosity (100 s^{-1})	0.236 Pa.s
Apparent viscosity (500 s^{-1})	0.0557 Pa.s

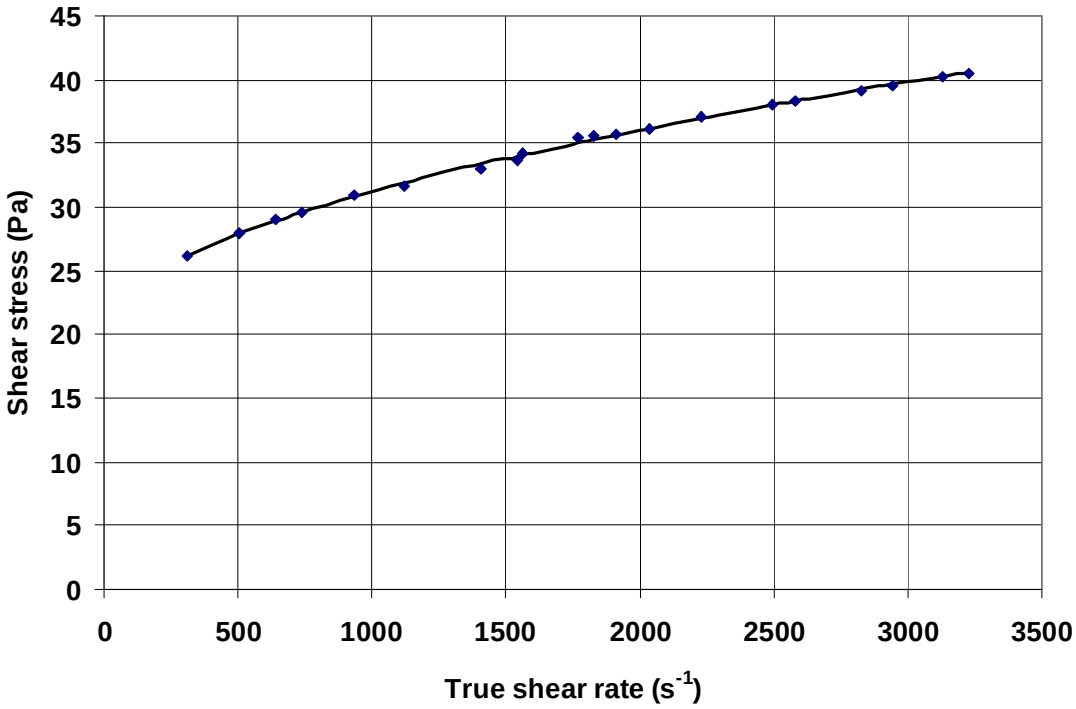

Rheogram 9% kaolin

10% KAOLIN

SLURRY PROPERTIES	
Solids Relative Density	2.65
Slurry Relative Density	1.165
Volumetric Concentration	10%
Yield Stress	21.311 Pa
Fluid Consistency Index	0.524 Pa.s^n
Flow Behaviour Index	0.468
Apparent viscosity (100 s^{-1})	0.258 Pa.s
Apparent viscosity (500 s^{-1})	0.062 Pa.s

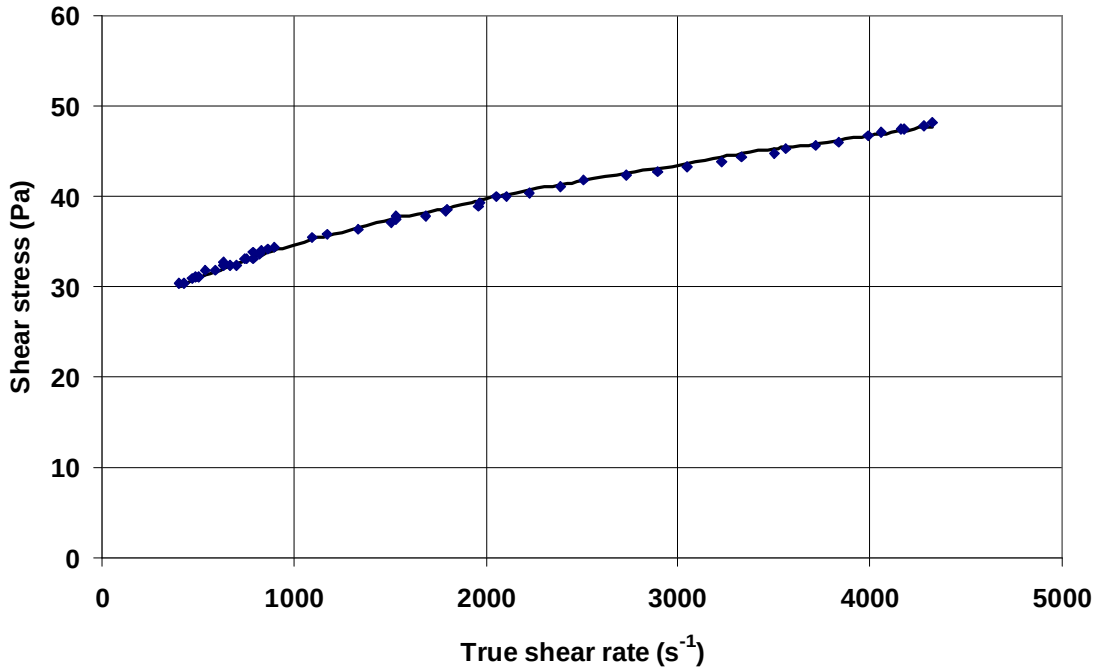

Rheogram -10% kaolin

3% BENTONITE

SLURRY PROPERTIES	
Slurry Relative Density	1.014
Concentration by mass	2.11%
Yield Stress	1.002 Pa
Fluid Consistency Index	0.0034 Pa.s^n
Flow Behaviour Index	1
Apparent viscosity (100 s^{-1})	0.013 Pa.s
Apparent viscosity (500 s^{-1})	0.0054 Pa.s

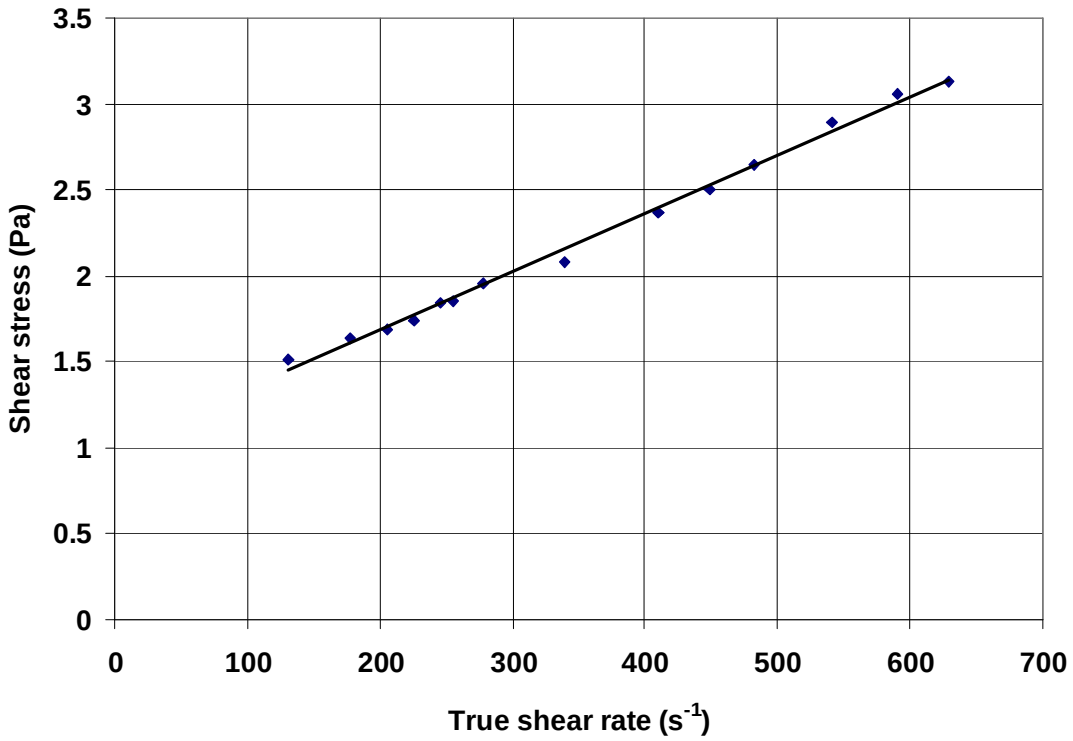

Rheogram 3% bentonite

4.5% BENTONITE

SLURRY PROPERTIES	
Slurry Relative Density	1.025
Concentration by mass	4.12%
Yield Stress	4.402 Pa
Fluid Consistency Index	0.0061 Pa.s^n
Flow Behaviour Index	1
Apparent viscosity (100 s^{-1})	0.0149 Pa.s
Apparent viscosity (500 s^{-1})	0.00501 Pa.s

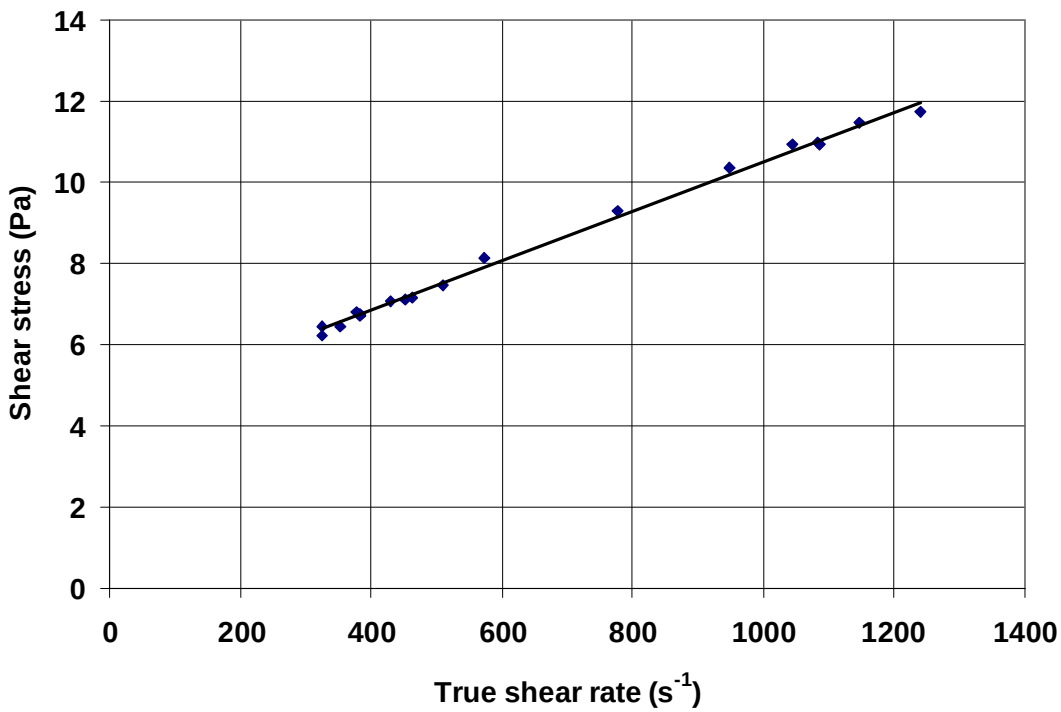

Rheogram 4.5% bentonite

6% BENTONITE

SLURRY PROPERTIES	
Slurry Relative Density	1.033
Concentration by mass	5.3%
Yield Stress	8.187 Pa
Fluid Consistency Index	0.0061 Pa.s^n
Flow Behaviour Index	1
Apparent viscosity (100 s^{-1})	0.0882 Pa.s
Apparent viscosity (500 s^{-1})	0.0227 Pa.s

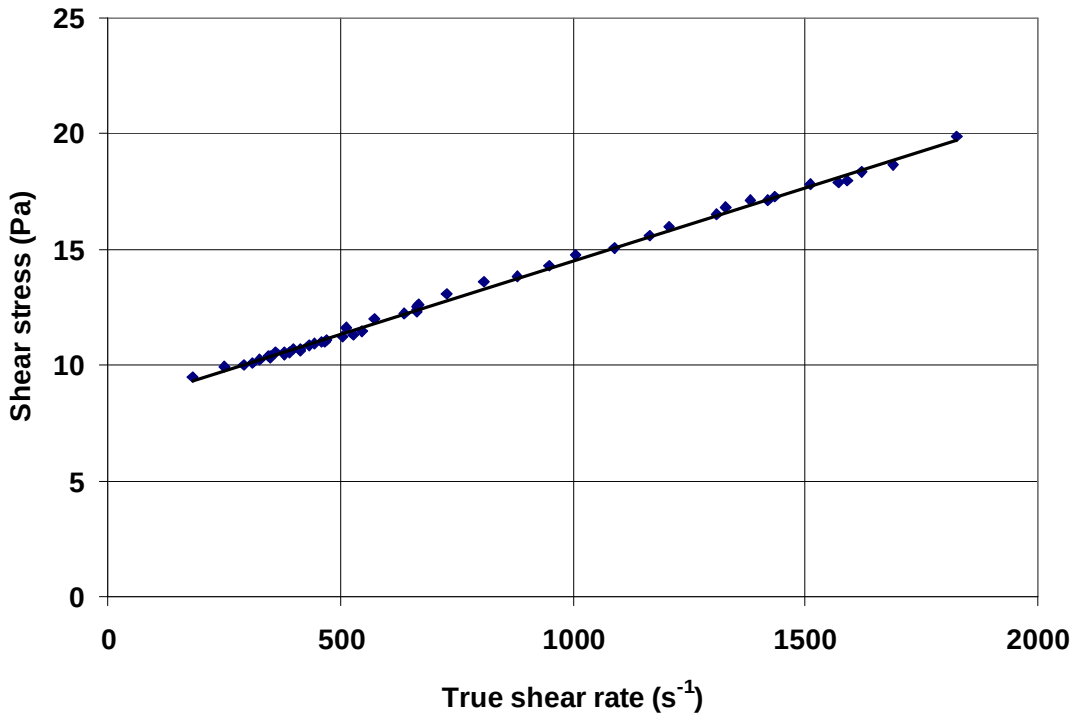

Rheogram 6% bentonite

6.2% BENTONITE

SLURRY PROPERTIES	
Slurry Relative Density	1.034
Concentration by mass	5.6%
Yield Stress	12.698 Pa
Fluid Consistency Index	0.006 Pa.s^n
Flow Behaviour Index	1
Apparent viscosity (100 s^{-1})	0.133 Pa.s
Apparent viscosity (500 s^{-1})	0.0314 Pa.s

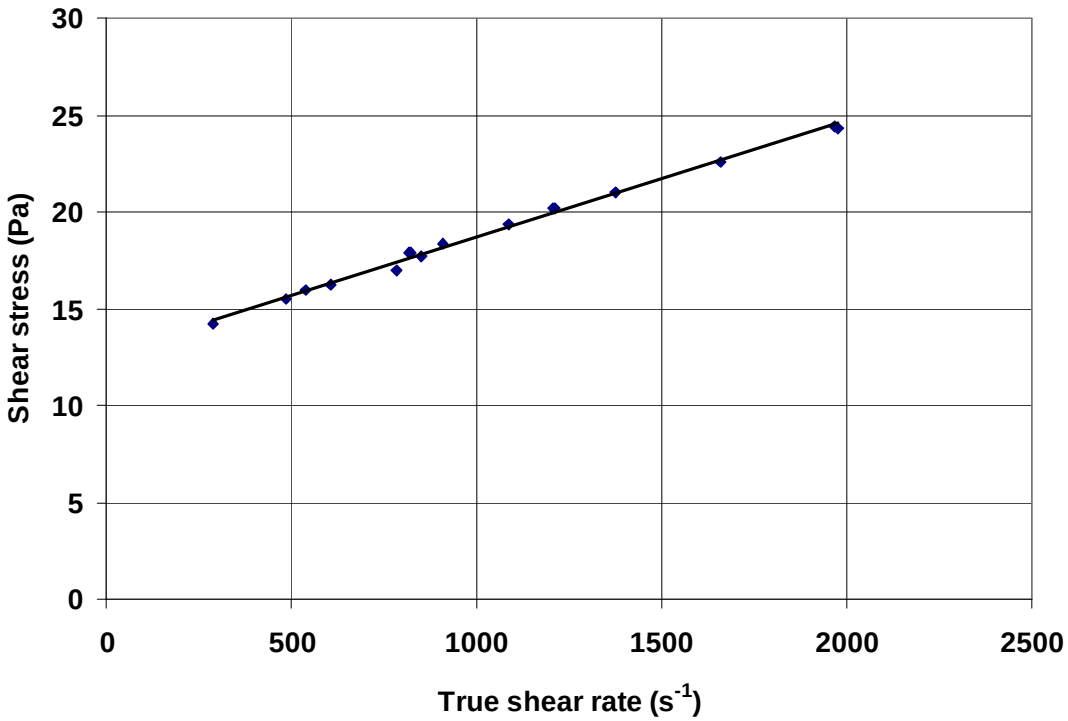

Rheogram 6.2% bentonite

1% CMC

SLURRY PROPERTIES	
Slurry Relative Density	1.0067
Concentration by mass	1%
Yield Stress	0 Pa
Fluid Consistency Index	0.063 Pa.s^n
Flow Behaviour Index	0.641
Apparent viscosity (100 s^{-1})	0.0121 Pa.s
Apparent viscosity (500 s^{-1})	0.0068 Pa.s

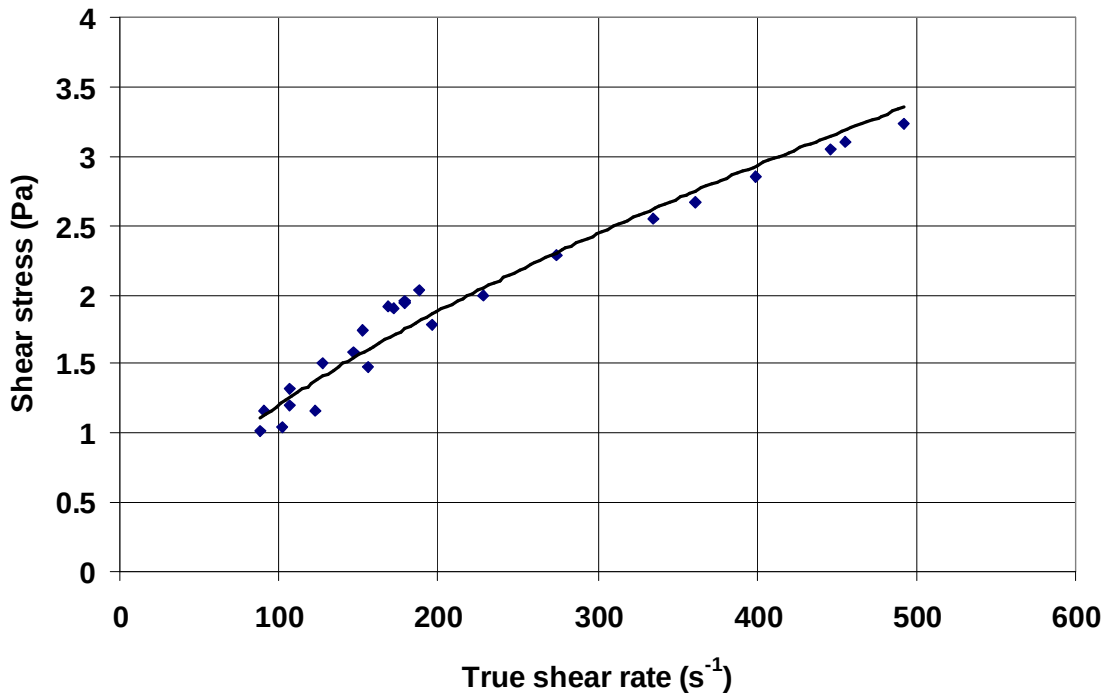

Rheogram 1% CMC

1.5% CMC

SLURRY PROPERTIES	
Slurry Relative Density	1.0086
Concentration by mass	1.5%
Yield Stress	0 Pa
Fluid Consistency Index	0.0181 Pa.s^n
Flow Behaviour Index	0.947
Apparent viscosity (100 s^{-1})	0.0142 Pa.s
Apparent viscosity (500 s^{-1})	0.013 Pa.s

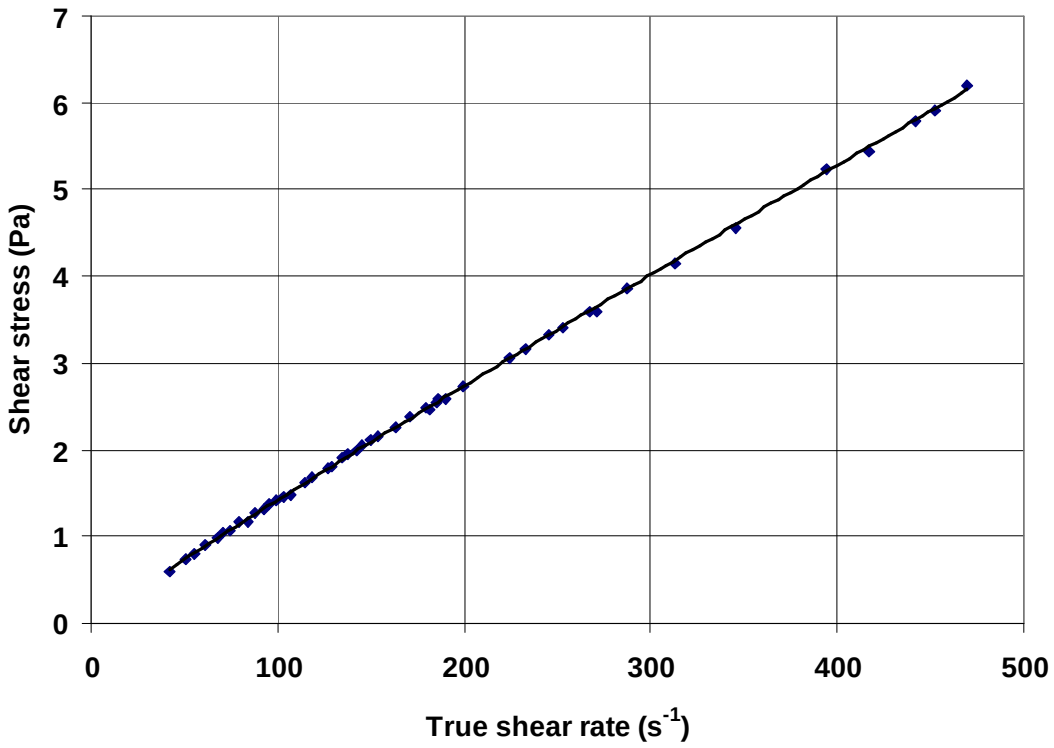

Rheogram 1.5% CMC

1.8% CMC

SLURRY PROPERTIES	
Slurry Relative Density	1.0107
Concentration by mass	1.8%
Yield Stress	0 Pa
Fluid Consistency Index	0.087 Pa.s^n
Flow Behaviour Index	0.765
Apparent viscosity (100 s^{-1})	0.0295 Pa.s
Apparent viscosity (500 s^{-1})	0.0202 Pa.s

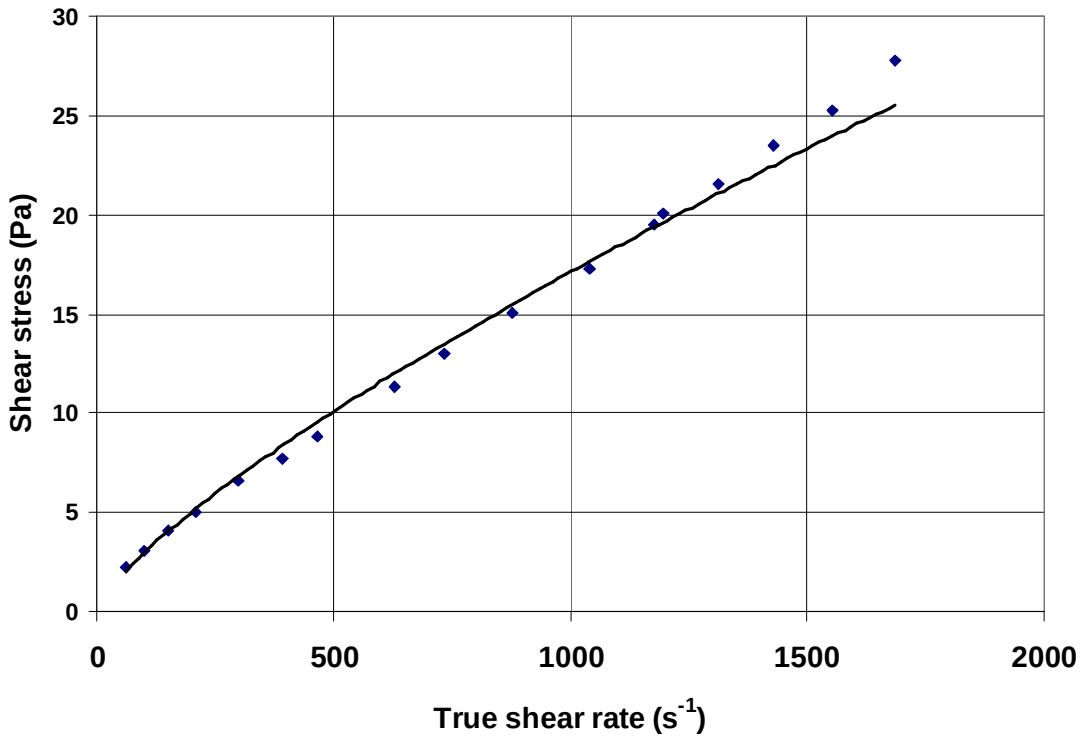

Rheogram 1.8% CMC

2.8% CMC

SLURRY PROPERTIES	
Slurry Relative Density	1.016
Concentration by mass	2.8%
Yield Stress	0 Pa
Fluid Consistency Index	0.197 Pa.s^n
Flow Behaviour Index	0.758
Apparent viscosity (100 s^{-1})	0.0646 Pa.s
Apparent viscosity (500 s^{-1})	0.0438 Pa.s

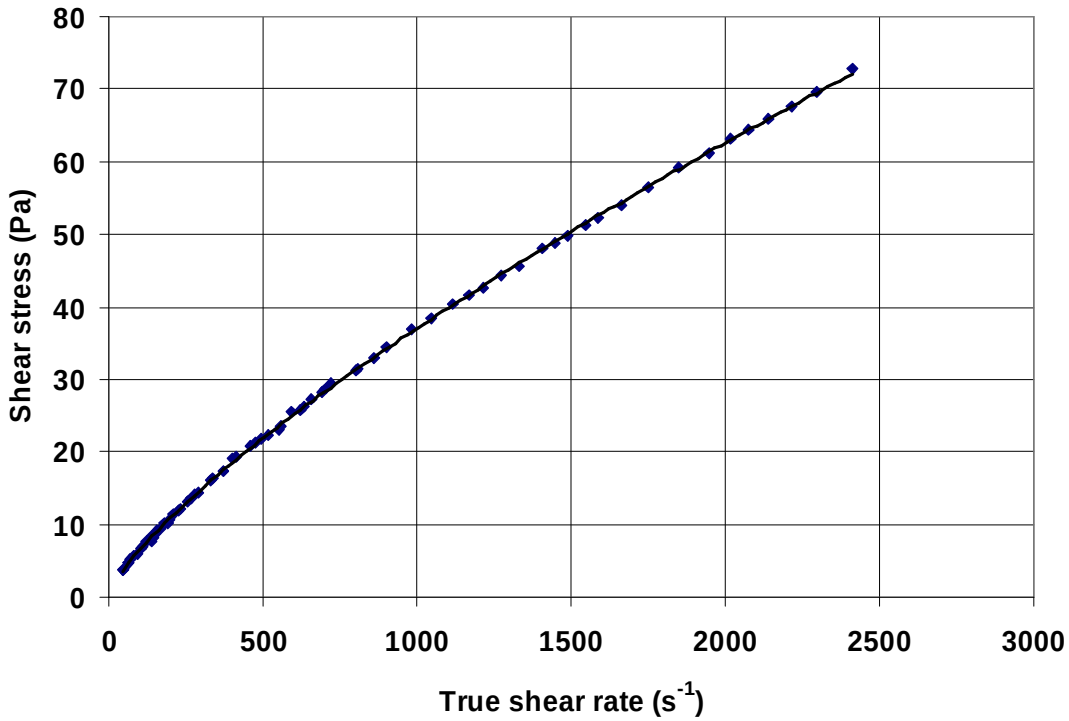

Rheogram 2.8% CMC

3% CMC

SLURRY PROPERTIES	
Slurry Relative Density	1.0182
Concentration by mass	3%
Yield Stress	0 Pa
Fluid Consistency Index	0.148 Pa.s^n
Flow Behaviour Index	0.8057
Apparent viscosity (100 s^{-1})	0.0605 Pa.s
Apparent viscosity (500 s^{-1})	0.0442 Pa.s

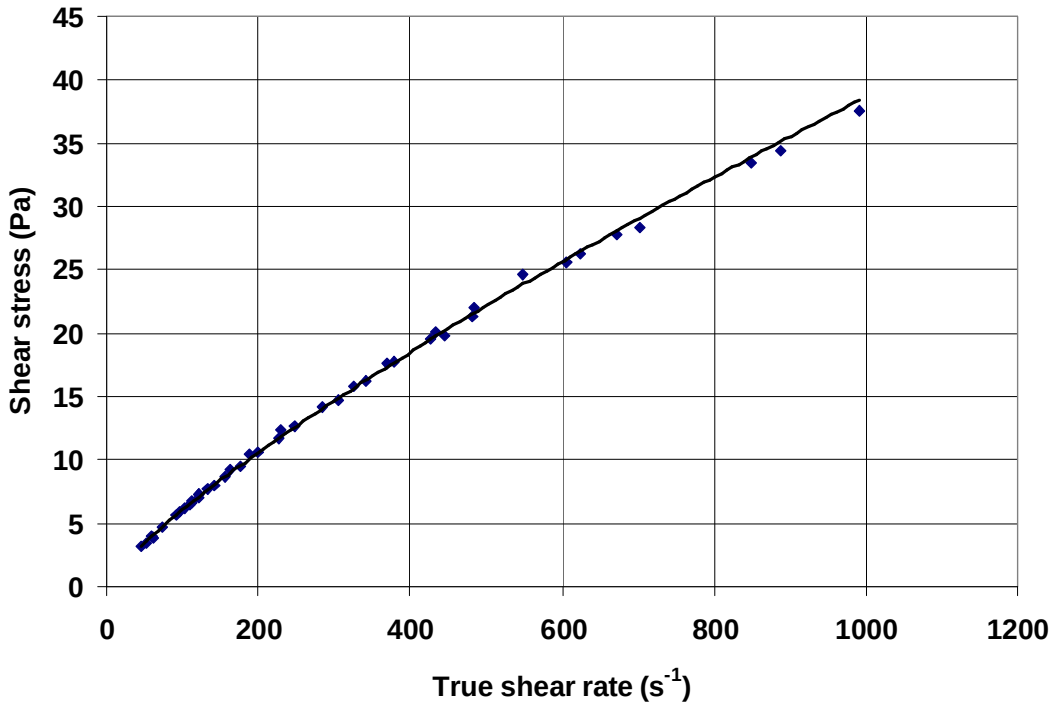

Rheogram 3% CMC

3.8 CMC

SLURRY PROPERTIES	
Slurry Relative Density	1.021
Concentration by mass	3.8%
Yield Stress	0 Pa
Fluid Consistency Index	0.572 Pa.s^n
Flow Behaviour Index	0.69
Apparent viscosity (100 s^{-1})	0.137 Pa.s
Apparent viscosity (500 s^{-1})	0.083 Pa.s

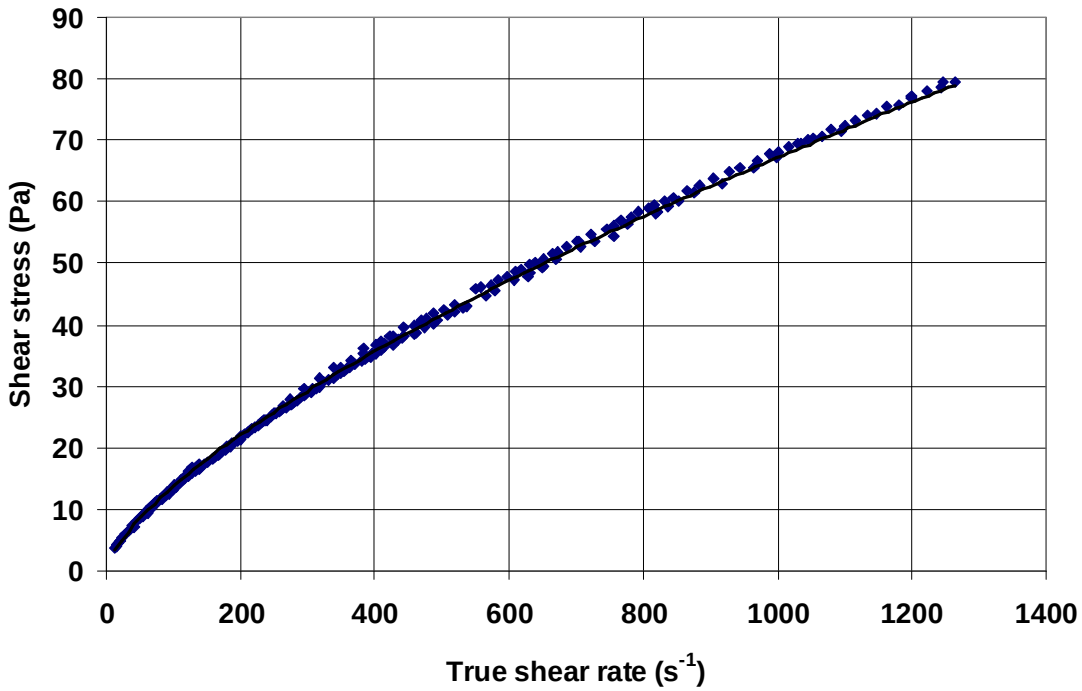

Rheogram 3.8% CMC

4% CMC

SLURRY PROPERTIES	
Slurry Relative Density	1.023
Concentration by mass	4%
Yield Stress	0 Pa
Fluid Consistency Index	0.372 Pa.s^n
Flow Behaviour Index	0.742
Apparent viscosity (100 s^{-1})	0.113 Pa.s
Apparent viscosity (500 s^{-1})	0.0748 Pa.s

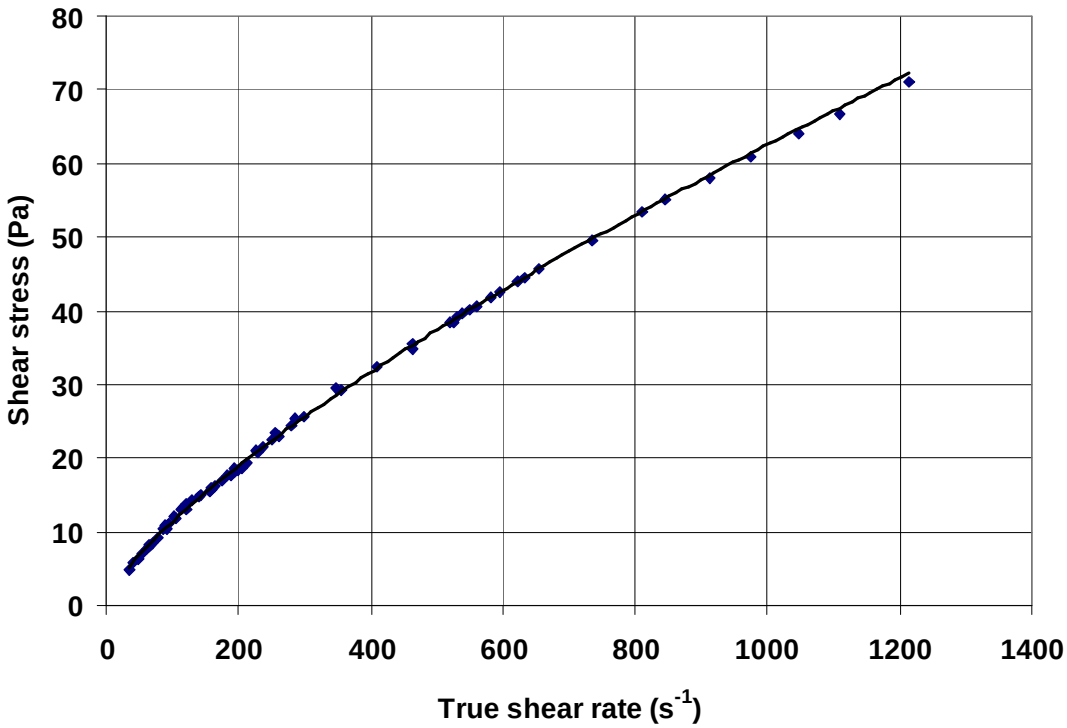

Rheogram 4% CMC

5.3% CMC

SLURRY PROPERTIES	
Slurry Relative Density	1.028
Concentration by mass	5.3%
Yield Stress	0 Pa
Fluid Consistency Index	0.841 Pa.s^n
Flow Behaviour Index	0.716
Apparent viscosity (100 s^{-1})	0.227 Pa.s
Apparent viscosity (500 s^{-1})	0.144 Pa.s

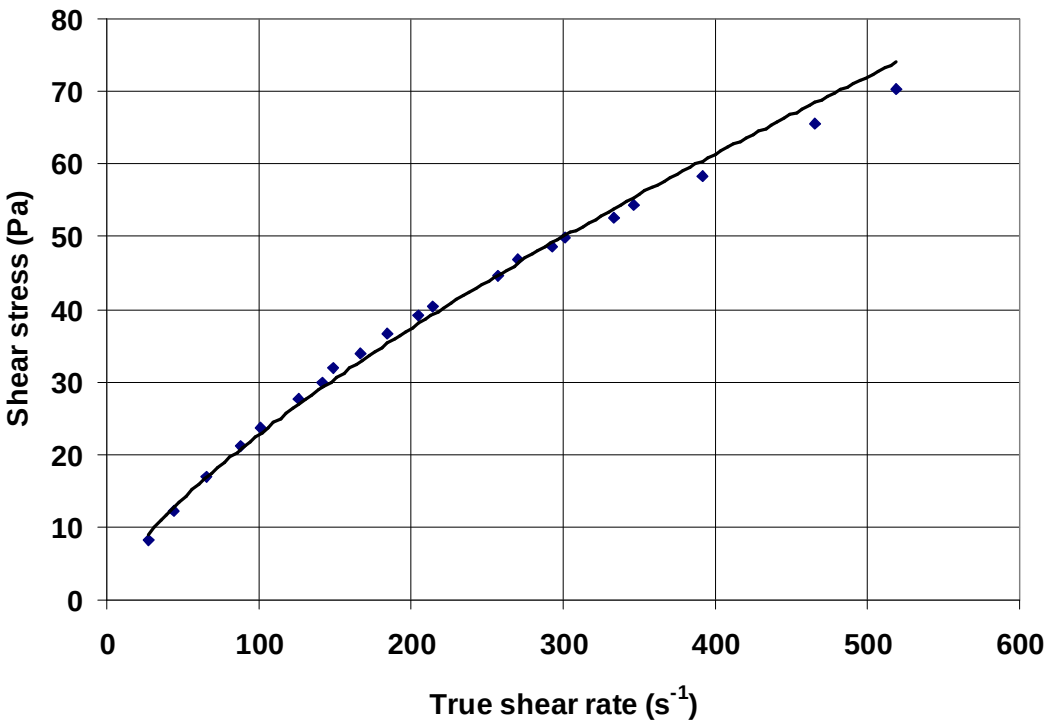

Rheogram 5.3% CMC

1% CARBOPOL

SLURRY PROPERTIES	
Slurry Relative Density	0.955
Concentration by mass	1%
Yield Stress	3.522 Pa
Fluid Consistency Index	0.287 Pa.s^n
Flow Behaviour Index	0.636
Apparent viscosity (100 s^{-1})	0.227 Pa.s
Apparent viscosity (500 s^{-1})	0.144 Pa.s

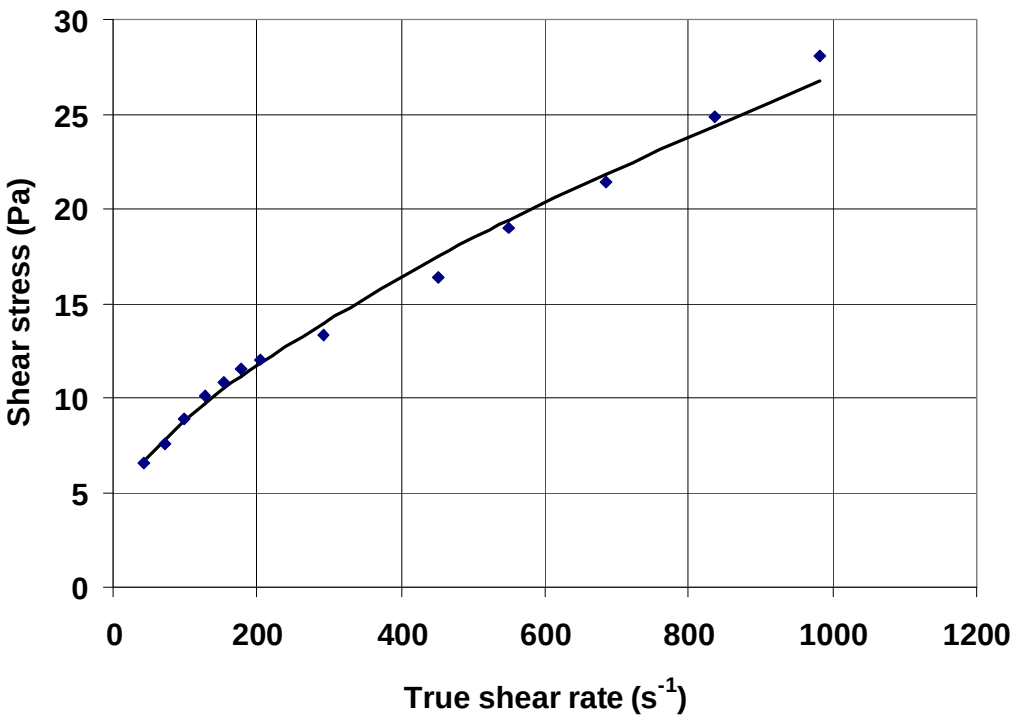

Rheogram 1% Carbopol

A2-FLUME DATA

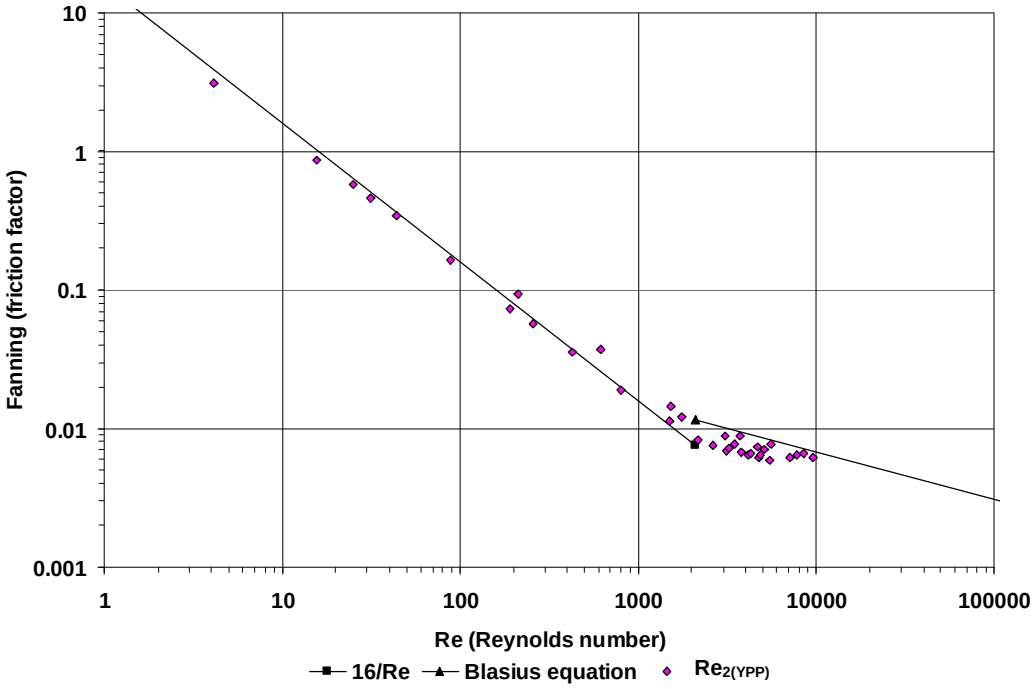

3% kaolin in 75 mm flume

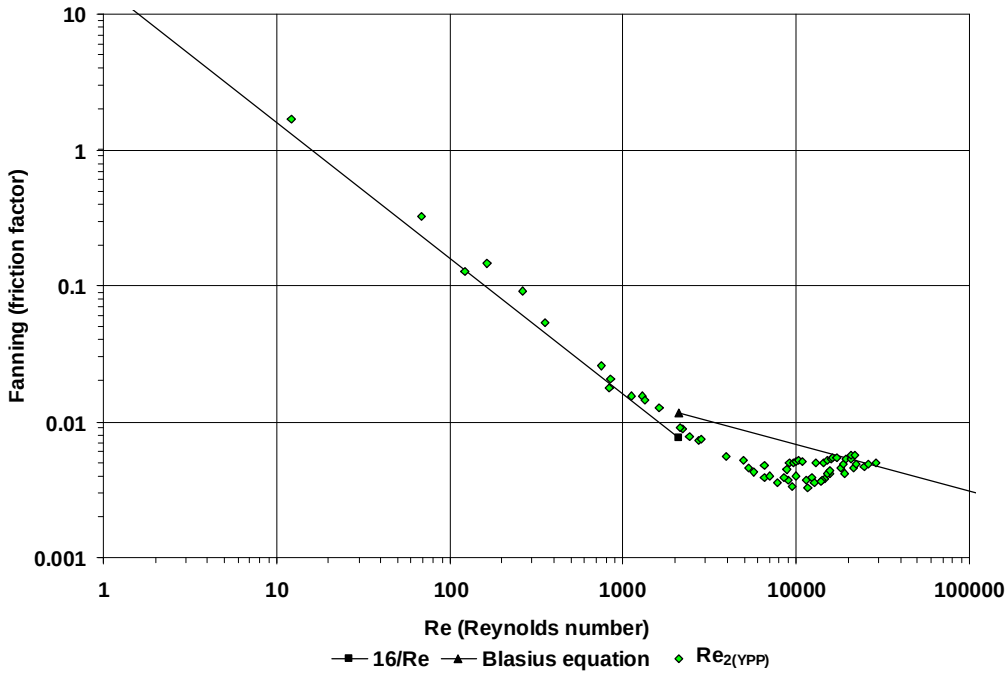

3% kaolin in 150 mm flume

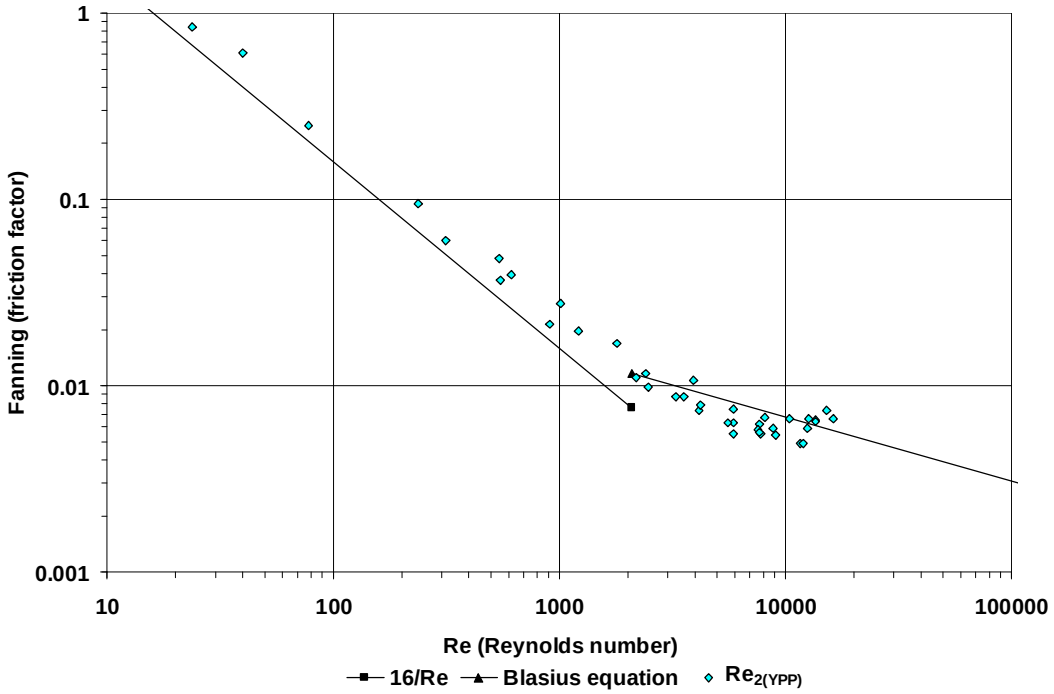

3% kaolin in 300 mm flume

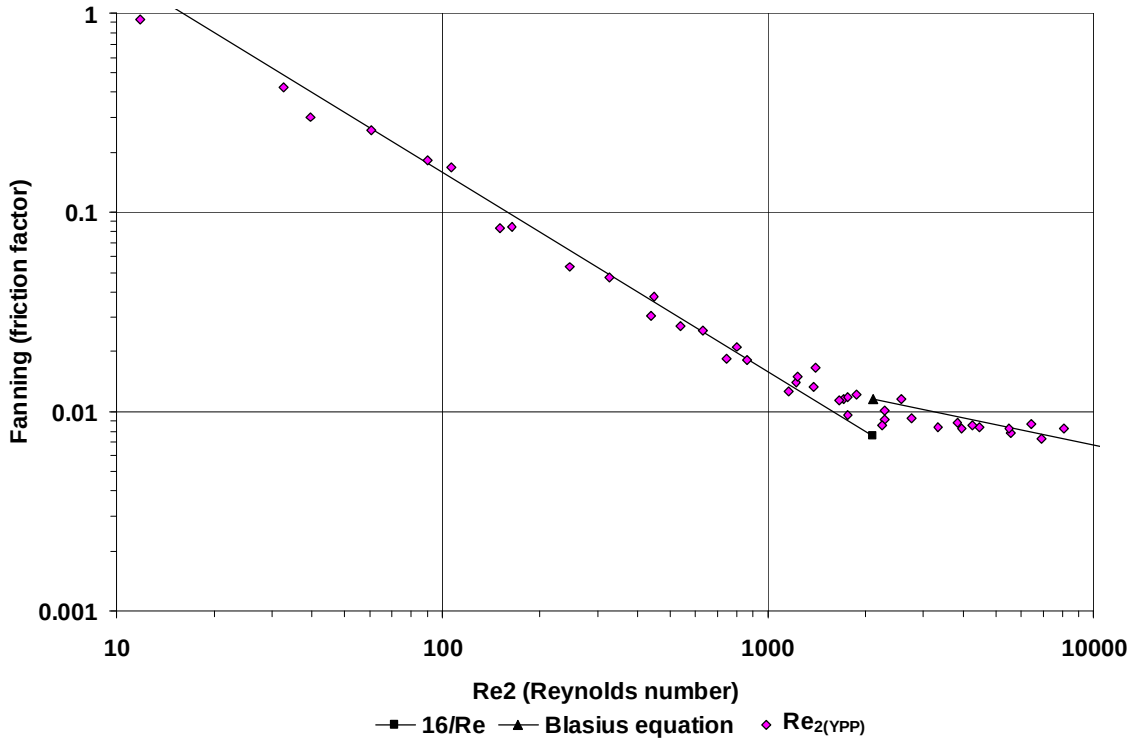

4.5% kaolin in 75 mm flume

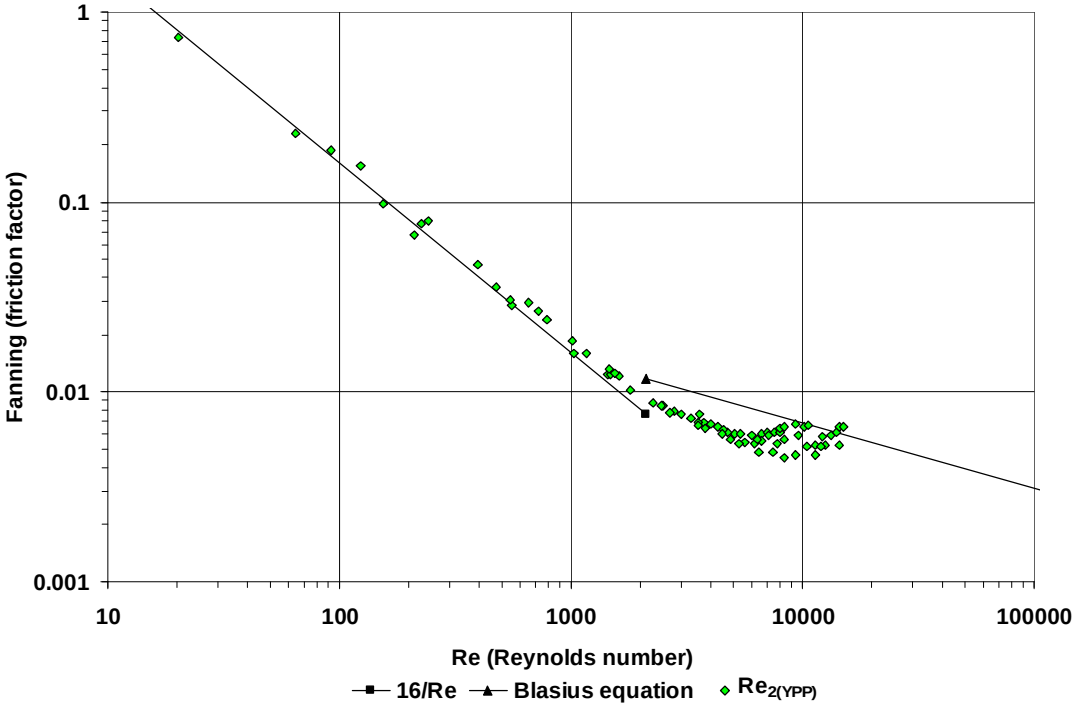

4.5% kaolin 150 mm flume

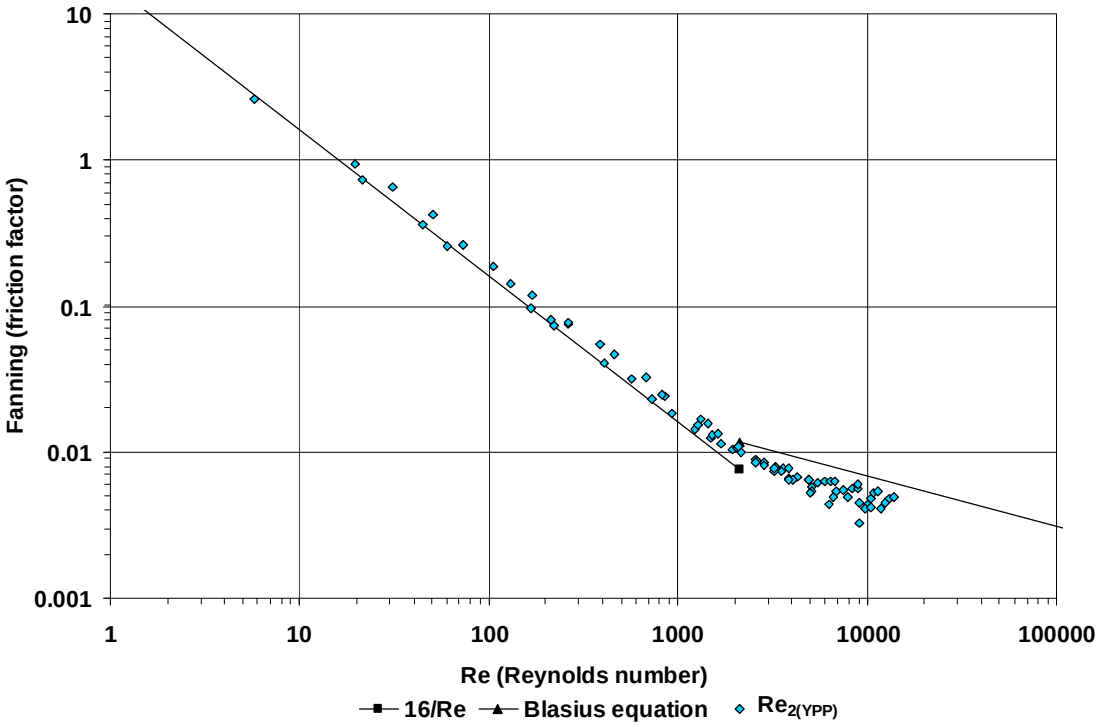

4.5% kaolin in 300 mm flume

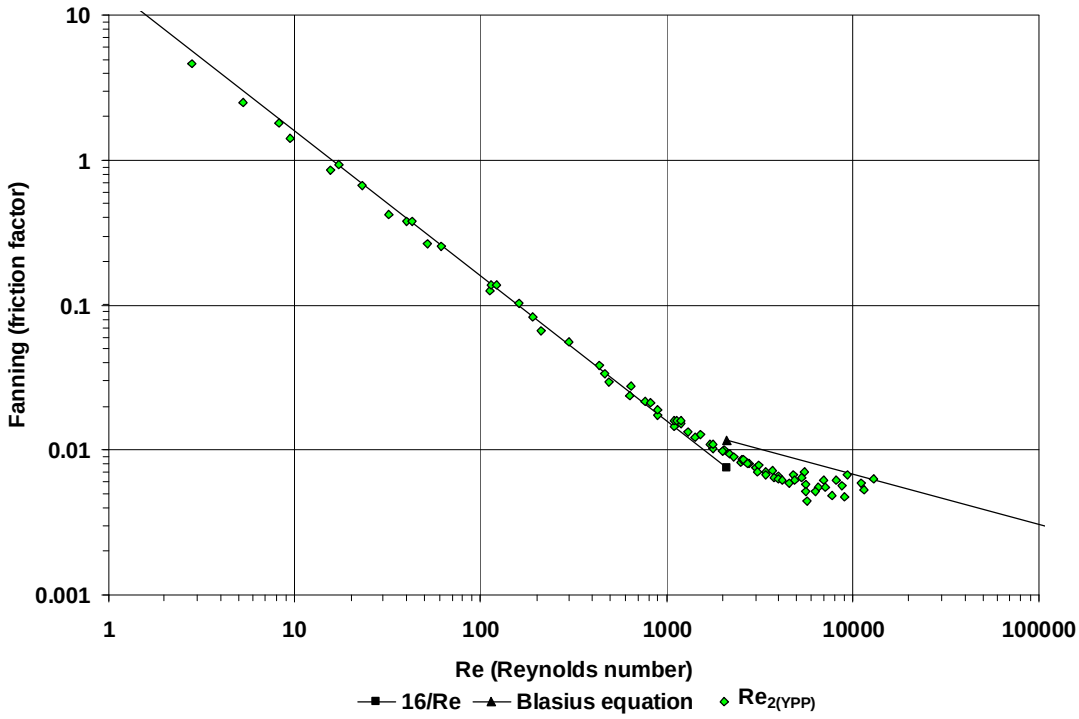

5.4% kaolin in 150 mm flume

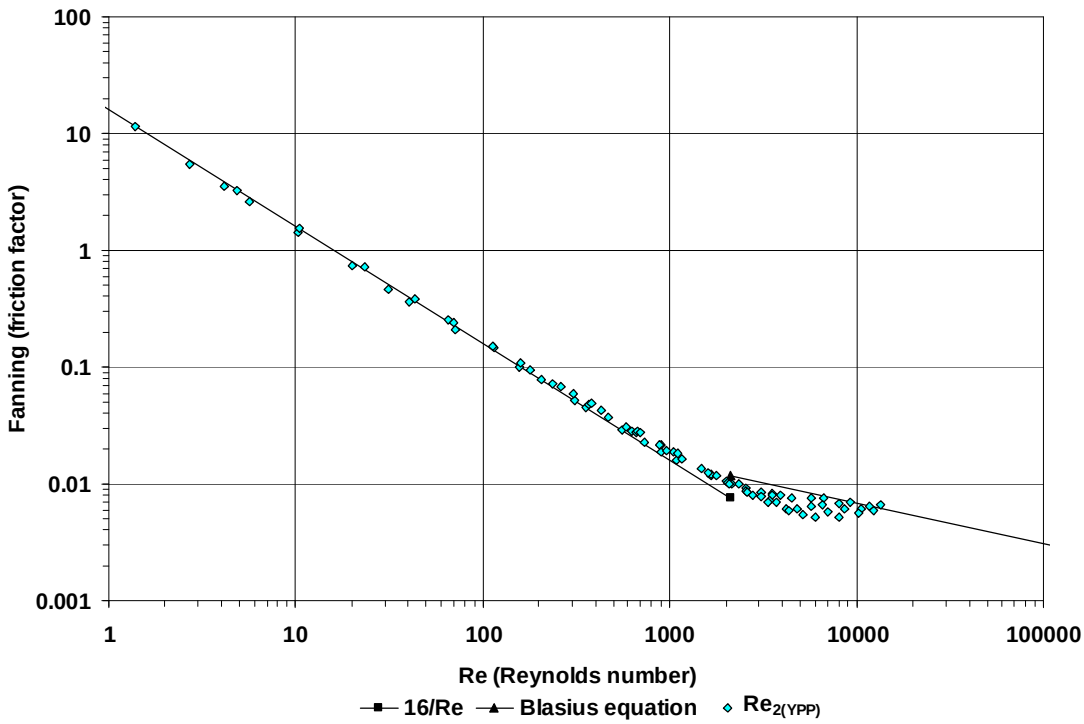

5.4% kaolin in 300 mm flume

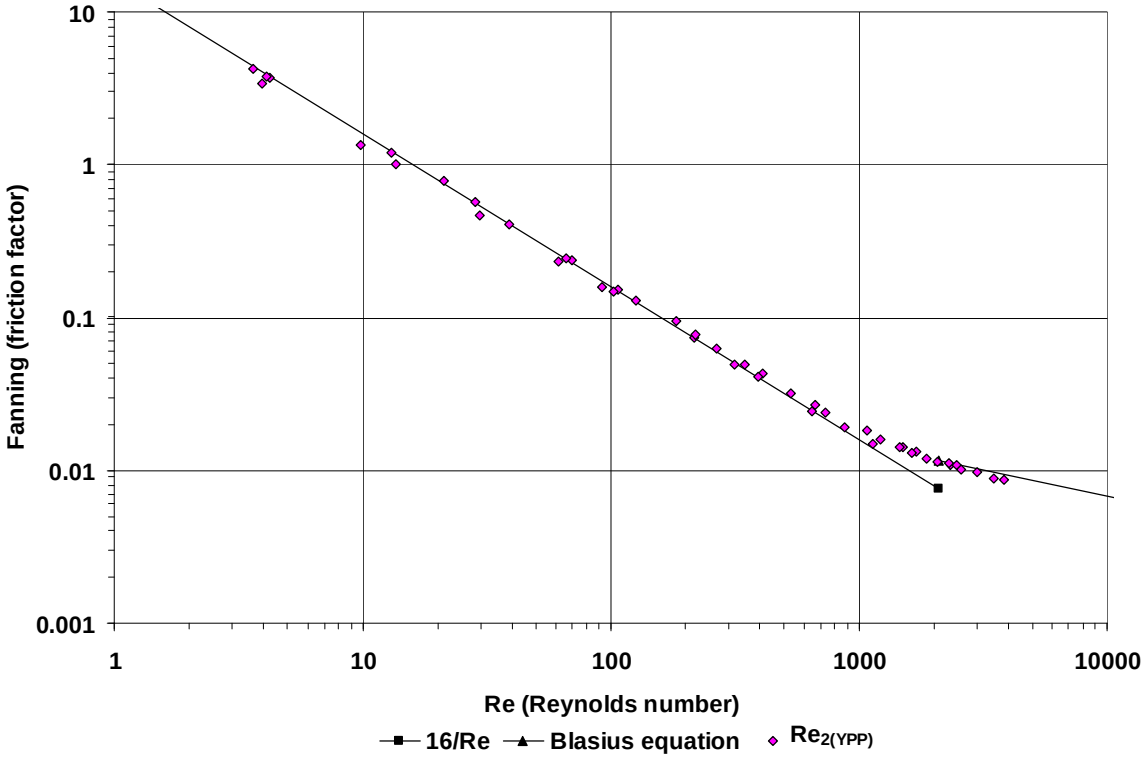

6% kaolin in 75 mm flume

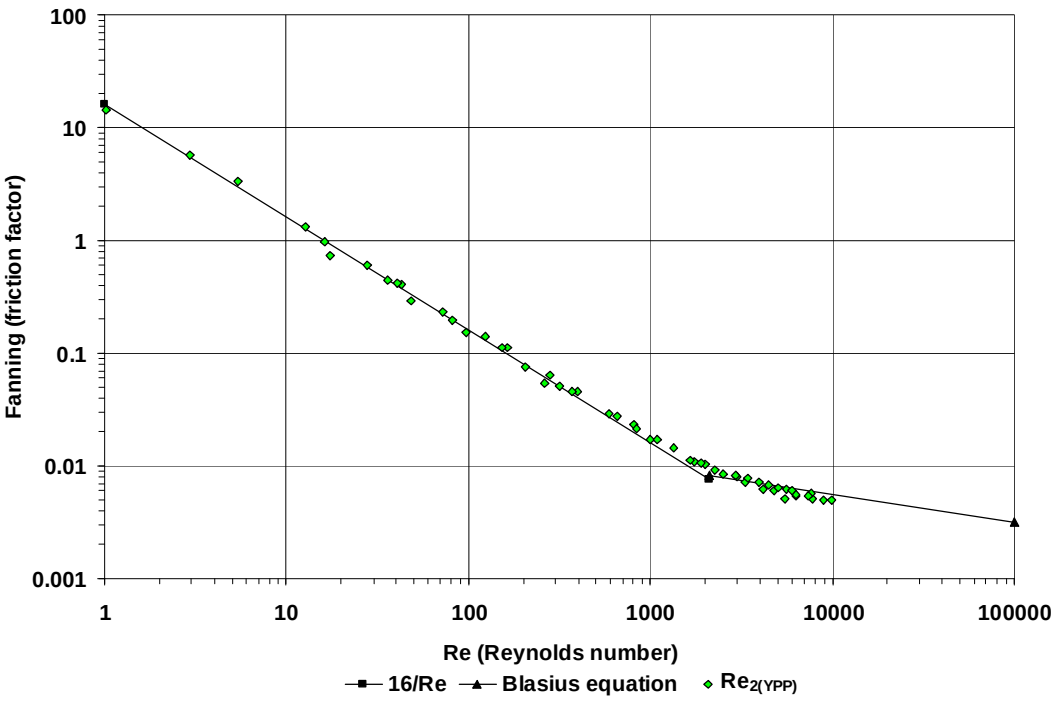

6% kaolin in 150 mm flume

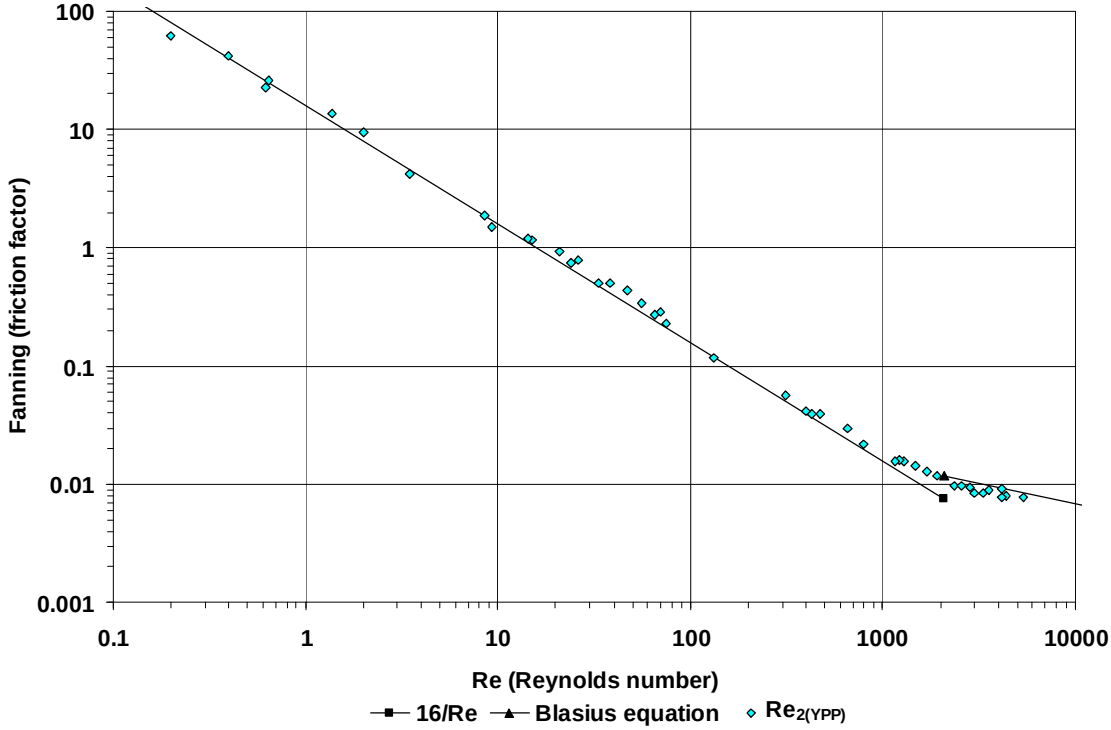

6% kaolin in 300 mm flume

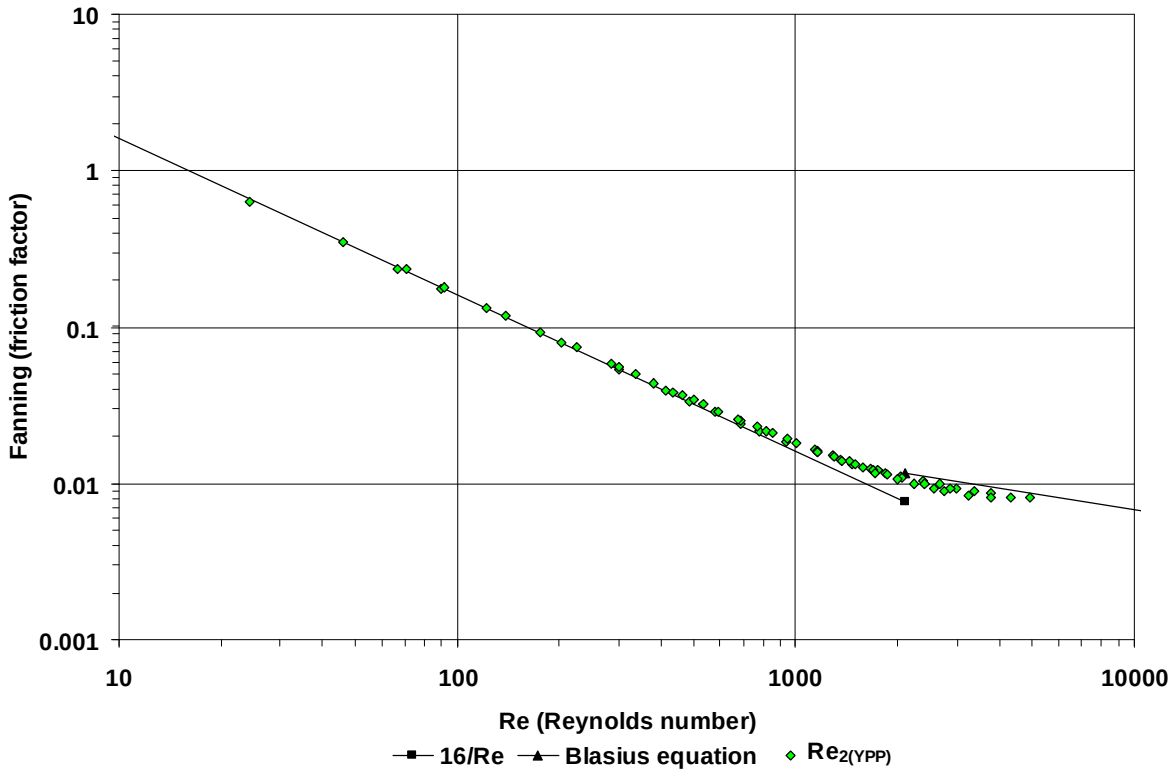

7.1% kaolin in 150 mm flume

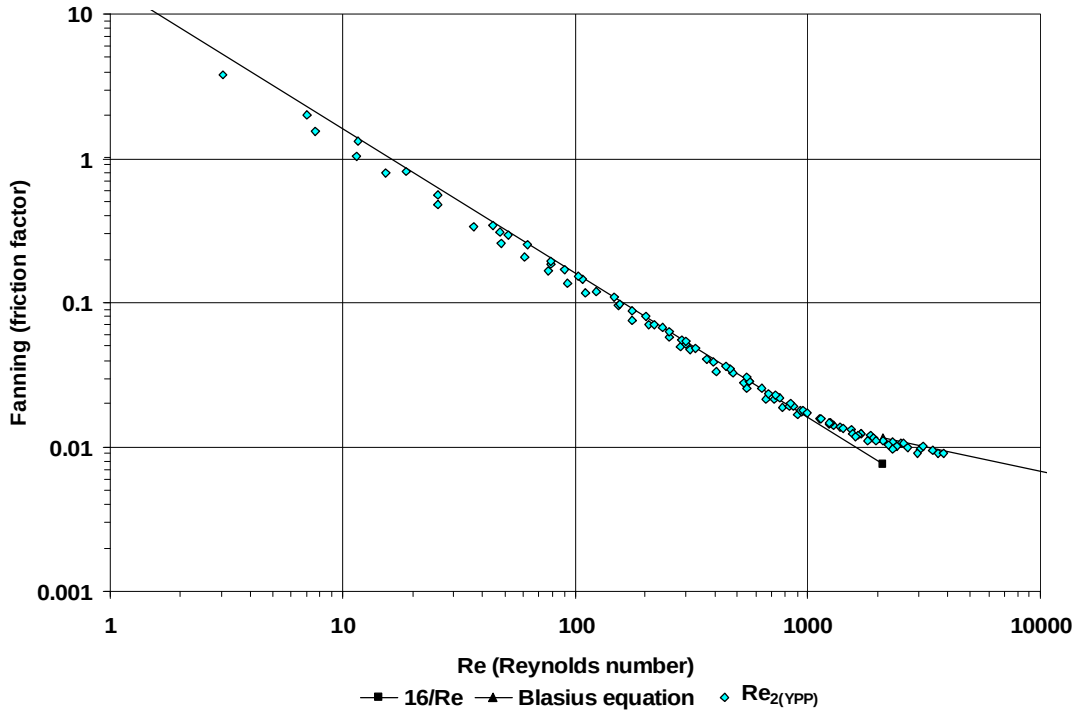

7.1% kaolin in 300 mm flume

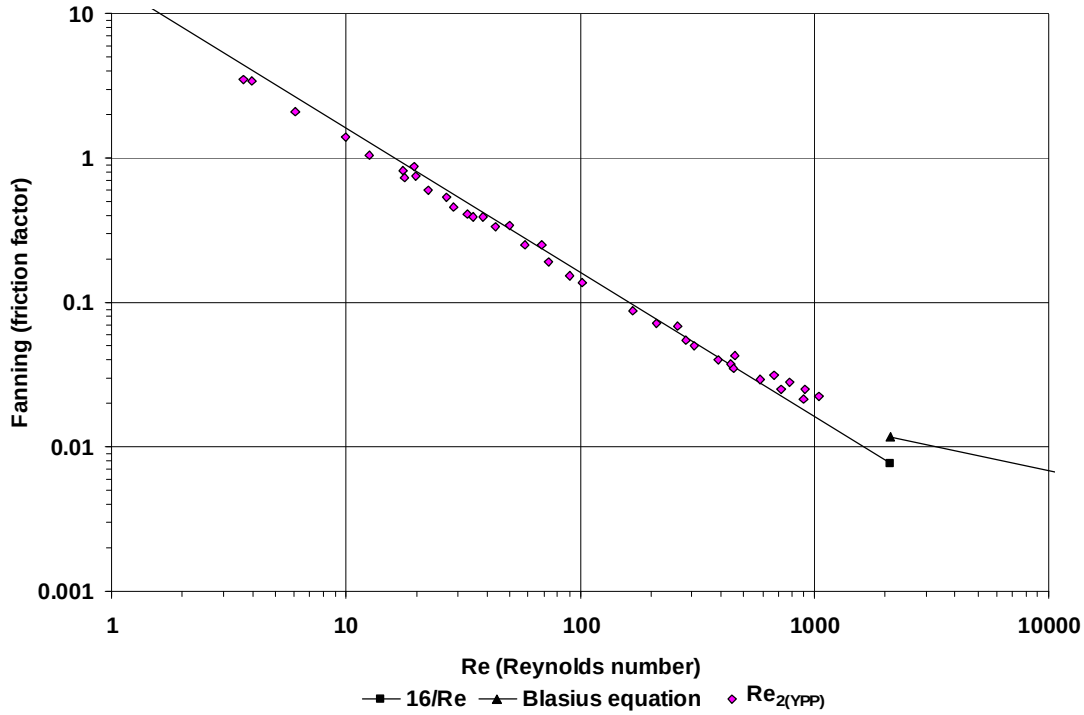

8% kaolin in 75 mm flume

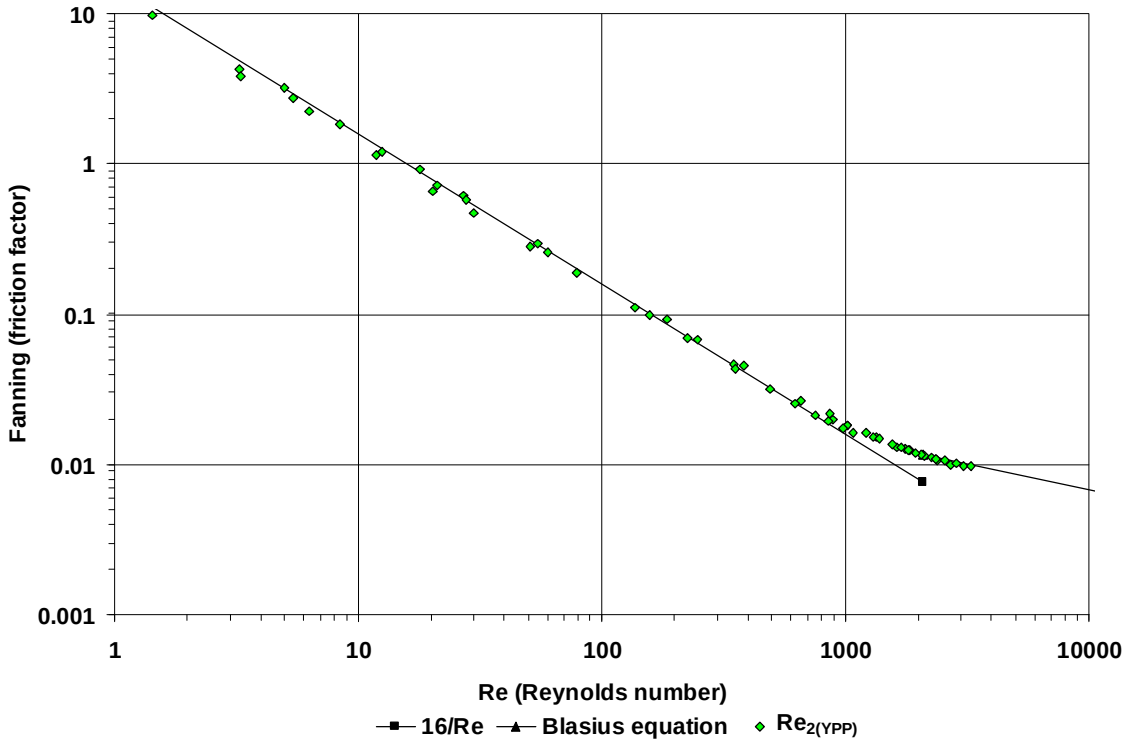

8% kaolin in 150 mm flume

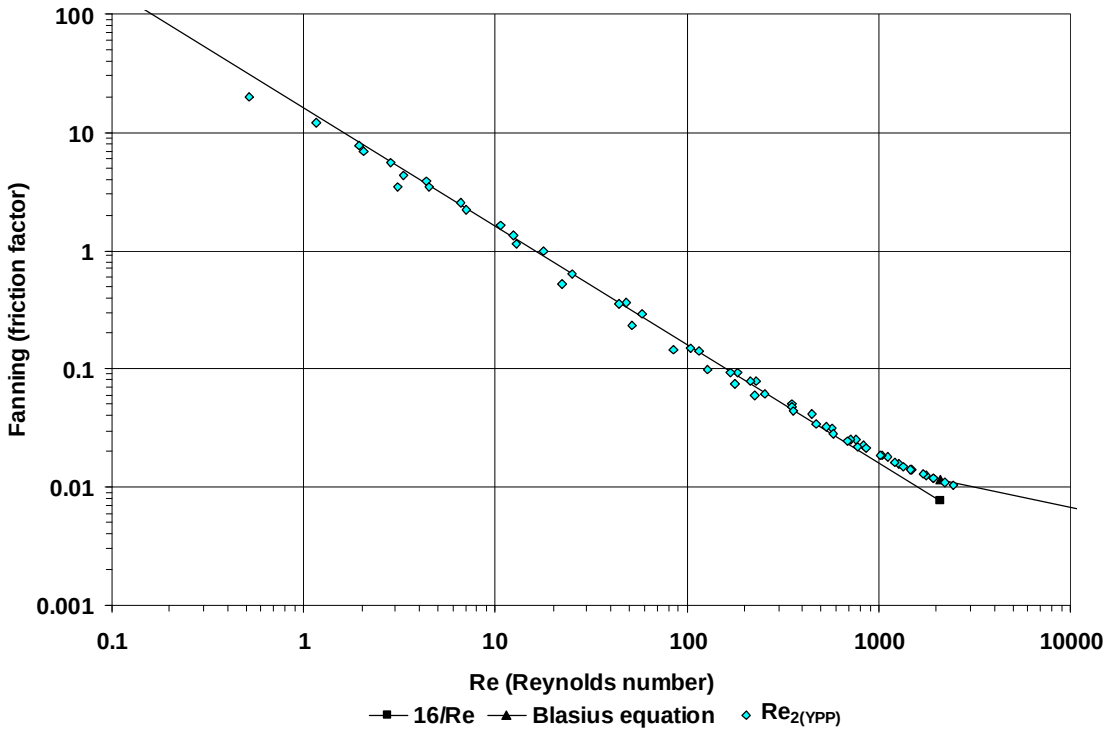

8% kaolin in 300 mm flume

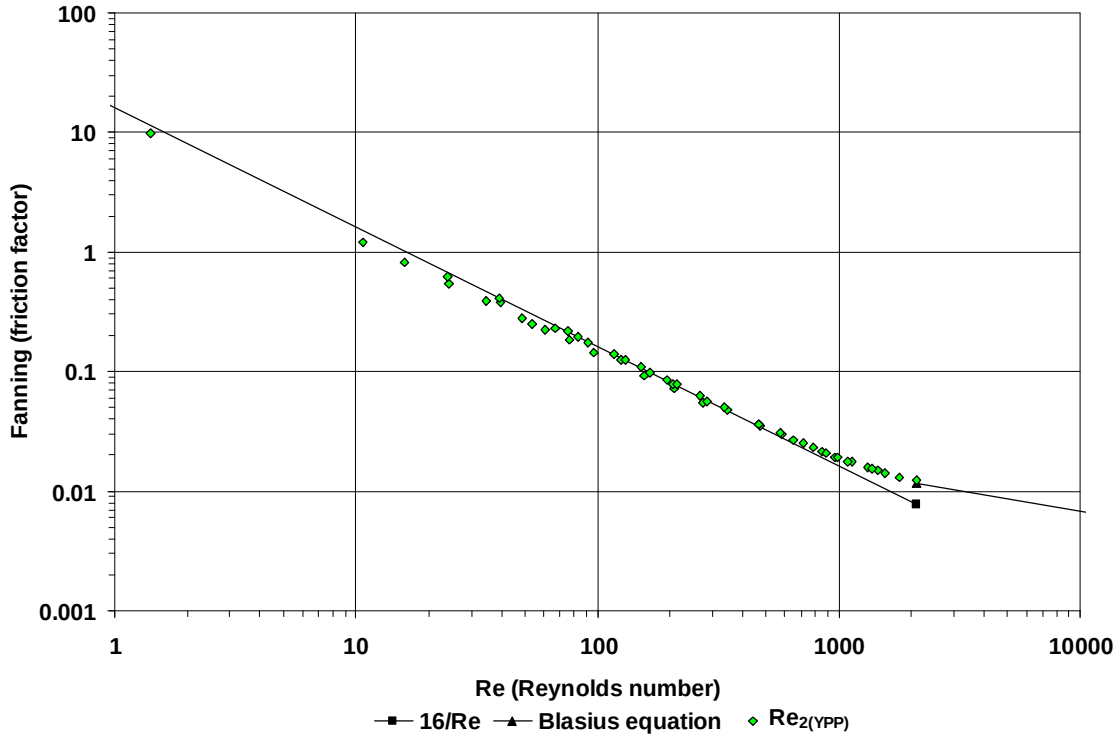

9% kaolin in 150 mm flume

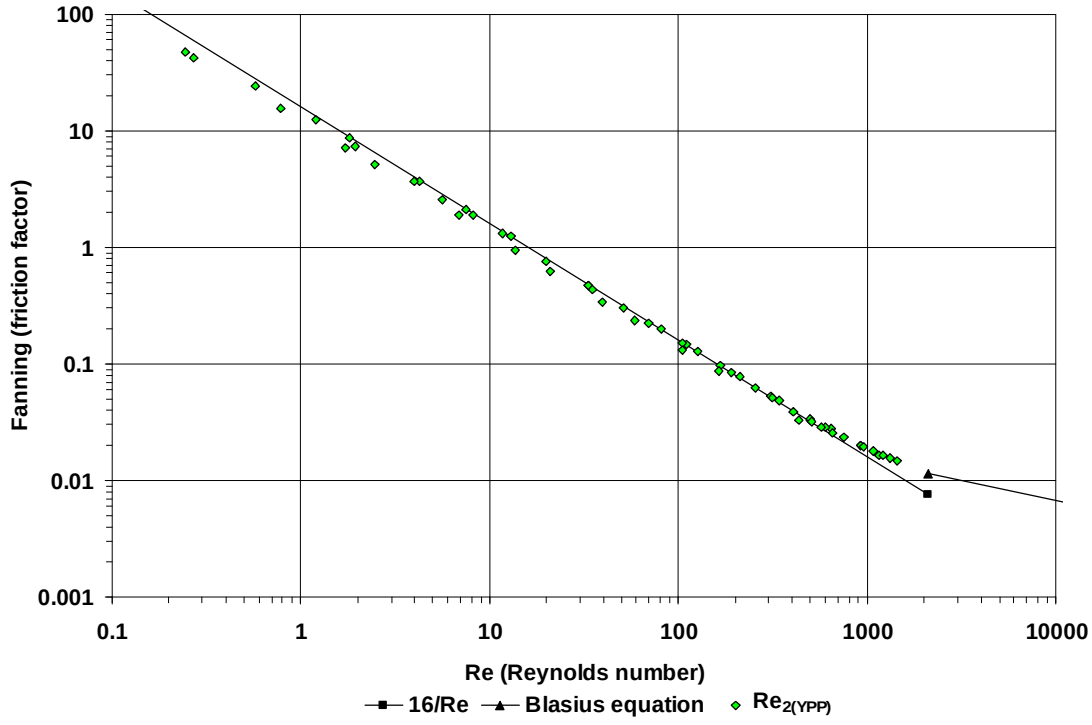

10% kaolin in 150 mm flume

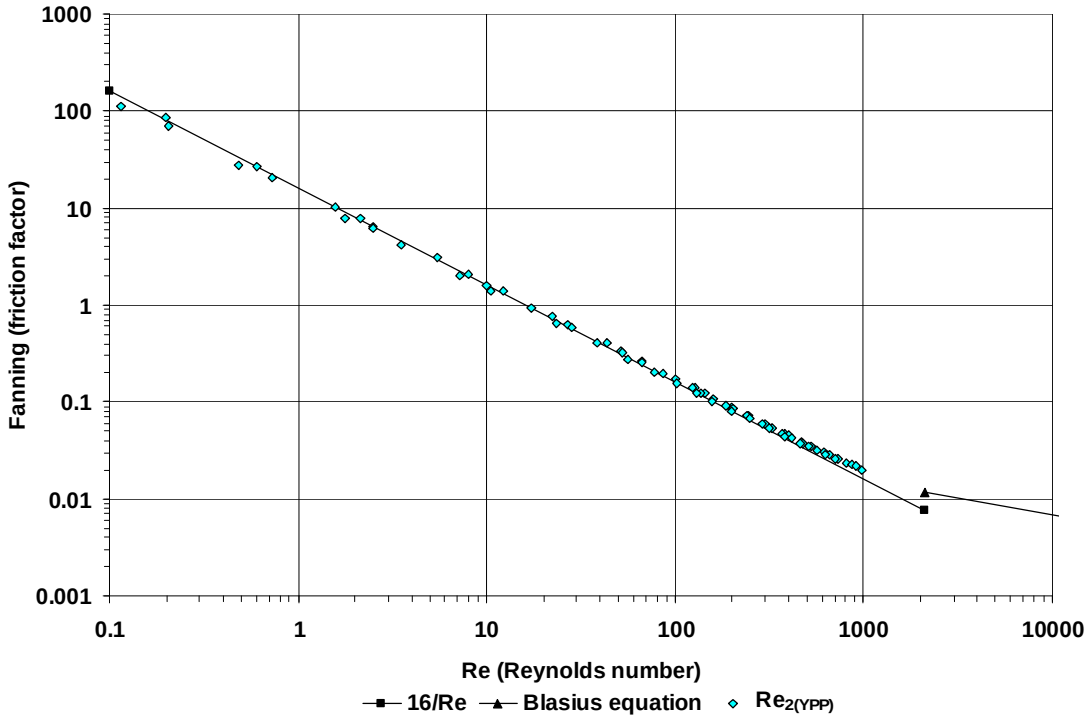

10% kaolin in 300 mm flume

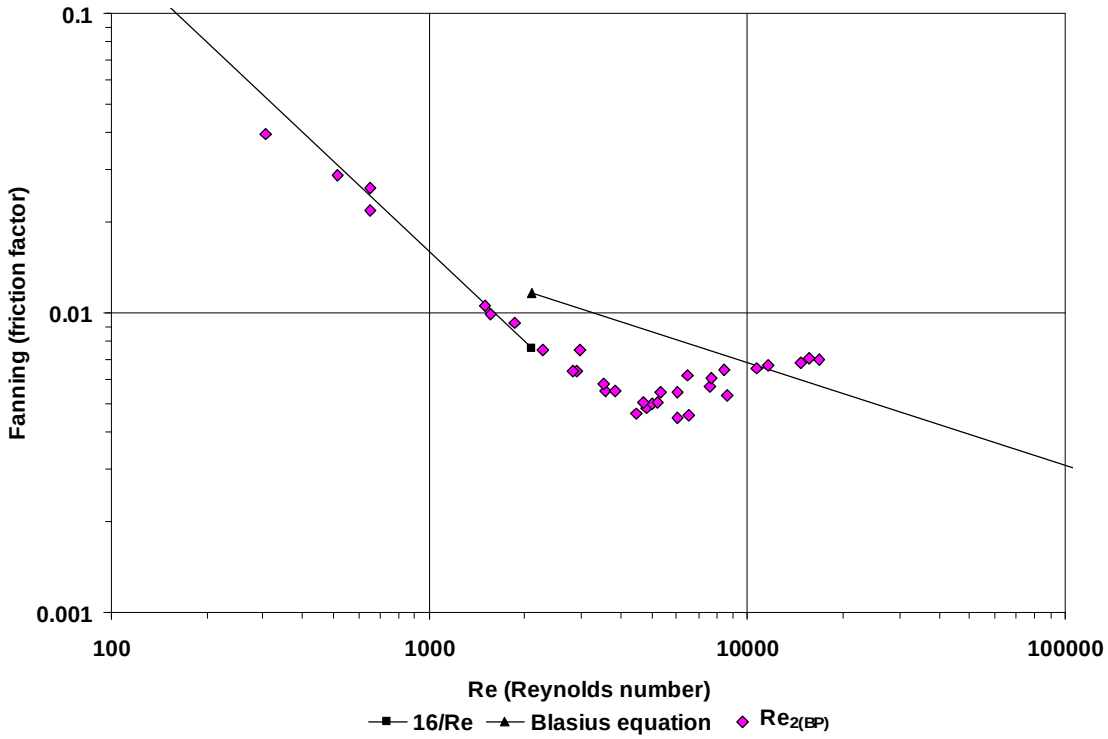

3% bentonite in 75 mm flume

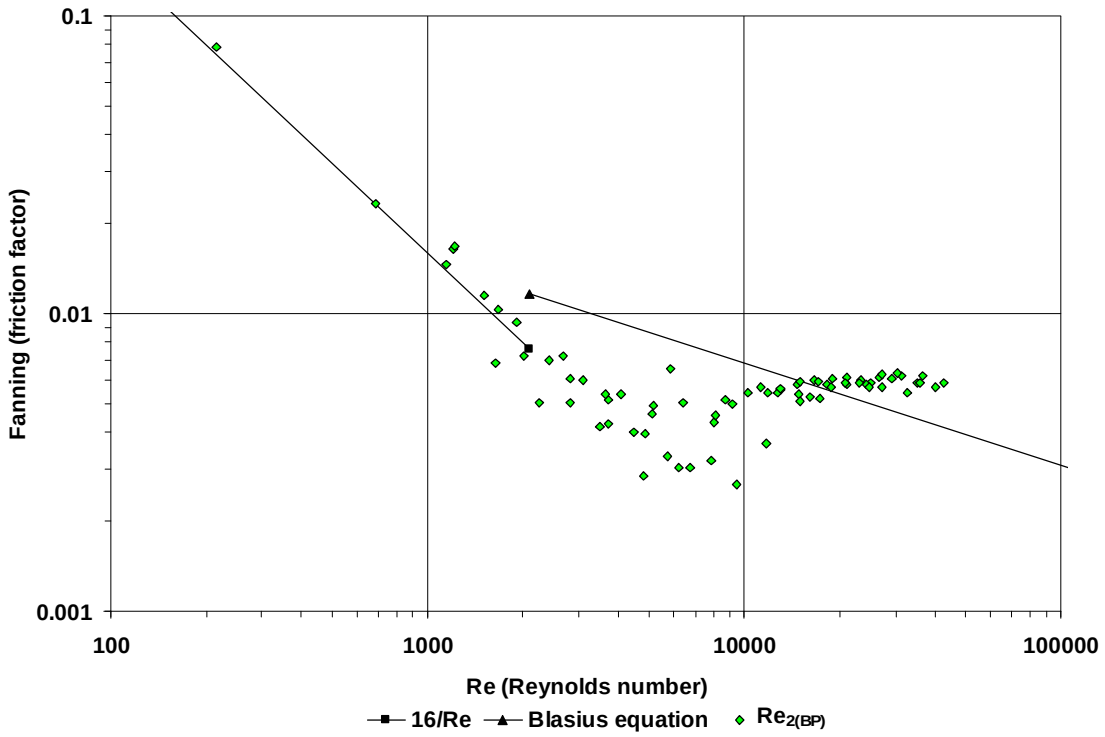

3% bentonite in 150 mm flume

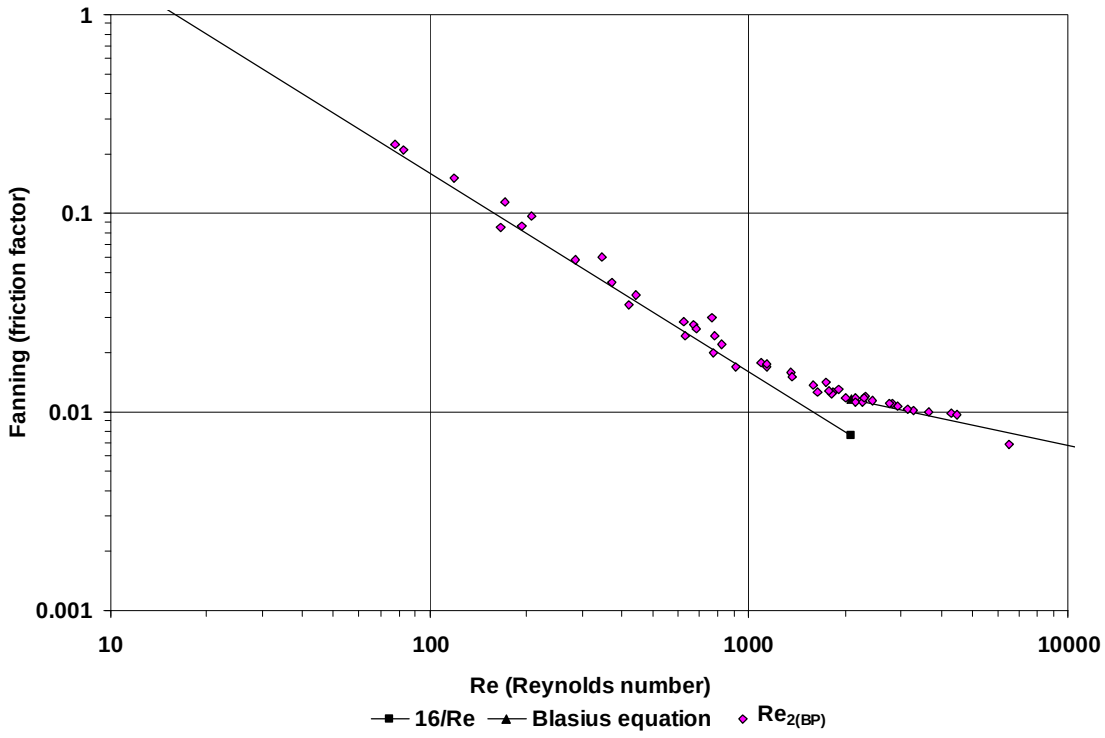

4.5% bentonite in 75 mm flume

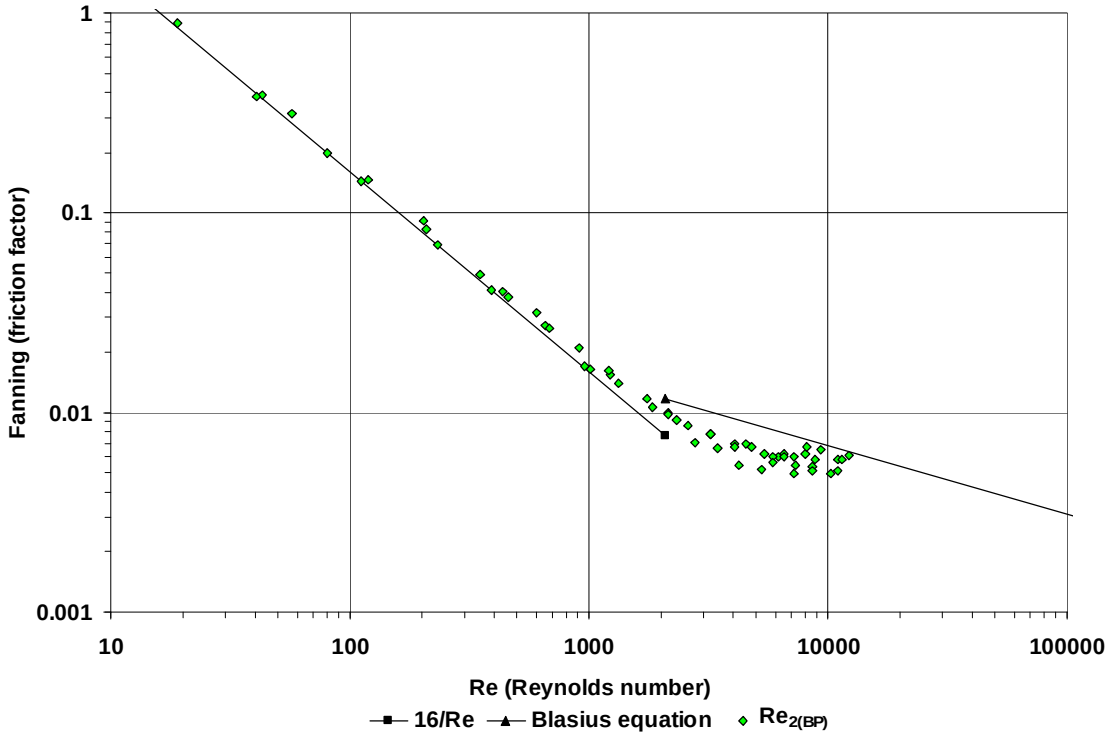

4.5% bentonite in 150 mm flume

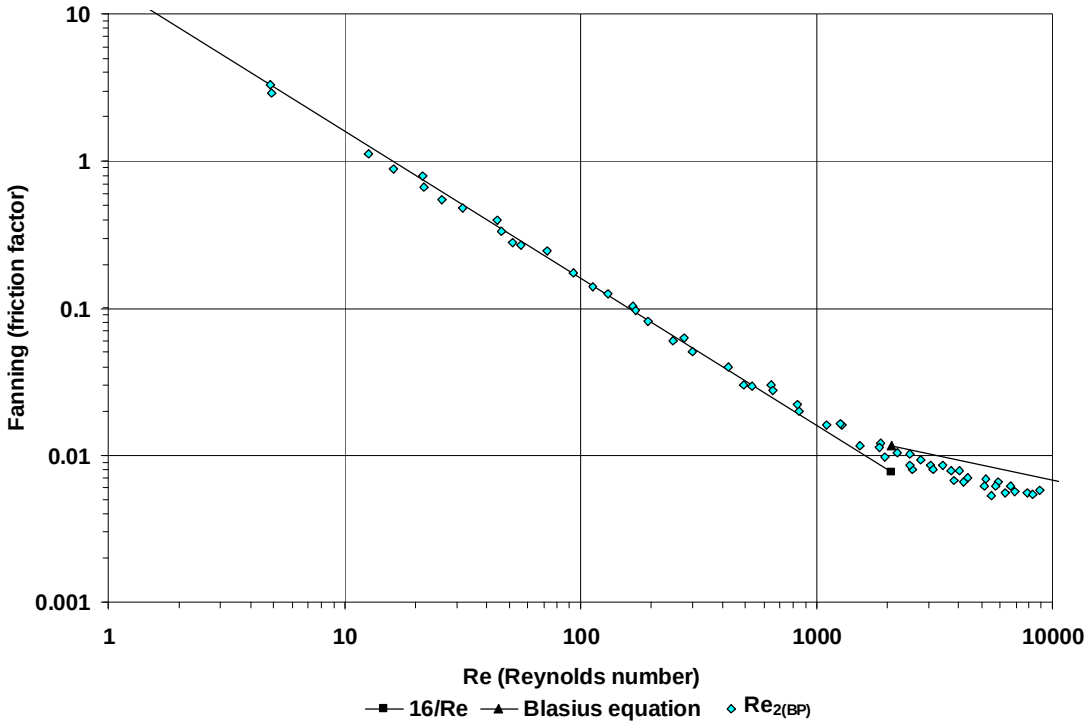

4.5% bentonite in 300 mm flume

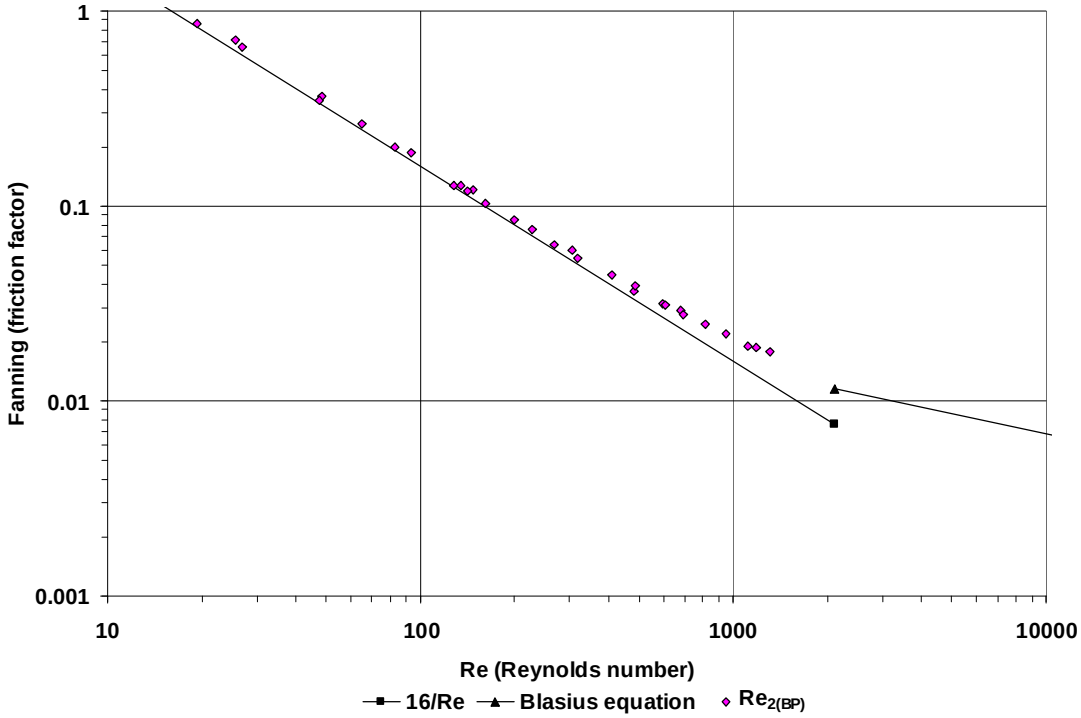

6% bentonite in 75 mm flume

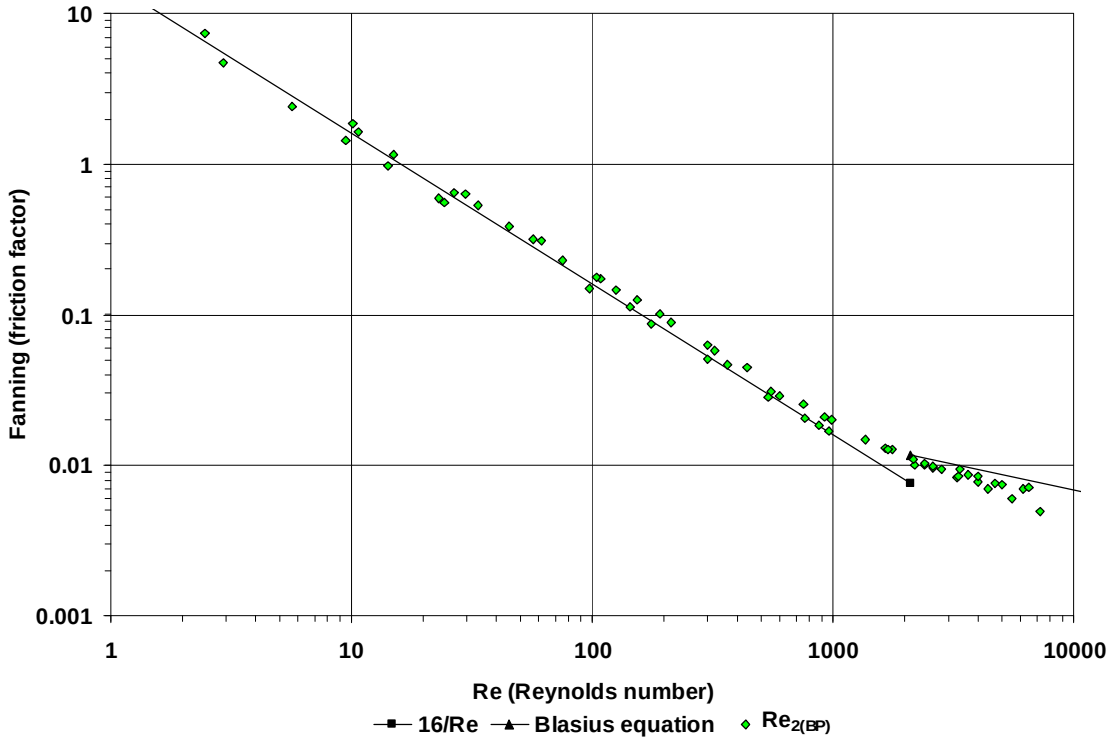

6% bentonite in 150 mm flume

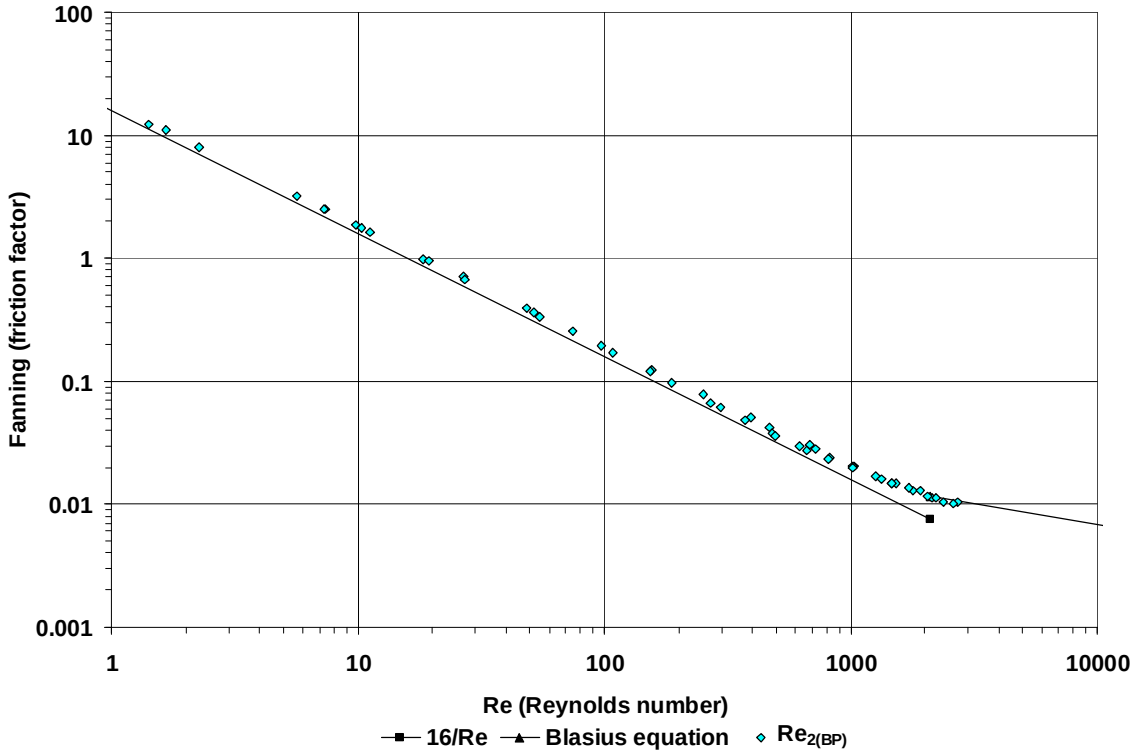

6% bentonite in 300 mm flume

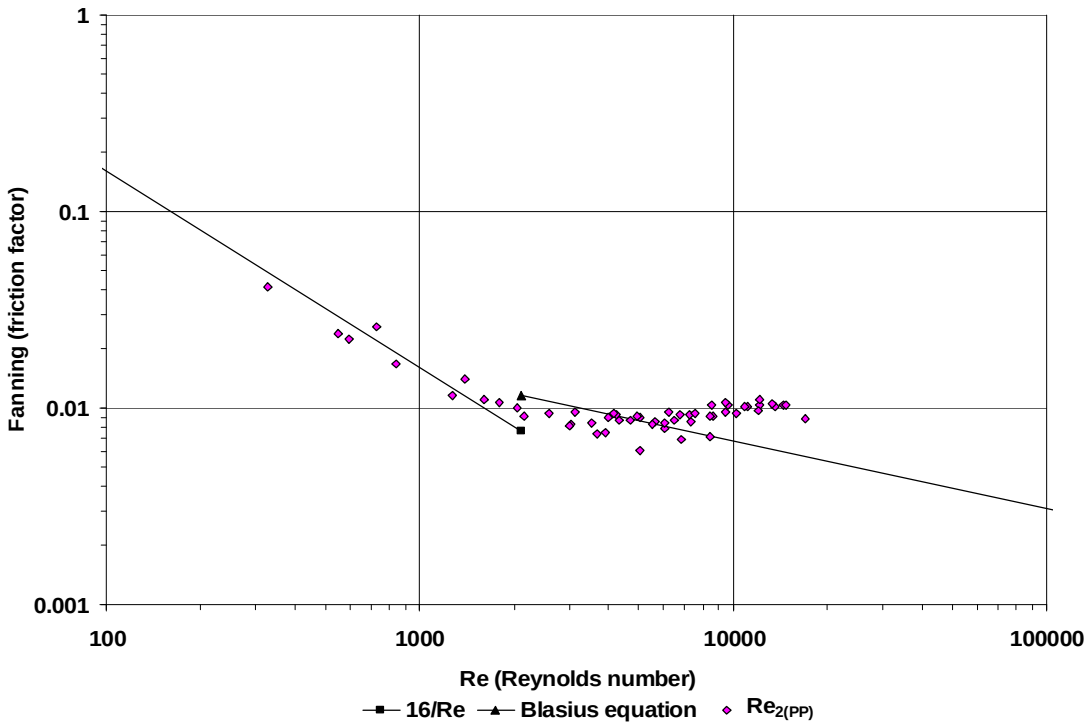

1% CMC in 75 mm flume

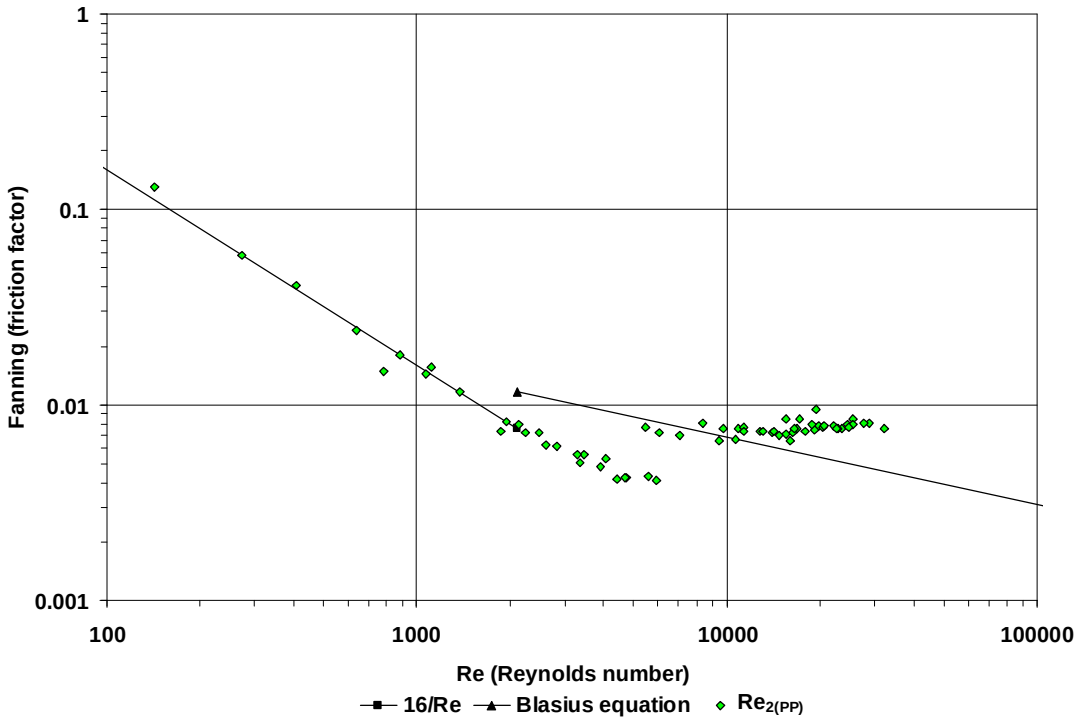

1% CMC in 150 mm flume

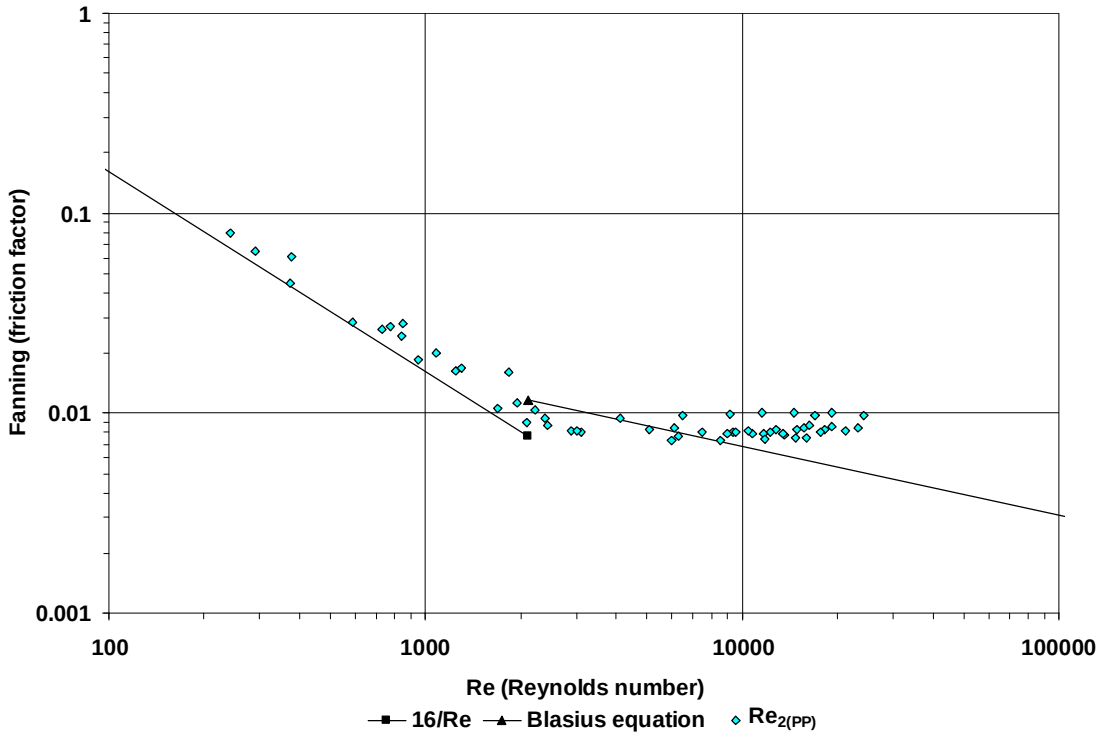

1% CMC in 300 mm flume

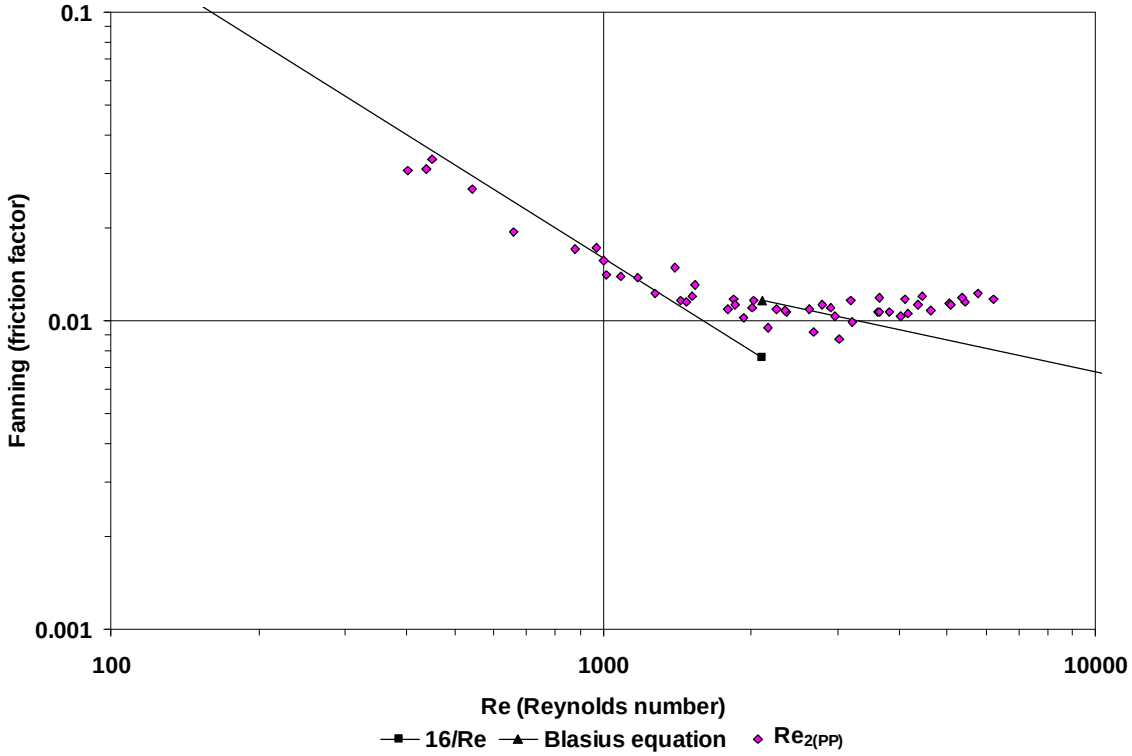

1.8% CMC in 75 mm flume

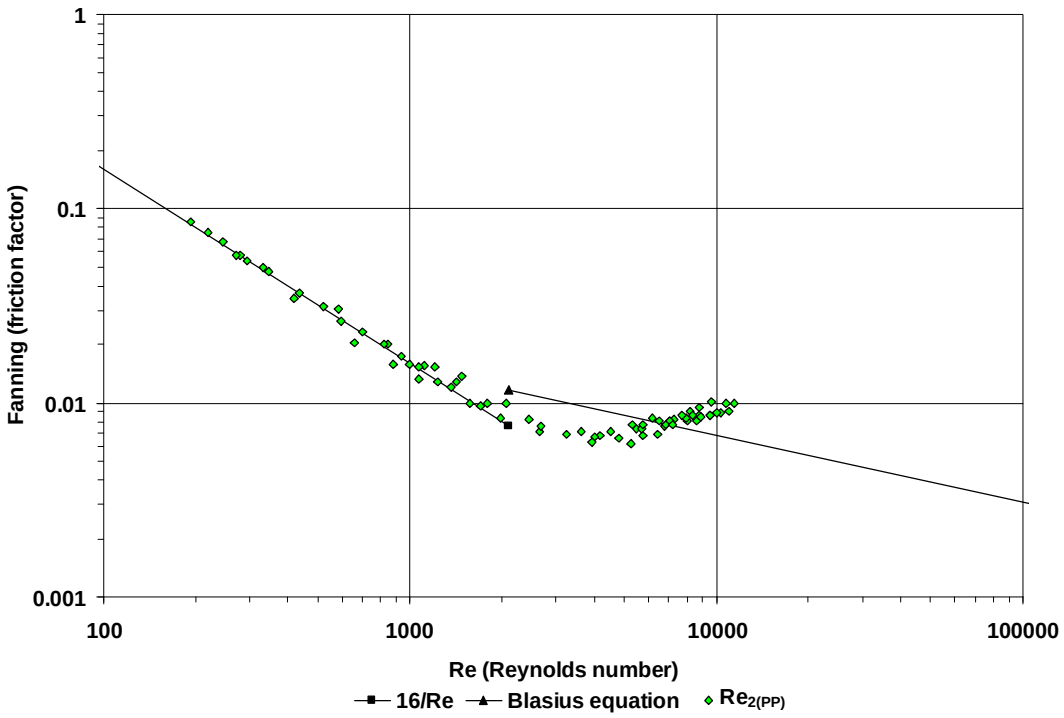

1.8% CMC in 150 mm flume

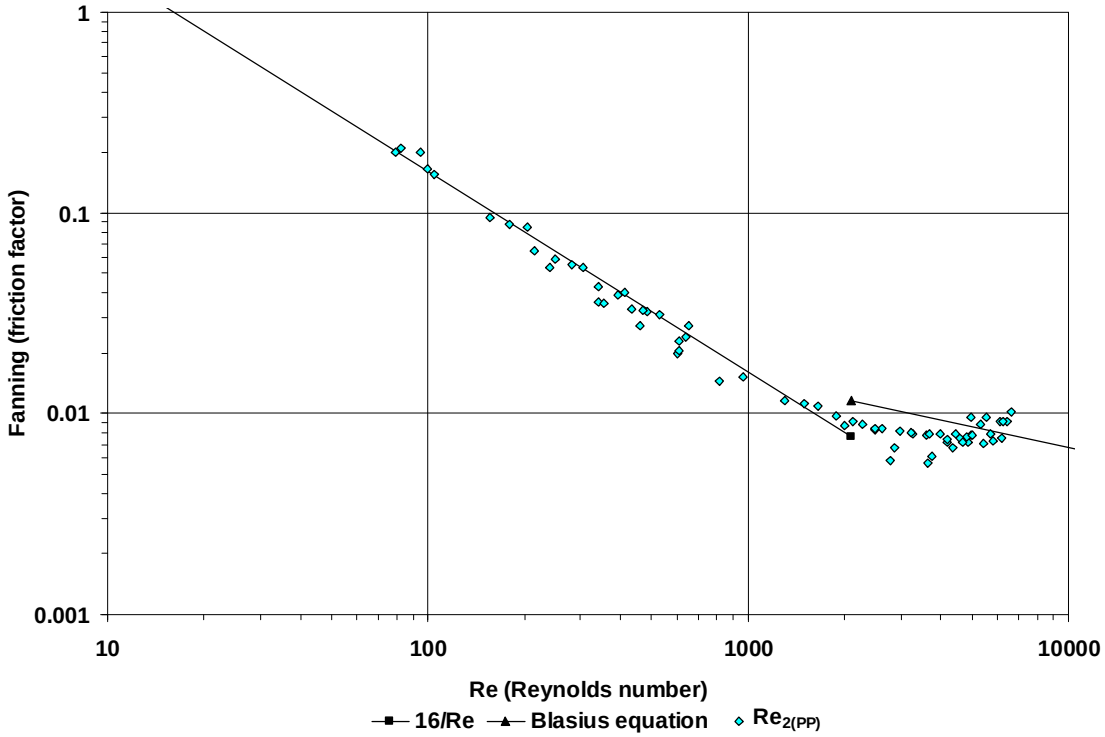

1.8% CMC in 300 mm flume

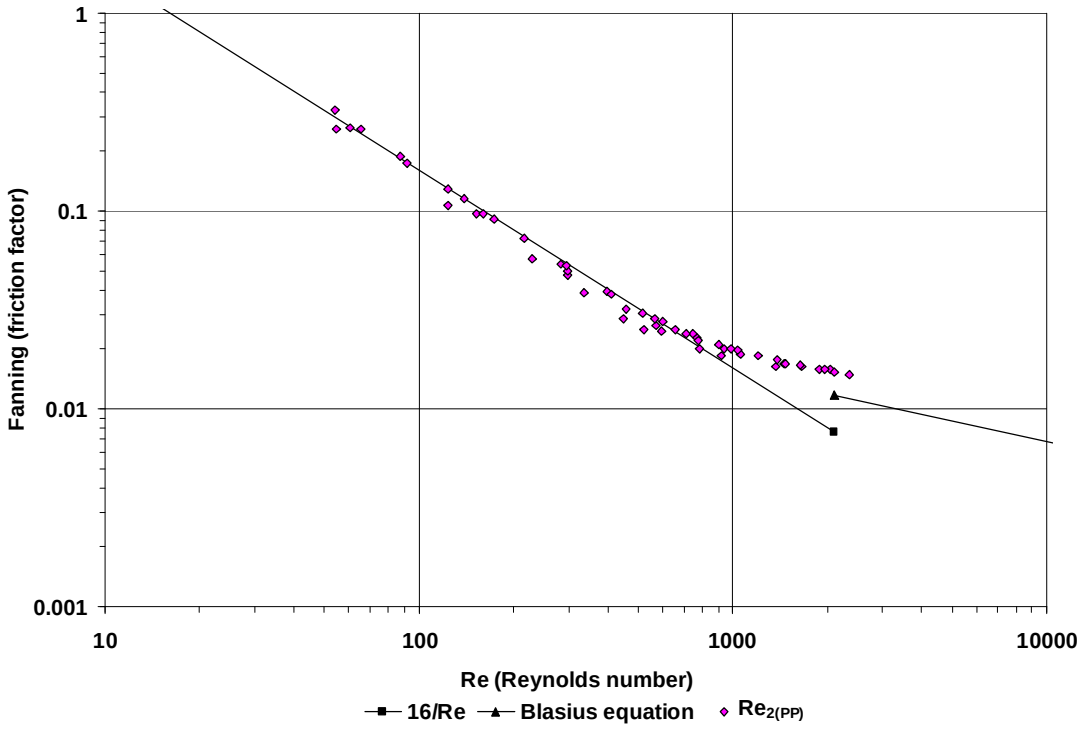

2.8% CMC in 75 mm flume

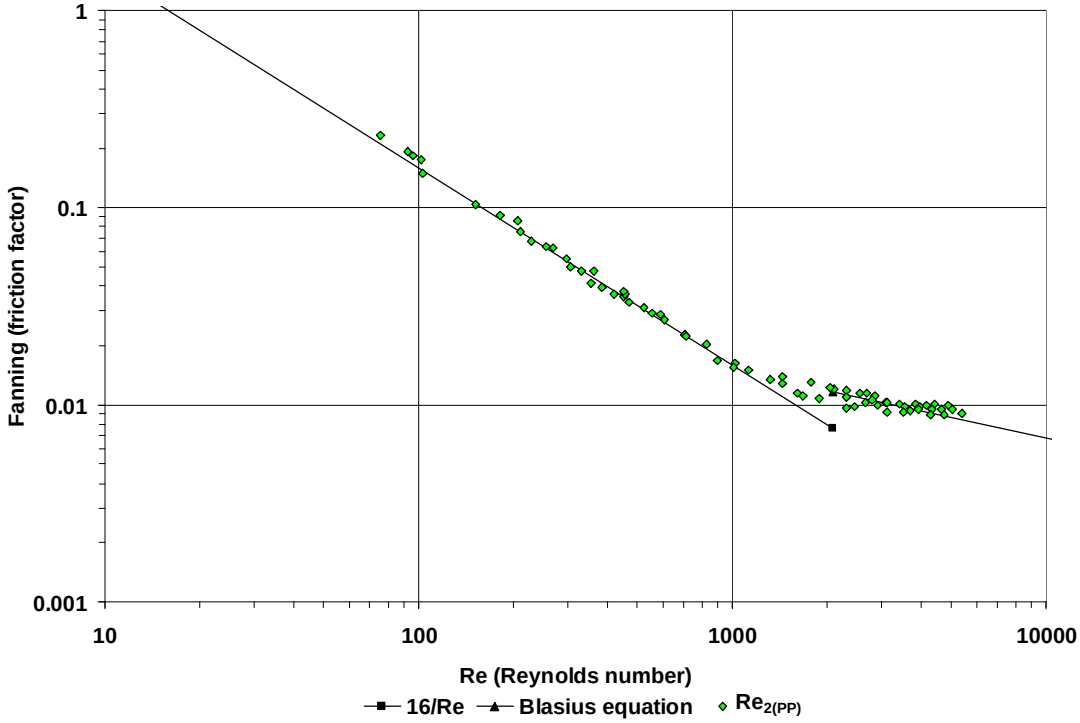

2.8% CMC in 150 mm flume

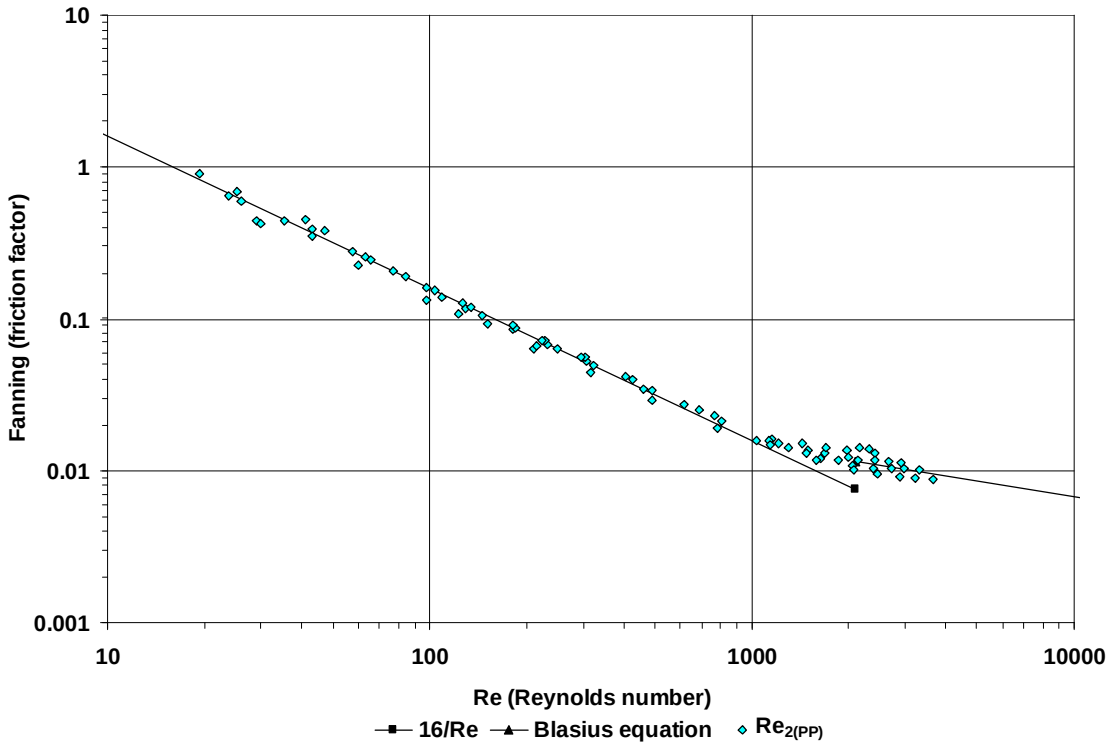

2.8% CMC in 300 mm flume

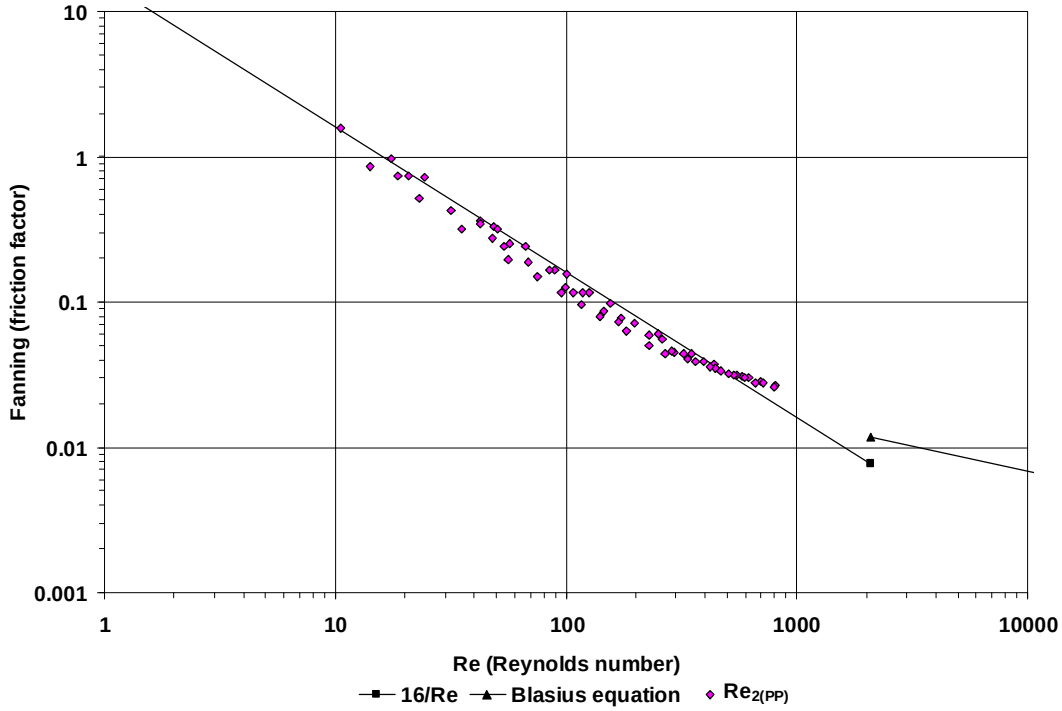

3.8% CMC in 75 mm flume

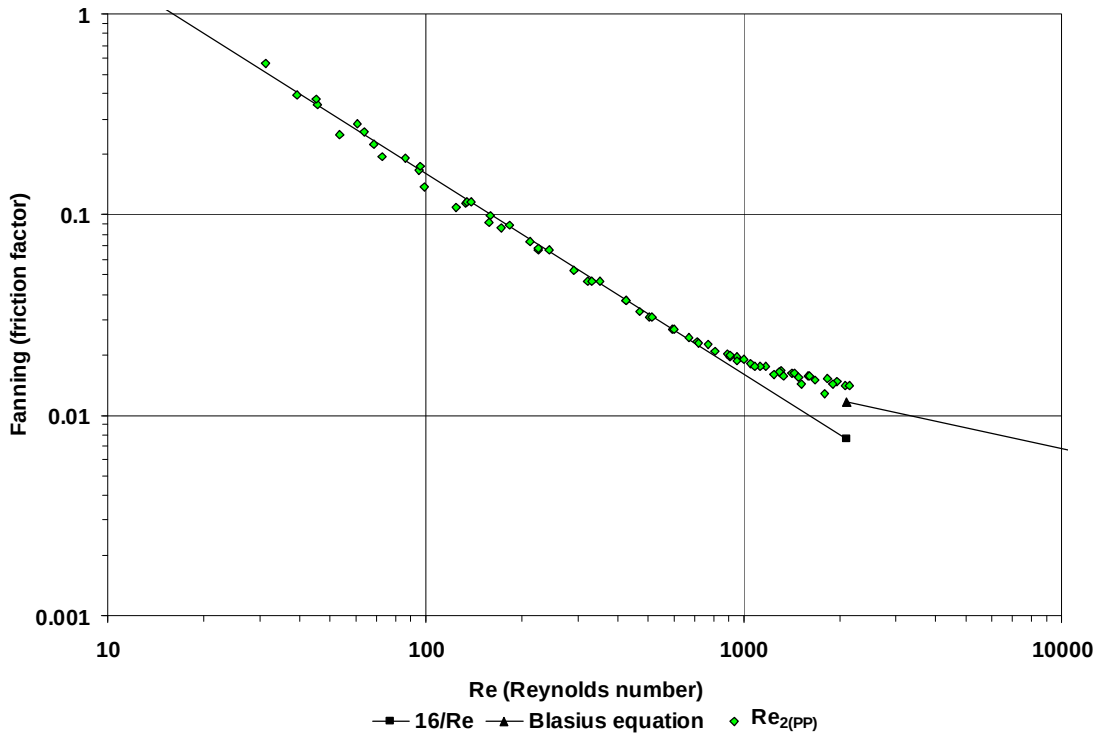

3.8% CMC in 150 mm flume

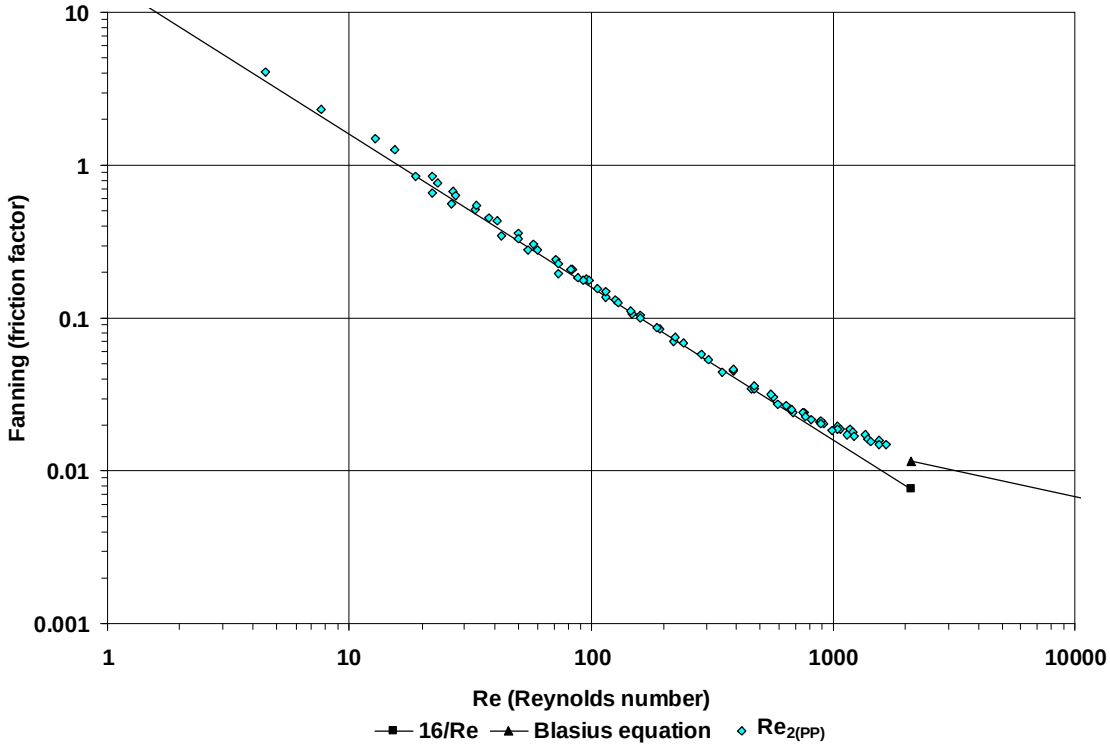

3.8% CMC in 300 mm flume

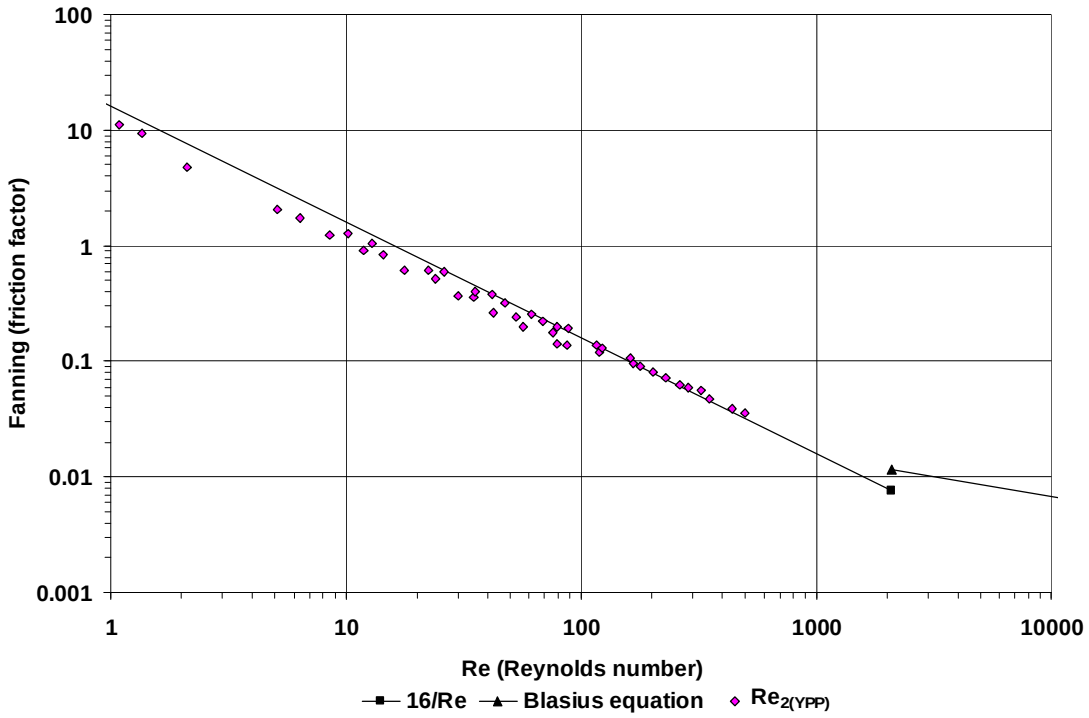

1% Carbopol in 75 mm flume

DRAWINGS OF THE FLUME AND PIPE VISCOMETER RIGS

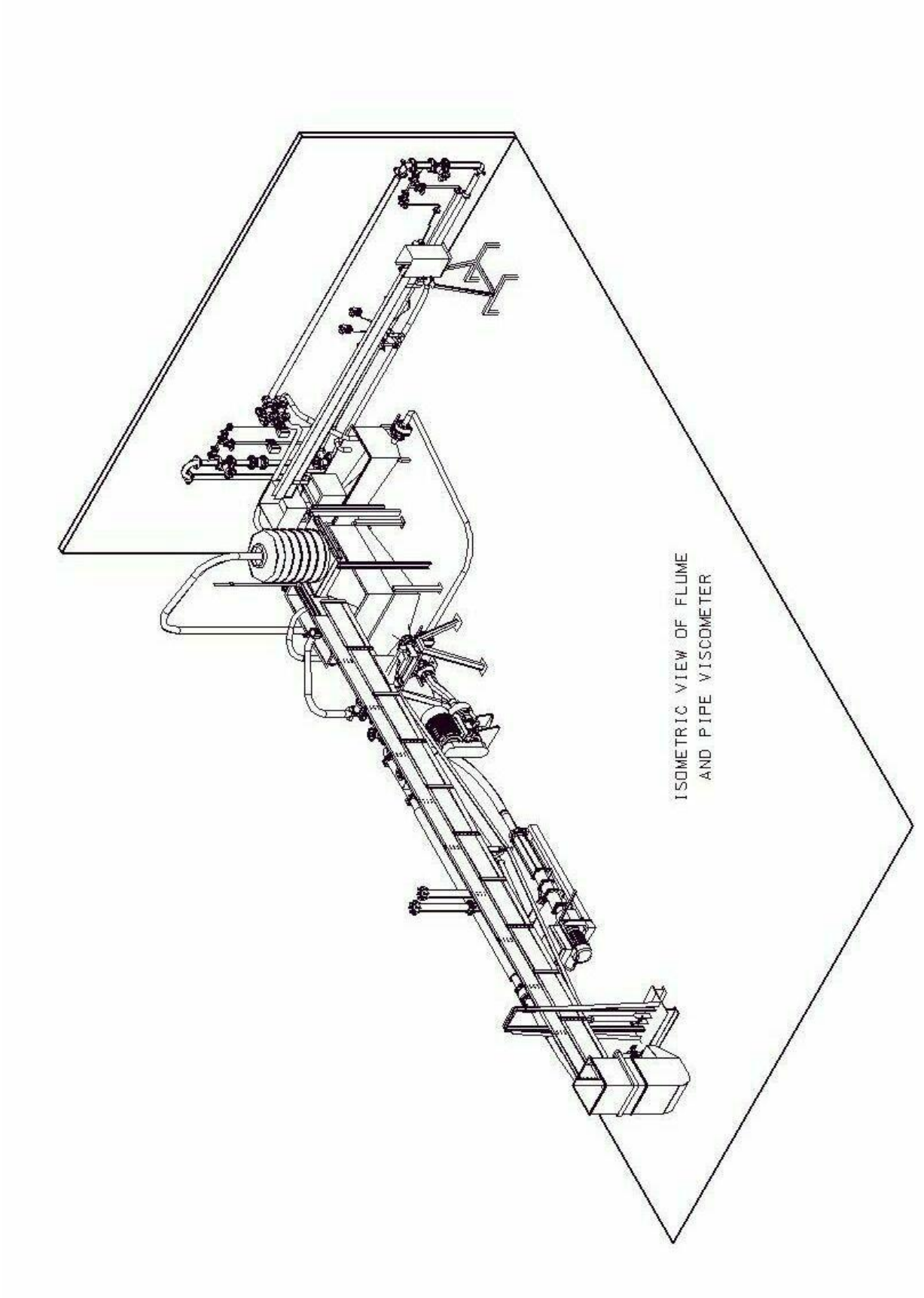

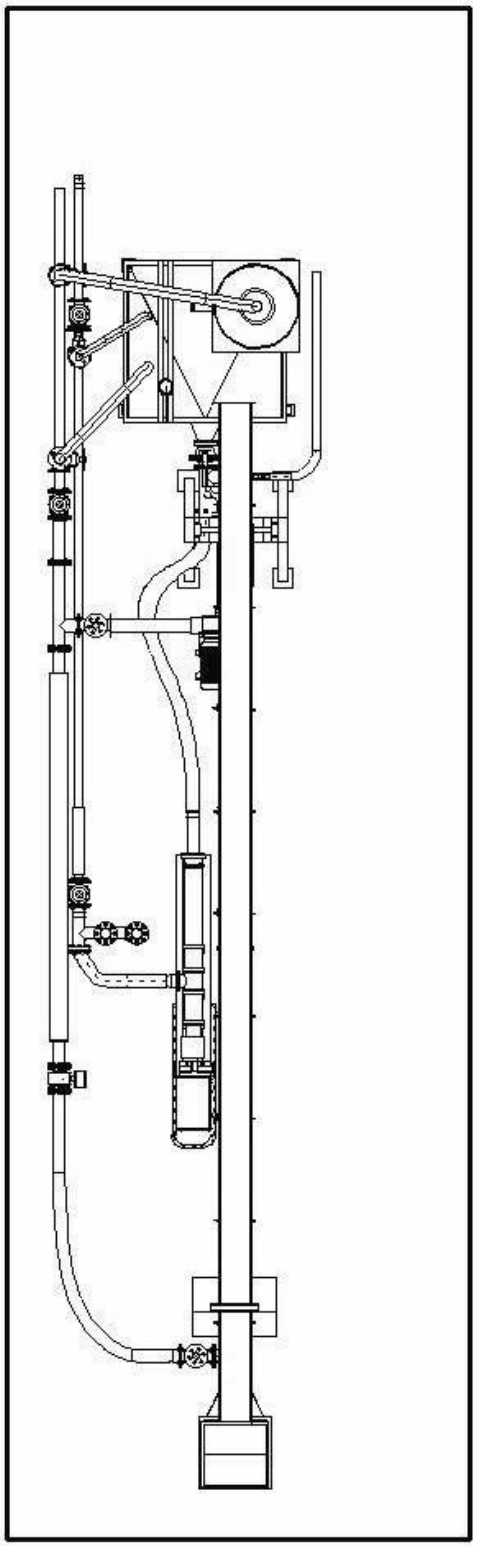

TOP VIEW
300mm FLUME

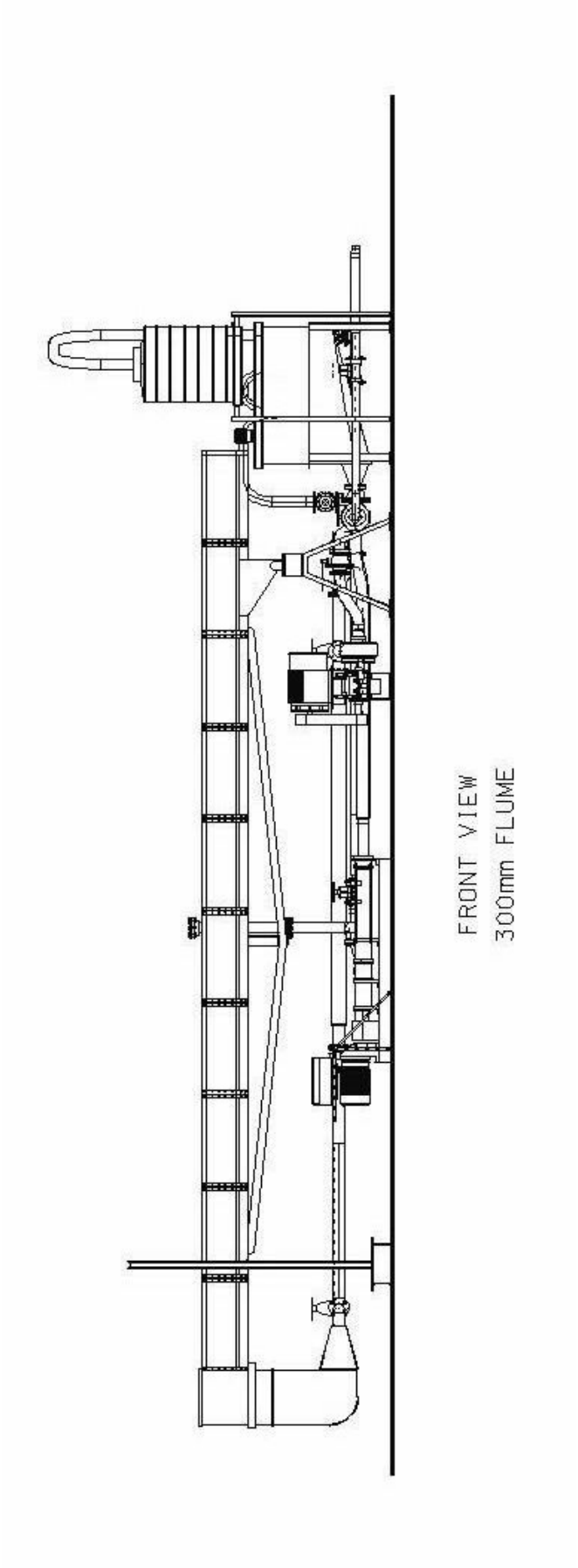
FRONT VIEW
300mm FLUME

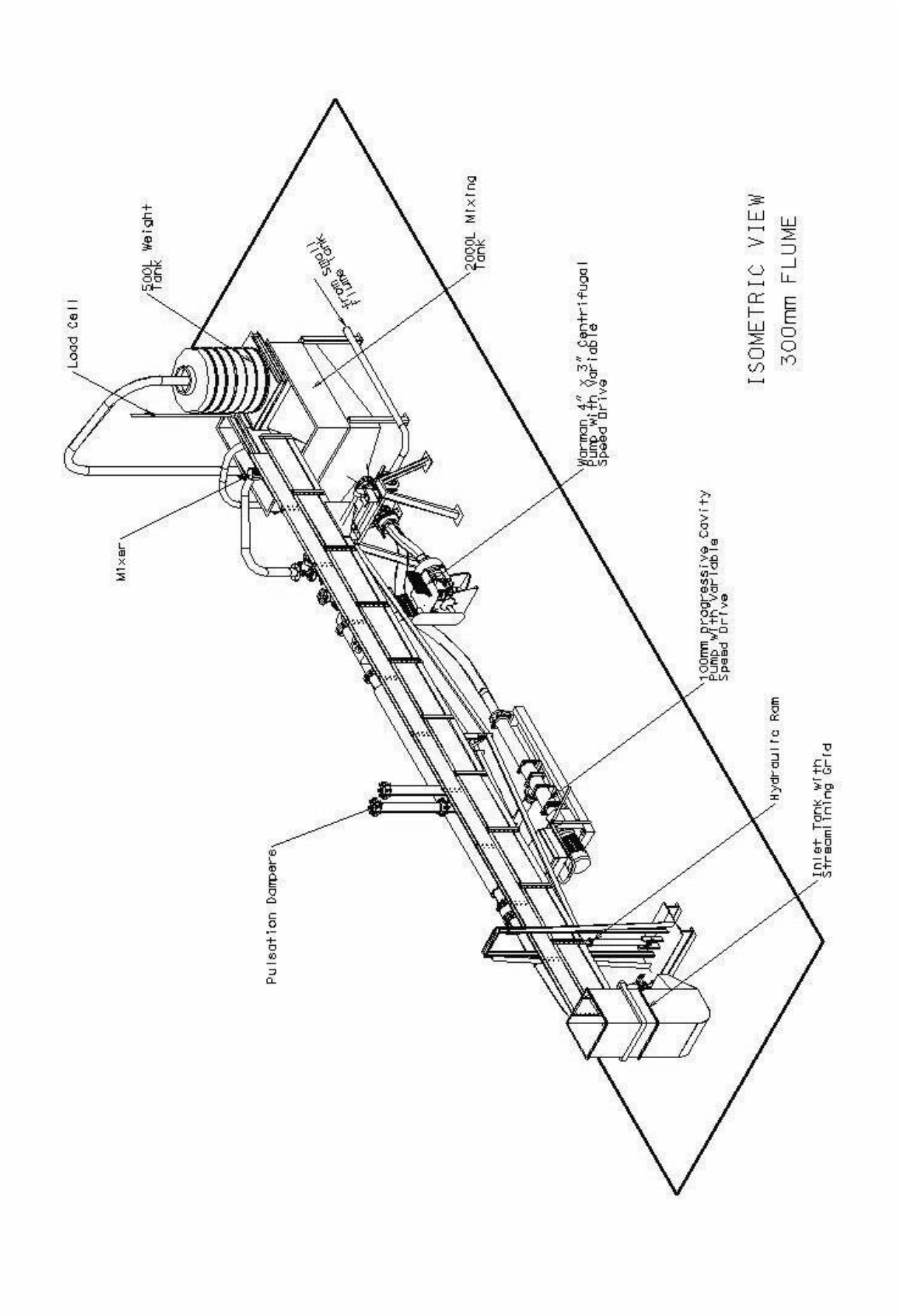
ISOMETRIC VIEW
300mm FLUME
Load Cell
500L Weight Tank
From Spoil Tank
2000L Mixing Tank
Warman 4" x 3" Centrifugal Pump with Variable Speed Drive
Mixer
100mm progressive Cavity Pump with Variable Speed Drive
Hydraulic Ram
Inlet Tank with Streamlining Grid
Pulsation Dampers

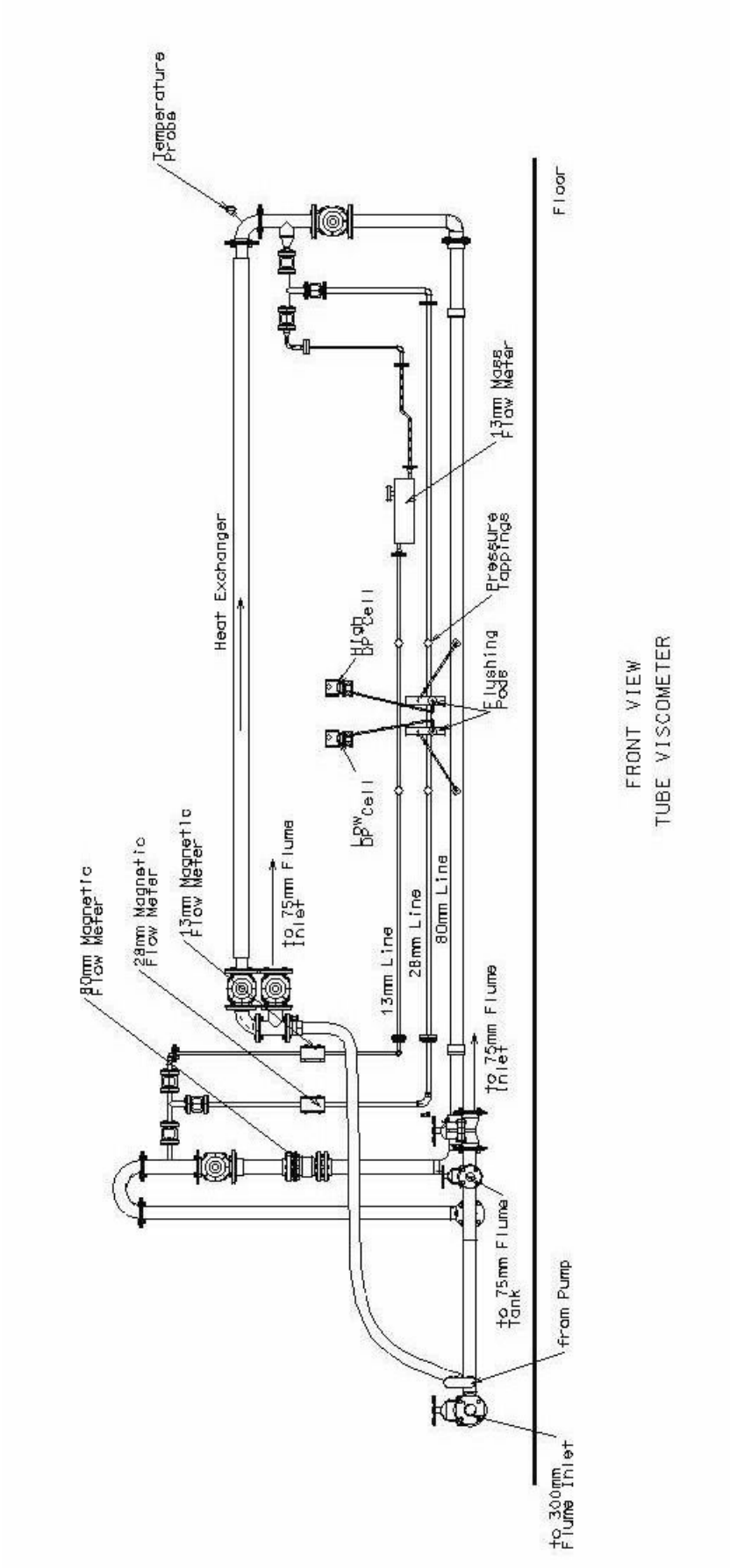
Temperature Probe
Floor
13mm Mass Flow Meter
Pressure Tappings
Heat Exchanger
High bP Cell
Flushing Ports
Low bP Cell
80mm Magnetic Flow Meter
28mm Magnetic Flow Meter
13mm Magnetic Flow Meter
to 75mm Fluma Inlet
13mm Line
28mm Line
80mm Line
to 75mm Fluma Inlet
to 75mm Fluma Tank
from Pump
to 300mm Fluma Inlet
FRONT VIEW
TUBE VISCOMETER

APPENDIX C

NEW DESIGN PROCEDURE FOR NON-NEWTONIAN SLURRIES IN RECTANGULAR OPEN CHANNELS

C.1 INTRODUCTION

In this appendix, the new design procedure for determining the flow depth and velocity of a rectangular flume transporting a non-Newtonian slurry is presented.

C.2 DETERMINATION OF SLURRY PROPERTIES

The following properties of the slurry need to be determined:

- The slurry relative density can be determined according to the procedure explained in Chapter 3.
- The rheological parameters $\tau_{y,}$ K and n need to be determined, preferably using a pipe viscometer. If that is not available, a rotary viscometer can be used. With the rheological parameters determined the apparent viscosity at shear rates 100 s^{-1} and 500 s^{-1} can be calculated.

C.3 INITIAL VALUES

Usually one needs to start with the volumetric throughput required or the slope or size limitation of the system.

The easiest is to set up a spreadsheet where one uses the optimisation function of the programme to speed up the process of recalculation.

The initial values to be selected are the slope of the flume and the width.

C.4 LAMINAR FLOW

The Reynolds number used is as follows:

$$Re_2 = \frac{8V^2\rho}{K\left(\frac{2V}{Rh}\right)^n + \tau_y}. \quad (C.1)$$

The fanning friction factor is as follows:

$$f = \frac{2\times g\times\left(\frac{B\times h}{2h+B}\right)\frac{1}{slope}}{V^2} \quad (C.2)$$

$$\text{or } V = \sqrt{\frac{2\times g\times\left(\frac{B\times h}{2h+B}\right)\frac{1}{slope}}{f}}. \quad (C.3)$$

In laminar flow: $f = 16/Re$. (C.4)

The process is as follows:

- Choose a Reynolds number.
- Calculate f (equation C.4).
- Value for the flow depth (h) is guessed.
- Calculate the velocity V (equation C.3).
- From that Re_2 can be calculated (equation C.1). This will differ from the chosen Reynolds number.
- Optimise the flow depth h until the two Reynolds numbers are the same.
- From this depth and velocity and the flow rate can easily be calculated.
- This process can easily be repeated for a range of Reynolds numbers.
- Determine the onset of transition as set out in Section C.5.

If the transition Reynolds number is known, lower Reynolds numbers can be now selected until required velocity flow rates or depths are obtained.

C.5 ONSET OF TRANSITION

To determine where the onset of transition occurs and the relationship of f = 16/Re stops, the following relationship needs to be determined:

$$Re_c = \frac{200}{\left(\mu_{app(100/s)}\right)^{0.21}} Fr + \frac{71}{\left(\mu_{app(100/s)}\right)^{0.75}} \quad (C.5)$$

where the Froude number is:

$$Fr = \frac{V}{\sqrt{gh}}. \quad (C.6)$$

To determine the Reynolds number at transition repeat the process above in C.4 and:

- Calculate the Froude number (equation C.6).
- Calculate the Re transition (equation C.5).
- Optimise the height h until Re_2 selected is the same as Re_c.

C.6 TURBULENT FLOW

The turbulent flow region must first be established before the onset of 'full turbulence' can be established

The velocity formula for turbulent flow is:

$$V = Re_* \left(2{,}5 \ln \frac{2R_h}{K} - 76{,}86\mu_{app\,500} - 9{,}45 \right) \quad (C.7)$$

$$\text{with } Re_* = \sqrt{gh \sin\alpha} \quad (C.8)$$

$$\text{and } R_h = \frac{2(Bh)}{B + 2h}. \quad (C.9)$$

The Reynolds number is the same as in laminar flow equation (C.1).

The fanning friction factor is as follows:

$$f_{turb} = 0.66 \left(\frac{2gh \sin\alpha}{V^2} \right) \quad (C.10)$$

The procedure is as follows:

- Select a depth a bit deeper than the depth obtained at the onset of transition.
- Calculate the hydraulic radius. Equation (C.9).
- Calculate the velocity. Equation (C.7).
- From this velocity, the Reynolds number, equation (C.1) and the friction factor, equation (C.10), can be determined.

Additional depths can be selected and the procedure can be repeated.

C.7 ONSET OF TURBULENCE

Before the final step in section C.6 can be performed, one needs to establish the start of 'full turbulence'.

The Reynolds number is as follows:

$$\mathrm{Re}_{c(turb)} = \frac{105}{\left(\mu_{app(500/s)}\right)^{0.52}}\mathrm{Fr} + \frac{108}{\left(\mu_{app(500/s)}\right)^{0.65}}. \qquad \text{(C.11)}$$

To determine the onset of 'full turbulence' the procedure is as follows:

- Complete all the steps in section C.6.
- Calculate the Froude number, Equation (C.6).
- Calculate the critical turbulent Reynolds number, Equation (C.11)
- The depth selected must yield the same Reynolds number by using Equation (C.11) and the Reynolds Re_2 number calculated in section C.6.

Now one can go back to the turbulent zone and continue selecting deeper h-values to obtain higher Reynolds numbers.

C.8 TRANSITION ZONE

The transition zone is not fixed and will vary with each variation of any of the parameters that can vary.

The way to establish the relationship is to obtain the Reynolds numbers and the friction factors at onset of transition as well as the onset of full turbulence. Then one can put a power law equation through the two points. The relationship will then be simple and similar to that in laminar flow.

C.9 NUMERICAL EXAMPLE

The following example will illustrate the procedure described in the previous sections.

The material is a 6% kaolin slurry and the flume size is 150 mm wide with a slope of 3 degrees.

The material properties are as follows:

K=		0.148466
n=		0.5171
t_y =		6.84
Density		1099
μ_{app}	100 1/s	0.084463
μ_{app}	500 1/s	0.021064
Slope =	degrees	3
Width =	m	0.15
k=		0.000003

Laminar Flow in Rectangular flumes Do Goalseek Range

Depth = m	V = m/s	Rh =	Q= l/s	Re = Calc	Re = selected	f (fanning) 16/Re =	Froude number	Rec (transition)
0.01594774	0.092	0.013151	0.22	**10**	10	1.600000	0.232268	531
0.017186529	0.307	0.013982	0.79	**105**	105	0.152381	0.747561	704
0.017678948	0.429	0.014307	1.14	**200**	200	0.080000	1.028988	799
0.018018146	0.524	0.014528	1.42	**295**	295	0.054237	1.247421	872
0.018283757	0.607	0.0147	1.66	**390**	390	0.041026	1.432237	934
0.018504978	0.680	0.014843	1.89	**485**	485	0.032990	1.595288	989
0.018696102	0.746	0.014965	2.09	**580**	580	0.027586	1.742766	1039
0.018865294	0.808	0.015074	2.29	**675**	675	0.023704	1.878387	1084
0.019017696	0.866	0.015171	2.47	**770**	770	0.020779	2.004593	1127
0.019156775	0.920	0.015259	2.64	**865**	865	0.018497	2.123088	1167
0.019284989	0.972	0.01534	2.81	**960**	960	0.016667	2.235116	1204
0.019404128	1.022	0.015416	2.97	**1055**	1055	0.015166	2.341620	1240
0.019515613	1.069	0.015486	3.13	**1150**	1150	0.013913	2.443334	1274
0.019620498	1.115	0.015552	3.28	**1245**	1245	0.012851	2.540843	1307
0.019717611	1.158	0.015613	3.42	**1338**	1338	0.011958	2.632682	1338

The onset of transition is at Reynolds number 1338. This was calculated by selecting a Reynolds number and optimising the depth until the Reynolds numbers are the same.

Turbulent Flow in Rectangular flumes

Depth (selected) m	V = m/s	Rh =	Q= l/s	Re =	f (fanning)	Froude number	Re Full Turbulence
0.040563	1.928442	0.026325	11.73	**3717**	0.00739197	3.057081	3717
0.041	1.941319	0.026509	11.94	**3767**	0.007372809	3.061051	3720
0.046	2.084284	0.028512	14.38	**4343**	0.007176077	3.102727	3753
0.051	2.220001	0.030357	16.98	**4927**	0.007013052	3.138582	3781
0.056	2.34943	0.032061	19.74	**5516**	0.006875529	3.169816	3805
0.061	2.473338	0.03364	22.63	**6111**	0.00675781	3.197305	3827
0.066	2.592348	0.035106	25.66	**6710**	0.006655804	3.221712	3846
0.071	2.706973	0.036473	28.83	**7312**	0.006566494	3.243548	3863
0.076	2.817646	0.037748	32.12	**7917**	0.006487597	3.263211	3878
0.081	2.924731	0.038942	35.54	**8525**	0.006417358	3.281020	3892
0.086	3.028542	0.040062	39.07	**9133**	0.006354399	3.297234	3905
0.091	3.129348	0.041114	42.72	**9744**	0.006297625	3.312064	3916
0.096	3.227386	0.042105	46.47	**10355**	0.00624615	3.325683	3927
0.101	3.322863	0.04304	50.34	**10968**	0.006199256	3.338238	3937
0.106	3.415961	0.043923	54.31	**11581**	0.006156347	3.349851	3946
0.111	3.506843	0.044758	58.39	**12195**	0.00611693	3.360627	3954
0.116	3.595653	0.04555	62.56	**12809**	0.006080588	3.370655	3962
0.121	3.682521	0.046301	66.84	**13423**	0.006046971	3.380011	3969
0.126	3.767566	0.047015	71.21	**14038**	0.00601578	3.388762	3976
0.131	3.850892	0.047694	75.67	**14653**	0.005986759	3.396966	3983
0.136	3.932596	0.048341	80.22	**15267**	0.005959685	3.404673	3989

The onset of full turbulence is found by optimising the depth until the Reynolds number is the same as the full turbulence Reynolds number.

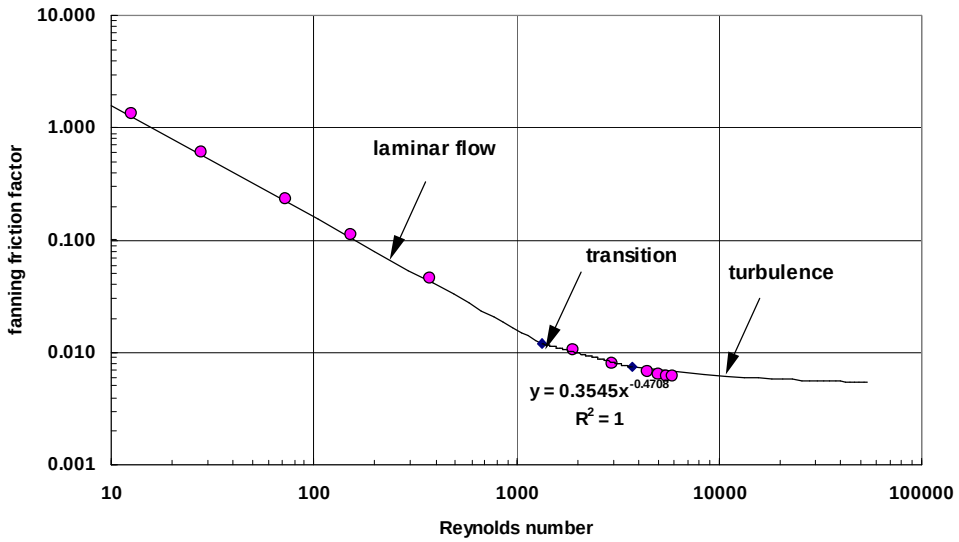

Figure C 1 Moody Diagram for 6% kaolin in 150 mm flume, 3 degree slope

In the transition range the relationship between Re and f is:

$$f = \frac{0.3551}{Re^{0.471}}. \qquad (C.12)$$

This relationship is valid between Re = 1338 and Re = 3717.

Transitional Flow in Rectangular flumes.

Depth = m	V = m/s	Rh =	Q= l/s	Re = Calc	Re = selected	f (fanning) 0.3551/(Re^.471)
0.019655472	1.155	0.015574	3.40	**1331**	1331	0.011991
0.02506	1.379	0.018784	5.18	**1900**	1900	0.010140
0.02962	1.549	0.021234	6.88	**2400**	2400	0.009084
0.03503	1.732	0.023878	9.10	**3000**	3000	0.008178
0.0415	1.926	0.026717	11.99	**3716**	3717	0.007392

Reynolds numbers can be manipulated in this region to obtain the required flow rates or velocities or flow depths.

APPENDIX D

FLUME DATA

The following section contains all the flume data which was used in the thesis.

The data sets are for tests in the three rectangular flumes of width 75 mm, 150 mm and 300 mm.

The channel slope, flow and flow depth as well as the rheological parameters are presented in tabular form for each of the tests.

The test fluids are kaolin, bentonite and CMC.

Material:	Kaolin
Concentration/vol:	3%
Density kg/m^3:	1050
Ty (Pa):	1.843
k (Pa.s^n):	0.002
n:	1.062
Flume width (mm):	75

SLOPE FLUME (degrees)	FLOW Q ($l.s^{-1}$)	DEPTH h (m)
4	0.159	0.0052
4	0.294	0.0057
4	0.604	0.0076
4	0.910	0.0100
4	1.259	0.0129
4	1.534	0.0138
4	1.839	0.0159
4	2.540	0.0199
2	5.548	0.0498
2	1.995	0.0227
2	1.477	0.0198
2	1.022	0.0150
2	0.552	0.0107
2	0.139	0.0083
1	0.024	0.0107
1	0.052	0.0116
1	0.070	0.0126
1	0.081	0.0129
1	0.100	0.0134
1	0.135	0.0127
1	0.200	0.0126
1	0.251	0.0136
1	0.350	0.0147
1	0.506	0.0153
1	0.828	0.0181
1	1.140	0.0205
1	1.468	0.0241
1	1.820	0.0273
1	2.172	0.0321
1	2.641	0.0363
1	3.043	0.0400
1	3.562	0.0459
1	4.076	0.0499
1	4.479	0.0548
1	5.567	0.0636

Material:	Kaolin
Concentration/vol:	3%
Density kg/m^3:	1049
Ty (Pa):	1.843
k (Pa.s^n):	0.002
n:	1.062
Flume width (mm):	150

SLOPE FLUME (degrees)	FLOW Q (l.s^{-1})	DEPTH h (m)
4	3.052	0.0111
4	4.063	0.0135
4	5.160	0.0159
4	6.212	0.0187
4	8.190	0.0228
4	10.956	0.0290
4	12.225	0.0323
4	14.291	0.0357
4	16.382	0.0403
4	20.345	0.0476
4	0.773	0.0053
4	0.528	0.0050
4	0.306	0.0040
3	0.976	0.0069
3	2.039	0.0092
3	3.056	0.0115
3	4.051	0.0139
3	4.993	0.0168
3	6.055	0.0195
3	7.296	0.0232
3	8.118	0.0255
3	10.922	0.0324
3	12.155	0.0358
3	14.363	0.0420
3	16.215	0.0458
3	18.394	0.0521
3	20.558	0.0569
3	0.324	0.0044
3	0.544	0.0060
3	0.785	0.0063
2	1.039	0.0090
2	2.225	0.0119
2	3.027	0.0141
2	4.239	0.0175
2	6.138	0.0228
2	8.249	0.0281
2	10.193	0.0367
2	12.574	0.0433
2	14.208	0.0480
2	16.483	0.0545
2	18.379	0.0599
2	20.452	0.0653
2	0.740	0.0083
2	0.518	0.0079
2	0.325	0.0074
2	0.148	0.0058

SLOPE FLUME (degrees)	FLOW Q (l.s^{-1})	DEPTH h (m)
1	1.153	0.0147
1	2.013	0.0171
1	3.114	0.0207
1	4.297	0.0255
1	6.299	0.0326
1	8.238	0.0372
1	10.211	0.0460
1	12.799	0.0569
1	14.219	0.0618
1	16.493	0.0705
1	18.365	0.0772
1	20.298	0.0832
1	0.128	0.0164
1	0.333	0.0180
1	0.579	0.0201
1	0.743	0.0203

Material:	Kaolin
Concentration/vol:	3%
Density kg/m^3:	1050
Ty (Pa):	1.727
k (Pa.s^n):	0.004
n:	0.955
Flume width (mm):	300

SLOPE FLUME (degrees)	FLOW Q (l.s^{-1})	DEPTH h (m)
4	1.432	0.0067
4	2.351	0.0074
4	3.025	0.0095
4	4.175	0.0104
4	5.245	0.0114
4	6.069	0.0130
4	8.107	0.0142
4	10.207	0.0178
4	12.411	0.0211
4	16.265	0.0256
3	2.004	0.0081
3	4.159	0.0104
3	6.048	0.0134
3	10.251	0.0185
3	15.249	0.0267
3	20.439	0.0346
3	0.724	0.0066
3	1.124	0.0073
2	2.462	0.0101
2	4.103	0.0130
2	6.118	0.0162
2	8.232	0.0193
2	10.146	0.0218
2	15.240	0.0313
2	20.394	0.0384
2	0.224	0.0081
2	0.556	0.0079
2	1.027	0.0089
2	1.555	0.0093
1	1.984	0.0144
1	4.050	0.0188
1	6.106	0.0231
1	8.135	0.0272
1	10.264	0.0296
1	15.383	0.0379
1	20.438	0.0472
1	0.286	0.0134
1	0.515	0.0133
1	1.070	0.0135
1	1.550	0.0147

Material:	Kaolin
Concentration/vol:	4.5%
Density kg/m^3:	1075
Ty (Pa):	3.510
k (Pa.s^n):	0.012
n:	0.836
Flume width (mm):	75

SLOPE	FLOW	DEPTH
FLUME	Q	h
(degrees)	(l.s^{-1})	(m)
2	0.100	0.0112
2	0.249	0.0122
2	0.519	0.0137
2	0.754	0.0156
2	1.045	0.0181
2	1.518	0.0222
2	2.031	0.0285
2	4.021	0.0421
2	6.104	0.0590
3	6.146	0.0490
3	4.065	0.0361
3	2.020	0.0237
3	0.995	0.0159
3	0.769	0.0122
3	0.506	0.0106
3	0.263	0.0089
3	0.100	0.0081
4	0.098	0.0064
4	0.263	0.0074
4	0.551	0.0090
4	0.763	0.0104
4	1.014	0.0121
4	2.152	0.0201
4	4.053	0.0319
4	6.293	0.0463
5	7.040	0.0456
5	4.099	0.0282
5	1.934	0.0169
5	1.031	0.0110
5	0.757	0.0087
5	0.550	0.0075
5	0.255	0.0059
5	0.094	0.0056
1	0.112	0.0213
1	0.234	0.0241
1	0.524	0.0273
1	0.743	0.0302
1	1.040	0.0315
1	1.525	0.0351
1	2.233	0.0409
1	3.983	0.0589
1	6.246	0.0821

Material:	Kaolin
Concentration/vol:	4.5%
Density kg/m^3:	1075
Ty (Pa):	3.510
k (Pa.s^n):	0.012
n:	0.836
Flume width (mm):	150

SLOPE FLUME (degrees)	FLOW Q ($l.s^{-1}$)	DEPTH h (m)
1	1.060	0.0235
1	2.078	0.0279
1	3.123	0.0306
1	4.103	0.0339
1	5.067	0.0372
1	6.209	0.0407
1	7.178	0.0449
1	8.288	0.0489
1	10.515	0.0568
1	12.518	0.0639
1	14.422	0.0708
1	16.284	0.0772
1	18.273	0.0823
1	20.611	0.0902
1	0.969	0.0251
1	0.606	0.0243
1	0.328	0.0239
2	1.028	0.0136
2	2.009	0.0158
2	3.115	0.0188
2	4.687	0.0235
2	5.393	0.0270
2	6.537	0.0291
2	8.281	0.0339
2	10.173	0.0394
2	12.482	0.0461
2	14.363	0.0518
2	16.573	0.0579
2	18.389	0.0626
2	20.469	0.0699
2	0.388	0.0129
2	0.633	0.0133
2	0.955	0.0136
3	1.128	0.0106
3	2.245	0.0126
3	3.036	0.0147
3	4.266	0.0176
3	5.181	0.0200
3	6.042	0.0222
3	6.990	0.0250
3	8.363	0.0292
3	10.522	0.0339
3	12.730	0.0415
3	14.600	0.0444
3	16.334	0.0508
3	18.304	0.0548
3	20.471	0.0600
3	0.966	0.0103
3	0.624	0.0096
3	0.332	0.0094

SLOPE FLUME (degrees)	FLOW Q ($l.s^{-1}$)	DEPTH h (m)
4	1.203	0.0086
4	2.056	0.0106
4	3.140	0.0131
4	4.418	0.0154
4	5.509	0.0180
4	6.237	0.0193
4	10.611	0.0287
4	12.353	0.0336
4	14.447	0.0376
4	18.557	0.0476
4	0.371	0.0073
4	0.679	0.0079
4	0.953	0.0081
5	0.988	0.0070
5	2.134	0.0095
5	3.034	0.0114
5	4.184	0.0145
5	5.337	0.0170
5	6.238	0.0180
5	8.378	0.0231
5	10.461	0.0272
5	12.076	0.0316
5	14.411	0.0346
5	16.507	0.0407
5	18.907	0.0461
5	20.626	0.0493
5	0.946	0.0069
5	0.599	0.0065
5	0.324	0.0054

Material:	Kaolin
Concentration/vol:	4.5%
Density kg/m^3:	1075
Ty (Pa):	3.510
k (Pa.s^n):	0.012
n:	0.836
Flume width (mm):	300

SLOPE FLUME (degrees)	FLOW Q ($l.s^{-1}$)	DEPTH h (m)
1	1.041	0.0218
1	2.197	0.0237
1	3.088	0.0244
1	4.329	0.0253
1	5.151	0.0266
1	6.245	0.0278
1	7.287	0.0296
1	8.218	0.0312
1	9.200	0.0327
1	10.552	0.0354
1	12.516	0.0384
1	14.108	0.0412
1	16.719	0.0455
1	18.684	0.0487
1	20.967	0.0529
1	0.943	0.0228
1	0.628	0.0221
1	0.307	0.0209
2	1.125	0.0121
2	2.026	0.0132
2	3.548	0.0151
2	4.046	0.0157
2	5.093	0.0170
2	6.245	0.0184
2	8.377	0.0212
2	10.422	0.0241
2	12.481	0.0268
2	12.495	0.0267
2	14.303	0.0291
2	16.505	0.0323
2	18.513	0.0352
2	20.511	0.0378
2	0.341	0.0124
2	0.691	0.0130
2	0.932	0.0130
3	2.022	0.0105
3	3.148	0.0116
3	4.269	0.0122
3	5.272	0.0134
3	6.159	0.0144
3	8.231	0.0167
3	12.256	0.0216
3	14.246	0.0241
3	16.651	0.0270
3	18.596	0.0292
3	20.584	0.0324
3	0.987	0.0095
3	0.598	0.0092
3	0.316	0.0091

SLOPE FLUME (degrees)	FLOW Q ($l.s^{-1}$)	DEPTH h (m)
4	1.544	0.0080
4	2.224	0.0089
4	3.058	0.0096
4	4.297	0.0108
4	5.143	0.0114
4	6.213	0.0122
4	8.500	0.0147
4	10.782	0.0172
4	12.498	0.0185
4	14.273	0.0202
4	16.465	0.0230
4	18.467	0.0257
4	20.336	0.0277
4	0.588	0.0070
4	0.325	0.0073
4	1.029	0.0079
5	1.208	0.0069
5	1.981	0.0075
5	3.140	0.0082
5	4.136	0.0091
5	5.149	0.0099
5	6.206	0.0105
5	8.335	0.0117
5	10.755	0.0150
5	12.199	0.0165
5	14.281	0.0182
5	16.359	0.0207
5	18.592	0.0231
5	20.514	0.0249
5	0.940	0.0065
5	0.630	0.0059
5	0.401	0.0047

Material:	Kaolin
Concentration/vol:	5.3%
Density kg/m^3:	1088
Ty (Pa):	4.985
k (Pa.s^n):	0.030
n:	0.717
Flume width (mm):	150

SLOPE FLUME (degrees)	FLOW Q ($l.s^{-1}$)	DEPTH h (m)
1	0.086	0.0298
1	0.189	0.0313
1	0.268	0.0323
1	0.367	0.0329
1	0.481	0.0334
1	0.703	0.0340
1	0.913	0.0347
1	1.449	0.0372
1	2.030	0.0377
1	3.356	0.0404
1	4.114	0.0436
1	5.271	0.0468
1	6.189	0.0496
1	8.098	0.0568
1	10.079	0.0631
1	15.116	0.0798
1	20.419	0.0980
1	24.363	0.1102
2	0.161	0.0154
2	0.290	0.0164
2	0.385	0.0164
2	0.487	0.0168
2	0.700	0.0176
2	0.914	0.0177
2	1.532	0.0186
2	2.145	0.0202
2	2.437	0.0212
2	2.835	0.0221
2	4.846	0.0276
2	3.083	0.0220
2	3.972	0.0247
2	6.069	0.0307
2	7.964	0.0365
2	10.020	0.0420
2	15.186	0.0563
2	21.917	0.0764
3	0.167	0.0109
3	0.276	0.0113
3	0.493	0.0118
3	0.579	0.0121
3	0.817	0.0123
3	1.013	0.0126
3	1.538	0.0137
3	2.011	0.0147
3	2.464	0.0160
3	2.994	0.0167
3	4.069	0.0194
3	6.114	0.0241
3	8.137	0.0291
3	10.003	0.0345
3	16.148	0.0487
3	22.011	0.0621

SLOPE FLUME (degrees)	FLOW Q ($l.s^{-1}$)	DEPTH h (m)
4	1.040	0.0103
4	1.489	0.0110
4	2.057	0.0121
4	2.522	0.0132
4	2.994	0.0144
4	3.242	0.0142
4	4.139	0.0164
4	5.162	0.0186
4	6.908	0.0226
4	8.672	0.0263
4	10.137	0.0297
4	15.097	0.0401
4	22.202	0.0579
4	26.103	0.0623
5	1.322	0.0093
5	2.129	0.0107
5	3.020	0.0123
5	4.536	0.0142
5	5.134	0.0163
5	6.102	0.0184
5	8.043	0.0219
5	10.192	0.0259
5	18.001	0.0411
5	28.125	0.0617
5	2.514	0.0115
5	3.548	0.0134
5	3.869	0.0143

Material:	Kaolin
Concentration/vol:	5.3%
Density kg/m^3:	1087.1
Ty (Pa):	4.985
k (Pa.s^n):	0.030
n:	0.717
Flume width (mm):	300

SLOPE FLUME (degrees)	FLOW Q (l.s^{-1})	DEPTH h (m)
1	0.243	0.0297
1	0.357	0.0299
1	0.443	0.0300
1	0.522	0.0302
1	0.699	0.0300
1	0.980	0.0302
1	1.221	0.0298
1	1.422	0.0307
1	1.964	0.0318
1	3.155	0.0342
1	3.715	0.0349
1	4.637	0.0356
1	5.021	0.0357
1	6.454	0.0366
1	7.662	0.0379
1	8.817	0.0392
1	10.099	0.0408
1	14.875	0.0482
1	19.618	0.0557
1	23.881	0.0624
1	30.455	0.0726
1	36.908	0.0824
1	44.008	0.0933
2	0.241	0.0150
2	0.366	0.0155
2	0.564	0.0159
2	0.795	0.0164
2	0.986	0.0164
2	1.363	0.0171
2	1.647	0.0175
2	2.061	0.0178
2	2.993	0.0182
2	3.644	0.0191
2	4.854	0.0203
2	5.549	0.0211
2	7.208	0.0228
2	8.632	0.0246
2	10.040	0.0267
2	16.127	0.0348
2	22.458	0.0433
2	33.385	0.0573
2	44.725	0.0712
3	0.698	0.0111
3	0.915	0.0114
3	1.187	0.0116
3	1.488	0.0121
3	1.845	0.0124
3	2.394	0.0128
3	2.565	0.0128
3	3.597	0.0142
3	4.839	0.0152
3	5.729	0.0159
3	6.970	0.0172
3	8.500	0.0191
3	10.153	0.0208
3	18.124	0.0303
3	23.588	0.0368
3	34.384	0.0487
3	45.172	0.0599

SLOPE FLUME (degrees)	FLOW Q (l.s^{-1})	DEPTH h (m)
4	1.270	0.0094
4	1.469	0.0097
4	2.106	0.0103
4	2.523	0.0106
4	3.536	0.0114
4	4.588	0.0123
4	5.475	0.0131
4	7.015	0.0147
4	8.377	0.0157
4	10.026	0.0177
4	17.417	0.0256
4	25.286	0.0339
4	35.672	0.0435
4	45.158	0.0527
5	1.306	0.0079
5	2.057	0.0086
5	1.793	0.0085
5	2.434	0.0091
5	3.419	0.0098
5	4.723	0.0108
5	5.605	0.0116
5	7.095	0.0128
5	8.460	0.0141
5	10.082	0.0156
5	16.007	0.0215
5	24.692	0.0299
5	35.437	0.0395
5	44.935	0.0486

Material:	Kaolin
Concentration/vol:	6%
Density kg/m^3:	1099
Ty (Pa):	6.840
k (Pa.s^n):	0.148
n:	0.517
Flume width (mm):	75

SLOPE FLUME (degrees)	FLOW Q ($l.s^{-1}$)	DEPTH h (m)
5	0.401	0.0129
5	0.223	0.0117
5	0.115	0.0112
5	0.581	0.0133
5	0.913	0.0148
5	1.343	0.0171
5	1.838	0.0196
5	2.561	0.0233
5	3.083	0.0264
5	3.438	0.0287
5	4.510	0.0341
5	5.567	0.0389
5	6.602	0.0439
4	4.899	0.0403
4	4.276	0.0374
4	2.956	0.0300
4	2.392	0.0263
4	0.892	0.0189
4	0.057	0.0128
4	0.202	0.0145
4	0.361	0.0154
4	0.622	0.0165
4	0.975	0.0180
3	1.127	0.0247
3	0.791	0.0236
3	0.584	0.0231
3	0.400	0.0220
3	0.248	0.0211
3	0.076	0.0185
3	0.081	0.0185
3	0.156	0.0198
3	0.862	0.0256
3	1.837	0.0292
3	3.032	0.0369
3	4.267	0.0450
3	5.128	0.0504
2	5.174	0.0662
2	3.942	0.0580
2	2.947	0.0506
2	1.802	0.0450
2	0.901	0.0401
2	0.795	0.0374
2	0.622	0.0358
2	0.388	0.0325
2	0.120	0.0279
2	0.244	0.0303
2	0.196	0.0288

Material:	Kaolin
Concentration/vol:	6%
Density kg/m3:	1099
Ty (Pa):	6.840
k (Pa.sn):	0.148
n:	0.517
Flume width (mm):	150

SLOPE FLUME (degrees)	FLOW Q (l.s-1)	DEPTH h (m)
5	0.103	0.0101
5	0.311	0.0106
5	0.677	0.0115
5	1.121	0.0120
5	1.760	0.0129
5	3.319	0.0152
5	5.171	0.0183
5	8.465	0.0231
5	11.234	0.0289
5	15.531	0.0361
5	19.757	0.0429
5	23.953	0.0496
4	1.129	0.0146
4	0.699	0.0139
4	0.370	0.0130
4	0.087	0.0117
4	23.972	0.0574
4	20.863	0.0505
4	15.319	0.0401
4	10.420	0.0312
4	8.437	0.0270
4	4.938	0.0204
4	3.553	0.0176
4	1.882	0.0157
3	0.264	0.0171
3	0.406	0.0175
3	0.685	0.0180
3	1.038	0.0186
3	1.738	0.0196
3	5.349	0.0259
3	8.496	0.0329
3	14.852	0.0469
3	17.981	0.0534
3	20.799	0.0591
3	23.960	0.0656
2	1.099	0.0275
2	0.705	0.0270
2	0.446	0.0256
2	0.097	0.0225
2	19.946	0.0732
2	23.999	0.0824
2	15.429	0.0614
2	10.472	0.0472
2	7.334	0.0390
2	4.948	0.0342
2	1.821	0.0249

SLOPE FLUME (degrees)	FLOW Q (l.s-1)	DEPTH h (m)
1	0.959	0.0532
1	1.855	0.0617
1	3.063	0.0711
1	5.174	0.0822
1	7.062	0.0899
1	11.537	0.1067
1	15.652	0.1213
1	24.013	0.1466
1	19.897	0.1348

Material:	Kaolin
Concentration/vol:	6%
Density kg/m^3:	1098.5
Ty (Pa):	6.840
k (Pa.s^n):	0.148
n:	0.517
Flume width (mm):	300

SLOPE FLUME (degrees)	FLOW Q ($l.s^{-1}$)	DEPTH h (m)
5	0.848	0.0112
5	2.978	0.0123
5	5.260	0.0142
5	7.229	0.0153
5	9.410	0.0176
5	15.650	0.0244
5	20.917	0.0296
5	0.121	0.0099
5	0.517	0.0114
5	0.710	0.0116
4	0.880	0.0132
4	2.875	0.0142
4	7.216	0.0183
4	13.461	0.0243
4	17.596	0.0285
4	20.874	0.0341
4	0.122	0.0121
4	0.533	0.0133
4	0.728	0.0133
3	1.210	0.0168
3	2.854	0.0177
3	7.284	0.0216
3	15.470	0.0308
3	20.821	0.0372
3	0.099	0.0145
3	0.549	0.0161
3	0.705	0.0164
2	1.192	0.0236
2	4.983	0.0265
2	10.383	0.0323
2	15.752	0.0390
2	21.012	0.0450
2	0.119	0.0223
2	1.939	0.0253
2	0.560	0.0222
2	0.795	0.0242
1	1.117	0.0428
1	5.198	0.0516
1	10.176	0.0576
1	15.639	0.0623
1	20.900	0.0686
1	0.135	0.0357
1	0.285	0.0425
1	0.729	0.0457

Material:	Kaolin
Concentration/vol:	7.1%
Density kg/m^3:	1118.3
Ty (Pa):	9.431
k (Pa.s^n):	0.625
n:	0.388
Flume width (mm):	150

SLOPE FLUME (degrees)	FLOW Q ($l.s^{-1}$)	DEPTH h (m)
1	1.416	0.0838
1	2.043	0.0888
1	2.497	0.0929
1	2.991	0.0964
1	4.085	0.1031
1	5.074	0.1087
1	6.231	0.1147
1	7.211	0.1197
1	8.133	0.1236
1	9.074	0.1284
1	10.107	0.1318
1	12.180	0.1410
1	14.361	0.1490
1	17.288	0.1592
1	19.022	0.1654
1	20.907	0.1709
2	1.145	0.0440
2	2.066	0.0471
2	2.520	0.0493
2	3.050	0.0511
2	4.130	0.0530
2	5.193	0.0545
2	6.317	0.0562
2	7.071	0.0576
2	7.987	0.0596
2	9.060	0.0618
2	10.107	0.0644
2	11.822	0.0685
2	14.813	0.0770
2	19.279	0.0889
2	21.304	0.0949
2	22.923	0.0993
2	26.139	0.1078
2	17.466	0.0841
3	1.032	0.0282
3	1.538	0.0295
3	2.206	0.0300
3	2.632	0.0316
3	3.136	0.0323
3	3.587	0.0327
3	4.053	0.0334
3	4.691	0.0340
3	5.351	0.0357
3	6.084	0.0371
3	7.172	0.0394
3	7.998	0.0413
3	9.067	0.0439
3	10.107	0.0462
3	12.432	0.0514
3	15.149	0.0579
3	19.034	0.0676
3	22.664	0.0763
3	27.439	0.0871

SLOPE FLUME (degrees)	FLOW Q ($l.s^{-1}$)	DEPTH h (m)
4	0.972	0.0210
4	2.155	0.0225
4	1.419	0.0215
4	2.772	0.0232
4	3.109	0.0242
4	4.160	0.0259
4	4.793	0.0268
4	5.609	0.0282
4	6.269	0.0297
4	7.100	0.0312
4	8.052	0.0334
4	8.955	0.0353
4	10.105	0.0378
4	11.967	0.0414
4	15.670	0.0499
4	20.315	0.0597
4	25.544	0.0710
5	1.890	0.0180
5	2.535	0.0189
5	2.987	0.0197
5	3.524	0.0206
5	4.294	0.0213
5	5.019	0.0228
5	6.104	0.0247
5	7.157	0.0269
5	8.079	0.0286
5	9.304	0.0309
5	10.187	0.0325
5	12.727	0.0375
5	16.621	0.0454
5	21.403	0.0550
5	28.511	0.0689

Material:	Kaolin
Concentration/vol:	7.1%
Density kg/m^3:	1118.5
Ty (Pa):	10.551
k (Pa.s^n):	0.834
n:	0.387
Flume width (mm):	300

SLOPE FLUME (degrees)	FLOW Q (l.s^{-1})	DEPTH h (m)
1	1.206	0.0633
1	2.054	0.0675
1	2.584	0.0691
1	3.038	0.0703
1	4.135	0.0732
1	5.140	0.0756
1	6.063	0.0774
1	7.007	0.0796
1	8.065	0.0813
1	9.082	0.0830
1	10.158	0.0849
1	13.634	0.0897
1	19.849	0.1023
1	22.889	0.0978
1	28.571	0.1044
1	33.360	0.1102
1	38.570	0.1170
1	44.609	0.1254
2	1.044	0.0353
2	2.172	0.0378
2	3.093	0.0391
2	4.131	0.0404
2	5.399	0.0417
2	6.042	0.0416
2	7.170	0.0423
2	8.103	0.0428
2	9.052	0.0432
2	10.153	0.0444
2	12.713	0.0457
2	15.924	0.0490
2	17.800	0.0509
2	20.168	0.0542
2	24.059	0.0591
2	27.408	0.0625
2	30.089	0.0662
2	34.154	0.0715
2	38.813	0.0772
2	44.036	0.0837
3	0.965	0.0249
3	2.016	0.0260
3	2.990	0.0268
3	4.149	0.0278
3	5.089	0.0286
3	6.119	0.0292
3	7.138	0.0296
3	8.110	0.0303
3	9.042	0.0311
3	10.247	0.0318
3	13.100	0.0345
3	17.043	0.0386
3	18.962	0.0405
3	23.351	0.0454
3	27.316	0.0499
3	30.588	0.0535
3	35.379	0.0589
3	39.500	0.0633
3	42.162	0.0665

SLOPE FLUME (degrees)	FLOW Q (l.s^{-1})	DEPTH h (m)
4	0.917	0.0184
4	1.635	0.0194
4	2.099	0.0198
4	2.561	0.0207
4	3.377	0.0210
4	4.076	0.0217
4	4.557	0.0219
4	5.020	0.0224
4	6.165	0.0232
4	6.963	0.0235
4	7.618	0.0241
4	8.577	0.0247
4	9.437	0.0254
4	10.159	0.0260
4	12.422	0.0278
4	16.255	0.0314
4	15.299	0.0305
4	19.676	0.0349
4	22.668	0.0378
4	25.454	0.0407
4	29.940	0.0454
4	35.637	0.0512
4	39.557	0.0559
4	42.539	0.0576
5	1.507	0.0160
5	2.040	0.0166
5	2.565	0.0173
5	3.105	0.0178
5	3.492	0.0177
5	3.929	0.0183
5	4.888	0.0185
5	5.603	0.0191
5	6.726	0.0197
5	7.555	0.0203
5	8.505	0.0210
5	9.421	0.0218

Material:	Kaolin
Concentration/vol:	8.0%
Density kg/m^3:	1133
Ty (Pa):	14.631
k (Pa.s^n):	0.057
n:	0.694
Flume width (mm):	75

SLOPE	FLOW	DEPTH
FLUME	Q	h
(degrees)	(l.s^{-1})	(m)
5	0.031	0.0307
5	0.030	0.0300
5	0.031	0.0309
5	0.035	0.0353
5	0.044	0.0437
5	0.051	0.0511
5	0.056	0.0564
5	0.061	0.0620
5	0.069	0.0701
4	0.032	0.0321
4	0.033	0.0329
4	0.033	0.0326
4	0.037	0.0366
4	0.041	0.0416
4	0.047	0.0473
4	0.054	0.0550
4	0.061	0.0621
4	0.073	0.0740
4	0.034	0.0346
4	0.036	0.0359
4	0.033	0.0336
4	0.032	0.0325
4	0.032	0.0324
4	0.031	0.0313
4	0.029	0.0291
3	0.044	0.0433
3	0.045	0.0447
3	0.047	0.0475
3	0.048	0.0480
3	0.049	0.0496
3	0.052	0.0518
3	0.052	0.0526
3	0.053	0.0531
3	0.063	0.0629
3	0.075	0.0752
3	0.080	0.0803
3	0.085	0.0857
3	0.091	0.0922

Material:	Kaolin
Concentration/vol:	8.0%
Density kg/m^3:	1133
Ty (Pa):	14.630
k (Pa.s^n):	0.057
n:	0.694
Flume width (mm):	150

SLOPE FLUME (degrees)	FLOW Q ($l.s^{-1}$)	DEPTH h (m)
5	0.021	0.0205
5	0.022	0.0222
5	0.024	0.0235
5	0.026	0.0264
5	0.031	0.0305
5	0.034	0.0346
5	0.039	0.0386
5	0.042	0.0424
5	0.047	0.0462
5	0.051	0.0515
5	0.055	0.0548
5	0.060	0.0603
5	0.019	0.0196
5	0.021	0.0207
4	0.025	0.0253
4	0.026	0.0263
4	0.027	0.0268
4	0.029	0.0289
4	0.032	0.0316
4	0.036	0.0356
4	0.040	0.0396
4	0.045	0.0445
4	0.049	0.0493
4	0.054	0.0536
4	0.058	0.0582
4	0.060	0.0603
4	0.067	0.0676
4	0.025	0.0245
4	0.023	0.0234
4	0.021	0.0215
3	0.036	0.0355
3	0.038	0.0376
3	0.026	0.0306
3	0.039	0.0397
3	0.042	0.0425
3	0.051	0.0507
3	0.055	0.0555
3	0.060	0.0605
3	0.065	0.0653
3	0.070	0.0705
3	0.075	0.0754
3	0.081	0.0806
3	0.084	0.0838
3	0.031	0.0313
3	0.033	0.0327

SLOPE FLUME (degrees)	FLOW Q ($l.s^{-1}$)	DEPTH h (m)
2	0.058	0.0577
2	0.062	0.0618
2	0.066	0.0657
2	0.069	0.0692
2	0.074	0.0735
2	0.076	0.0764
2	0.077	0.0773
2	0.080	0.0802
2	0.084	0.0842
2	0.089	0.0887
2	0.094	0.0948
2	0.099	0.0994
2	0.105	0.1052
2	0.052	0.0515

Material:	Kaolin
Concentration/vol:	8.0%
Density kg/m^3:	1133
Ty (Pa):	14.630
k (Pa.s^n):	0.057
n:	0.694
Flume width (mm):	300

SLOPE FLUME (degrees)	FLOW Q ($l.s^{-1}$)	DEPTH h (m)
5	0.019	0.0192
5	0.019	0.0188
5	0.018	0.0183
5	0.020	0.0194
5	0.021	0.0207
5	0.022	0.0218
5	0.023	0.0230
5	0.024	0.0242
5	0.026	0.0257
5	0.028	0.0274
5	0.030	0.0292
5	0.031	0.0309
5	0.033	0.0328
4	0.022	0.0216
4	0.023	0.0228
4	0.023	0.0235
4	0.024	0.0242
4	0.025	0.0253
4	0.027	0.0263
4	0.028	0.0274
4	0.029	0.0290
4	0.030	0.0302
4	0.032	0.0319
4	0.034	0.0333
4	0.036	0.0355
4	0.038	0.0374
3	0.030	0.0300
3	0.029	0.0294
3	0.028	0.0284
3	0.031	0.0308
3	0.033	0.0329
3	0.034	0.0339
3	0.035	0.0351
3	0.037	0.0364
3	0.038	0.0377
3	0.039	0.0391
3	0.041	0.0408
3	0.043	0.0425
3	0.045	0.0448

SLOPE FLUME (degrees)	FLOW Q ($l.s^{-1}$)	DEPTH h (m)
2	0.043	0.0426
2	0.043	0.0436
2	0.044	0.0442
2	0.046	0.0461
2	0.050	0.0497
2	0.051	0.0516
2	0.052	0.0521
2	0.053	0.0529
2	0.053	0.0535
2	0.055	0.0547
2	0.056	0.0560
2	0.058	0.0577
2	0.060	0.0593
1	0.114	0.1137
1	0.110	0.1089
1	0.105	0.1043
1	0.100	0.0990
1	0.094	0.0936
1	0.089	0.0877
1	0.079	0.0784
1	0.074	0.0737

Material:	Kaolin
Concentration/vol:	9.0%
Density kg/m^3:	1149.4
Ty (Pa):	20.448
k (Pa.s^n):	0.267
n:	0.535
Flume width (mm):	150

SLOPE FLUME (degrees)	FLOW Q (l.s^{-1})	DEPTH h (m)
1	2.172	0.1515
1	2.837	0.1578
2	2.403	0.1019
2	3.083	0.1075
2	4.011	0.1128
2	5.048	0.1181
2	6.277	0.1179
2	1.000	0.1181
2	6.285	0.1236
2	7.290	0.1283
2	8.496	0.1336
2	10.081	0.1403
2	14.146	0.1544
2	17.790	0.1680
2	21.802	0.1792
3	2.217	0.0626
3	2.994	0.0651
3	4.149	0.0694
3	5.102	0.0728
3	6.160	0.0747
3	7.224	0.0765
3	8.145	0.0771
3	10.081	0.0803
3	13.733	0.0846
3	18.102	0.0948
3	23.231	0.1065
3	26.755	0.1146
4	1.972	0.0432
4	3.060	0.0456
4	3.739	0.0467
4	4.068	0.0481
4	5.043	0.0488
4	6.038	0.0498
4	7.086	0.0509
4	8.569	0.0530
4	10.094	0.0557
4	12.906	0.0612
4	16.122	0.0679
4	18.795	0.0738
4	22.787	0.0826
4	25.937	0.0895
5	2.167	0.0337
5	3.195	0.0348
5	3.926	0.0359
5	5.140	0.0373
5	6.283	0.0385
5	7.226	0.0398
5	8.503	0.0419
5	10.081	0.0443
5	12.204	0.0483
5	15.702	0.0555
5	18.528	0.0613
5	22.055	0.0681
5	28.434	0.0813

Material:	Kaolin
Concentration/vol:	10.0%
Density kg/m^3:	1165
Ty (Pa):	21.311
k (Pa.s^n):	0.524
n:	0.468
Flume width (mm):	150

SLOPE FLUME (degrees)	FLOW Q ($l.s^{-1}$)	DEPTH h (m)
5	1.487	0.0342
5	2.250	0.0352
5	2.945	0.0366
5	4.046	0.0380
5	5.391	0.0394
5	7.280	0.0414
5	9.423	0.0471
5	0.913	0.0340
5	0.673	0.0331
5	0.309	0.0312
5	12.268	0.0510
5	14.329	0.0529
5	16.155	0.0586
5	18.006	0.0622
5	20.219	0.0668
4	1.133	0.0444
4	2.068	0.0477
4	3.458	0.0507
4	4.482	0.0520
4	6.089	0.0545
4	8.129	0.0565
4	10.328	0.0595
4	12.161	0.0635
4	14.250	0.0665
4	17.056	0.0714
4	18.386	0.0755
4	20.248	0.0787
4	0.323	0.0403
4	0.654	0.0430
4	0.940	0.0444
3	1.085	0.0618
3	2.293	0.0692
3	3.418	0.0745
3	4.202	0.0782
3	6.454	0.0836
3	8.493	0.0867
3	12.079	0.0892
3	14.332	0.0919
3	16.496	0.0948
3	18.160	0.0983
3	20.445	0.1029
3	10.570	0.0862
3	3.286	0.0738
3	0.935	0.0637
3	0.618	0.0603
3	0.310	0.0560

SLOPE FLUME (degrees)	FLOW Q ($l.s^{-1}$)	DEPTH h (m)
2	1.259	0.1096
2	2.163	0.1123
2	3.208	0.1176
2	4.241	0.1247
2	6.409	0.1364
2	8.299	0.1455
2	12.407	0.1605
2	16.267	0.1686
2	0.321	0.0846
2	0.303	0.0846
2	0.612	0.0949
2	0.930	0.0974

Material:	Kaolin
Concentration/vol:	10.0%
Density kg/m^3:	1165
Ty (Pa):	21.311
k (Pa.s^n):	0.524
n:	0.468
Flume width (mm):	300

SLOPE FLUME (degrees)	FLOW Q ($l.s^{-1}$)	DEPTH h (m)
5	0.986	0.0285
5	2.184	0.0307
5	3.119	0.0313
5	3.970	0.0320
5	5.651	0.0328
5	6.126	0.0333
5	7.323	0.0336
5	8.192	0.0339
5	9.330	0.0347
5	10.582	0.0349
5	11.099	0.0356
5	12.207	0.0361
5	13.085	0.0365
5	14.270	0.0368
5	15.228	0.0377
5	16.167	0.0379
5	17.345	0.0387
5	18.362	0.0396
5	19.268	0.0405
5	20.072	0.0406
5	0.615	0.0285
5	0.298	0.0262
4	0.800	0.0344
4	1.527	0.0364
4	1.965	0.0379
4	3.016	0.0387
4	4.358	0.0402
4	5.092	0.0411
4	6.253	0.0412
4	7.085	0.0419
4	8.123	0.0420
4	9.306	0.0427
4	10.228	0.0430
4	11.289	0.0431
4	12.129	0.0435
4	13.139	0.0442
4	14.043	0.0444
4	15.252	0.0451
4	16.005	0.0457
4	17.286	0.0467
4	18.261	0.0469
4	19.949	0.0483
4	0.230	0.0356
4	0.645	0.0351

SLOPE FLUME (degrees)	FLOW Q ($l.s^{-1}$)	DEPTH h (m)
3	1.103	0.0474
3	2.369	0.0507
3	3.257	0.0526
3	4.228	0.0534
3	6.121	0.0565
3	8.107	0.0577
3	10.322	0.0585
3	12.127	0.0586
3	14.197	0.0592
3	16.304	0.0598
3	18.200	0.0606
3	20.503	0.0620
3	0.561	0.0450
3	0.280	0.0426
2	1.399	0.0718
2	2.086	0.0759
2	3.134	0.0791
2	3.844	0.0805
2	6.112	0.0854
2	8.193	0.0888
2	10.201	0.0910
2	12.267	0.0932
2	14.385	0.0951
2	16.431	0.0963
2	18.348	0.0969
2	20.747	0.0973
2	0.302	0.0616
2	0.655	0.0650

Material:	Bentonite
Concentration/vol:	3.0%
Density kg/m^3:	1014
Ty (Pa):	1.002
k (Pa.s^n):	0.003
n:	1.000
Flume width (mm):	75

SLOPE FLUME (degrees)	FLOW Q (l.s^{-1})	DEPTH h (m)
1	0.106	0.0065
1	0.205	0.0084
1	0.401	0.0104
1	0.581	0.0120
1	0.754	0.0137
1	0.925	0.0150
1	0.900	0.0166
1	1.148	0.0166
1	1.339	0.0189
1	1.497	0.0208
1	1.823	0.0250
1	2.346	0.0305
1	4.115	0.0485
1	5.031	0.0557
2	5.038	0.0461
2	4.096	0.0387
2	2.490	0.0260
2	1.991	0.0214
2	1.512	0.0175
2	1.079	0.0121
2	0.807	0.0103
2	0.631	0.0089
2	0.449	0.0074
2	0.254	0.0058
2	0.106	0.0046
3	0.108	0.0039
3	0.255	0.0049
3	0.473	0.0064
3	0.741	0.0084
3	0.967	0.0098
3	5.177	0.0404
3	6.171	0.0473
3	7.184	0.0532

Material:	Bentonite
Concentration/vol:	3.0%
Density kg/m^3:	1014
Ty (Pa):	1.002
k (Pa.s^n):	0.003
n:	1.000
Flume width (mm):	150

SLOPE FLUME (degrees)	FLOW Q (l.s^{-1})	DEPTH h (m)
1	4.309	0.0239
1	6.111	0.0326
1	8.117	0.0416
1	10.216	0.0505
1	13.267	0.0614
1	16.619	0.0722
1	19.333	0.0808
1	22.729	0.0919
2	2.229	0.0106
2	4.118	0.0171
2	6.100	0.0261
2	8.111	0.0329
2	10.351	0.0399
2	13.392	0.0488
2	16.192	0.0567
2	19.354	0.0646
2	22.400	0.0721
3	2.213	0.0086
3	4.157	0.0171
3	6.187	0.0235
3	8.254	0.0287
3	10.437	0.0341
3	13.268	0.0409
3	16.526	0.0493
3	19.328	0.0555
3	22.463	0.0628
4	1.985	0.0087
4	4.061	0.0153
4	6.176	0.0211
4	8.228	0.0259
4	10.509	0.0306
4	13.369	0.0380
4	16.220	0.0441
4	19.452	0.0491
4	22.424	0.0561
5	2.089	0.0087
5	4.178	0.0140
5	6.072	0.0189
5	8.224	0.0238
5	10.423	0.0280
5	13.550	0.0335
5	16.386	0.0396
5	19.472	0.0447
5	22.352	0.0502
5	1.404	0.0072
5	1.085	0.0054
5	0.872	0.0039
5	0.660	0.0037
5	0.418	0.0029
5	0.287	0.0033

SLOPE FLUME (degrees)	FLOW Q (l.s^{-1})	DEPTH h (m)
4	0.334	0.0030
4	0.430	0.0036
4	0.607	0.0042
4	0.803	0.0049
4	1.020	0.0052
4	1.261	0.0055
4	1.553	0.0076
3	1.525	0.0069
3	1.279	0.0063
3	1.018	0.0058
3	0.826	0.0051
3	0.405	0.0044
3	0.629	0.0045
2	0.460	0.0063
2	0.603	0.0062
2	0.816	0.0070
2	1.220	0.0083
2	1.506	0.0091
2	1.045	0.0075
1	1.324	0.0116
1	1.038	0.0103
1	0.806	0.0099
1	0.613	0.0093
1	0.417	0.0084
1	0.209	0.0079

Material:	Bentonite
Concentration/vol:	4.5%
Density kg/m^3:	1025
Ty (Pa):	4.402
k (Pa.s^n):	0.006
n:	1.000
Flume width (mm):	75

SLOPE	FLOW	DEPTH
FLUME	Q	h
(degrees)	(l.s^{-1})	(m)
1	4.535	0.0836
1	4.022	0.0806
1	3.504	0.0779
1	2.453	0.0672
1	1.380	0.0603
1	1.066	0.3265
3	0.270	0.0138
3	0.557	0.0142
3	0.843	0.0156
3	1.122	0.0179
3	1.441	0.0207
3	1.958	0.0240
3	2.474	0.0279
3	2.960	0.0323
3	4.011	0.0399
3	5.006	0.0460
3	0.366	0.0155
2	0.368	0.0228
2	0.356	0.0228
2	0.559	0.0223
2	0.802	0.0230
2	1.208	0.0264
2	1.501	0.0293
2	1.979	0.0316
2	2.463	0.0359
2	2.945	0.0397
2	3.490	0.0441
2	4.044	0.0486
2	4.569	0.0528
2	5.036	0.0570
5	0.337	0.0096
5	0.604	0.0114
5	1.065	0.0126
5	1.230	0.0141
5	1.532	0.0161
5	2.104	0.0196
5	4.079	0.0316
5	5.908	0.0366
4	3.995	0.0340
4	6.075	0.0470
4	3.066	0.0281
4	2.502	0.0245
4	2.066	0.0214
4	1.454	0.0179
4	1.142	0.0143
4	0.870	0.0133
4	0.565	0.0114
4	0.012	0.0095
4	0.300	0.0095
4	0.300	0.0114
4	0.556	0.0111

Material:	Bentonite
Concentration/vol:	4.5%
Density kg/m^3:	1025
Ty (Pa):	4.402
k (Pa.s^n):	0.006
n:	1.000
Flume width (mm):	150

SLOPE FLUME (degrees)	FLOW Q (l.s^{-1})	DEPTH h (m)
1	1.232	0.0390
1	0.944	0.0411
1	0.629	0.0414
1	2.272	0.0445
1	4.492	0.0490
1	6.968	0.0554
1	9.683	0.0643
1	12.423	0.0709
1	11.925	0.0710
1	14.028	0.0760
1	17.990	0.0839
1	21.103	0.0884
2	2.225	0.0188
2	4.524	0.0260
2	7.047	0.0331
2	9.511	0.0396
2	12.299	0.0475
2	14.192	0.0515
2	18.227	0.0617
2	21.307	0.0707
2	0.337	0.0150
2	0.610	0.0162
2	0.911	0.0166
2	1.226	0.0170
3	1.228	0.0135
3	0.946	0.0122
3	0.632	0.0122
3	0.305	0.0113
3	2.005	0.0143
3	4.591	0.0209
3	7.261	0.0279
3	9.653	0.0326
3	11.949	0.0383
3	14.226	0.0436
3	18.124	0.0532
3	21.271	0.0621
4	1.994	0.0117
4	4.528	0.0177
4	6.931	0.0225
4	9.538	0.0281
4	12.279	0.0335
4	14.114	0.0384
4	18.082	0.0485
4	21.473	0.0530
4	0.335	0.0084
4	0.622	0.0088
4	0.976	0.0097
4	1.226	0.0105

SLOPE FLUME (degrees)	FLOW Q (l.s^{-1})	DEPTH h (m)
5	1.247	0.0090
5	0.941	0.0075
5	0.611	0.0074
5	2.273	0.0103
5	4.546	0.0149
5	6.961	0.0199
5	9.491	0.0252
5	12.322	0.0302
5	14.493	0.0343
5	18.066	0.0427
5	21.178	0.0490

Material:	Bentonite
Concentration/vol:	4.5%
Density kg/m^3:	1025
Ty (Pa):	5.410
k (Pa.s^n):	0.004
n:	1.000
Flume width (mm):	300

SLOPE FLUME (degrees)	FLOW Q (l.s^{-1})	DEPTH h (m)
1	1.944	0.0349
1	1.946	0.0370
1	4.495	0.0366
1	6.985	0.0388
1	9.625	0.0424
1	12.261	0.0469
1	14.142	0.0460
1	18.229	0.0523
1	22.351	0.0561
1	1.250	0.0346
1	0.925	0.0336
1	0.577	0.0337
2	0.300	0.0176
2	0.672	0.0187
2	1.001	0.0194
2	1.301	0.0197
2	1.968	0.0194
2	4.518	0.0225
2	7.085	0.0248
2	9.567	0.0277
2	12.495	0.0314
2	14.036	0.0332
2	18.100	0.0385
2	21.137	0.0416
3	2.042	0.0125
3	4.596	0.0160
3	7.039	0.0184
3	9.606	0.0213
3	12.250	0.0246
3	14.230	0.0263
3	18.201	0.0310
3	21.444	0.0344
3	0.309	0.0099
3	0.614	0.0105
3	0.939	0.0113
3	1.249	0.0114
4	0.292	0.0074
4	0.668	0.0087
4	0.952	0.0091
4	1.242	0.0094
4	2.171	0.0104
4	4.539	0.0128
4	7.201	0.0155
4	9.689	0.0178
4	12.168	0.0203
4	14.158	0.0226
4	18.238	0.0270
4	21.127	0.0289

SLOPE FLUME (degrees)	FLOW Q (l.s^{-1})	DEPTH h (m)
5	2.061	0.0086
5	4.531	0.0107
5	7.048	0.0134
5	9.630	0.0152
5	12.223	0.0182
5	14.226	0.0203
5	18.197	0.0238
5	21.566	0.0274
5	0.284	0.0064
5	0.657	0.0072
5	0.959	0.0068
5	1.252	0.0068

Material:	Bentonite
Concentration/vol:	6.0%
Density kg/m^3:	1032.8
Ty (Pa):	12.698
k (Pa.s^n):	0.006
n:	1.000
Flume width (mm):	75

SLOPE FLUME (degrees)	FLOW Q (l.s^{-1})	DEPTH h (m)
5	0.944	0.0273
5	1.512	0.0283
5	2.011	0.0304
5	2.532	0.0344
5	2.945	0.0374
5	3.430	0.0397
5	3.962	0.0425
5	4.570	0.0451
5	5.030	0.0483
5	6.013	0.0550
5	1.067	0.0295
5	0.822	0.0285
5	0.588	0.0286
5	0.440	0.0286
4	1.449	0.0409
4	0.684	0.0457
4	0.959	0.0402
4	1.883	0.0419
4	2.504	0.0480
4	2.938	0.0485
4	3.498	0.0530
4	4.006	0.0542
4	4.533	0.0574
3	4.061	0.0835
3	3.485	0.0832
3	2.500	0.0745
3	3.012	0.0798
3	2.036	0.0757
3	1.496	0.0737
3	0.973	0.0752

Material:	Bentonite
Concentration/vol:	6.0%
Density kg/m^3:	1033
Ty (Pa):	8.187
k (Pa.s^n):	0.006
n:	1.000
Flume width (mm):	150

SLOPE FLUME (degrees)	FLOW Q ($l.s^{-1}$)	DEPTH h (m)
1	0.363	0.0801
1	0.676	0.0835
1	0.969	0.0858
1	1.252	0.0858
1	1.585	0.0888
1	1.930	0.0852
2	1.559	0.0378
2	1.224	0.0384
2	0.931	0.0379
2	0.606	0.0391
2	0.301	0.0405
3	0.366	0.0242
3	0.640	0.0231
3	0.919	0.0246
3	1.227	0.0246
3	1.522	0.0257
4	1.520	0.0180
4	1.229	0.0175
4	0.920	0.0170
4	0.589	0.0163
4	0.283	0.0154
5	0.336	0.0129
5	0.657	0.0133
5	0.940	0.0140
5	1.236	0.0140
5	1.532	0.0148
5	2.000	0.0146
5	4.470	0.0188
5	7.042	0.0242
5	9.644	0.0286
5	12.276	0.0322
5	15.897	0.0363
5	18.188	0.0460
5	20.647	0.0510
4	2.019	0.0167
4	4.522	0.0223
4	7.078	0.0277
4	9.559	0.0330
4	12.083	0.0382
4	16.100	0.0469
4	18.457	0.0519

SLOPE FLUME (degrees)	FLOW Q ($l.s^{-1}$)	DEPTH h (m)
3	2.066	0.0223
3	4.370	0.0284
3	7.027	0.0340
3	9.534	0.0393
3	11.918	0.0455
3	16.593	0.0583
3	17.817	0.0599
3	20.803	0.0668
2	2.007	0.0350
2	4.513	0.0397
2	6.994	0.0477
2	9.579	0.0533
2	11.852	0.0593
2	16.006	0.0706
2	18.170	0.0761
2	20.206	0.0815
1	1.965	0.0841
1	4.444	0.0951
1	7.111	0.1124
1	9.513	0.1148
1	12.469	0.1123
1	16.145	0.1216
1	18.527	0.1307
1	20.454	0.1375

Material:	Bentonite
Concentration/vol:	6.0%
Density kg/m^3:	1034
Ty (Pa):	12.698
k (Pa.s^n):	0.006
n:	1.000
Flume width (mm):	300

SLOPE FLUME (degrees)	FLOW Q (l.s^{-1})	DEPTH h (m)
5	0.281	0.0185
5	0.615	0.0191
5	1.193	0.0195
5	21.017	0.0332
5	18.970	0.0305
5	17.108	0.0287
5	15.391	0.0273
5	13.177	0.0256
5	11.309	0.0243
5	8.979	0.0230
5	7.116	0.0227
5	5.020	0.0212
5	2.983	0.0201
5	1.977	0.0194
4	2.081	0.0252
4	3.015	0.0257
4	5.084	0.0269
4	7.004	0.0271
4	9.009	0.0280
4	11.070	0.0288
4	13.138	0.0306
4	15.275	0.0324
4	17.053	0.0340
4	19.001	0.0359
4	18.985	0.0347
4	21.165	0.0371
4	0.310	0.0221
4	0.756	0.0237
4	0.946	0.0239
4	1.212	0.0239
3	1.232	0.0335
3	0.930	0.0332
3	0.594	0.0334
3	20.217	0.0438
3	18.880	0.0430
3	15.004	0.0393
3	13.143	0.0382
3	10.883	0.0353
3	8.990	0.0343
3	7.056	0.0344
3	5.093	0.0346
3	2.997	0.0343
3	2.068	0.0337
2	2.141	0.0565
2	3.048	0.0586
2	5.035	0.0592
2	7.086	0.0575
2	9.158	0.0567
2	10.937	0.0562
2	12.921	0.0563
2	14.952	0.0565
2	17.575	0.0593
2	20.464	0.0606

Material:	CMC
Concentration/vol:	1.0%
Density kg/m^{-3}:	1006.7
Ty (Pa):	0.000
k (Pa.s^{n}):	0.060
n:	0.655
Flume width (mm):	75

SLOPE FLUME (degrees)	FLOW Q (l.s^{-1})	DEPTH h (m)
1	0.092	0.006
1	0.159	0.007
1	0.332	0.009
1	0.612	0.013
1	0.970	0.018
1	1.238	0.022
1	1.565	0.027
1	2.003	0.032
1	2.799	0.042
1	3.782	0.054
1	4.976	0.067
1	5.774	0.071
2	2.804	0.033
2	3.852	0.042
2	4.894	0.052
2	5.734	0.059
2	0.117	0.005
2	0.310	0.007
2	0.599	0.010
2	0.958	0.013
2	1.193	0.017
2	1.503	0.020
2	2.108	0.023
3	0.148	0.005
3	0.298	0.006
3	0.594	0.008
3	0.961	0.013
3	1.216	0.015
3	1.521	0.017
3	1.957	0.021
3	2.787	0.028
3	3.822	0.037
3	5.002	0.046
3	6.135	0.055

SLOPE FLUME (degrees)	FLOW Q (l.s^{-1})	DEPTH h (m)
4	3.115	0.029
4	3.810	0.033
4	4.964	0.042
4	5.877	0.047
4	6.890	0.054
4	0.141	0.004
4	0.305	0.005
4	0.593	0.008
4	0.877	0.010
4	1.199	0.013
4	1.518	0.016
4	1.993	0.019
5	1.235	0.012
5	0.861	0.008
5	0.612	0.007
5	0.328	0.005
5	2.259	0.020
5	3.762	0.029
5	4.841	0.037
5	5.804	0.043
5	6.726	0.045

Material:	CMC
Concentration/vol:	1.0%
Density kg/m^3:	1006.7
Ty (Pa):	0.000
k (Pa.s^n):	0.060
n:	0.655
Flume width (mm):	150

SLOPE FLUME (degrees)	FLOW Q (l.s^{-1})	DEPTH h (m)
1	1.161	0.011
1	1.925	0.015
1	4.476	0.029
1	6.741	0.039
1	9.140	0.052
1	11.755	0.062
1	13.496	0.069
1	16.278	0.079
1	18.321	0.088
1	20.280	0.098
1	0.153	0.006
1	0.323	0.007
1	0.653	0.009
1	0.090	0.005
2	0.181	0.005
2	0.291	0.004
2	0.656	0.006
2	0.938	0.007
2	1.272	0.009
2	2.102	0.011
2	4.520	0.024
2	6.753	0.032
2	9.251	0.040
2	11.982	0.049
2	13.460	0.056
2	16.585	0.064
2	18.210	0.074
2	20.252	0.075
3	1.954	0.009
3	4.549	0.021
3	6.664	0.027
3	9.227	0.036
3	11.892	0.041
3	13.464	0.046
3	16.586	0.054
3	18.275	0.059
3	20.420	0.066
3	0.313	0.004
3	0.636	0.005
3	0.906	0.006
3	1.240	0.007
3	1.514	0.008

SLOPE FLUME (degrees)	FLOW Q (l.s^{-1})	DEPTH h (m)
4	0.342	0.004
4	0.643	0.005
4	0.971	0.006
4	1.267	0.006
4	1.979	0.010
4	4.351	0.017
4	6.840	0.024
4	9.231	0.030
4	11.761	0.037
4	13.495	0.041
4	16.542	0.049
4	20.389	0.058
5	2.051	0.010
5	4.512	0.017
5	6.802	0.022
5	9.258	0.029
5	11.762	0.034
5	13.644	0.038
5	16.613	0.045
5	20.410	0.052
5	0.342	0.004
5	0.624	0.004
5	0.907	0.005
5	1.280	0.006

Material:	CMC
Concentration/vol:	1.0%
Density kg/m^3:	1006.7
Ty (Pa):	0.000
k (Pa.s^n):	0.060
n:	0.655
Flume width (mm):	300

SLOPE FLUME (degrees)	FLOW Q ($l.s^{-1}$)	DEPTH h (m)
1	1.856	0.010
1	4.276	0.018
1	6.758	0.024
1	11.445	0.035
1	13.644	0.039
1	16.302	0.045
1	18.615	0.049
1	22.886	0.056
1	0.393	0.006
1	0.592	0.007
1	0.912	0.008
1	1.520	0.009
2	1.491	0.008
2	0.892	0.006
2	0.611	0.005
2	0.269	0.004
2	1.803	0.008
2	4.306	0.014
2	6.750	0.019
2	9.115	0.023
2	11.659	0.027
2	13.969	0.031
2	17.358	0.037
2	21.375	0.043
3	1.923	0.007
3	4.390	0.012
3	6.785	0.016
3	8.940	0.020
3	11.660	0.024
3	13.928	0.027
3	17.307	0.032
3	22.025	0.038
3	0.206	0.003
3	0.584	0.005
3	0.888	0.005
3	1.527	0.007

SLOPE FLUME (degrees)	FLOW Q ($l.s^{-1}$)	DEPTH h (m)
4	1.479	0.006
4	0.858	0.005
4	0.579	0.004
4	0.297	0.004
4	1.934	0.006
4	4.364	0.011
4	6.729	0.015
4	9.165	0.018
4	12.126	0.022
4	14.442	0.026
4	17.531	0.029
4	22.576	0.035
5	1.760	0.006
5	4.536	0.011
5	6.906	0.015
5	9.163	0.018
5	12.193	0.022
5	14.656	0.025
5	17.400	0.029
5	23.112	0.035
5	0.571	0.004
5	1.198	0.005
5	0.907	0.005
5	1.280	0.006

Material:	CMC
Concentration/vol:	1.8%
Density kg/m^3:	1010.7
Ty (Pa):	0.000
k (Pa.s^n):	0.087
n:	0.765
Flume width (mm):	75

SLOPE	FLOW	DEPTH
FLUME	Q	h
(degrees)	(l.s^{-1})	(m)
5	0.290	0.007
5	0.577	0.008
5	0.879	0.011
5	1.190	0.013
5	1.466	0.015
5	1.980	0.018
5	2.951	0.025
5	3.770	0.031
5	4.900	0.039
5	5.713	0.044
5	6.665	0.051
5	7.590	0.056
4	3.008	0.028
4	3.792	0.033
4	4.700	0.040
4	5.728	0.048
4	6.675	0.055
4	0.260	0.007
4	0.564	0.010
4	0.868	0.012
4	1.164	0.014
4	1.484	0.016
4	2.065	0.021
3	2.093	0.024
3	1.470	0.019
3	1.207	0.016
3	0.912	0.013
3	0.621	0.011
3	2.763	0.028
3	3.822	0.040
3	4.758	0.047
3	5.703	0.055
2	3.853	0.047
2	3.095	0.038
2	4.744	0.053
2	5.740	0.062
2	0.297	0.010
2	0.608	0.013
2	0.849	0.015
2	1.146	0.018
2	1.512	0.022
2	2.129	0.028
1	2.156	0.036
1	1.467	0.028
1	1.191	0.025
1	0.899	0.021
1	0.544	0.016
1	0.324	0.013
1	2.573	0.041
1	3.843	0.056
1	4.778	0.066

Material:	CMC
Concentration/vol:	1.8%
Density kg/m^3:	1010.7
Ty (Pa):	0.000
k (Pa.s^n):	0.087
n:	0.765
Flume width (mm):	150

SLOPE FLUME (degrees)	FLOW Q ($l.s^{-1}$)	DEPTH h (m)
5	2.029	0.011
5	4.361	0.016
5	6.543	0.021
5	9.038	0.029
5	11.579	0.036
5	13.082	0.040
5	15.586	0.047
5	18.131	0.052
5	20.183	0.057
5	0.293	0.005
5	0.598	0.006
5	0.920	0.008
5	1.197	0.009
5	1.477	0.010
4	1.457	0.010
4	1.150	0.009
4	0.880	0.008
4	0.626	0.008
4	0.297	0.006
4	4.398	0.017
4	6.742	0.024
4	9.098	0.031
4	11.858	0.038
4	13.161	0.041
4	15.754	0.049
4	17.958	0.054
4	20.050	0.060
3	1.929	0.012
3	4.264	0.019
3	6.651	0.025
3	2.891	0.015
3	9.049	0.033
3	11.465	0.042
3	13.359	0.047
3	15.650	0.054
3	18.089	0.060
3	20.104	0.067
3	0.291	0.006
3	0.589	0.008
3	0.399	0.007
3	0.906	0.009
3	1.170	0.010
3	1.465	0.011

SLOPE FLUME (degrees)	FLOW Q ($l.s^{-1}$)	DEPTH h (m)
2	1.447	0.013
2	1.185	0.012
2	0.856	0.011
2	0.543	0.009
2	0.422	0.009
2	0.287	0.008
2	2.013	0.014
2	3.006	0.018
2	4.082	0.021
2	6.465	0.030
2	9.035	0.039
2	11.545	0.049
2	13.248	0.054
2	15.694	0.063
2	18.080	0.071
2	20.010	0.077
1	2.202	0.020
1	2.821	0.022
1	4.101	0.028
1	6.473	0.037
1	8.987	0.049
1	11.395	0.062
1	13.356	0.070
1	15.785	0.083
1	17.956	0.089
1	19.866	0.097
1	0.293	0.010
1	0.435	0.011
1	0.600	0.012
1	0.906	0.014
1	1.214	0.015
1	1.477	0.017

Material:	CMC
Concentration/vol:	1.8%
Density kg/m^3:	1010.7
Ty (Pa):	0.000
k (Pa.s^n):	0.105
n:	0.775
Flume width (mm):	300

SLOPE FLUME (degrees)	FLOW Q ($l.s^{-1}$)	DEPTH h (m)
1	2.037	0.015
1	4.265	0.020
1	3.189	0.018
1	6.666	0.024
1	9.095	0.030
1	11.752	0.035
1	13.383	0.039
1	15.686	0.042
1	17.935	0.047
1	20.241	0.052
1	7.225	0.026
1	0.306	0.009
1	0.570	0.010
1	0.890	0.012
1	1.183	0.013
1	1.471	0.014
2	0.283	0.007
2	0.578	0.008
2	0.875	0.009
2	1.194	0.010
2	1.458	0.011
2	1.891	0.011
2	4.285	0.015
2	6.687	0.019
2	9.020	0.023
2	11.539	0.027
2	13.192	0.029
2	15.712	0.033
2	17.997	0.036
2	19.928	0.039
3	1.837	0.010
3	4.425	0.014
3	6.713	0.017
3	6.729	0.017
3	9.002	0.020
3	11.476	0.023
3	13.562	0.026
3	15.627	0.031
3	17.944	0.035
3	20.043	0.037
3	0.304	0.006
3	0.617	0.007
3	0.881	0.008
3	1.177	0.009
3	1.476	0.009

SLOPE FLUME (degrees)	FLOW Q ($l.s^{-1}$)	DEPTH h (m)
4	1.497	0.007
4	1.177	0.007
4	0.884	0.006
4	0.590	0.006
4	0.295	0.005
4	4.714	0.012
4	6.634	0.013
4	9.056	0.016
4	11.555	0.020
4	13.311	0.023
4	15.667	0.027
4	17.904	0.029
4	19.929	0.033
4	1.966	0.008
5	6.780	0.013
5	9.055	0.015
5	11.632	0.020
5	13.406	0.022
5	15.659	0.025
5	18.114	0.028
5	20.087	0.032
5	0.299	0.005
5	0.615	0.005
5	0.882	0.006
5	1.186	0.007
5	1.456	0.007

Material:	CMC
Concentration/vol:	2.8%
Density kg/m^3:	1016
Ty (Pa):	0.000
k (Pa.s^n):	0.197
n:	0.758
Flume width (mm):	75

SLOPE FLUME (degrees)	FLOW Q ($l.s^{-1}$)	DEPTH h (m)
1	0.130	0.015
1	0.297	0.020
1	0.573	0.025
1	0.866	0.030
1	1.211	0.035
1	1.469	0.039
1	1.857	0.046
1	2.796	0.059
1	3.778	0.074
2	4.372	0.059
2	2.869	0.044
2	1.816	0.033
2	0.118	0.011
2	0.294	0.014
2	0.579	0.018
2	0.919	0.022
2	1.195	0.025
0	0.000	0.000
3	1.432	0.024
3	1.204	0.022
3	0.919	0.019
3	0.510	0.015
3	0.278	0.012
3	0.117	0.009
3	1.804	0.027
3	2.761	0.036
3	3.713	0.045
3	4.714	0.053
4	1.182	0.019
4	0.910	0.016
4	0.628	0.014
4	0.275	0.010
4	0.091	0.007
4	1.908	0.025
4	2.892	0.033
4	3.759	0.040
4	4.789	0.047
4	5.677	0.055
4	0.148	0.009
4	0.197	0.009
4	0.445	0.012

SLOPE FLUME (degrees)	FLOW Q ($l.s^{-1}$)	DEPTH h (m)
5	0.133	0.007
5	0.210	0.009
5	0.321	0.010
5	0.432	0.011
5	0.602	0.012
5	0.892	0.015
5	1.194	0.017
5	1.496	0.019
5	1.623	0.020
5	2.792	0.029
5	4.394	0.040
5	5.032	0.045
5	6.028	0.051

Material:	CMC
Concentration/vol:	2.8%
Density kg/m^3:	1016
Ty (Pa):	0.000
k (Pa.s^n):	0.769
n:	0.197
Flume width (mm):	150

SLOPE FLUME (degrees)	FLOW Q (l.s^{-1})	DEPTH h (m)
1	1.776	0.027
1	2.830	0.032
1	4.230	0.039
1	6.616	0.051
1	9.022	0.063
1	11.585	0.075
1	13.728	0.085
1	16.185	0.096
1	18.064	0.105
1	20.044	0.114
1	0.315	0.015
1	0.600	0.018
1	0.900	0.021
1	1.191	0.023
1	1.490	0.025
2	1.469	0.019
2	1.186	0.018
2	0.881	0.016
2	0.603	0.014
2	0.320	0.011
2	1.945	0.020
2	2.789	0.022
2	4.344	0.028
2	6.644	0.036
2	8.994	0.045
2	11.753	0.055
2	13.753	0.061
2	16.257	0.069
2	20.161	0.082
3	1.998	0.017
3	2.831	0.019
3	4.189	0.023
3	6.624	0.032
3	8.999	0.038
3	11.350	0.045
3	13.773	0.051
3	16.350	0.059
3	18.105	0.064
3	20.095	0.070
3	0.301	0.009
3	0.621	0.011
3	0.866	0.013
3	1.188	0.014
3	1.494	0.015

SLOPE FLUME (degrees)	FLOW Q (l.s^{-1})	DEPTH h (m)
4	1.465	0.013
4	1.219	0.013
4	0.890	0.011
4	0.586	0.010
4	0.302	0.008
4	1.868	0.014
4	4.308	0.021
4	6.569	0.026
4	9.044	0.034
4	11.587	0.039
4	13.643	0.045
4	16.154	0.051
4	17.927	0.056
4	19.974	0.062
5	2.062	0.014
5	2.777	0.015
5	4.220	0.019
5	6.618	0.025
5	8.933	0.030
5	11.473	0.036
5	13.939	0.041
5	16.142	0.046
5	18.259	0.052
5	20.076	0.055
5	0.280	0.007
5	0.662	0.009
5	0.887	0.010
5	1.171	0.011
5	1.488	0.012

Material:	CMC
Concentration/vol:	2.8%
Density kg/m^3:	1016
Ty (Pa):	0.000
k (Pa.s^n):	0.368
n:	0.658
Flume width (mm):	300

SLOPE FLUME (degrees)	FLOW Q ($l.s^{-1}$)	DEPTH h (m)
1	1.932	0.021
1	2.008	0.021
1	2.873	0.024
1	4.285	0.027
1	6.698	0.032
1	9.039	0.038
1	11.725	0.043
1	13.810	0.048
1	16.189	0.053
1	19.912	0.060
1	0.324	0.012
1	0.331	0.012
1	0.629	0.015
1	0.963	0.016
1	1.194	0.018
1	1.469	0.020
2	1.428	0.015
2	1.170	0.014
2	0.898	0.013
2	0.730	0.012
2	0.410	0.010
2	0.202	0.009
2	2.422	0.017
2	3.344	0.019
2	5.654	0.023
2	8.102	0.027
2	10.457	0.032
2	12.788	0.036
2	15.272	0.040
2	17.467	0.045
2	18.974	0.047
2	19.776	0.048
3	2.057	0.014
3	2.813	0.016
3	4.300	0.018
3	6.858	0.021
3	8.994	0.024
3	11.475	0.027
3	13.782	0.031
3	16.094	0.034
3	18.123	0.037
3	20.224	0.040
3	0.298	0.008
3	0.207	0.007
3	0.502	0.009
3	0.736	0.010
3	0.927	0.011
3	1.295	0.012
3	1.596	0.013

SLOPE FLUME (degrees)	FLOW Q ($l.s^{-1}$)	DEPTH h (m)
4	1.555	0.011
4	1.457	0.011
4	1.187	0.010
4	0.858	0.009
4	0.549	0.008
4	0.330	0.007
4	0.210	0.006
4	1.897	0.012
4	2.887	0.014
4	4.352	0.016
4	6.653	0.018
4	9.030	0.021
4	11.607	0.024
4	13.785	0.027
4	16.132	0.030
4	18.107	0.032
4	20.581	0.035
5	2.304	0.012
5	3.312	0.013
5	5.754	0.015
5	7.968	0.018
5	10.606	0.020
5	12.847	0.023
5	15.342	0.025
5	17.506	0.028
5	20.525	0.031
5	0.197	0.005
5	0.448	0.007
5	0.667	0.008
5	0.841	0.008
5	1.329	0.010
5	0.306	0.006
5	0.346	0.007
5	0.399	0.007
5	1.702	0.010

Material:	CMC
Concentration/vol:	3.8%
Density kg/m^3:	1021
Ty (Pa):	0.000
k (Pa.s^n):	0.606
n:	0.678
Flume width (mm):	75

SLOPE FLUME (degrees)	FLOW Q ($l.s^{-1}$)	DEPTH h (m)
5	1.046	0.022
5	0.648	0.019
5	0.424	0.016
5	0.283	0.014
5	0.111	0.011
5	0.212	0.013
5	0.050	0.008
5	1.478	0.026
5	1.950	0.030
5	2.861	0.037
5	3.791	0.045
5	4.883	0.055
4	1.930	0.033
4	3.088	0.044
4	3.764	0.051
4	4.900	0.061
4	5.765	0.068
4	0.087	0.011
4	0.233	0.013
4	0.200	0.014
4	0.238	0.015
4	0.400	0.017
4	0.566	0.019
4	0.876	0.022
4	1.190	0.026
4	1.530	0.028
3	1.538	0.032
3	1.192	0.030
3	0.873	0.026
3	0.597	0.023
3	0.429	0.020
3	0.291	0.018
3	0.219	0.016
3	0.112	0.013
3	1.816	0.037
3	2.778	0.047
3	3.747	0.058
3	4.647	0.068
3	5.585	0.077

SLOPE FLUME (degrees)	FLOW Q ($l.s^{-1}$)	DEPTH h (m)
2	5.466	0.096
2	4.719	0.086
2	3.807	0.074
2	2.935	0.061
2	2.027	0.048
2	0.597	0.027
2	0.402	0.023
2	0.284	0.021
2	0.191	0.018
2	0.115	0.015
2	0.898	0.032
2	1.056	0.034
2	0.643	0.028
1	0.640	0.040
1	0.855	0.046
1	1.073	0.051
1	0.465	0.035
1	0.282	0.028
1	0.184	0.025
1	0.112	0.020
1	3.580	0.103
1	2.808	0.089
1	1.970	0.071
1	1.365	0.058

Material:	CMC
Concentration/vol:	3.8%
Density kg/m^3:	1021
Ty (Pa):	0.000
k (Pa.s^n):	0.453
n:	0.724
Flume width (mm):	150

SLOPE FLUME (degrees)	FLOW Q ($l.s^{-1}$)	DEPTH h (m)
1	1.974	0.041
1	4.264	0.058
1	2.886	0.049
1	6.518	0.071
1	8.826	0.083
1	11.226	0.095
1	12.922	0.106
1	15.714	0.119
1	17.995	0.132
1	19.271	0.137
0	0.000	0.000
0	0.000	0.000
1	0.651	0.026
1	0.904	0.031
1	1.202	0.033
1	1.494	0.036
2	1.593	0.027
2	1.249	0.025
2	0.918	0.023
2	0.636	0.021
2	0.461	0.018
2	0.335	0.017
0	0.000	0.000
2	2.092	0.030
2	3.057	0.035
2	4.700	0.041
2	6.969	0.049
2	9.325	0.058
2	11.471	0.066
2	13.575	0.075
2	16.131	0.084
2	18.533	0.093
3	2.254	0.025
3	3.299	0.029
3	5.248	0.035
3	7.440	0.042
3	9.843	0.050
3	11.822	0.056
3	14.212	0.064
3	16.704	0.072
3	17.041	0.073
0	0.000	0.000
3	0.346	0.013
3	0.575	0.016
3	0.731	0.018
3	1.090	0.020
3	1.288	0.021
3	1.683	0.023

SLOPE FLUME (degrees)	FLOW Q ($l.s^{-1}$)	DEPTH h (m)
4	1.748	0.020
4	1.324	0.018
4	1.025	0.017
4	0.735	0.015
4	0.484	0.014
4	0.367	0.012
4	2.468	0.023
4	3.536	0.026
4	5.660	0.031
4	7.896	0.038
4	10.364	0.044
4	12.149	0.050
4	14.615	0.057
4	17.044	0.064
4	18.839	0.069
5	2.682	0.021
5	3.779	0.024
5	6.085	0.029
5	8.389	0.035
5	10.642	0.040
5	13.173	0.045
5	15.242	0.053
5	17.559	0.059
5	18.433	0.061

Material:	CMC
Concentration/vol:	3.8%
Density kg/m^3:	1021
Ty (Pa):	0.000
k (Pa.s^n):	0.606
n:	0.678
Flume width (mm):	300

SLOPE FLUME (degrees)	FLOW Q ($l.s^{-1}$)	DEPTH h (m)
1	1.869	0.029
1	2.969	0.033
1	4.311	0.038
1	6.616	0.043
1	8.845	0.049
1	11.242	0.053
1	13.277	0.058
1	15.968	0.064
1	17.557	0.067
1	18.520	0.069
1	0.443	0.018
1	0.128	0.013
0	0.000	0.000
1	0.604	0.020
1	0.927	0.022
1	1.179	0.025
1	1.526	0.026
2	1.624	0.021
2	1.682	0.021
2	1.243	0.019
2	0.916	0.018
2	0.624	0.015
2	0.441	0.014
2	0.324	0.013
2	0.168	0.010
2	2.099	0.022
2	3.073	0.025
2	4.711	0.028
2	7.066	0.032
2	9.420	0.036
2	11.476	0.040
2	13.569	0.043
2	16.085	0.048
2	18.561	0.052
3	2.276	0.019
3	3.340	0.021
3	5.188	0.025
3	7.438	0.028
3	9.749	0.031
3	14.120	0.037
3	16.468	0.041
3	18.831	0.044
3	0.366	0.010
3	0.465	0.012
3	0.679	0.013
3	0.947	0.014
3	1.288	0.016
3	1.671	0.017

SLOPE FLUME (degrees)	FLOW Q ($l.s^{-1}$)	DEPTH h (m)
4	1.926	0.015
4	1.565	0.015
4	1.276	0.014
4	1.040	0.013
4	0.738	0.012
4	0.525	0.011
4	0.373	0.010
4	2.423	0.017
4	3.546	0.019
4	5.647	0.022
4	7.820	0.024
4	10.459	0.028
4	12.266	0.030
4	14.572	0.033
4	17.128	0.036
4	19.363	0.039
5	2.646	0.016
5	4.520	0.019
5	6.206	0.021
5	8.389	0.023
5	10.720	0.025
5	12.571	0.027
5	15.985	0.031
5	17.724	0.033
5	19.068	0.035
5	0.213	0.008
5	0.414	0.009
5	0.544	0.010
5	0.798	0.011
5	1.094	0.012
5	1.347	0.013
5	1.610	0.013
5	1.953	0.014

Material:	Carbopol
Concentration/vol:	1.0%
Density kg/m^3:	955
Ty (Pa):	3.520
k (Pa.s^n):	0.287
n:	0.636
Flume width (mm):	75

SLOPE FLUME (degrees)	FLOW Q (l.s^{-1})	DEPTH h (m)
1	0.017	0.021
1	0.074	0.029
1	0.135	0.033
1	0.197	0.037
1	0.253	0.040
1	0.347	0.044
1	0.505	0.048
1	0.670	0.053
1	0.857	0.058
1	1.151	0.065
1	1.386	0.074
2	0.014	0.010
2	0.071	0.015
2	0.132	0.018
2	0.193	0.020
2	0.258	0.021
2	0.358	0.024
2	0.502	0.027
2	0.755	0.032
2	0.851	0.037
2	1.148	0.041
2	1.394	0.045
3	0.016	0.009
3	0.074	0.012
3	0.134	0.014
3	0.196	0.016
3	0.256	0.017
3	0.346	0.019
3	0.395	0.020
3	0.560	0.023
3	0.756	0.024
3	1.145	0.029
3	1.391	0.033
4	0.015	0.007
4	0.069	0.009
4	0.131	0.012
4	0.189	0.013
4	0.251	0.014
4	0.345	0.016
4	0.554	0.018
4	0.715	0.019
4	0.791	0.020
4	1.030	0.022
4	1.255	0.023
4	1.449	0.025

APPENDIX E

DIMENSIONAL ANALYSIS OF THE YIELD PSEUDOPLASTIC MODEL

The wall shear stress is a function of the following:

Mixture density (ρ_m),

Characteristic length (L),

Mean velocity (V),

Yield stress (τ_y)

Fluid consistency index (K)

Flow behaviour index (n)

Using the Buckingham π method, the following dimensionless groups result:-

$$\Pi_1 = \frac{\tau_0}{\rho V^2} \qquad \text{E.1}$$

$$\Pi_2 = \frac{\tau_y}{\rho_m V^2} \qquad \text{E.2}$$

$$\Pi_3 = \frac{8\rho V^{2-n} L^n}{K} \qquad \text{E.3}$$

and $\Pi_4 = n$ E.4

These four dimensionless groups, using appropriate constants, are conventionally manipulated so that the Fanning friction factor is a function of Reynolds number and Hedström number.

The Reynolds number developed by Slatter (1994) which was adapted in this thesis for open channel flow (chapter 5 equation 5.7, 5.8 and 5.9) has not been derived from dimensional analysis and since dimensional analysis has traditionally played such an important role in the formulation of Reynolds numbers, thus deserves some comment.

Dimensional analysis is based on the premise that the functional relationship between the problem variables is multiplicative and exponential. This method is therefore unable to resolve the additive nature of the fundamental rheological relationship of:

$$\tau = \tau_y + K\left(-\frac{du}{dr}\right)^n, \qquad \text{E.8}$$

(Slatter and Lazarus, 1993).

One of the underlying aims of this thesis was to produce a single criterion for transition (as in Newtonian flow; Re_2=2100). Clearly, the route following dimensional analysis cannot produce a single criterion.

This approach has been adopted by Hanks (1979) and it is disappointing to note that this sophisticated approach has to date not yielded good results (Slatter and Wasp, 2000). This was for pipe flow - arguably much simpler than open channel flow.

Therefore the approach adopted in this thesis does not accommodate the dimensional analysis route.

While this may not satisfy the requirements of absolute scientific rigour, it has the potential to produce workable engineering solutions until more rigorous successful approaches are developed.